PREPARATION OF HIGH DENSITY POLYETHYLENE AND POLY (BUTYLENE SUCCINATE) FILLED WITH BIO-FILLERS FROM EGGSHELL

Wanikorn Buakaew

A Thesis Submitted in Partial Fulfillment of the Requirements for the

Degree of Master of Engineering in Polymer Engineering

Suranaree University of Technology

Academic Year 2013

การเตรียมพอลิเอทิลีนชนิดความหนาแน่นสูงและพอลิบิวทิลีนซัคซิเนต ที่เติมสารตัวเติมชีวภาพจากเปลือกไข่

นายวนิกร บัวแก้ว

วิทยานิพนธ์นี้เป็นส่วนหนึ่งของการศึกษาตามหลักสูตรปริญญาวิศวกรรมศาสตรมหาบัณฑิต
สาขาวิชาวิศวกรรมพอลิเมอร์
มหาวิทยาลัยเทคโนโลยีสุรนารี
ปีการศึกษา 2556

PREPARATION OF HIGH DENSITY POLYETHYLENE AND POLY (BUTYLENE SUCCINATE) FILLED WITH BIO-FILLERS FROM EGGSHELL

Suranaree University of Technology has approved this thesis submitted in partial fulfillment of the requirements for a Master's Degree.

Thesis Examining Committee

(Asst. Prof. Dr. Nitinat Suppakarn)
Chairperson

(Asst. Prof. Dr. Wimonlak Sutapun)
Member (Thesis Advisor)

(Assoc. Prof. Dr. Yupaporn Ruksakulpiwat)
Member

(Prof. Dr. Sukit Limpijumnong)
Vice Rector for Academic Affairs and Innovation

(Assoc. Prof. Flt. Lt. Dr. Kontorn Chamniprasart)
Dean of Institute of Engineering

วนิกร บัวแก้ว : การเตรียมพอลิเอทิลีนชนิดความหนาแน่นสูงและพอลิบิวทิลีนซัคซิเนตที่เติมสารตัวเติมชีวภาพจากเปลือกไข่ (PREPARATION OF HIGH DENSITY POLYETHYLENE AND POLY (BUTYLENE SUCCINATE) FILLED WITH BIO-FILLERS FROM EGGSHELL) อาจารย์ที่ปรึกษา : ผู้ช่วยศาสตราจารย์ ดร.วิมลลักษณ์ สุตะพันธ์, 207 หน้า.

ในการศึกษานี้ เปลือกไข่ไก่ถูกใช้เป็นสารตัวเติมเสริมแรงสำหรับการเตรียมวัสดุเชิงประกอบพอลิเอทิลีนชนิดความหนาแน่นสูงและวัสดุเชิงประกอบพอลิบิวทิลีนซัคซิเนต โดยเปลือกไข่ถูกเตรียมให้อยู่ในรูปของผงเปลือกไข่บดและผงเปลือกไข่ตกตะกอน โดยตรวจสอบผลของปริมาณสารตัวเติม ขนาดอนุภาคสารตัวเติม และสารช่วยเพิ่มความเข้ากันได้ ที่มีผลต่อสมบัติทางกายภาพของวัสดุเชิงประกอบ

จากการศึกษาสมบัติทางกายภาพของวัสดุเชิงประกอบของพอลิเอทิลีนชนิดความหนาแน่นสูงและผงเปลือกไข่บด พบว่าการเพิ่มปริมาณผงเปลือกไข่บดช่วยเพิ่มมอดุลัสของยังค์ของวัสดุเชิงประกอบ แต่มีผลต่อการลดลงของสมบัติทางกลอื่นๆ และปริมาณผลึกของวัสดุเชิงประกอบ นอกจากนี้ พบว่าขนาดและปริมาณเปลือกไข่บดไม่มีผลต่ออุณหภูมิการเสื่อมสลาย อุณหภูมิการหลอมละลายและอุณหภูมิการตกผลึกของเมทริกซ์พอลิเอทิลีนชนิดความหนาแน่นสูง แต่การยืดตัว ณ จุดขาด และความทนทานต่อแรงกระแทกของวัสดุเชิงประกอบพอลิเอทิลีนชนิดความหนาแน่นสูงถูกปรับปรุงจากการใช้ผงเปลือกไข่บดที่มีอนุภาคเฉลี่ยที่เล็กลง ปริมาณผลึกของพอลิเอทิลีนชนิดความหนาแน่นสูงไม่ขึ้นอยู่กับขนาดของอนุภาคของผงเปลือกไข่บด นอกจากนี้พอลิเอทิลีนชนิดความหนาแน่นสูงกราฟต์มาเลอิกแอนไฮไดรด์ช่วยลดความเปราะของวัสดุเชิงประกอบของพอลิเอทิลีนชนิดความหนาแน่นสูงและผงเปลือกไข่บด ในขณะที่ยางเอทิลีนโพรพิลีนกราฟต์มาเลอิกแอนไฮไดรด์ส่งผลต่อการลดลงของสมบัติทางกลของวัสดุเชิงประกอบพอลิเอทิลีนชนิดความหนาแน่นสูงที่เติมผงเปลือกไข่บด

การศึกษาสมบัติทางกายภาพของวัสดุเชิงประกอบของพอลิเอทิลีนชนิดความหนาแน่นสูงและผงเปลือกไข่ตกตะกอน พบว่าการเพิ่มปริมาณผงเปลือกไข่ตกตะกอนช่วยเพิ่มมอดุลัสของยังค์และมอดุลัสแรงดัดของวัสดุเชิงประกอบ แต่มีผลต่อการลดลงของสมบัติทางกลอื่นๆ ผงเปลือกไข่ตกตะกอนทำให้อุณหภูมิการเสื่อมสลายของเมทริกซ์พอลิเอทิลีนชนิดความหนาแน่นสูงเพิ่มขึ้นอย่างมีนัยสำคัญ และปริมาณผงเปลือกไข่ตกตะกอนไม่มีผลต่ออุณหภูมิการการหลอมละลาย และอุณหภูมิการการตกผลึกของเมทริกซ์พอลิเอทิลีนชนิดความหนาแน่นสูงเช่นกัน ส่วนปริมาณผลึกของเมทริกซ์พอลิเอทิลีนชนิดความหนาแน่นสูงลดลงเล็กน้อยเมื่อปริมาณผงเปลือกไข่ตกตะกอน

เพิ่มขึ้น ในเชิงเปรียบเทียบ สมบัติทางกลของวัสดุเชิงประกอบของพอลิเอทิลีนชนิดความหนาแน่นสูงที่ 20 เปอร์เซ็นต์โดยน้ำหนักของผงเปลือกไข่บดไม่แตกต่างกันมากเมื่อเทียบกับวัสดุเชิงประกอบของพอลิเอทิลีนชนิดความหนาแน่นสูงที่ 20 เปอร์เซ็นต์โดยน้ำหนักของผงเปลือกไข่ตกตะกอน ส่วนอุณหภูมิการเสื่อมสลาย และอุณหภูมิการหลอมละลายของวัสดุเชิงประกอบพอลิเอทิลีนชนิดความหนาแน่นสูงเหล่านั้นก็ไม่แตกต่างกัน อย่างไรก็ตาม พอลิเอทิลีนชนิดความหนาแน่นสูงที่เติมผงเปลือกไข่บดมีความเหนียว ความทนทานต่อแรงกระแทก อุณหภูมิการตกผลึก และปริมาณผลึกสูงกว่าพอลิเอทิลีนชนิดความหนาแน่นสูงที่เติมผงเปลือกไข่ตกตะกอน

จากการศึกษาสมบัติทางกายภาพของวัสดุเชิงประกอบของพอลิบิวทิลีนซัคซิเนตกับผงเปลือกไข่บด พบว่ามอดุลัสของยังค์ของวัสดุเชิงประกอบถูกปรับปรุงเมื่อปริมาณของผงเปลือกไข่บดเพิ่มขึ้น ส่วนปริมาณผงเปลือกไข่บดไม่มีผลต่ออุณหภูมิการเสื่อมสลาย และอุณหภูมิการหลอมละลายของเมทริกซ์พอลิบิวทิลีนซัคซิเนต การเติมผงเปลือกไข่บดลงไปในพอลิบิวทิลีนซัคซิเนตทำให้อุณหภูมิการตกผลึกและปริมาณผลึกของเมทริกซ์พอลิบิวทิลีนซัคซิเนตลดลง จากการศึกษาสมบัติทางกายภาพของวัสดุเชิงประกอบของพอลิบิวทิลีนซัคซิเนตกับผงเปลือกไข่ตกตะกอน พบว่าการเพิ่มปริมาณผงเปลือกไข่ตกตะกอนมีผลต่อการลดลงของความทนทานต่อแรงดึงสูงสุด การยืด ณ จุดขาด ความทนทานต่อแรงกระแทก อุณหภูมิการตกผลึกและปริมาณผลึก นอกจากนี้ ผงเปลือกไข่ตกตะกอนไม่มีผลต่ออุณหภูมิการเสื่อมสลาย และอุณหภูมิการหลอมละลายของเมทริกซ์พอลิบิวทิลีนซัคซิเนต ในเชิงเปรียบเทียบ วัสดุเชิงประกอบพอลิบิวทิลีนซัคซิเนตที่ 20 เปอร์เซ็นต์โดยน้ำหนักของสารตัวเติมเปลือกไข่ตกตะกอน มีความทนทานต่อแรงกระแทก ความทนทานแรงดัด และอุณหภูมิการเสื่อมสลายต่ำกว่าวัสดุเชิงประกอบพอลิบิวทิลีนซัคซิเนตที่ 20 เปอร์เซ็นต์โดยน้ำหนักของสารตัวเติมเปลือกไข่บด อย่างไรก็ตาม พอลิบิวทิลีนซัคซิเนตที่เติมผงเปลือกไข่ตกตะกอนมีอุณหภูมิการตกผลึก และปริมาณผลึกสูงกว่าพอลิบิวทิลีนซัคซิเนตที่เติมผงเปลือกไข่บดเล็กน้อย

สาขาวิชา วิศวกรรมพอลิเมอร์ ลายมือชื่อนักศึกษา _____

ปีการศึกษา 2556 ลายมือชื่ออาจารย์ที่ปรึกษา _____

WANIKORN BUAKAEW : PREPARATION OF HIGH DENSITY POLYETHYLENE AND POLY (BUTYLENE SUCCINATE) FILLED WITH BIO-FILLERS FROM EGGSHELL. THESIS ADVISOR : ASST. PROF. WIMONLAK SUTAPUN, Ph.D., 207 PP.

HIGH DENSITY POLYETHYLENE/POLY (BUTYLENE SUCCINATE)/ EGGSHELL/COMPOSITE/COMPATIBILIZER

In this work, chicken eggshell was used as a reinforcing filler for preparing high density polyethylene (HDPE) composite, and poly (butylene succinate) (PBS) composite. The eggshell was prepared as eggshell powder (ESP), and precipitated eggshell powder (PESP). Effect of the filler content, filler size, and compatibilizers on physical properties of those composites was investigated.

For ESP/HDPE composites, increasing ESP content enhanced Young's modulus of HDPE composite but had negative effect on other mechanical properties, and degree of crystallinity (X_c) of the composite. In addition, ESP content and size did not influence decomposition temperature (T_d), melting temperature (T_m) and crystallizing temperature (T_c) of HDPE matrix. However, with smaller particle size of ESP, elongation at break, and impact strength of HDPE composite, matrix were enhanced. Crystallinity of the filled HDPE did not depend on ESP particle size. In addition, High density polyethylene grafted with maleic anhydride (HDPE-g-MAH) helped reduce brittleness of ESP/HDPE composite. Nevertheless, ethylene propylene rubber grafted with maleic anhydride (EPR-g-MAH) had negative effect on mechanical properties of the ESP/HDPE composite.

For PESP/HDPE composite, increasing PESP content improved Young's modulus and flexural modulus of the composite but had negative effect on other mechanical properties. In addition, PESP significantly increased T_d of HDPE matrix and PESP content insignificantly affected T_m, and T_c of HDPE matrix, as well. Crystallinity of HDPE matrix slightly decreased with increasing PESP content. In comparison, mechanical properties of HDPE composite at 20 wt.% ESP were not much different from those of the composites at 20 wt.% PESP. Also, T_d, and T_m of those composites were not different. However, HDPE filled with ESP had higher toughness, impact strength, T_c, and X_c than HDPE filled with PESP.

For ESP/PBS composite, increasing ESP content improved Young's modulus of the composite. ESP content did not affect T_d, and T_m of PBS matrix. Adding ESP into PBS resulted in decreased T_c, and X_c of PBS matrix. For PESP/PBS composite, increasing PESP content had negative effect on tensile strength, elongation at break, impact strength, T_c, and X_c. In addition, PESP did not affect T_d, and T_m of PBS matrix. In comparison, PBS composite at 20 wt.% PESP had lower impact strength, flexural strength, and T_d than the composite at 20 wt.% ESP. However, PBS filled with PESP had slightly higher T_c, and X_c than the PBS filled with ESP.

School of Polymer Engineering Student's Signature _____

Academic Year 2013 Advisor's Signature _____

ACKNOWLEDGEMENTS

I would like to thank Suranaree University of Technology for financial support and Center of Excellence on Petrochemical and Materials Technology for research assistantship.

I am deeply grateful to my thesis advisor, Asst. Prof. Dr. Wimonlak Sutapun, who always gives me a kind suggestions and supports me throughout the period of master study. In addition, I would like to express my appreciation to Asst. Prof. Dr. Nitinat Suppakarn and Assoc. Prof. Dr. Yupaporn Ruksakulpiwat for their valuable suggestions and guidance given as committee members.

My sincere thanks also go to all of the faculty and staff members of School of Polymer Engineering for their help and assistance through the course of this work. The special thanks are also attributed to SUT farm for supplying chicken eggshell, Scientific Promotion Co., Ltd. for kindly supplying air jet sieving machine (Retsch, AS 200 jet), and Chemical Innovation Co., Ltd. for supplying maleic anhydride grafted high density polyethylene (Fusabond® MB100D, DuPont™). Special thanks are extended to my good friends especially Miss Ladawan Srisuwan for their helps and encouragement.

Finally, I would like to thank my parents, Mr. Somboon and Mrs. Sungwan Buakaew, my maternal uncle, Mr. Sungwean Kaewthep, and my younger brother, Mr. Phadungkiat Buakaew, who give me a valuable life with their endless love, supports, understandings and encouragement throughout my life.

Wanikorn Buakaew

TABLE OF CONTENTS

Page

TABLE OF CONTENTS (Continued)

Page

TABLE OF CONTENTS (Continued)

Page

TABLE OF CONTENTS (Continued)

Page

TABLE OF CONTENTS (Continued)

Page

TABLE OF CONTENTS (Continued)

Page

TABLE OF CONTENTS (Continued)

Page

TABLE OF CONTENTS (Continued)

Page

LIST OF TABLES

Table **Page**

LIST OF TABLES (Continued)

Table **Page**

LIST OF TABLES (Continued)

Table **Page**

LIST OF TABLES (Continued)

Table **Page**

LIST OF TABLES (Continued)

Table **Page**

LIST OF FIGURES

Figure **Page**

LIST OF FIGURES (Continued)

Figure **Page**

LIST OF FIGURES (Continued)

Figure **Page**

LIST OF FIGURES (Continued)

Figure **Page**

LIST OF FIGURES (Continued)

Figure **Page**

LIST OF FIGURES (Continued)

Figure **Page**

LIST OF FIGURES (Continued)

Figure **Page**

LIST OF FIGURES (Continued)

Figure **Page**

SYMBOLS AND ABBRAVIATIONS

ESP	=	Eggshell powder
PESP	=	Precipitated eggshell powder

CHAPTER I

INTRODUCTION

1.1 Background

World consumption of thermoplastic materials is increasing in some sectors such as construction, agriculture, and automotive; aerospace; and electronic parts (Wang et al., 2007). The commercial plastics major consumed in Thailand are polyethylene (PE), polypropylene (PP), and polyvinyl chloride (PVC) as shown in Table 1.1. Even though, some of them are good in weathering resistance and mechanical strength, and they have emerged as ideal materials for automobile and consumer products (Tanniru et al., 2005), these synthetic thermoplastics are non biodegradable. Nowadays, biodegradable polymers have been increasingly used as environmental friendly materials. The most popular biodegradable polymers are aliphatic thermoplastic polyesters such as poly (lactic acid) (PLA), poly (butylene succinate) (PBS), and poly (ε-caprolactone) (PCL). As a matter of fact, their price is quite high, 10$/kg (source: Fresh Bag Co., Ltd) therefore they are not economically commercialized for consumer product. In addition, thermoplastics, non biodegradable and biodegradable, are seldom used as neat plastic but compounded with mineral fillers to improve some certain properties like stiffness and strength, and also to reduce material cost for consumer product. Presently, another criteria to be considered in the mineral filler selection is whether it is eco-friendly/environmental friendly material, and renewable.

High density polyethylene is one of the most consumed thermoplastics in Thailand. It is a semi-crystalline polymer. The demand market of HDPE is increasing because of its expanded application, especially for automotive and structural applications. However, there is some limitation in engineering design for applying HDPE in certain application that requires high stiffness and/or strength especially in structural application. To improve these limitations, HDPE is needed to compound with reinforcing fillers. It would be beneficial for environment if HDPE is compounded with eco-friendly or bio-filler that also meets the requirement of mechanical enhancement and material cost reduction.

Table 1.1 Usage of the most common types of plastic in Thailand (Petroleum Institute of Thailand, 2012).

Plastic type	**Usage (%)**
PE (LDPE, LLDPE and HDPE)	38.7
Polypropylene (PP)	23.3
Polyvinyl chloride (PVC)	9.5
Polyethylene terephthalate (PET)	7.8
Acrylonitrile butadiene styrene (ABS)	5.9
Polyamide (PA)	4.3
Others	10.3
Total	100

Nowadays, the development of eco-friendly biodegradable polymers has gained increasing attention because of growing worldwide recognition of the need to reduce global environmental pollution. However, the biodegradable polymers are not yet widely used because they are expensive. PBS has been attracting much attention due to its general physical properties similar to those of commercial non biodegradable product derived from LLDPE, LDPE, and PP. It has been predicted that within the next 5 years, consumer products from PBS will be successfully commercialized and soon replace those non biodegradable plastics. The drawback for commercializing PBS consumer product is its high price. One method to reduce the price and enhance mechanical performance of PBS was blending or compounding with low cost and eco-friendly fillers. There are many studies concerning the use of bio-fiber and bio-flour to reinforce PBS composite system such as rice-husk (RHF) and red algae fibre (Y.F. Shih et al., 2006; M. W. Lee et al., 2008). Many works have been shown the use of bio mineral filler to produce biodegradable PBS composite such as bone-based hydroxyapatite (HA)/PBS composite (Guo, Zhang and Zhang, 2013) and oyster shell $CaCO_3$/PBS composite (Funabashi, Ninomiya, Flores and Kunioka, 2010). It was confirmed that the bio filler, organic filler, and mineral filler, improved tensile modulus of those PBS composites. Up until now, there is few bio filler of choice for reinforcing and compounding PBS; therefore effort must be put in for finding novel bio filler for PBS. The bio filler must be not expensive, is able to enhance mechanical properties and reduce material cost, and is renewable.

The mineral fillers are a vital and significant part of the plastic industry. Their worldwide mineral filler consumption in plastics is currently estimated to be over 10 million tons per annum (Stadelman and Cotterill, 1995). The most commonly mineral

fillers used in non bio and biodegradable plastic industry are calcium carbonate, clay, talc, silica, mica, wollastonite, glass fiber and glass beads (Elleithy et al., 2010). The mostly used fillers in Thailand, for the plastic compounding are shown in Table 1.2.

Table 1.2 Mineral fillers consumed by plastic industry in Thailand (Source: Department of Primary Industries and Mines Thailand, 2012).

Fillers types	Calcite	Talc	Clay	Diatomite	Others	Total
Consumption (wt.%)	56.3	7.2	4.7	1.8	29.7	100

For compounding HDPE, among those mineral fillers, particulate calcium carbonate ($CaCO_3$) is widely used as a reinforcing filler. There are two types of calcium carbonate used as mineral filler for plastics compounding, ground calcium carbonate (GCC) and precipitated calcium carbonate (PCC). The characteristics of GCC and PCC are shown in Table 1.3. GCC is manufactured by conventional extracting, grinding and sieving methods. Commercial GCC grade contain 90.0-99.5 wt% $CaCO_3$ (Xanthos, 2005). GCC are generally used as filler with an interesting performance (stiffness and strength)/price ratio. PCC is interesting because it has regular crystalline shape, small particle size and narrow particle size distribution (Renaudin et al., 2008). It is used to fulfill specific needs like processing aid, impact modifier etc. (Renaudin et al., 2008). However, it is much more expensive than GCC thus limiting its uses.

Table 1.3 Basic properties of GCC and PCC (Wypych, 2010; Zweifel et al., 2008).

Properties	Unit	GCC	PCC
Loss of ignition at 950^{o}C	%	43.5	44
Density	g/cm^{3}	2.7	2.9
Refractive index	-	1.48-1.65	1.7
Decomposition (onset temperature)	^{o}C	550	550
Particle size range	µm	0.2-10	0.1-2
Hardness	Mohs	3	3
Purity	%	90-99.5	99.5-100

In addition, PCC is currently produced by a lime soda process, a calcium chloride process, and a carbonation process. Calcium chloride process is one to the most used process for preparing PCC. The chemical reaction of the process includes $CaCl_2$ solution preparation and precipitation, as shown in equation (1.1) and (1.2) (Kobeleva and Poilov, 2007).

$$CaCO_3 + 2HCl \longrightarrow CaCl_2 + CO_2 + H_2O \quad (1.1)$$

$$CaCl_2 + Na_2CO_3 \longrightarrow CaCO_3 + 2NaCl \quad (1.2)$$

However, calcium carbonate filler is normally derived from natural resources such as sedimentary rock, limestone, and volcanic rock. For production the filler, more than 5 million tons of sedimentary rock has been consumed annually. The natural resources take long time to sediment in nature. In order to slowdown the rate

of natural resource consumption, renewable sources should be looked for. Those sources might come from either plants or animals.

Currently, a new eco-friendly or bio-filler is interesting because it is derived from renewable bio-source which is abundant. Interestingly, the chicken eggshell, a waste product from hatchery, food industry etc., comprises calcium carbonate ($CaCO_3$) as high as 94 wt.%, close to purity of ground calcium carbonate (GCC) filler. Furthermore, it is generated by reproducible source. Most of eggshell is commonly disposed without any utilization. For the past five year, several researches have proved that eggshell powder is good reinforcing filler for thermoplastics comparable to GCC.

Pakdeechote et al. (2010) have studied the preparation of ESP for HDPE. Moreover, the use of ESP as a filler in other thermoplastics was also studied such as LDPE (Shuhadah and Supri, 2009), PP (Dangtungee et al., 2008), polyaniline (PANI) (Ghani and Young, 2010), and epoxy (Ji et al., 2009). It was found that incorporation of ESP into those thermoplastics enhanced Young's modulus of the filled thermoplastics. Therefore, using ESP as bio-filler has gained advantages because it is renewable, environmentally compatible, and not expensive.

Using eggshell fillers to reinforce HDPE has some benefit in terms of mechanical enhancement, price reduction and also more environmental compatibility of ESP filled HDPE. Eggshell filler is able to prepare as ground eggshell and precipitated eggshell. However, there is no study concerning effect of eggshell particle size and effect of compatibilizer type and content on physical properties of ESP/HDPE composites. In addition, HDPE-filled with precipitated eggshell has not been studied yet.

For compounding HDPE with ESP, the maleic anhydride grafted high density polyethylene (HDPE-g-MAH), and maleic anhydride grafted ethylene propylene rubber (EPR-g-MAH) were used as compatibilizers. It was expected that compatibilization of the filled HDPE would be enhanced by two mechanism as shown in Figure 1.1. Firstly, it was the interaction between hydroxyl groups attacked to MAH groups of those compatibilizers. Secondly, it was the well mixing between HDPE main chains and molecular backbones of HDPE-g-MAH, and the coexisting between HDPE main chains and molecular backbones of EPR-g-MAH with the rubbery amorphous phase of HDPE matrix. It was expected that this coexistence would impart ductility of the rigid particle filled HDPE.

As mentioned previously, eggshell filler is good bio filler for thermoplastics, therefore it was expected that the eggshell filler, ground eggshell, and precipitated eggshell, could be a good eco-friendly filler for PBS, as well.

In addition, eggshell filler was expected that it would compatible to PBS according to its polar surface. This would enhance eggshell filler and PBS matrix interfacial adhesion. Using chicken eggshell filler for reinforcing PBS has not been investigated that. This study would add filler of choice for PBS.

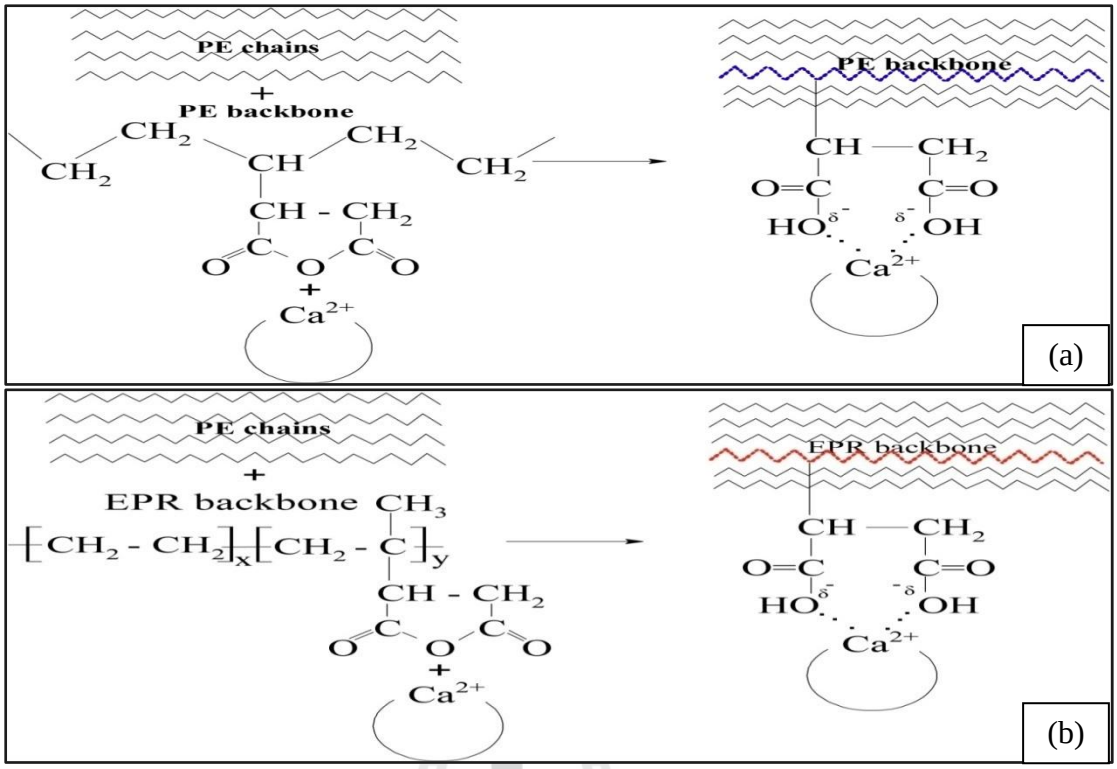

Figure 1.1 Schematic representing the mechanism of surface modification with maleic anhydride grafted high density polyethylene (HDPE-g-MAH) (a), and maleic anhydride grafted ethylene propylene rubber (EPR-g-MAH) (b) in $CaCO_3$/HDPE composites (Li et al., 2006; Chow et al., 2005).

1.2 Statement of motivation

Chicken eggshell has been reported that it is a calcium carbonate-rich material. Commonly, eggshell is disposed without any utilization even though it comprised valuable calcium carbonate up to 94 wt.% (Xanthos, 2005). Thus, eggshell is interesting, apart from high in calcium carbonate content, because it is derived from renewable bio-source, low cost and abundant. Interestingly, this calcium carbonate from eggshell can be used as alternative filler for HDPE and PBS. Most importantly, eggshell filler would enhance environmental friendliness to HDPE-derived product,

on the other hand, eggshell filler would reduce material cost for commercializing PBS product, and help prolong natural resources for GCC and PCC production. The advantages of utilization of eggshell as a bio-filler for polymer are its renewable sources, reduction of waste and reduction energy consumed for producing calcium carbonate mineral.

In this research, the chicken eggshell was used as reinforcing filler for HDPE and PBS. The eggshell bio-filler was prepared in a form of eggshell powder (ESP) with membrane removal and precipitated eggshell powder (PESP). For HDPE and PBS filled with eggshell filler, effect of filler content, filler sizes and compatibilizer was investigated.

1.3 Research objectives

The main objectives of this research are as follows:

(i) To prepare bio-reinforcing filler from eggshell as an alternative filler in a form of eggshell powder (ESP), and precipitated eggshell powder (PESP).

(ii) To prepare composites of HDPE filled with eggshell powder (ESP) and precipitated eggshell powder (PESP).

(iii) To prepare bio-composites of PBS filled with eggshell powder (ESP) and precipitated eggshell powder (PESP).

(iv) To determine effect of bio-reinforcing size, filler content and compatibilization on mechanical properties, flow behavior, crystallinity and fracture morphology of HDPE and PBS composites.

1.4 Scope and limitation of the research

Chicken eggshell was used in two forms: eggshell powder (ESP) and precipitated eggshell powder (PESP). The ESP with an average particle size of 13.96, 20.35, and 35.30 μm were used for preparing HDPE composites. The calcium chloride process was carried out to prepare PESP.

The composites of HDPE and PBS were prepared with various ESP contents of 10, 20, 30, and 40 wt%. The maleic anhydride grafted high density polyethylene (HDPE-g-MAH) and maleic anhydride grafted ethylene propylene rubber (EPR-g-MAH) were used as compatibilizers for HDPE-filled with ESP with various contents of 2, 5, 8, and 10 wt.%.

The composites of HDPE and PBS were prepared with PESP contents of 5, 10, and 20 wt.%.

The chemical composition and crystal form of ESP and PESP were determined. The thermal properties of ESP, PESP, neat HDPE, neat PBS, HDPE composites and PBS composites were examined. Moreover, mechanical properties (tensile properties, flexural properties and impact properties), flow behavior, thermal, crystallinity and fracture morphology of those composites were investigated.

CHAPTER II

LITERATURE REVIEW

2.1 Avian eggshell

2.1.1 Structure of egg and eggshell

An egg composes of three main parts; eggshell, albumen or white, and yolk. The yolk is surrounded by albumen, which in turn is enveloped by eggshell membranes and finally a hard eggshell (USDA, 2000). The egg comprises approximately 30 wt.% yolk, 60 wt.% albumen and 10 wt.% shell (Stadelman and Cotterill, 1995), as presented in Figure 2.1.

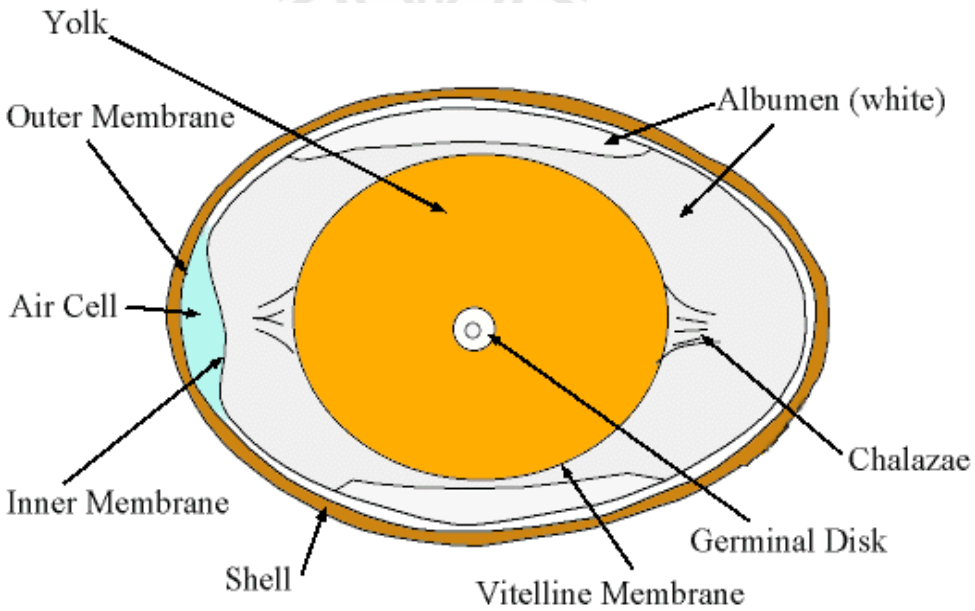

Figure 2.1 Schematic of different parts of egg structure.

(Source: http://foodsafety.suencs.com/060909-egg-basics-for-the-consumer).

Eggshell is a combination of both inorganic and organic components. Calcium carbonate in the form of calcite is the main component of eggshell about 94 wt.%, which presents a density of 2.710 g cm^{-1} (Carvalho, Araujo and Castro, 2011). The other components were reported as 1 wt.% magnesium carbonate, 1 wt.% calcium phosphate, and organic materials such as type X collagen, sulfated polysaccharides, and other proteins about 4 wt.% (Hassan, Rangari, Rana and Jeelani, 2013). The eggshell calcium carbonate consists in the vertical crystal layer, palisade layer and mammilary knob layer as shown in Figure 2.2 (Dennis et al., 1996). The inner most layer of calcite – mammilary layer (~100 μm) grows on the outer egg membrane and creates the base on which the palisade layer constitutes the thickest part (~200 μm) of the eggshell. The top layer is the vertical layer (~5-8 μm) covered by the organic cuticle (Dobiasova et al., 2008). Moreover, the numerous pore canals are distributed at the outer eggshell surface about 7,000-17,000 pores per egg, but these are unevenly over the shell surface (Stadelman and Cotterill, 1995; Carvalho, Araujo and Castro, 2011).

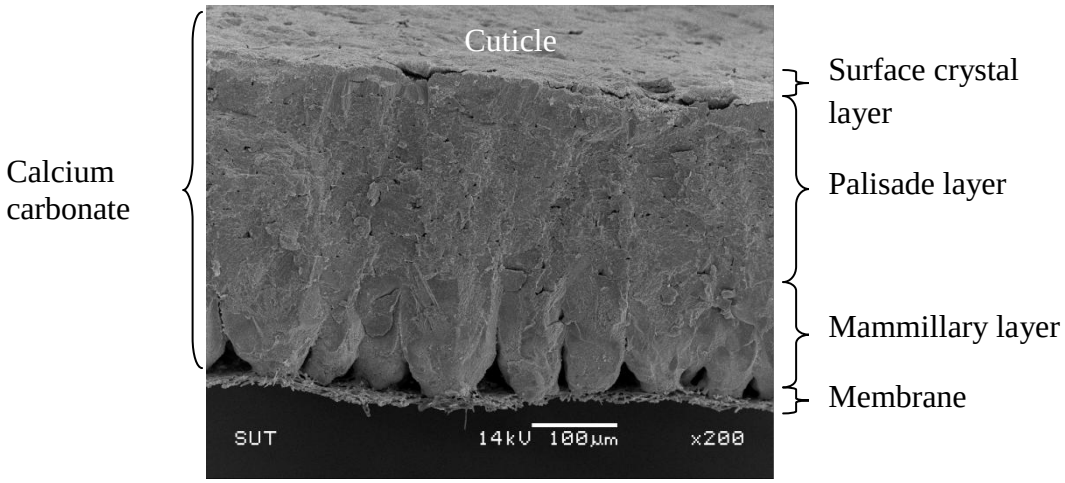

Figure 2.2 SEM micrograph of a cross-fractured chicken eggshell structure.

The vertical crystal layer consists of short with their long axes oriented toward the shell surface. The palisade layer is a very dense and hard. Its crystalline structure is form by calcification of calcium carbonate. The mammilary knob layer has a core and is interconnected to protein fibers of the outer shell membrane (Mine, 2008).

The innermost structure associated with the eggshell is a meshwork of interwoven fibers known as the shell membranes as shown in Figure 2.3. This structure, organized into inner and outer layers of differing fiber sizes, contains collagens Type I, Type V and Type X (Hincke et al., 2008; Mine, 2008).

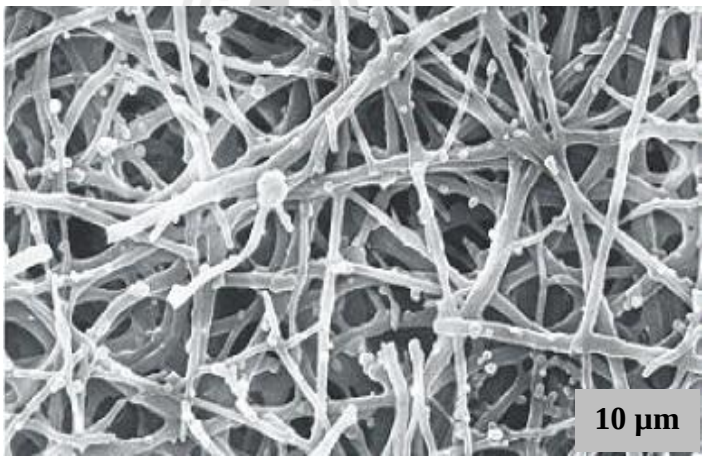

Figure 2.3 Interwoven of protein fiber within eggshell membrane (Scala et al., 2000).

2.1.2 Chemical composition of eggshell

The avian eggshell consists of calcium carbonate ($CaCO_3$) as the major component in the form of calcite (Gongruttananun, 2011). It was reported that all eggshells had similar chemical content to commercial $CaCO_3$ (Jai et al., 2007). The minor components are phosphorous (P) and magnesium (Mg) and a few of other

components; *i.e.* Si, Al, Na, K, F, Cl, Sr, Fe, Li, Ba, Zn and Zr (Gil and Mok, 2007; Goran et al., 2010). The mammilary layer is the major source of calcium. Phosphorous was detected in the cone region but the most of phosphate and magnesium has been found in the outer portion of the shell (Salam et al., 2006).

Avian eggshell membranes are composed of proteins with disulfide groups and carbohydrate. The outer organic cuticle is rich in cystein (42.7%), and in the inner membrane cystein can exceed 95% (Dauphin et al., 2006). In addition, the uronic acid, sialic acid and nitrogen were found in eggshell and shell membranes. Uronic acid concentrations are similar between the inner shell membrane and outer shell membrane but approximately five-fold higher in the organic matter. Sialic acid concentrations are highest in the organic matter of eggshell and higher in the inner than in the outer shell membrane. Nitrogen concentrations are lowest in the organic matter of eggshell but relatively constant between the two shell membranes. Amino acid analysis showed that the content of glycine and alanine are higher and those of proline and hydroxyproline are lower in eggshell layers compared to shell membranes (Miksik et al., 2003). In addition, the chemical structures of cystein, uronic acid, sialic acid, glycine, alanine, proline and hydroxyproline are shown in Figure 2.4.

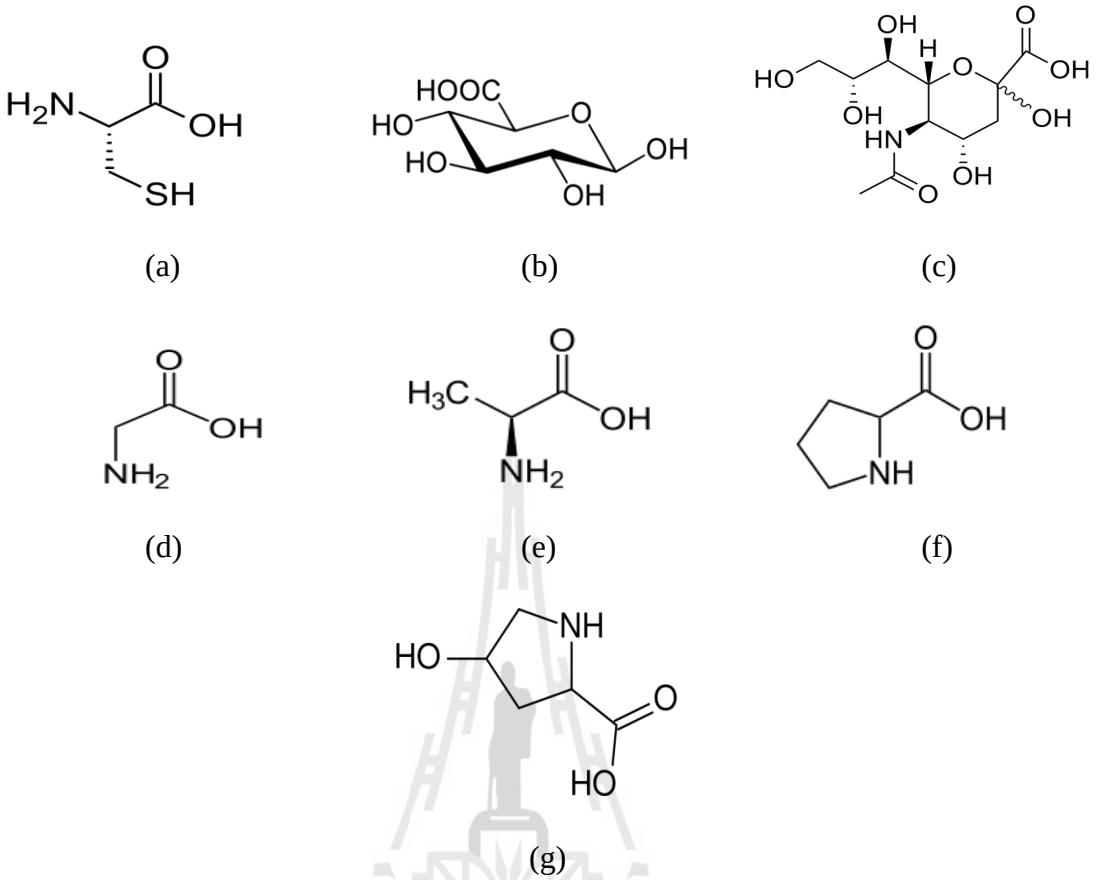

Figure 2.4 Chemical structures of cystein (a), uronic acid (b), sialic acid (c), glycine (d), alanine (e), proline (f), and hydroxyproline (g).

2.1.3 Eggshell matrix proteins

The eggshell mineral is associated with an organic matrix composing of proteins, glycoprotein and proteoglycans, termed “eggshell matrix protein”. They are progressively incorporated from the precursor milieu (uterine fluid) during calcification. Their function is thought to participate in its antimicrobial defenses (Rose and Hincke, 2009). The eggshell matrix protein can be divided into three types: eggshell specific, bone protein and egg white protein (Sim et al., 2000). Ovocleidin-17, ovocleidin-116, ovocalyxin-32 and ovocalyxin-36 were in group of eggshell

specific. Osteopontin was in a group of bone protein. The example of protein in egg white proteins group was ovalbumin, ovotransferrin and lysozyme (Sim et al., 2000).

Ovocleidin-17 was the first matrix protein purified to homogeneity. It is synthesized in the tubular gland cells of the uterus and secreted into the uterine fluid in relative abundance during the calcification growth phase. It is present throughout the entire calcified part of the shell (Sim et al., 2000). Ovocleidin 116, this protein is secreted in the uterine fluid during the active calcification phase and is abundant in the palisade layer of the eggshell (Mine, 2008). Ovocalyxin-32 is secreted by the surface epithelial cells of the uterus in the uterine fluid during the terminal phase of calcification and consequently is mainly localized in the most external part of the shell (palisade layer, vertical crystal layer and cuticle) (Mine, 2008). Ovocalyxin-36 is localized to the eggshell membranes and is most abundant near the calcified shell (Sim et al., 2000).

Osteopontin is localized in the core of the non-mineralized shell membrane fibers, in mammillae, and in the outermost part of palisade layer of the shell (Pines et al., 1996). Ovalbumin is the first egg white protein that was also observed in the eggshell. Lysozyme and ovotransforrin, two other major egg white proteins, were also identified in the eggshell. They were found to be present mainly in the basal parts of the shell (eggshell membrane, mammillae) (Gautron and Nys, 2007).

2.2 Application of eggshell

Eggshells can be utilized for various purposes that minimize their effect on environmental pollution. Eggshells present healthy, balanced calcium due to its trace

amounts of other minerals and is probably the best natural source of calcium. The utilization of eggshell in a form of powder is mostly used. The chicken eggshell and its membranes are an inexpensive and abundant waste material which exhibit interesting characteristics for many potential applications such as medical and cosmetic applications. Due to the high nutrient content of calcium, magnesium and phosphorous, the eggshell can be utilized as a fertilizer, soil conditioner or an additive for animal feed (Yoo et al., 2009; Glatz et al., 2011). Moreover, the associated eggshell membranes have a high content of bioactive components, as well as properties of moisture retention and biodegradability which have potential use for clinical, cosmetics, nutraceutical and nanotechnology applications (Yoo et al., 2009; King, 2011). Furthermore, the eggshell powder after calcination have been also used for biosorption of heavy metal (Cr, Cd or Cu) (Chojnacka, 2005; Jai et al., 2007) and dyes and as a template to synthesize metal nanoparticles (Cordeiro and Hincke, 2011). The combination of nanosized calcium phosphate ($Ca(PO_4)_2$) biomaterials synthesized from eggshell and eggshell membrane show promise to develop drug delivery system and nanowires for electronic devices (Cordeiro and Hincke, 2011). For polymeric materials, eggshell powder was used as a reinforcing filler in, for example, LDPE (Shuhadah and Supri, 2009), HDPE (Pakdeechote, 2010), PP (Dangtungee and Shawaphun, 2008), epoxy (Ji, Zhu, Qi and Zeng, 2009) and SBR (Saeb, Dakhel, Khonakdar, Heinrich and Wagenknecht, 2012).

2.3 Preparation of eggshell powder for polymer composites

A method of preparing eggshell powder comprises the step of reducing the size of raw eggshells to a particle size sufficient for the intended use (Suzuki et al.,

2012). Ball milling is a common comminuting method of producing fine powder in many industrial fields. The tumbling with centrifugal and planetary action has been used recently in the preparation of fine powder from a variety of materials such as mineral, ores, alloys, chemicals, glass, ceramics and plant materials. The planetary five balls with 20 mm-diameter mill can reduce particles to fine powder though the imposition of impact and friction force (Tsai et al., 2008). Therefore, eggshell powder was obtained. In addition, Tsai et al (2008) reported that when the grinding time increases from 10 to 60 min, the pore properties of ESP sample also increase as a result of the development of fine powder. It indicated that a more energy is applied at a longer time; the fragmentation continues to occur according to the crack evolution and size reduction.

Moreover, the method for preparation eggshell particles was prepared in another way. Hassan et al. (2013) reported that the synthesize bio-$CaCO_3$ nanoparticles derived from eggshells using the top-down approach of mechanical attrition and ultrasonic irradiation. TEM studies clearly showed that the particles have an irregular platelet shape of 10 nm. BET surface area measurements showed that synthesized bio-$CaCO_3$ nanoparticles have 179.4% higher surface area than the starting eggshell powder. The results clearly showed that the mechanical attrition followed by ultrasonic irradiation can be successfully used in the synthesis of high surface area bio- $CaCO_3$ nanoparticles.

Mosaddegh, Hassankhani, Pourahmadi and Ghazanfari (2013) studied the nano-$CaCO_3$ based on chicken eggshell waste by using a convenient ball mill–assisted preparation with different ball milling time. They found that the eggshell particle size decreased with increasing milling time from 30 min to 4 hr. The BET surface area

analysis showed a higher surface area of 4.0351 m^2 g^{-1} with the average particle size of 3 μm for eggshell with ball milling time of 4 hr, indicating that the higher the ball milling time can create the fine particles of ESP.

Another method is to use a meat processing machine to grind eggshells into a powder, and then mix the powder with water to separate the membrane. The shell sinks and the membrane stays suspended in the water. The eggshell without membrane was obtained (Glatz et al., 2011).

2.4 Thermal decomposition of eggshell and eggshell powder

Eggshell decomposed in three different thermal events. The first event around 51°C is endothermic and is attributed to the removal of physically adsorbed water on the eggshell. The second event about 324°C is exothermic, and related to decomposition of organic matter (Freire and Holanda, 2006). The third event around 765.3°C is endothermic, and is caused by decomposition of calcium carbonate as shown in equation (2.1) (Freire and Holanda, 2006).

$$CaCO_3\,(s) \xrightarrow{\triangle} CaO\,(s) + CO_2\,(g) \qquad (2.1)$$

Dasgupta et al. (2004) reported that the weight loss of eggshell below 250°C, which is due to evaporation of the physical absorbed water. At the temperature below 450°C all the organics decomposed. Within the temperatures range of 750°C and 900°C, almost all the calcium carbonate decomposes into calcium oxide (CaO) with a DTGA peak at 850°C.

Murakami et al. (2007) reported that the thermal decomposition process of eggshell powder occurred at the temperature of 771.5^{o}C with mass loss of 42.5%, which corresponds to carbon dioxide release.

2.4.1 Calcination of eggshell

The calcined eggshell was prepared in several temperatures. For example, washed and uncrushed raw eggshell was calcined in an air atmosphere at various temperatures up to 1000^{o}C, for 1 hr at each temperature (Lee and Oh, 2003).

Krishna et al. (2007) reported that chicken's eggshell was heated in a box furnace at 900^{o}C for 2 hr to decompose organic matter and convert the calcium carbonate to calcium oxide. After atmospheric atmosphere, calcium oxide was turned into calcium hydroxide. The product was finely ground in an agate pestle and mortar.

Another method for calcined eggshell preparation was reported. The eggshells were rinsed several times with deionized water to remove impurity and interference materials such as organics and salts. Then, the sample was dried at 100^{o}C for 24 h in the dry oven. Calcinations were performed in the furnace at 800^{o}C for 2 h after crushing the dried sample. Finally, samples having 40-100 mesh separated with a vibration selector were used (Jai et al., 2007).

2.5 Precipitated calcium carbonate (PCC)

2.5.1 Preparation of PCC

Currently, precipitated calcium carbonate (PCC) can be produced by three different processes, i.e. a lime soda process, a calcium chloride process and a carbonation process (Teir, Eloneva and Zevanhoven, 2005). In the lime soda process, Calcium hydroxide is reacted with sodium carbonate, from which the calcium

carbonate is precipitated. In the calcium chloride process, calcium hydroxide is reacted with ammonium chloride, forming ammonia gas and a calcium chloride solution. After purification, this solution is further reacted with sodium carbonate to form a calcium carbonate precipitate and a sodium chloride solution. In the carbonation process, at high temperature, calcium carbonate decomposed into calcium oxide. The presence of moisture, calcium oxide absorbs water and changes to calcium hydroxide. After that, calcium hydroxide is reacted with carbon dioxide to form calcium carbonate. However, a disadvantage of lime soda and carbonation processes is difficult to obtain the calcium carbonate. Therefore, the most widely used is calcium chloride process. This was reported by Kobeleva and Poilov (2007). They reported that PCC can produce by the reaction of calcium chloride and sodium carbonate solution as shown in equation (2.2).

$$CaCl_2\,(l) + Na_2CO_3\,(l) \longrightarrow CaCO_3\,(s) + 2NaCl\,(l) \qquad (2.2)$$

Popescu, Isopescu, Matei, Fagarasan and Plesu (2013) studied the preparation of precipitated calcium carbonate in the presence of ammonia and alkylamines. Precipitated calcium carbonate was obtained by CO_2 bubbling in $CaCl_2$ solution. Ammonia and alkylamines were used to enhance CO_2 absorption and control the polymorphic phases. Vaterite and calcite mixtures were obtained.

2.5.2 Factor affecting the size, shape and surface of PCC particle

PCC can usually produced in three crystal forms; calcite, vaterite and aragonite. In addition, crystalline shapes, particle sizes and surfaces of PCC can be controlled by condition of precipitation such as temperature and pH (Popescu, Isopescu, Matei, Fagarasan and Plesu, 2013).

Kobeleva and Poilov (2007) reported that the PCC particle size was decreased with increasing concentration and flow rate of Na_2CO_3 reactant into $CaCl_2$ solution. Moreover, their particle size was decreased as increasing the agitation from 3.3 to 11.0 rps. A change in the temperature of precipitation was effected in shape of calcium carbonate. A change in the temperature of precipitation, PCC particles was in calcite, vaterite and aragonite at the temperature about 90, 60 and 20^{o}C, respectively.

Xu, Zhao, Lai and Hao (2011) studied the effect of polyethylene glycon (PEG) with difference molecular weight and concentration on the phase and morphology of $CaCO_3$. The PCC was obtained from the reaction between the $CaCl_2$ and Na_2CO_3 solution. The concentration of $CaCl_2$ and $NaCO_3$ was 0.05 mol L^{-1}. PEG was used as an additive at the concentration of 0.002, 0.005 and 0.010 mol L^{-1}, respectively. At high concentration of PEG, They found that aragonite and calcite were obtained, whereas calcite could be obtained by the use of PEG as the additive at concentration of 0.002 mol L^{-1}.

Sabriye, Pişkin, Özgül and Özdemir (2012) studied the effect of the process condition on crystal structure of PCC from fly ash by adding sodium carbonate into fly ash leachate with distilled water. It was found that when sodium carbonate is added as the solid form, calcite crystal was form in rhombohedral structure. On the other hand, calcite crystal structure was in scalenohedral form when the sodium carbonate solution was added. Furthermore, they found that the reaction time, temperature, sodium carbonate concentration have no significance on the PCC polymorph.

2.5.3 Thermal decomposition of PCC

Popescu, Isopescu, Matei, Fagarasan and Plesu (2013) studied the thermal decomposition of calcium carbonate polymorphs precipitated. Vaterite and calcite mixtures were studied. From TGA and DTGA curves, they found that the PCC sample showed a small weight loss about 2%, in the temperature range from 25 to 600^{o}C, corresponding to the decomposition of adsorbed carbonate species, with a main endothermic peak at 553^{o}C. The exothermic peak from 459^{o}C was assigned to the vaterite–calcite phase transition. The main endothermic decomposition process took place in the temperature from 600 to 790^{o}C delaying the growth rate of more stable polymorphs. A stable polymorphic phase of calcite, the decomposition temperature of calcite was maximum rate at 750^{o}C with 43.6% weight loss, corresponding to the transformation temperature range of the $CaCO_3$ into CaO.

2.6 Calcium carbonate ($CaCO_3$) filled HDPE

High density polyethylene (HDPE), semi-crystalline polymer, is widely used as an engineering polymer with high-tonnage production due to its distinctive mechanical and physical properties. Because of its low toughness, weather resistance and environmental stress cracking resistance as compared to engineering polymers, its application in many areas has been limited. To improve these advantages, HDPE has been reinforced with reinforcing fillers (Elleithy et al., 2010). In fact, most of the studies of modification of semi-crystalline polymers with rigid particulate fillers reported a significant decreased of toughness compared to neat polymer, i.e., the observation on calcite/HDPE composite and iron powder/HDPE composites. On the contrary, several researches have revealed an increased in toughness with rigid fillers

in some systems such as HDPE/calcium carbonate composites and filled polyethylene with calcium carbonate. In this research, the effect of content, particle size and compatibilization of calcium carbonate filled HDPE was reviewed.

2.6.1 Effect of $CaCO_3$ content on mechanical properties of $CaCO_3$/HDPE composite

Suwanprateeb (2000) found that tensile yield stress decreases with increasing filler volume fraction whereas the compressive yield stress increased as the amount of filler was increased. In general, tensile properties of materials are largely determined by flaws and submicroscopic cracks. These flaws act as weak points in the materials. In contrast, the cracks do not play such an important role in compression test because the applied stresses tend to close them rather than open them. Thus, compression properties tend to be characteristic of the pure polymer, while tension tests are more characteristic of the flaws in the material. Calcium carbonate–polyethylene composites are composed of rigid fillers dispersed in a ductile polymer matrix. These rigid fillers can act as defects in the composites if the filler is weak or the interface adhesion between fillers and matrix is not strong.

Tanniru and Misra (2005) studied the influence of the addition of 5-20 % $CaCO_3$ into HDPE on tensile modulus and yield stress of composites. They concluded that the tensile modulus of HDPE composite increased with increasing $CaCO_3$ content. This was because the reinforcement effect of $CaCO_3$ as well as an increase in percentage of crystallinity increased the modulus of composites when increasing $CaCO_3$ content. On the contrary, they also believed that the yield stress of HDPE was affected by the increasing of $CaCO_3$ content. This was attributed to the nucleating effect of $CaCO_3$. The nucleating effect of $CaCO_3$ decreased the spherulite

size (a negative effect on yield stress) and retarded the positive effect of increase in degree of crystallinity on the yield stress.

Teixeira et al. (2005) explained that the addition of $CaCO_3$ provoked a decrease on the impact strength, stress at break and yield stress properties of HDPE composite. On the other hand, Young's modulus of the composite increased with increasing $CaCO_3$ content.

Chafide, Ali, Mohsin, Elleity and Al-Zahrani (2012) studied the mechanical properties of $CaCO_3$/HDPE nanocomposites. The $CaCO_3$/HDPE nanocomposites were prepared from masterbatch by melt blending in twin screw extruder at 0, 10 and 20 wt.% $CaCO_3$ masterbatch. The DSC analysis showed a decrease in crystallinity of $CaCO_3$/HDPE nanocomposites with the increase of $CaCO_3$ loading. This was due to the presence of nanofiller which could restrict the movement of the polymer chain segments and reduced the free volume/spaces available to be occupied by the macromolecules, thus, hindered the crystal growth. However, there was an increase in crystallization temperature about 1–2 °C with the addition of $CaCO_3$. It was suggested that the $CaCO_3$ nanoparticles acted as nucleating agent. In melt rheology study, the complex viscosities of $CaCO_3$/HDPE nanocomposites were higher than the HDPE matrix and increased with the increasing of $CaCO_3$ masterbatch loading. The DMA results showed that the storage modulus increased with the increasing of nano-$CaCO_3$ contents. The improvement was more than 40 %, as compared to that of neat HDPE. Additionally, the tensile test results showed that with the addition of $CaCO_3$ masterbatch, modulus elasticity of nanocomposites sample increased while yield stress decreased.

2.6.2 Effect of particle size of $CaCO_3$ on mechanical properties of $CaCO_3$/HDPE composite

Bartczak et al. (1999) studied notched Izod impact energy of the $CaCO_3$/HDPE composite. HDPE was modified with three different sizes of calcium carbonate particles at 25 vol.% $CaCO_3$. They found that the modification of HDPE with calcium carbonate led to increase the impact energy of the HDPE in all three sizes of $CaCO_3$. This increase was considerably depended on the size of $CaCO_3$ particles. The impact energy of composites increased by only 20% for $CaCO_3$ diameter of 3.50 μm, by more than 700% for $CaCO_3$ diameter of 0.70 μm compared with neat HDPE. The increase in toughness of the $CaCO_3$/HDPE composite considerably depended on the particle size of calcium carbonate. This was because the mean interparticle ligament thickness of the matrix dropped to values below 0.6 μm.

Shi, Wang and Cai (2013) studied preparation and characterization of the $CaCO_3$/HDPE composites with various shapes and size of $CaCO_3$. $CaCO_3$ with various shapes and sizes was prepared using $CaCl_2$ and Na_2CO_3 aqueous solutions. HDPE/ 4 wt.% $CaCO_3$ composites were prepared using a Haake Rotational Rheometer. The addition of $CaCO_3$ into HDPE, the tensile yield strength of the composites was higher than that of HDPE. Sphere-like $CaCO_3$ is the best form in improving the thermal stability and cubic $CaCO_3$ can cause negative effect to the toughness. The impact strength of the composites is significantly increased with decreasing $CaCO_3$ particle size. SEM examination of the fractured surfaces of the composites shows that $CaCO_3$ reacted in cavitations and lance functions which increase the impact strength of the composites.

2.6.3 Effect of compatibilization on mechanical properties of $CaCO_3$/HDPE composite

Sahnoune, Cuesta and Crespy (1999) studied the modification of the tensile yield strength of $CaCO_3$ filled HDPE by the incorporation of (Styrene-Ethylene/Butylene-Styrene) triblock copolymers (SEBS). Two types of elastomers were used, (Styrene-Ethylene/Butylene-Styrene) triblock copolymers (SEBS) and (Styrene-Ethylene/Butylene-Styrene) triblock copolymers grafted with maleic anhydride (MA-g-SEBS). It was found that the grafted and ungrafted SEBS had different effects on the tensile strength and impact strength of HDPE/$CaCO_3$ composite. MA-g-SEBS encapsulating mineral particles, entailed an increase in impact strength. The ungrafted SEBS dispersed in the matrix had no positive effect. These results showed that the location of the elastomer has a pronounced influence on the tensile and impact properties of filled polymers. The formation of an elastomer interphase with high molecular mobility may act as a bumper interlayer around filler particles, which absorbs the impact energy and prevents the initiation of cracks. Moreover the adhesion created by the elastomer interphase may also prevent the propagation of cracks at the interface.

Li et al. (2000) studied HDPE/sulfonated EPDM-treated $CaCO_3$ blends. Sulfonated ethylene-propylene-diene monomer terpolymer (H-SEPDM) was used to treated $CaCO_3$ particles. The particles were encapsulated by H-SEPDM through the reaction of sulfonic acid group in H-SEPDM. The treated $CaCO_3$ was blended with HDPE, a brittle ductile transition occurs at 30 wt.% $CaCO_3$. The impact strength of the blend raises sharply at 25-30 wt.% $CaCO_3$, more than 70 J/m and four

times higher than that of 30 wt.% $CaCO_3$, without much loss of its yield strength and modulus.

Lazzeri, Zebarjad, Pracella, Cavalier and Rosa (2004) studied the influence of stearic acid treatment of the particles on mechanical properties of precipitated calcium carbonate (PCC)/HDPE composites. The HDPE composite was prepared at 10 vol.% PCC. The addition of stearic acid was slightly decreased in Young's modulus and yield stress of the composites, in comparison with uncoated PCC/HDPE composites, while impact strength progressively increased.

Xie, Liu, Ou and Yang (2005) studied the microstructure, impact strength, and rheological properties of blends consisting of high-density polyethylene (HDPE) and maleated poly (ethylene-octene) (POEg) and/or calcium carbonate ($CaCO_3$). They found that the improvement of impact strength of HDPE/POEg was limited due to the miscibility between them. The introduction of $CaCO_3$ had a negative impact on the toughness of the matrix because of the poor interfacial adhesion. In ternary blends of HDPE/POEg/$CaCO_3$, an elastomer layer was formed around $CaCO_3$ particles due to the strong interaction between POEg and $CaCO_3$, which improves the HDPE-$CaCO_3$ interfacial strength and the toughness of the blends. A significant enhancement of dynamic viscosity, storage modulus, and the low-shear viscosity were observed as the results of the high miscibility of HDPE with POEg and strong interaction between POEg and $CaCO_3$.

Xu, Zou, Shi, Feng and Gong (2005) investigated the effect of the unsaturated hyperbranched polyester coated $CaCO_3$ particles (UH20-coated $CaCO_3$) on mechanical properties of $CaCO_3$/HDPE composites. The incorporation of UH20-coated $CaCO_3$ into HDPE decreased the mechanical properties such as tensile

strength, elongation at break and impact strength with increasing UH20-coated $CaCO_3$ content.

Phueakbuakhao, Ouajai and Kreua-Ongarjnukool (2008) presented the mechanical properties and morphology of recycled high density polyethylene (r-HDPE) filled with 10 wt.% $CaCO_3$. The influence of treatment of $CaCO_3$ with various coupling agents, including stearic acid (SA), aminopropyltriethoxy silane (AMPTES), glycidoxypropyltrimethoxy silane (GPTMS) and maleic anhydride grafted HDPE (MA-g-HDPE), was investigated. This study clearly demonstrated that the addition of coupling agent to $CaCO_3$ modifies the mechanical properties of the r-HDPE/$CaCO_3$ composites. It was also found that each coupling agent gives rise to increases in a particular mechanical properties due to its characteristics. In the case of AMPTES, the best mechanical properties was observed at 2 wt.% whereas GPTMS and MA-g-HDPE showed the best performance at 3 wt.% and 4 wt.%, respectively. SEM micrographs of the fractured surfaces of the composites revealed a strong interfacial interaction between r-HDPE and $CaCO_3$, resulting in improvement of the fracture toughness.

Mnif, Massardier, Kallel and Elleuch (2010) studied phase structure of composite polypropylene (PP)/ethylene–propylene–rubber (EPR)/coated nano-$CaCO_3$ composites. They found that the morphology was the core–shell structure in which EPR acts as the shell part encapsulating coated nano-$CaCO_3$. In this case, EPR-g-MAH copolymer did not improved the interface between (PP/EPR) and nanoparticles but PEP propylene ethylene copolymer should be preferentially localized at the interface of PP and (EPR/nano-$CaCO_3$) phases generating an improved adherence, which would ensure a better cohesion of the whole material. According to the nature

of the compatibilizers and surface treatment, it is believed that the synergistic effect of both the EPR elastomer and $CaCO_3$ nanoparticles should account for the balanced performance of the ternary composites.

2.7 ESP filled polymers

The composites are materials consisting of two or more identifiable constituents of different natures. Special consideration has been give to those composites which consist of synthetic fibers or mineral particle with a high modulus with reinforcement embedded in comparatively lower modulus matrix. However, due to the petroleum-derived products or the environmental hazard, a growing effort has emerged in recent years on the research, development and application of biocomposites. A biocomposite contains at least one constituent that is derived from renewable resources such avian eggshell (Toro et al., 2007). Polyolefin composites normally used inorganic fillers such as calcium carbonate or talc (Elleithy et al., 2010). The chicken eggshell is an aviculture byproduct that has been listed worldwide as one of waste environmental problem. There have been several attempts to use eggshell powder for several polymers such as PP and PE. The literature on this topic was reviewed as the following.

2.7.1 ESP filled polypropylene (PP)

Dangtungee and Shawaphun (2008) studied the mechanical properties of polypropylene filled with eggshell powder. The mechanical properties of the composites were studied by tensile tester, impact tester and scanning electron microscope (SEM). PP compounded with egg shell particles in various ESP filler loadings, ranging from 5 to 30 wt%. They found that the tensile stress for both PP

compounds decreased with increasing amounts of ESP filler. The young's modulus result was found to increase with increasing amount of ESP filler. An increase in ESP filler, over all the impact strength was increased.

Toro et al. (2007) studied the Young's modulus of $CaCO_3$/PP comparing to that of ESP/PP composite. They found that ESP with particle size of 8.4 μm led to a higher in Young's modulus of composites than $CaCO_3$ with particle sizes of 17.1, 2.0 and 0.7 μm. This was due to PP/ESP composites having better phase continuity than $CaCO_3$/PP composites.

2.7.2 ESP filled low density polyethylene (LDPE)

Shuhadah and Supri. (2009) studied the effect of chemical modification on the mechanical properties of ESP/LDPE composites with and without modifications (NaOH-isophalic acid). It indicated that tensile strength, elongation at break of the composite decreased with increasing ESP content. The addition of isopthalic acid, the interfacial adhesion between LDPE and ESP was improved leading to enhance the tensile strength and elongation at break, as compared to the unmodified LDPE/ESP composites.

2.7.3 ESP filled polyester

Hassan, Aigbodion and Patrick (2012) studied the effect of the eggshell particles on mechanical properties of ESP/polyester composites. The ESP particles were used as reinforcement in polyester matrix at 10-50 wt.% ESP. They showed that the hardness values, tensile and flexural strength of the ESP/polyester composite increased with increasing ESP content.

2.7.4 ESP filled epoxy

Ji, Zhu, Qi and Zeng (2009) studied the incorporation of ESP into epoxy resin. The particle size of ESP (D_{50}) was 1.23 μm and ESP content 0-10 mass%. They found that when the epoxy resin composite contains 5.0 mass% ESP, the impact strength of the composite reaches 16.7 kJ/m^2, compared with 9.7 kJ/m^2 of a neat epoxy resin. The impact strength still remains 12.3 kJ/m^2 when the composite contains 10 mass% ESP, indicating that ESP is an excellent filler to improve toughness of the epoxy resin. This was due to the strong interaction between the reactive amine group on the surface of ESP and carbonyl group of epoxy resin.

2.7.5 ESP filled elastomers

Saeb, Dakhel, Khonakdar, Heinrich and Wagenknecht (2012) studied the effect of particle size and dispersion of nano ESP and nano $CaCO_3$ on thermomechanical properties and curing characteristics of the ESP or $CaCO_3$ particles filled elastomers such as NBR, SBR and NR. The average particle size of ESP and $CaCO_3$ was 50 and 349 nm, respectively. The fillers content were 5, 10 and 15 phr. It was observed that the ultimate tensile properties of SBR and NR nanocomposites were improved to some extent when 5 phr of ESP nanofiller was added to the rubber compound compared to $CaCO_3$. In the case of NBR nanocompounds, the mechanical properties were seemingly comparable, irrespective of the type of nanofiller. This contradictive behavior could be attributed to the alteration of crosslink density due to particular filler–matrix interaction while using mineral and natural fillers. The results of the rheometric study revealed that using ESP rather than $CaCO_3$ slightly increases the scorch time of all types of prepared nanocomposites, whereas a significant drop in the optimum curing time was seen for NBR nanocomposites containing ESP biofiller.

Moreover, TGA curves showed similar thermal stability for SBR nanocomposites containing ESP and $CaCO_3$ fillers. Finer particle size of $CaCO_3$ and higher porosity of ESP at high and low loading levels were respectively the main reasons for improvement of ultimate properties.

Intharapat, Kongnoo and Kateungngan (2012) investigated the effect of three types of eggshell calcium carbonate (ECC), eggshell calcium carbonate treated with a temperature at 600^{o}C (ECC-600) and commercial $CaCO_3$ on mechanical properties of epoxidized natural rubber (ENR) composites. The average particle size of $CaCO_3$, ECC, and ECC-600 was 15, 26 and 29 μm with BET surface area of 2.112, 2.532 and 1.902 m^2/g, respectively. They found that tensile strength, tear strength, hardness, tension set of ECC filled ENR were greater than that of $CaCO_3$ and ECC-600. This was due to better filler-rubber interaction through high surface area and the organic part of ECC particles. It was expected that the larger surface area of ECC and a polar amine ($-NH_2$) groups in protein existed in particles hence greater the interaction and stronger the interfacial adhesion between the ECC and rubber matrix.

2.8 Mineral filled poly (butylene succinate)

In recent years, eco-friendly biodegradable polymers and plastics have gained increasing attention because of growing recognition worldwide of the need to reduce global environmental pollution. These biodegradable materials can be completely degraded into natural ecosystems such as active sludge, natural soil, lake and marine. Accordingly, the biodegradability of biodegrade polymers corresponds to the ability to be chemically transformed by the action of biological enzymes or microorganisms.

Poly (butylene succinate) (PBS) is one of the commercially used biodegradable polymers with a range of interesting properties including good mechanical properties, melt processing, biodegradability and compostability. PBS is produced by the condensation reaction of the glycols 1,4-butanediol and aliphatic dicarboxylic acid, which is succinic acid (Y. F. Shih et al., 2008). In recent year, PBS can be compound with several fillers to reduction of cost or other proposes. The literature on this topic was reviewed as the following.

2.8.1 Calcium carbonate derived oyster shell filled PBS

Funabashi, Ninomiya, Flores and Kunioka (2010) investigated the mechanical properties of oyster shell powder/PBS composites. The biobased $CaCO_3$ derived from oyster shell was prepared at 10-40 wt.%. They reported that the both values of strength and strain at break decreased with increasing filler content. Therefore, mechanical properties of PBS polymers could not be improved by the addition of oyster powders.

2.8.2 Silica (SiO_2) filled PBS

Bian et al. (2010) studied the influence of silica nanoparticles on the nonisothermal crystallization behavior, crystal structure, and mechanical properties of the SiO_2/PBS nanocomposites. The silica content was 0, 1, 3, 6 and 10 wt.%. It was revealed that the crystallization peak temperature of the SiO_2/PBS nanocomposites was higher than that of neat PBS at various cooling rates. The half-time of crystallization decreased with increasing silica loading; this indicated the nucleating role of silica nanoparticles. A study of the nucleation activity revealed that the silica nanoparticles had a good nucleation effect on PBS. The crystallization activation

energy increased with increasing silica content. In addition, the modulus and yield strength were enhanced with the addition of silica nanoparticles into the PBS matrix.

Vassiliou, Bikiaris, Mabrouk and Kontopoulou (2011) studied the effect of fumed silica (SiO_2) on properties of SiO_2/PBS composites. The PBS composites was prepared at 0.5, 1.0, 2.5 and 5.0 wt.% SiO_2. The addition of SiO_2 into PBS matrix, the SiO_2 acted as nucleating agents, increasing the crystallization rate of PBS. On the other hand, the degree of crystallinity was slightly reduced. In addition, tensile strength and Young's modulus were significantly increased with increasing SiO_2 content.

2.8.3 Organo-montmorillonite (OMMT) filled PBS

Phua et al. (2011) investigated the effect of OMMT content on mechanical properties of the OMMT/PBS nanocomposites. It was found that the optimum tensile strength and elongation at break were observed at 2% OMMT/PBS composite. With increasing OMMT content, at 4-10 wt.% OMMT, the modulus of the composite were increased.

2.8.4 Hydroxyapatite (HA) filled PBS

Guo, Zhang and Zhang (2013) investigated the mechanical and crystallization behavior of HA/PBS composites. With increasing HA content, the crystallization of HA/PBS composites decreased and crystallization onset shifted to a lower temperature. The diameter of spherulites increased at first and decreased with a further HA content. At the same time, the crystallization rate became slow when the HA content was no more than 15 wt.% and increased when HA content reached 20 wt.%. In addition, tensile modulus, flexural strength and flexural modulus were increased with increasing HA content.

CHAPTER III

EXPERIMENTAL

3.1 Materials

Chicken eggshell waste of Bovans Goldline and ISA Brown hybrid breed was obtained from SUT farm, Suranaree University of Technology. A commercial injection grade of high density polyethylene (HDPE, EL-Lene™ H5814J) was purchased from SCG Chemicals Co., Ltd. Poly (butylene succinate) (PBS, GS Pla AZ91TN) was purchased from Mitsubishi Chemical Performance Polymer, Inc. High density polyethylene grafted with maleic anhydride (HDPE-g-MAH, Fusabond® MB100D, DuPont™) was kindly supplied by Chemical Innovation Co., Ltd. Ethylene propylene rubber grafted with maleic anhydride (EPR-g-MAH, Exxerlor™ VA1803, ExxonMobil) was purchased from Global Connections Co., Ltd. Some physical properties of HDPE, PBS, HDPE-g-MAH, and EPR-g-MAH were summarized in Table 3.1. Hydrochloric acid (HCl 37%), sodium carbonate (Na_2CO_3) and sodium hydroxide (NaOH) were obtained from Carlo Erba Reagent. All of these reagents were an analytical grade.

Table 3.1 Some physical properties of HDPE, PBS, HDPE-g-MAH, and EPR-g-MAH.

Properties	Unit	HDPE	PBS	HDPE-g-MAH	EPR-g-MAH
Density	g/cm^3	0.958	1.260	0.960	0.863
Melt flow index (@ 190°C, 2.16 kg)	g/10 min	11.4*	35.4*	2.0**	3.3**
Melting point	°C	131	110	136	-
Maleic anhydride content	wt.%	-	-	0.90	1.14

* MFI obtained from the laboratory

** MFI obtained from the datasheet

3.2 Preparation of membrane-peeled eggshell powder (ESP)

First of all, chicken eggshell waste was washed with tapped water to remove residues and eggshell membranes were then peel off from the washed eggshell. After that, the eggshell was cleaned with tapped water again and dried in an open air for 24 hr. This eggshell was named as "membrane-peeled eggshell". To prepare ESP via a ball milling, thousand grams of the membrane-peeled eggshell were ground for 24 hr within a 5,830 ml cylindrical porcelain pot under a rotational speed of 40 rpm. The grinding media for the milling process were 30 balls of 25 mm-diameter, 40 balls of 20 mm-diameter, and 60 balls of 15 mm-diameter.

In order to study effect of membrane-peeled eggshell particle size on physical properties of HDPE composite, ground membrane-peeled eggshell powder (ESP) was prepared into three particle ranges, 45-63 μm using screen sieves of 325 and 230 mesh no., 32-45 μm using screen sieves of 450 and 325 mesh no., and smaller than 25

μm using screen sieve of 500 mesh no. To obtained ESP having particle size smaller than 25 μm; an air jet sieving machine (Retsch, AS 200Jet) was used for sieving process. Three particle size ranges of ESP, 45-63 μm, 32-45 μm, and smaller than 25 μm were named ESP1, ESP2 and ESP3 respectively.

3.3 Preparation of precipitated eggshell powder (PESP)

For preparing precipitated eggshell powder (PESP), 100 g ESP was dissolved in 1000 ml of 1 M hydrochloric acid solution. After ESP was completely dissolved, pH of the solution was adjusted to be neutral using 0.5 M sodium hydroxide solution. Then, the solution was then filtered using the Buchner filter equipment. After that, 1 M sodium carbonate solution was slowly added with a dropping rate of 2 ml/min into the filtered solution while the solution was continuously being stirred at a speed of 800 rpm using a 3.5 cm of Teflon-coated magnetic bar. After the sodium carbonate solution was completely dropped. The solution was still continuously stirred at the same speed to allow eggshell $CaCO_3$ precipitation to be completed. After that, the precipitated eggshell powder (PESP) was filtered using the Buchner filter equipment and subsequently rinsed several times with deionized water to remove residual chemicals. Subsequently, PESP was dried in an oven at 70^{o}C for 24 hr. It was then kept in a desiccator for further characterization, and HDPE and PBS composite preparation.

3.4 Preparation of ESP/HDPE composites

HDPE filled with ESP3 were prepared in an internal mixer (Hakke, Rheomix 3000p). ESP3 was dried in an oven overnight at 70^{o}C before mixed with HDPE at

ESP3 contents of 10, 20, 30 and 40 wt.%. The mixing process was operated at 190^{o}C under a rotor speed of 70 rpm and a mixing time of 15 min. At first, HDPE was melted for 5 min and then ESP3 was added into a mixing chamber. The ESP3/HDPE composites were ground using a grinding machine before further molded into test specimens using an injection machine (Chuan Lih Fa, CLF 80T).

For studying the effect of ESP particle size on the flow, mechanical and thermal properties of HDPE composites, the composites were prepared with three different sizes of ESP, ESP1, ESP2 and ESP3, at 20 wt.%. The mixing process was operated at the same process of ESP3 filled HDPE.

In order to study effect of compatibilization on physical properties of HDPE composite, HDPE-g-MAH and EPR-g-MAH were used as a compatibilizer. HDPE filled with 20 wt.% ESP2 were prepared at 2, 5, 8 and 10 wt.% HDPE-g-MAH or EPR-g-MAH (based on HDPE). To prepare compatibilized ESP2/HDPE composites, a mixture of HDPE and a compatibilizer at predetermined composition was first melted for 5 min in an internal mixer (Hakke Rheomix 3000p) and then ESP2 was added into a mixing chamber. The compatibilized ESP2/HDPE composites from the mixing process were ground by a grinding machine before further molded into test specimens using an injection machine (Chuan Lih Fa, CLF 80T).

To prepare test specimens, the injection process was carried out at a melting temperature of 200^{o}C, a screw speed of 130 rpm, an injection speed of 19.5 mm/sec, a holding pressure of 840 kg/cm^{2} and a mold temperature of 30^{o}C.

3.5 Preparation of PESP/HDPE composite

HDPE filled with various contents of PESP were prepared in an internal mixer (Hakke, Rheomix 3000p). The contents of PESP were 5, 10 and 20 wt%. PESP was dried in an oven overnight at 70^{o}C before mixed with HDPE. The mixing process was operated at 190^{o}C under a rotor speed of 70 rpm and mixing time of 15 min. The molding process was operated at the same procedure of ESP filled ESP/HDPE preparation.

3.6 Preparation of ESP/PBS composite and PESP/PBS composite

PBS filled with ESP3 was prepared in an internal mixer (Hakke, Rheomix 3000p). The various contents of ESP3 were 10, 20, 30 and 40 wt%. The ESP3 was dried overnight in an oven at 70^{o}C before mixed with PBS. To prepare ESP3/PBS composite, PBS was first melted for 2 min in an internal mixer and ESP3 was then added into a mixing chamber. The mixing process was operated at 120^{o}C under a rotor speed of 60 rpm and a mixing time of 3 min.

For prepared PBS filled with PESP, it was also prepared in an internal mixer at PESP content of 5, 10 and 20 wt%. The mixing process was operated at the same process of ESP3 filled ESP3/PBS preparation.

To prepared test specimens, PBS composites were ground and further molded by an injection machine (Chuan Lih Fa, CLF 80T). The injection molding was carried out with a melting temperature of 190^{o}C, a screw speed of 130 rpm, an injection speed of 47 mm/sec, a holding pressure of 617 kg/cm^{2} and a mold temperature of 30^{o}C.

3.7 Characterization of ESP and PESP

3.7.1 Particle size and size distribution

The particle size and size distribution of ESP1, ESP2, ESP3 and PESP were determined via the particle size analyzer (Malvern, Mastersizer S) with a range lens of 300RF and a beam length of 2.40 mm. Deionized water was used as a medium and 0.1%w/v sodium hexametaphosphate was used as a surfactant for the characterization.

3.7.2 Specific surface area

The specific surface area (BET) and pore size of ESP1, ESP2, ESP3, and PESP were determined by the N_2 adsorption–desorption analyzer (Micromeritics, ASAP 2010). Before the measurement, each sample was degassed at 110^{o}C for 24 hr in vacuum.

3.7.3 Crystal form

The X-ray diffractometer (XRD, Bruker, D5005) was used to determine crystal polymorph of ESP1, ESP2, ESP3 and PESP. The measurement was carried out using CuKα radiation (λ = 0.15406 nm) with an accelerating voltage of 40 kV and a current of 40 mA, 2θ between 5 and 70^{o}C, a scan step of 0.02^{o}, and a scan speed of 0.5 s/step.

3.7.4 Chemical compositions

X-ray fluorescence spectrometer (XRF, Philips, PW2400) was used to quantitatively determine composition of calcium and other elements of ESP1, ESP2, ESP3 and PESP. The investigation was performed using K_α radiation under an accelerating voltage of 80-100 kV and a current of 24-30 mA.

3.7.5 Decomposition temperature

Thermal decomposition temperature vs weight loss of ESP1, ESP2, ESP3, and PESP was monitored by the thermogravimetric analyzer (TGA, Mettler Toledo, TGA/DSC1). The temperature range for the analysis was 30 to 1,000^{o}C with a heating rate of 20°C/min under a nitrogen atmosphere.

3.7.6 Particle morphology

The particle morphology of ESP1, ESP3, ESP3 and PESP was investigated by the scanning electron microscope, (SEM, JEOL, JSM 6010LV), with an accelerating voltage of 14 kV. The sample was coated with gold for 10 min prior to investigation.

3.8 Characterization of HDPE and PBS composites

3.8.1 Flow property

Melt flow index (MFI) of neat HDPE, neat PBS, HDPE composites and PBS composites was tested according to ASTM D1238 using the melt flow indexer (Kayeness, D4004HV) at a temperature of 190^{o}C and a stand weight of 2.16 kg.

3.8.2 Mechanical properties

Tensile properties of neat HDPE, neat PBS, HDPE composites and PBS composites were determined in accordance with ASTM D638. The universal testing machine (Instron, model 5565) equipped with a load cell of 5 kN was employed in a uniaxial tension at a crosshead speed of 10 mm/min and a gauge length of 50 mm. At least five specimens were tested.

Flexural properties of neat HDPE, neat PBS, HDPE composites and PBS composites were tested according to ASTM D790 under the universal testing machine (Instron, model 5565) with a load cell of 5 kN at a crosshead speed of 14 mm/min and a fixed span length of 53 mm. At least five specimens were tested.

Unnotched Izod impact strength, following ASTM D256, of neat HDPE, neat PBS, HDPE composites and PBS composites was evaluated under the impact tester (Atlas, BPI) equipped with 5.4 J hammer. At least five specimens were tested.

3.8.3 Fracture surface morphology

Fracture surface morphology of neat HDPE, neat PBS, HDPE composites and PBS composites was investigated by the scanning electron microscope (SEM, JOLE, JSM 6010LV) operated at an accelerating voltage of 20 kV. The test specimens were fractured under liquid nitrogen and coated with gold for 10 min prior to investigation.

3.8.4 Decomposition temperature

Thermal decomposition of neat HDPE, neat PBS, HDPE composites and PBS composites was investigated by the thermogravimetric analyzer (TGA, Mettler Toledo, TGA/DSC1). The sample was heated from 30 to 1,000^{o}C with a heating rate of 20°C/min under a nitrogen atmosphere.

3.8.5 Melting temperature, crystallization temperature and degree of crystallinity

Melting temperature (T_m), crystallization temperature (T_c) and degree of crystallinity (X_c) of neat HDPE, neat PBS and their composites were determined using the differential scanning calorimetry (DSC, Perkin Elmer, Model UNIX DSC-

7). Each sample was heated from 30 to 180^{o}C, holded at 180^{o}C for 5 min and cooled to 30^{o}C, and then reheated to 180^{o}C under a nitrogen atmosphere. The rate of heating and cooling was 10^{o}C/min. Melting temperature, crystallization temperature and degree of crystallinity were obtained according to ASTM D3417. The degree of crystallinity was calculated by equation (3.1) shown below.

$$X_c(\%) = \left[\left(\frac{\Delta H_f}{\Delta H_{f*}}\right)(W_f)\right] \times 100 \qquad (3.1)$$

Where ΔH_f is the enthalpy of fusion of the sample.

ΔH_{f*} is the enthalpy of fusion of a 100% crystalline HDPE and PBS.

ΔH_{f*} HDPE= 292.6 J/g (Sahebian, Zebarjadand and Sajjad, 2009).

ΔH_{f*} PBS= 110.3 J/g (Phua, Chow and Ishak, 2011).

W_f is the weight fraction of polymer matrix.

CHAPTER IV

RESULTS AND DISCUSSION

4.1 Characterization of ESP and PESP

4.1.1 Particle size, size distribution and specific surface area of ESP and PESP

The particle size and size distribution as well as specific surface area of eggshell powder after sieving with screen sieves of 325-230 mesh no (ESP1), 450-325 mesh no (ESP2), 500 mesh no (ESP3) and precipitated eggshell powder (PESP) are shown in Table 4.1. The ESP1, ESP2 and ESP3 had a volume average diameter of 35.30, 20.35, and 13.96 μm respectively. Furthermore, the particles size range of ESP3 was lower than that of ESP2 and ESP1.

Comparatively, a volume average diameter of PESP was 14.54 μm which is close to that of ESP3. However, the particles size range of PESP was lower than that of ESP3, as presented in Table 4.1. The size distribution curves of these ESP and PESP are shown in Figure 4.3.

In addition, the specific surface area of ESP3 was higher than that of ESP2 and ESP1. On the other hand, the specific surface area of ESP3 was lower than that of PESP, as observed from SEM micrograph in Figure 4.3 (c) and (d).

Table 4.1 The particle size, size distribution and specific surface area of ESP1, ESP2, ESP3 and PESP.

Material	Particle size distribution (μm)				Range (μm)	BET surface area (m^2/g)
	D [4,3]	D [0,1]	D [0,5]	D [0,9]		
ESP 1	35.30	2.33	33.69	74.41	0.34-100.57	3.7073
ESP 2	20.35	3.46	18.47	39.60	0.34-54.40	3.9027
ESP 3	13.96	2.64	12.37	27.56	0.34-40.02	4.2308
PESP	14.54	4.46	13.47	26.26	0.34-34.32	4.4729

4.1.2 Crystal form of ESP and PESP

X-ray diffraction (XRD) patterns of ESP1, ESP2, ESP3, PESP and $CaCO_3$ were comparatively illustrated in Figure 4.1. The pattern of ESP1, ESP2, ESP3 and $CaCO_3$ was well matched which is the pattern of calcite polymorph with a crystal system of rhombohedral structure (JCPD number 01-071-1663, a= 4.98900, b=4.98900, c=17.06200, α=90°, β=90°, γ=120°). The strongest peak of the calcium carbonate eggshell occurred at 2θ of 29.5^o. This is similar to the XRD pattern of ESP stated by Witoon (2011). This implied that the grinding process did not made any transformation of crystal form of ESP1, ESP2 and ESP3.

In addition, the pattern of PESP shows two polymorph characteristics of calcite with a crystal system of rhombohedral structure (JCPD number 01-072-1652, a=4.9900, b=4.9900, c=17.00200, α=90°, β=90°, γ=120°), and vaterite with a crystal system of hexagonal structure (JCPD number 01-072-6506, a=4.13000, b=4.13000, c= 8.49000, α=90°, β=90°, γ=120°). In addition, the strongest peak

located at 2θ of 29.5° was assigned to the pattern of calcite crystal and the peaks located at 2θ of 24.9°, 27.0° and 32.8° were assigned to the pattern of vaterite crystal.

Moreover, these XRD patterns of ESP and PESP were in good agreement with their results obtained from SEM microscopy as shown in Figure 4.4 (a-d) which are mentioned in 4.1.5.

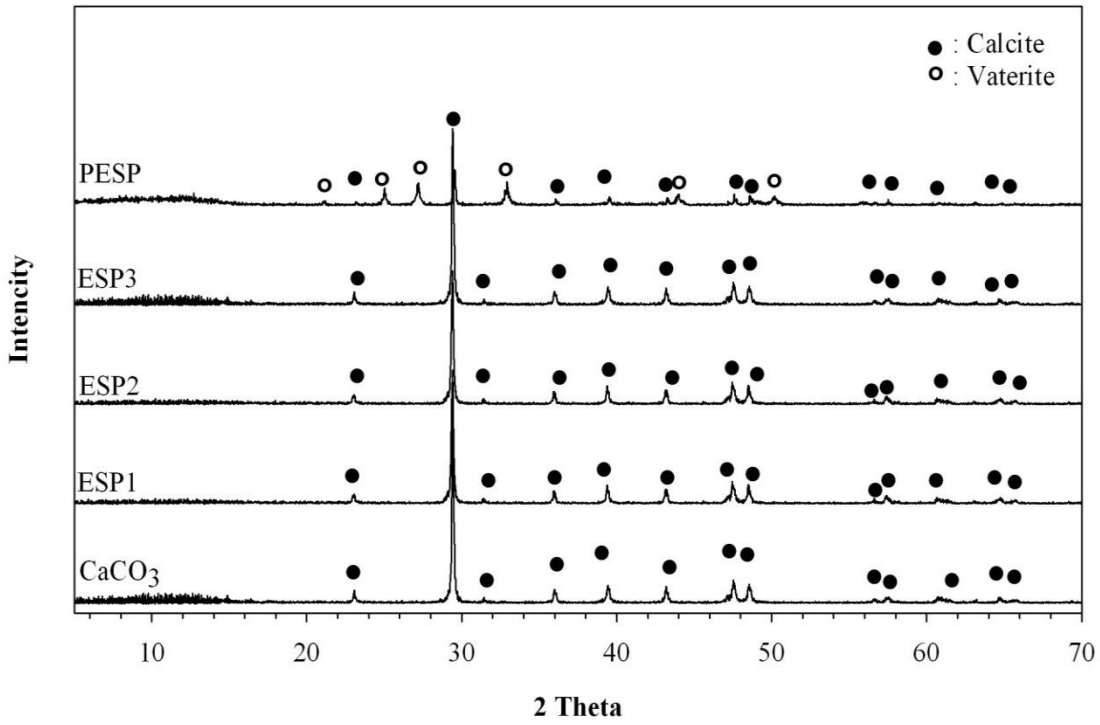

Figure 4.1 XRD patterns of ground $CaCO_3$, ESP1, ESP2, ESP3, and PESP.

4.1.3 Chemical composition of ESP and PESP

The elemental composition of eggshell powder (ESP) and precipitated eggshell powder (PESP) determined by X-ray fluorescence (XRF) spectrometer is shown in Table 4.2. The Ca content in ESP1, ESP2, ESP3 and PESP was approximately 38.04 to 39.37 wt.% which much higher than that of other elements

composing in ESP and PESP. Furthermore, it has been reported that the Ca content of ESP was about 38.00 to 39.00 wt.% (Schaafsma and Beelen, 1999; Schaafsma et al., 2000). Mijan, Kin and Kwak (2013) also reported that Ca content of ESP was about 38.6 wt.%. In addition, Freire and Holanda (2006) reported that the ESP had the Ca composition of 50.2 wt.%. The Ca content of ESP prepared by grinding and sieving into three particle ranges was insignificantly different. Nevertheless, the PESP had higher the Ca content than ESP1, ESP2 and ESP3. This might be because some organic compounds of eggshell matrix were removed during the dissolving ESP with HCl acid. The removal of some organic compounds from PESP was evident from the TGA and DTGA result, which was mentioned in the result following section 4.1.4. In addition, other minor compositions in ESP1, ESP2, ESP3 and PESP were Mg, Na, S, P, K and Cl and trace amount of Al, Si, Sr, Fe, Ba and Zn (Jai, Wook, Kyu, Gil and Mok, 2007).

Table 4.2 Elemental composition of ESP1, ESP2, ESP3, and PESP.

Elements	**Content (wt.%)**			
	ESP1	**ESP2**	**ESP3**	**PESP**
Ca	38.04	38.86	38.54	39.37
Mg	0.11	0.51	0.33	0.75
Na	0.87	0.35	0.50	0.42
S	0.37	0.11	0.12	0.11
P	0.40	0.22	0.14	0.34
K	0.11	0.08	0.12	<0.01
Cl	0.22	<0.01	0.11	<0.01
Si	0.06	0.06	0.04	0.04
Sr	<0.01	<0.01	<0.01	0.16
Al, Fe, Ba, Zn	<0.01	<0.01	<0.01	<0.01

4.1.4 Decomposition temperature of ESP and PESP

TGA and DTGA curves of ESP1, ESP2, ESP3, and PESP were shown in Figure 4.2 (a) and (b), respectively. From TGA and DTGA curves, ground eggshell powder showed two major thermal transitions. The first transition occurred at 324-327^{o}C, was derived from the decomposition of organic compound of eggshell matrix (Sutapun et al., 2013). The second transition at 814^{o}C, 809^{o}C, and 777^{o}C were derived from thermal decomposition of eggshell calcium carbonate. Freire and Holanda (2006) reported that the decomposition temperatures of eggshell organic compound and eggshell calcium carbonate were around 324.0^{o}C and 765.3^{o}C, respectively. In addition, Hassan, Rangari, Rana and Jeelani (2013) also reported that the decomposition temperatures of eggshell appeared at around 310^{o}C and 700-800^{o}C were derived from the decomposition of organic matter containing in eggshell matrix and calcium carbonate depositing in eggshell, respectively. The results showed that thermal stability of eggshell calcium carbonate decreased with reduction in particle size of eggshell powder. Furthermore, the smaller particle size had larger surface area that contributes to high efficiency of heat transfer (Mohamed, Yusupand and Maitra, 2012). Therefore, with larger surface of ESP3, it decomposed at lowest temperature, in comparison with that ESP1 and ESP2.

TGA and DTGA curves of PESP also showed two thermal transitions. The first transition at 324^{o}C was derived from the decomposition of organic compound of eggshell. The second transition occurred at 789^{o}C, was derived from the decomposition of eggshell calcium carbonate.

Moreover, the first transition of PESP observed from the TGA curve shows lower transition weight loss than the ground ESP. Accordingly, DTGA curve

of PESP shows almost a flat line in the temperature range of eggshell organic compound decomposition than ground ESP indicating that organic compositions of PESP were almost completely removed. In addition, PESP exhibited lower thermal decomposition temperature than ESP2 and ESP1. This might be because the vaterite crystal form of PESP was the most unstable polymorph. Popescu, Isopescu, Matei, Fagarasan and Plesu (2013) reported that the thermal decomposition of the vaterite crystal form of precipitated calcium carbonate was around 459 to 553^{o}C. Nevertheless, PESP showed slightly higher thermal decomposition temperature than ESP3. This was due to the some aggregation of the PESP particles as shown in Figure 4.4 (d), indicating that PESP had high thermal decomposition temperature, in comparison with ESP3.

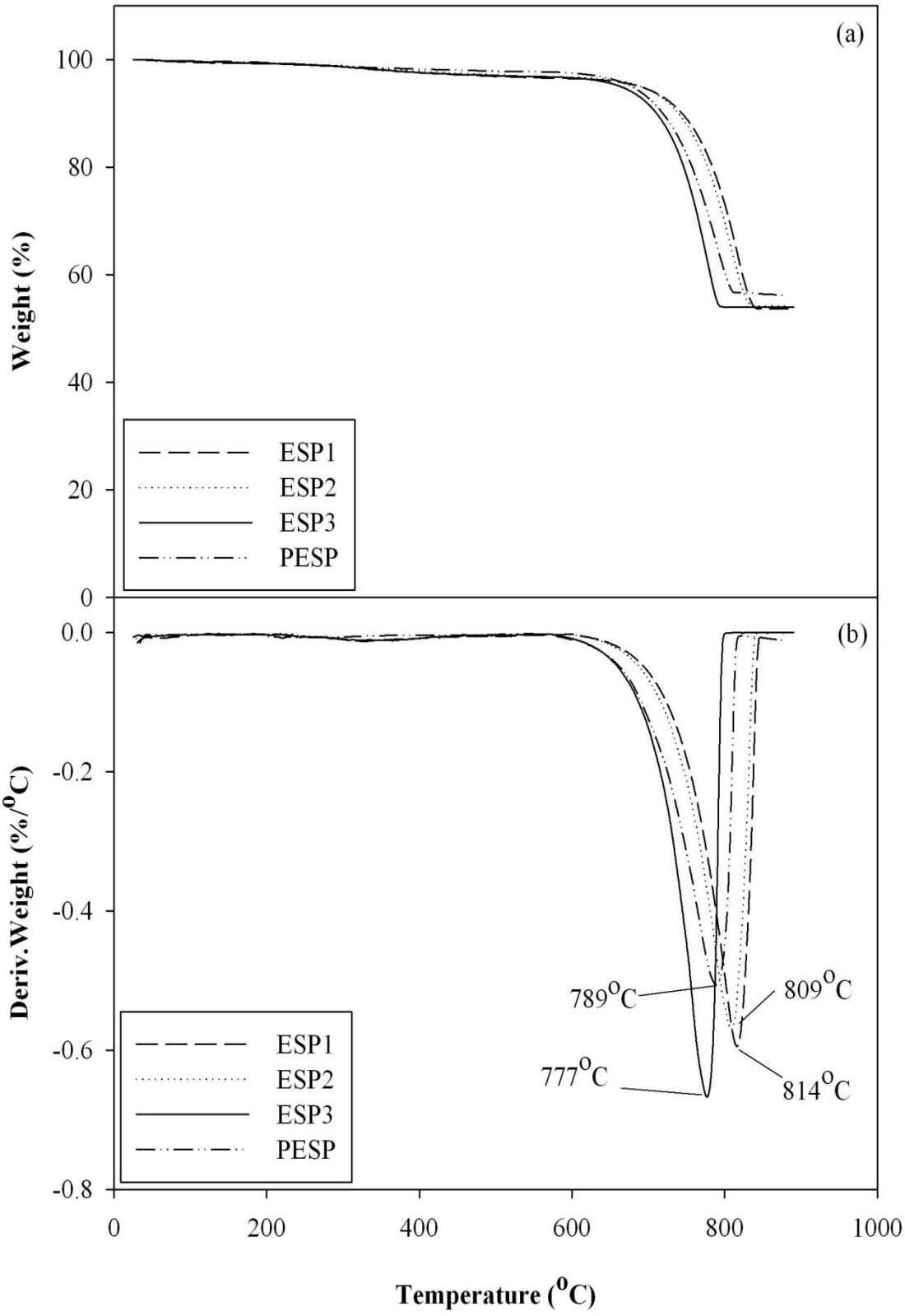

Figure 4.2 TGA (a) and DTGA (b) curves of ESP1, ESP2, ESP3, and PESP.

4.1.5 Particle morphology of ESP and PESP

SEM micrographs of ESP1, ESP2, ESP3, and PESP are shown in Figure 4.3. It was observed that ESP1, ESP2 and ESP3 particles were in cubic and irregular shape, with a rough surface. The cubic shape was a particular shape of calcite polymorph. After grinding and sieving process, the eggshell matrix protein still partly left on ESP1, ESP2 and ESP3 particles. Moreover, the ESP1, ESP2 and ESP3 formed the agglomeration as shown in Figure 4.3 (a), (b) and (c) respectively.

The PESP particle exhibits two characteristic shapes which was in cubic and sphere shape. Furthermore, the SEM micrograph of PESP shows very fine particles of smooth surface with homogeneous size distribution. After the precipitation step, the eggshell matrix protein was not observed at the PESP surfaces. However, it was confirmed from TGA curve that the organic compound was partly left on PESP particle after the eggshell precipitation. In addition, the particles of PESP formed the aggregation, as observed in Figure 4.3 (d). The sphere of PESP was a characteristic of vaterite polymorph. It was reported that precipitated of calcium carbonate from the mixing of calcium chloride and sodium carbonate would give rise to the PCC particle with sphere shape (Kirboga and Oner, 2013).

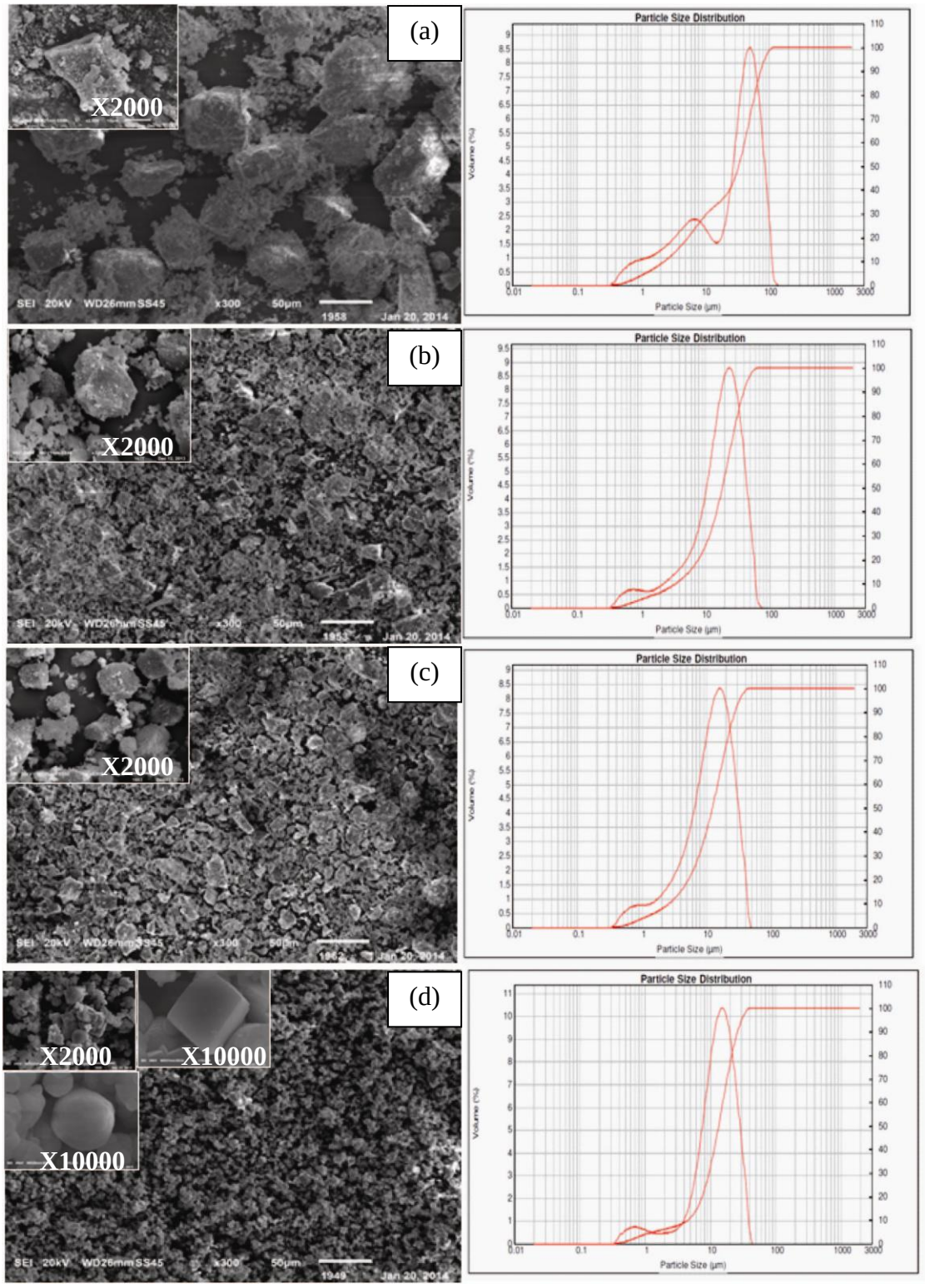

Figure 4.3 SEM micrographs (X300) and size distribution curve of ESP1 (a), ESP2 (b), ESP3 (c), and PESP (d).

4.2 Characterization of membrane peeled ESP/HDPE composites

4.2.1 Effect of ESP content on physical properties of ESP3/HDPE composites

4.2.1.1 Flow property

The melt flow index (MFI) of neat HDPE and ESP3/HDPE composite at various ESP3 contents is summarized in Table 4.3. It was found that MFI of HDPE composites decreased with increasing ESP3 content. This was because the hard and rigid particles of ESP3 restricted the mobility and flow of the polymer matrix (Yun Fu, Qiao Feng, Lauke and Wing Mai, 2008).

Table 4.3 Melt flow index of neat HDPE and ESP3/HDPE composites.

ESP3 content (wt.%)	MFI (g/10 min)
0	11.47
10	7.05
20	6.08
30	6.04
40	5.10

4.2.1.2 Stress-strain behavior

The tensile stress-strain behavior of neat HDPE and ESP3/HDPE composite at various ESP3 content are shown in Figure 4.4. It presents that neat HDPE and HDPE composite at 10 wt.% ESP3 did not break within an instrumentation limit of 800% elongation. At a tension rate 10 mm/min, the tensile

stress-strain curve of HDPE composite at 20 wt.% ESP3 shows cold drawing region before the specimen fractured. This was because the ESP filler restricted the mobility of the HDPE matrix as mentioned in 4.2.1.1. Moreover, the strain hardening behavior was not observed from tensile curve of 20 wt.% ESP3/HDPE composite. In addition, tensile curve of HDPE composite at 30 and 40 wt.% ESP3 exhibited necking zone without cold drawing region before fractured. This suggested that the interfacial debonding of the HDPE matrix from the ESP3 particle was extended when the ESP3 was added more into the HDPE matrix (Bartczak, Argon, Cohen and Weinberg, 1999).

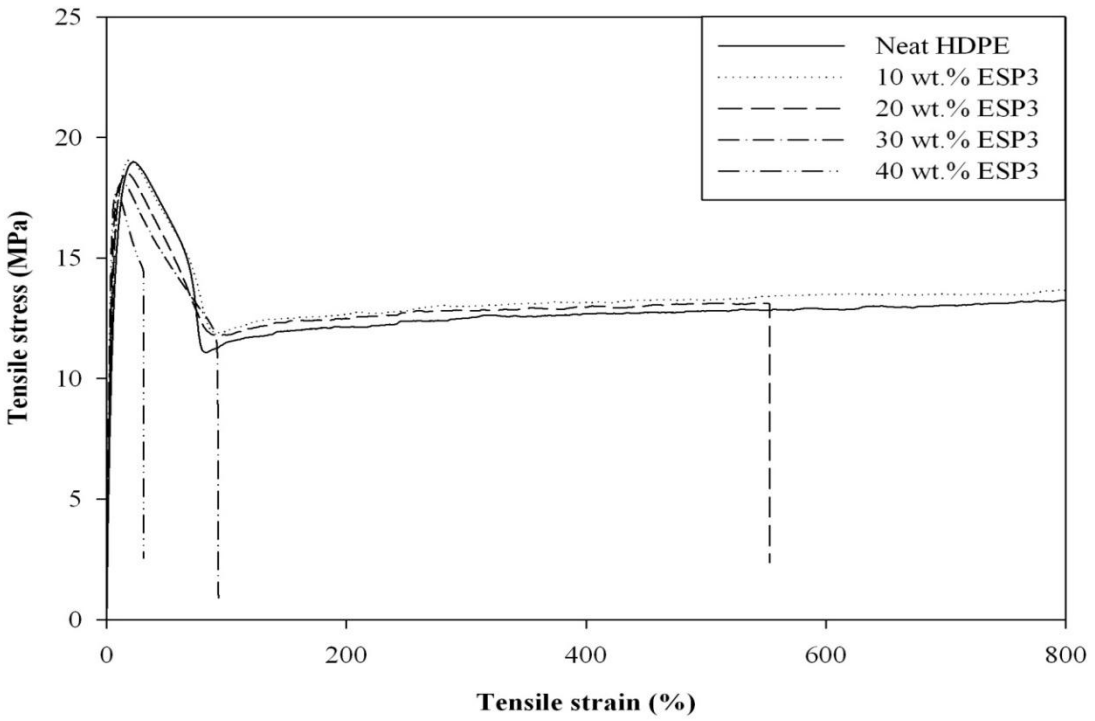

Figure 4.4 Tensile stress-strain curves of neat HDPE and ESP3/HDPE at various ESP3 contents.

4.2.1.3 Mechanical properties

From plots of yield strength and tensile stress at break versus ESP3 content of ESP3/HDPE composite as shown in Figure 4.5, it was revealed that yield strength of the composite gradually decreased with increasing ESP3 content. This was because voids at ESP3-HDPE interface was a weakening point. The void acted as a stress concentration by which interfacial HDPE matrix was in the vicinity of magnified as a result the matrix yielded at lower applied stress with more added ESP3 (Suwanprateeb, 2000; Bartczak, Argon, Cohen and Weinberg, 1999; Suwanprateeb, Tiemprateeb, Kangwantrakool and Hemachandra, 1998). Moreover, Figure 4.5 also shows tensile stress at break of ESP3/HDPE composites. The result showed that tensile stress at break of neat HDPE and HDPE composite at 10 wt.% ESP3 was not observed because the specimens did not rupture within instrumentation limit. Nevertheless, at 20-40 wt.% ESP3, tensile stress at break was slightly decreased with increased ESP3 content. The addition of ESP3 diminished ability to plastically flow of the matrix.

In addition, Young's modulus of the composites was improved by addition of ESP3. This was caused by the incorporation of rigid particle of ESP3 which is stiffer than HDPE. With increasing ESP3 content, elongation at break of ESP3 filled HDPE decreased and was much lower than that of unfilled HDPE as shown in Figure 4.6. The addition of ESP3 diminished ability to plastically flow of the matrix. This is an indication that with higher content of ESP3, the HDPE composite lossed ability to absorb applied energy prior to composite fracture. This result well corresponded with the result obtained from an impact test of the HDPE composite as presented in Table 4.4.

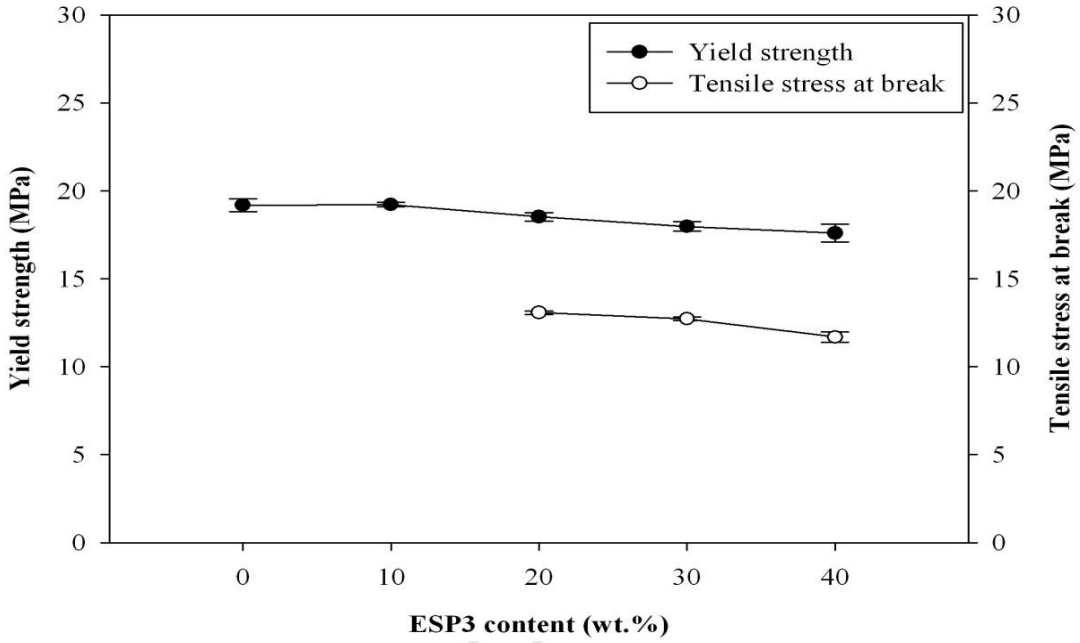

Figure 4.5 Plots of yield strength and tensile stress at break vs ESP3 content of ESP3/HDPE composites.

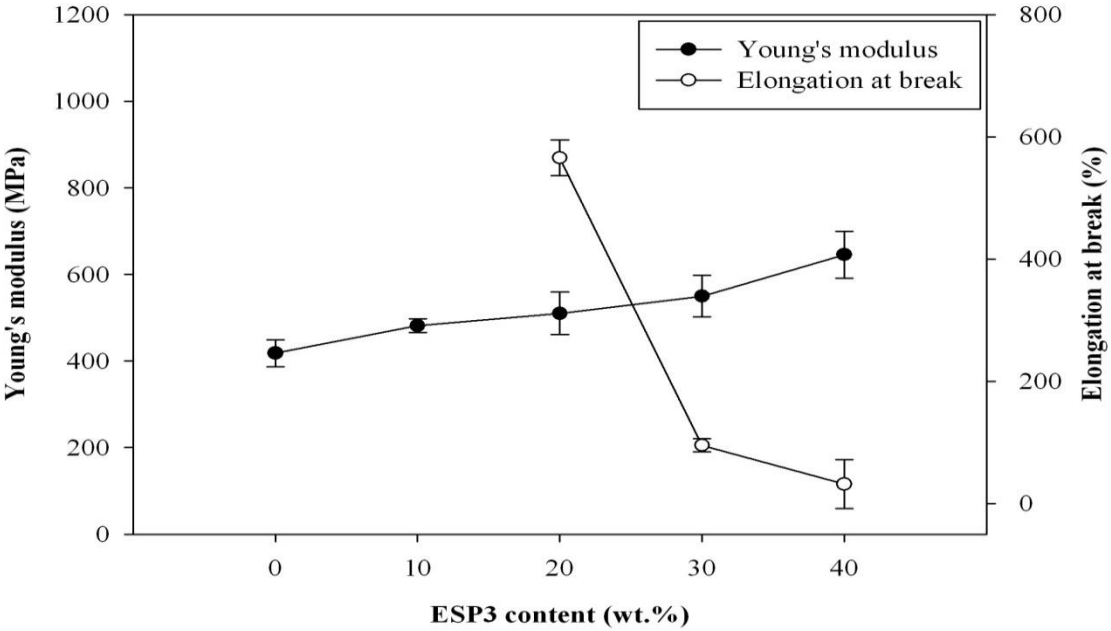

Figure 4.6 Plots of Young's modulus and elongation at break vs ESP3 content of ESP3/HDPE composites.

Figure 4.7 shows flexural modulus of neat HDPE and ESP3/HDPE composites. The flexural modulus of HDPE improved with the incorporation of ESP3. As increasing ESP3 content, the flexural modulus significantly increased. The addition of ESP3 diminished ability to plastically flow of the matrix. This was due to the incorporation of stiffness ESP3 particle. In addition, the flexural strength of the composites was slightly increased with increasing ESP3 content. In addition, the tensile and flexural properties of HDPE composites at various ESP3 contents are summarized in Table 4.5.

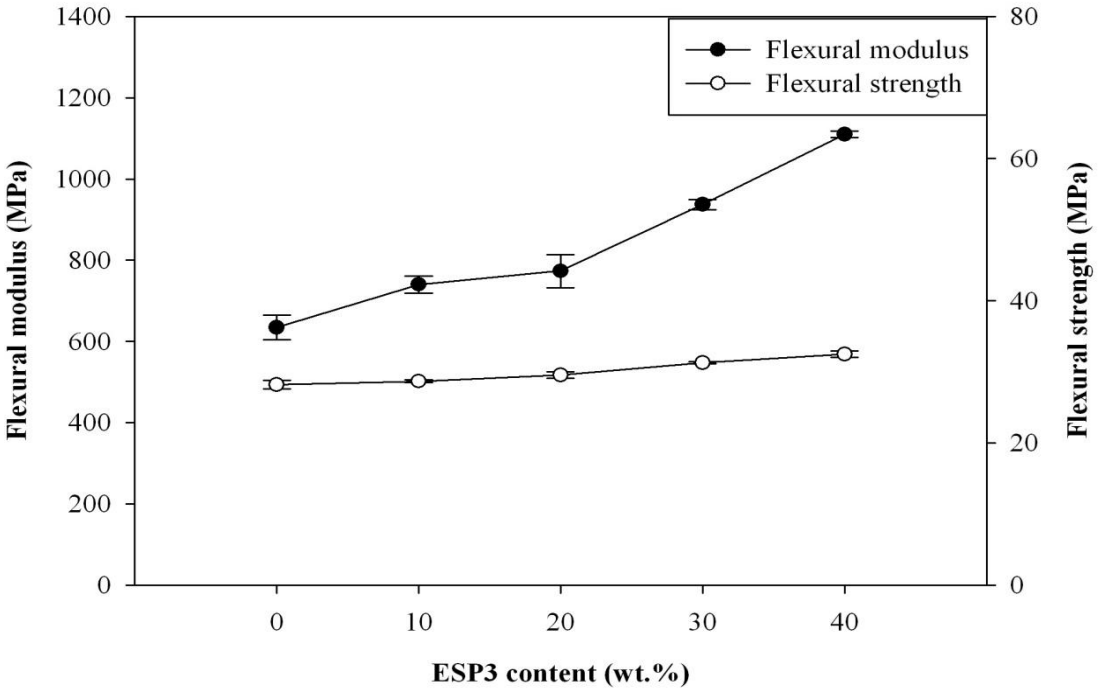

Figure 4.7 Plot of flexural modulus and flexural strength vs ESP3 content of ESP3/HDPE composites.

Impact strength of neat HDPE and HDPE composites at various ESP3 contents is shown in Table 4.4. The HDPE composite with higher content in ESP3 had lower impact strength than that of the composite with lower ESP3 content and lower than that of unfilled HDPE. This was because the addition of ESP3 diminished ability to absorb impact energy prior to composite rupture. However, the HDPE composite at 10 wt.% ESP3 and neat HDPE did not rupture within an instrumentation limit.

Table 4.4 Impact strength of neat HDPE and HDPE composite at various ESP3 contents.

ESP3 content (wt.%)	**Impact strength (kJ/m^2)**
0	>130
10	>130
20	58.87±6.00
30	27.01±0.64
40	16.49±0.26

Table 4.5 Tensile and flexural properties of neat HDPE and ESP3/HDPE composite at various ESP3 contents.

ESP3 Content (wt.%)	Young's modulus (MPa)	Elongation at break (%)	Yield strength (MPa)	Tensile stress at break (MPa)	Flexural modulus (MPa)	Flexural strength (MPa)
0	418.1±31.7	Not break	19.1±0.3	Not break	634.5±30.5	28.2±0.6
10	481.5±16.6	Not break	19.2±0.1	Not break	739.7±21.1	28.6±0.1
20	510.0±49.8	565.7±29.3	18.5±0.2	13.0±0.1	773.3±40.9	29.5±0.4
30	549.9±48.7	95.4±11.6	17.9±0.2	12.7±0.1	936.9±12.0	31.2±0.1
40	645.6±54.8	31.6±40.4	17.6±0.5	11.6±0.3	1109.6±8.3	32.4±0.4

4.2.1.4 Fracture surface morphology

SEM micrographs of ESP3/HDPE composites shown in Figure 4.12 illustrate that HDPE composite has a rough fracture surface with agglomerated eggshell particles. The higher the ESP3 content, the poorer the ESP dispersed within HDPE matrix. Moreover, it can be seen that voids at fracture surface of the composite increased with increasing ESP3 content. This was due to the poor interfacial adhesion between the interface of ESP3 and HDPE matrix and leading to brittleness of the composite with more added ESP3. This was responsible for the decrease of yield strength, tensile stress at break and impact strength. In addition, the surface topology of HDPE matrix indicated that it still ruptured in a ductile manner as same as neat HDPE.

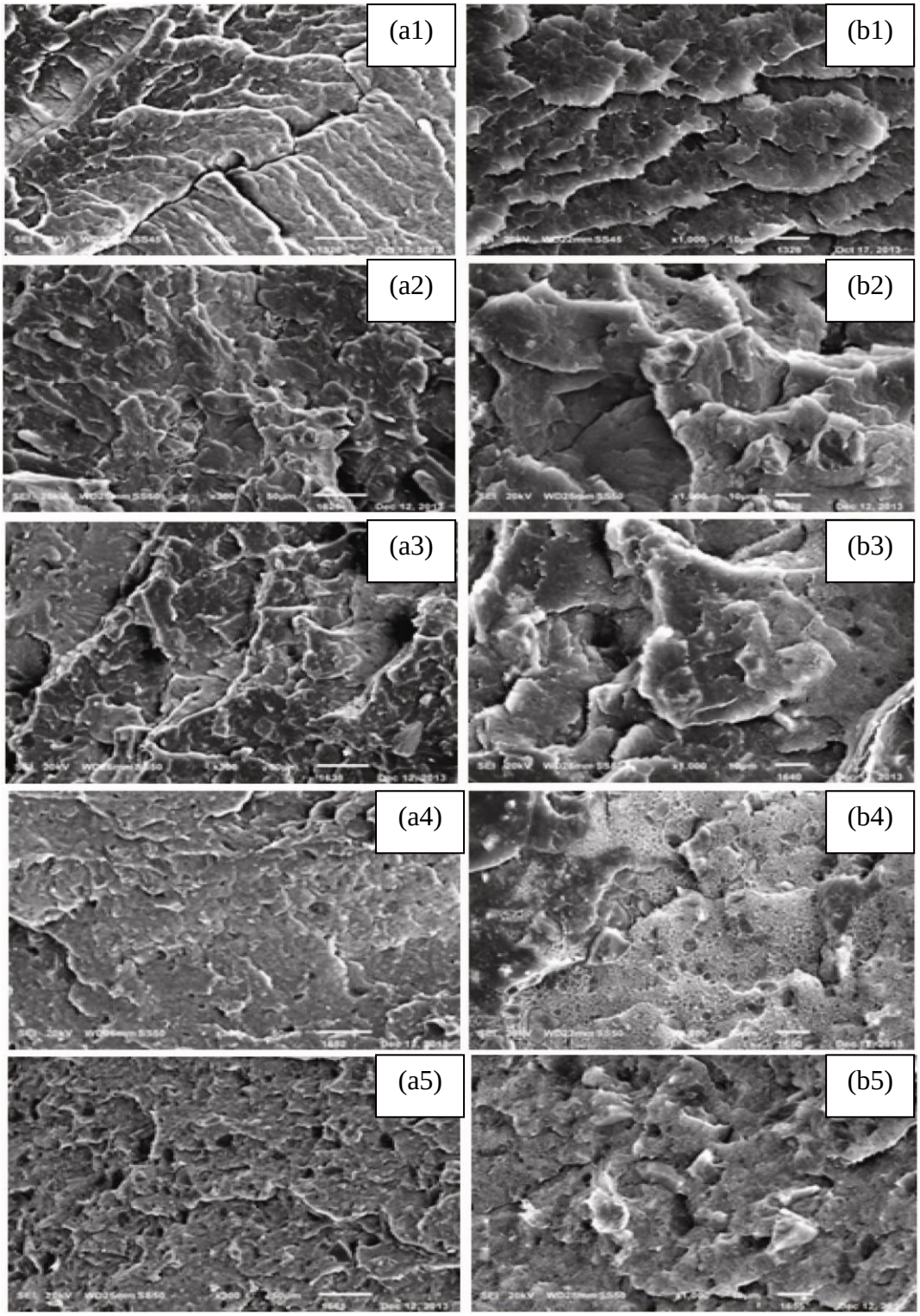

Figure 4.8 SEM micrographs (x300 (a) and x1000 (b)) of neat HDPE (1) and ESP3/HDPE composite at 10 (2), 20 (3), 30 (4) and 40 (5) wt.% ESP3.

4.2.1.5 Decomposition temperature

TGA and DTGA curves of neat HDPE and HDPE composite at various ESP3 contents are shown in Figure 4.9. Neat HDPE thermally decomposed as a single transition at 483^{o}C whereas ESP3/HDPE composites decomposed with two thermal transitions. The first transition, due to decomposition of HDPE matrix, was at 484^{o}C for the filled HDPE with 10, 20, 30 and 40 wt.% ESP3. This indicated that the filled ESP3 did not influence thermal decomposition of HDPE matrix. The second transition derived from thermal decomposition of eggshell calcium carbonate was around 726, 754, 764 and 777^{o}C for HDPE filled with 10, 20, 30 and 40 wt.% ESP3, respectively. The decomposition temperature of ESP3 filler increased with increasing ESP3 content. Similar observation was investigated by Pakdeechote (2010). This was possibly due to the strong effect of filler content and particle-particle interaction as increasing filler content (Osman, Atallah, Schweizer and Ottinger, 2004). Furthermore, TGA curevs show the percentage of HDPE and ESP3 corresponding to the mixing ratios. The final weight after the decomposition is calcium oxide (CaO). The residual of CaO after decomposition of the composite at 10, 20, 30 and 40 wt.% ESP3 was 5, 11, 16 and 21 wt.%, respectively. In addition, the characteristic peak of organic eggshell matrix was not observed.

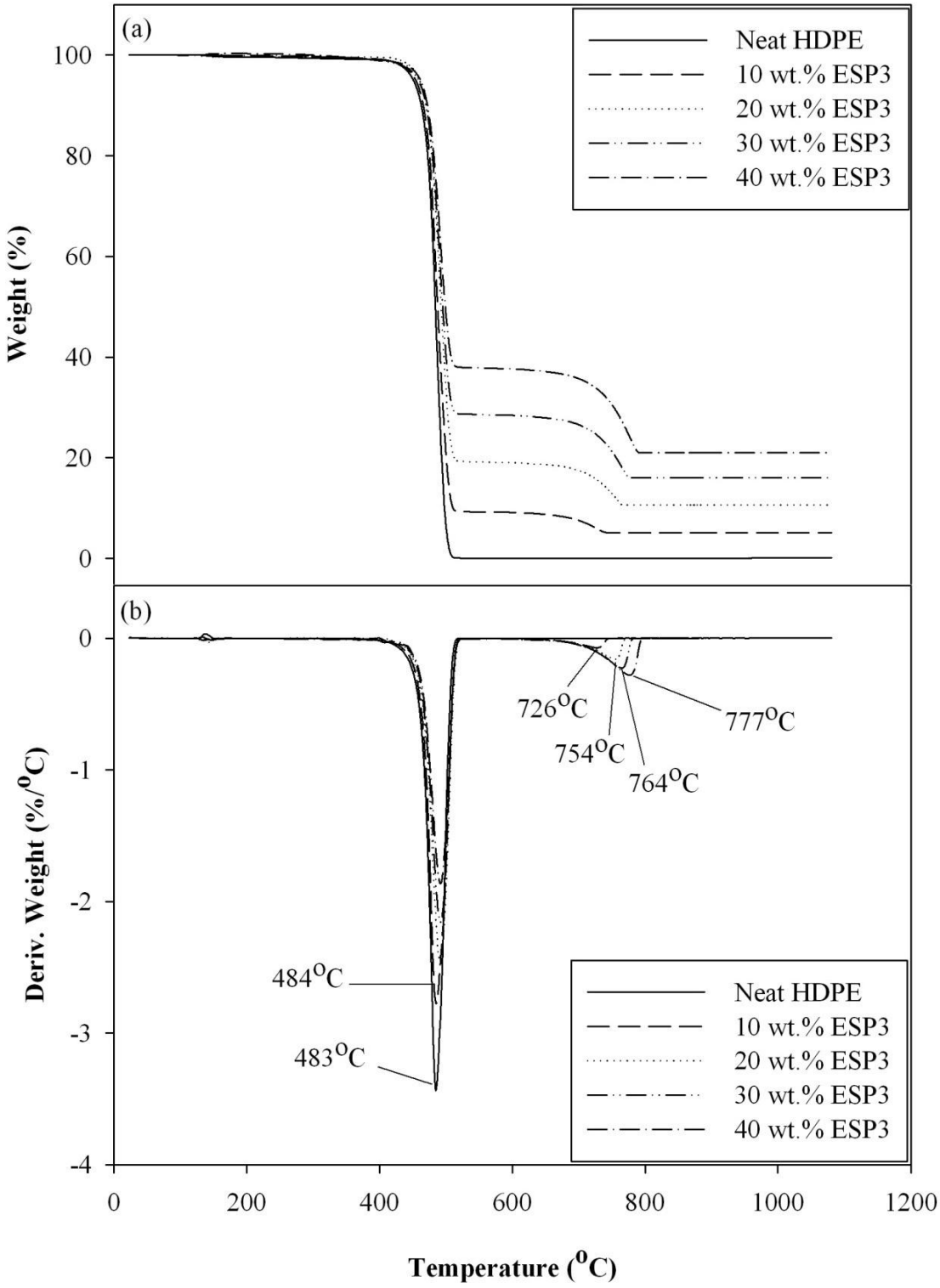

Figure 4.9 TGA and DTGA curves of neat HDPE and HDPE composite at 10, 20, 30 and 40 wt.% ESP3.

4.2.1.6 Melting and crystallization temperature

DSC curves of neat HDPE and ESP3/HDPE composites at vartous ESP3 contents are shown in Figure 4.10. In the first heating curve, neat HDPE and ESP3/HDPE composites, showed a single melting behavior during heating process. It revealed that melting temperature of HDPE did not change when ESP3 was added. With increasing ESP content, HDPE melting temperatures did not change as well, as observed from Figure 4.10 (a). This indicated that ESP3 did not disturb melting process of HDPE matrix. In addition, the second heating curves of neat HDPE and ESP3/HDPE composites are presented in Figure 4.10 (b). The second heating curves of neat HDPE and ESP3/HDPE composites showed a single melting behavior after the removal of thermal history. Comparatively, the melting temperature obtained from the first heating and second heating scan of neat HDPE and ESP3/HDPE composites was not significantly different.

Figure 4.11 shows DSC curves obtained from the first cooling of neat HDPE and ESP3/HDPE composites. It was found that the adding ESP3 into HDPE exhibited insignificant effect on crystallization temperature. It clearly indicated that ESP3 did not act as a nucleating agent for HDPE matrix. This is due to ESP3 particles obstructed the HDPE chain mobility for reentry into specific lamellar.

Degree of crystallinity of HDPE composite decreased with increasing ESP content. With increasing ESP composition, HDPE chains were more obstructed to crystallize by the added ESP. However, degree of crystallinity obtained from the second heating scan was higher than that of the first heating scan. This might be due to the removal of thermal history by the slow rate of the second heating. After the 1^{st} heating scan, the composites was slowly cooled down at a cooling rate of

10^{o}C/min to room temperature. During slow rate of cooling, more HDPE molecules was able to crystallize and rearrage themself into and within spherulites and lamellar, respectively. Therefore, X_c from the 2^{nd} heating scan was higher than that obtained from the 1^{st} heating scan. In addition, melting temperature, crystallization temperature and degree of crystallinity of neat HDPE and HDPE composite at 10, 20, 30 and 40 wt.% ESP3 are shown in Table 4.6.

As previously mentioned in section in 4.2.1.2, ESP3/HDPE composite at 20 wt.% ESP3 showed cold drawing region before the specimen frectured within an instrumentation limit of 800% elongation. Therefore, the HDPE composite was further prepared with ESP1, ESP2 and ESP3 at 20 wt.% in order to study the effect of particle sizes and interfacial modification on physical properties of the composites.

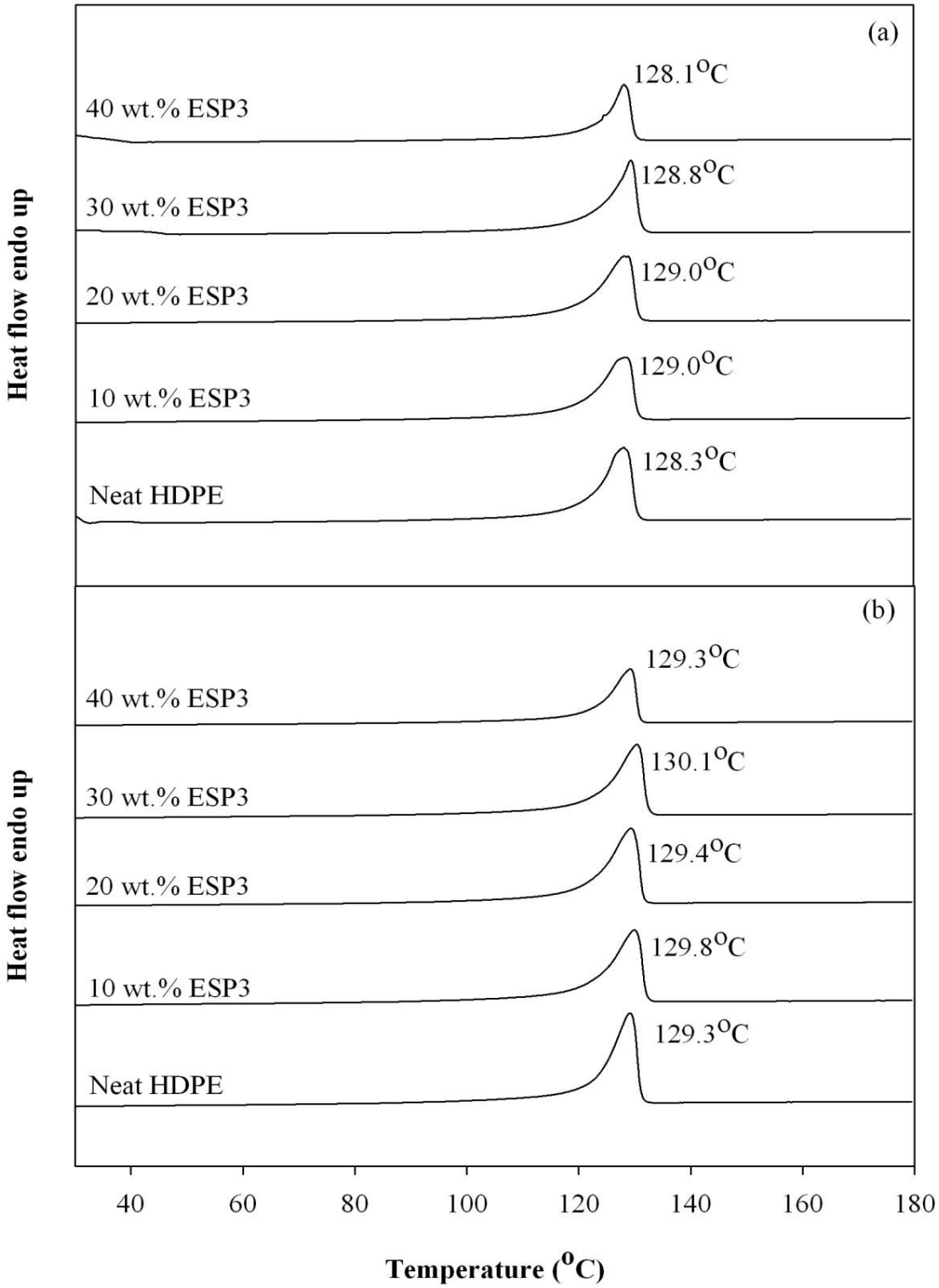

Figure 4.10 DSC curves of 1st heating (a) and 2nd heating (b) scan of neat HDPE and ESP3/HDPE composites.

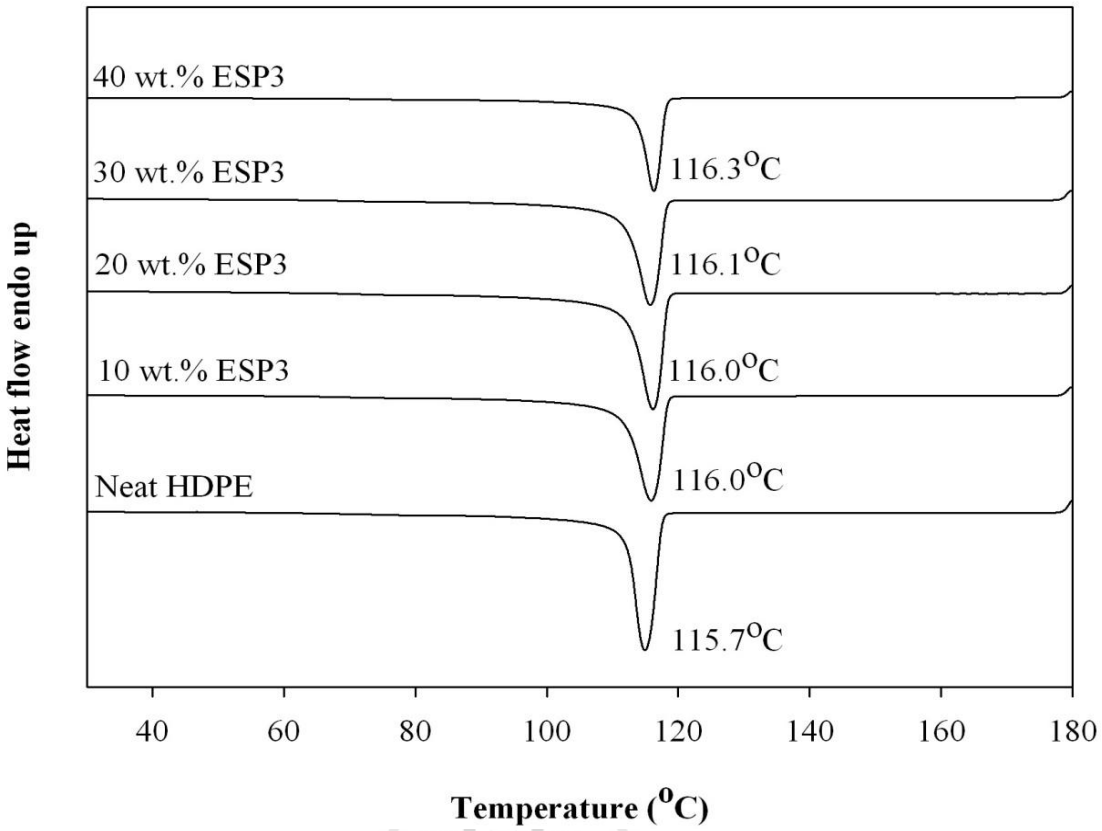

Figure 4.11 DSC curves obtained from the 1st cooling scan of neat HDPE and ESP3/HDPE at 10, 20, 30 and 40 wt.% ESP3.

Table 4.6 Melting temperature (T_m), crystallization temperature (T_c) and degree of crystallinity (X_c) of neat HDPE and HDPE composite at various ESP3 contents.

ESP3 content (wt.%)	T_d (^oC)		T_m (^oC)		T_c (^oC)	Delta H (J/g)		X_c (%)	
	HDPE	ESP3	1st scan	2nd scan		1st scan	2nd scan	1st scan	2nd scan
Neat HDPE	483	-	128.3	129.3	115.7	206.3	227.9	70.5	77.9
10	484	726	129.0	129.8	116.0	229.7	245.8	70.6	75.6
20	484	754	129.0	129.4	116.0	252.6	272.2	69.1	74.4
30	484	764	128.8	130.1	116.1	279.3	311.4	66.8	74.5
40	484	777	128.1	129.3	116.3	318.2	362.6	65.3	74.4

4.2.2 Effect of ESP particle size on physical properties of 20 wt.% ESP/HDPE composites

4.2.2.1 Flow property

Melt flow index (MFI) of neat HDPE and HDPE composite filled with ESP1, ESP2 and ESP3 is shown in Table 4.7. The number average particle size of ESP1, ESP2 and ESP3 was 35.30, 20.35 and 13.96 μm with the particle range of 0.34-100.57, 0.34-54.40, and 0.34-40.02 μm, respectively, as mentioned previously. Neat HDPE showed higher MFI than ESP/HDPE composites. Furthermore, MFI of the composites insignificantly changed with ESP particle sizes.

Table 4.7 MFI of neat HDPE and HDPE composites filled with ESP1, ESP2 and ESP3 at 20 wt.%.

ESP content (wt.%)	MFI (g/10 min)		
	ESP1	ESP2	ESP3
0	11.89		
20	6.51	7.10	6.08

4.2.2.2 Stress-strain behavior

Figure 4.12 shows tensile stress-strain curves of neat HDPE and HDPE composites prepared with ESP1, ESP2 and ESP3. Neat HDPE did not break within an instrumentation limit of 800% elongation. In addition, the tensile stress-strain curves of 20 wt.% ESP/HDPE composites prepared with ESP1, ESP2 and ESP3 showed cold drawing region without strain hardening before the specimen fractured. However, HDPE composite prepared with ESP3 had the highest ultimate

elongation. This was because the size distribution of ESP3 was quite homogenous and narrow. Moreover, the voids size from the HDPE composite prepared with smaller particle of ESP3 were lower extended than that of the composite prepared with larger particle of ESP2 and ESP1. These voids acted as stress concentrator which made the composite prepared with ESP3 fractured at higher stress (Zuiderduin, Westzaan, Huetink and Gaymans, 2003). Furthermore, the strain hardening behavior was not observed from tensile curves of the HDPE composites.

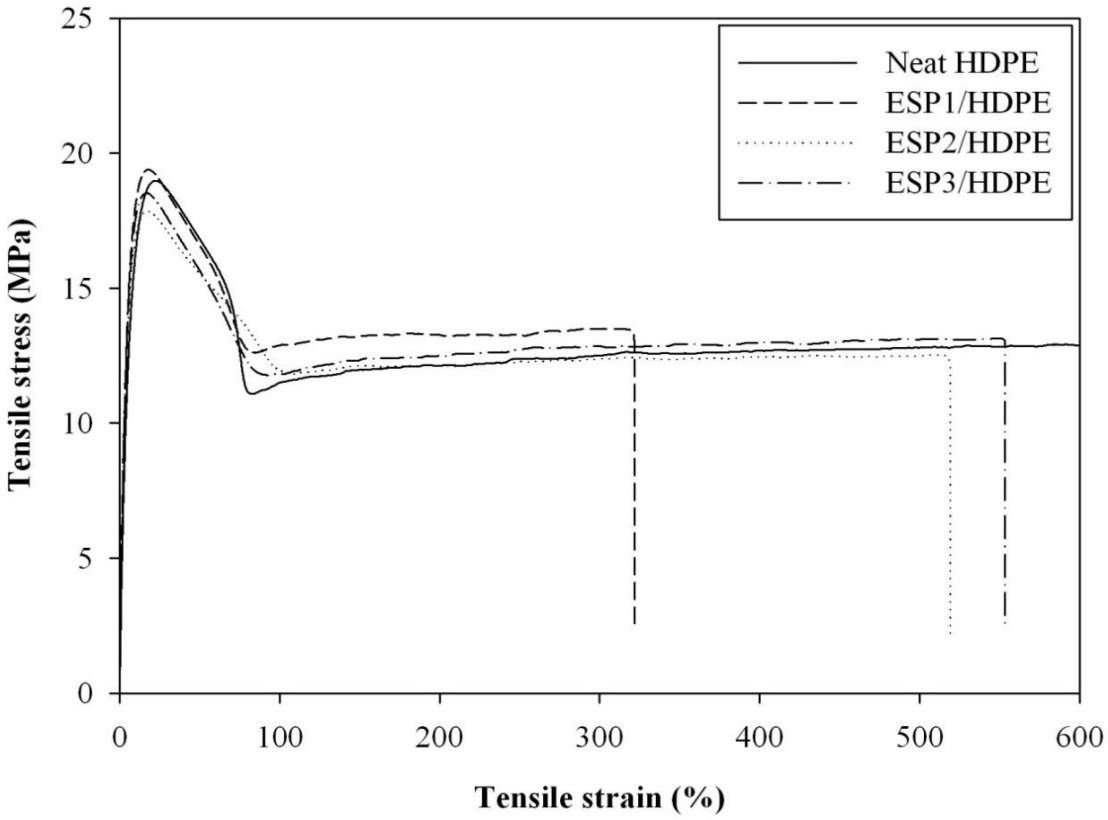

Figure 4.12 Tensile stress-strain curves of neat HDPE and ESP/HDPE composites prepared with ESP1, ESP2 and ESP3 at 20 wt.%.

4.2.2.3 Mechanical properties

For tensile properties, eggshell particle size did not signifinicantly affect Young's modulus, tensile stress at break, and yield strength, of filled HDPE composites, as observed from Figure 4.13 and 4.14. Neat HDPE did not break within an instrumentation limit. However, elongation at break of ESP/HDPE composite related to a particle size of eggshell. Elongation at break of the composite with smaller ESP particle size of ESP2 and ESP3 was higher than that of the composite with the larger size of ESP1. This is an indication that, under tensile deformation, the HDPE composite with smaller eggshell particle size had higher ductility than the HDPE composites with larger eggshell particle size. This was because the voids size from the HDPE composite prepared with smaller particle of ESP3 were lower extended than that of the composite prepared with larger particle of ESP2 and ESP1. These voids acted as stress concentrator which made the composite prepared with ESP3 fractured at higher stress (Zuiderduin, Westzaan, Huetink and Gaymans, 2003). This result well corresponded with the result obtained from an impact test of the HDPE composite in which the composite with smaller size of ESP had higher impact strength than the one with larger particle size. Additionally, mechanical properties of neat HDPE and HDPE composites filled with ESP1, ESP2 and ESP3 are summarized in Table 4.8.

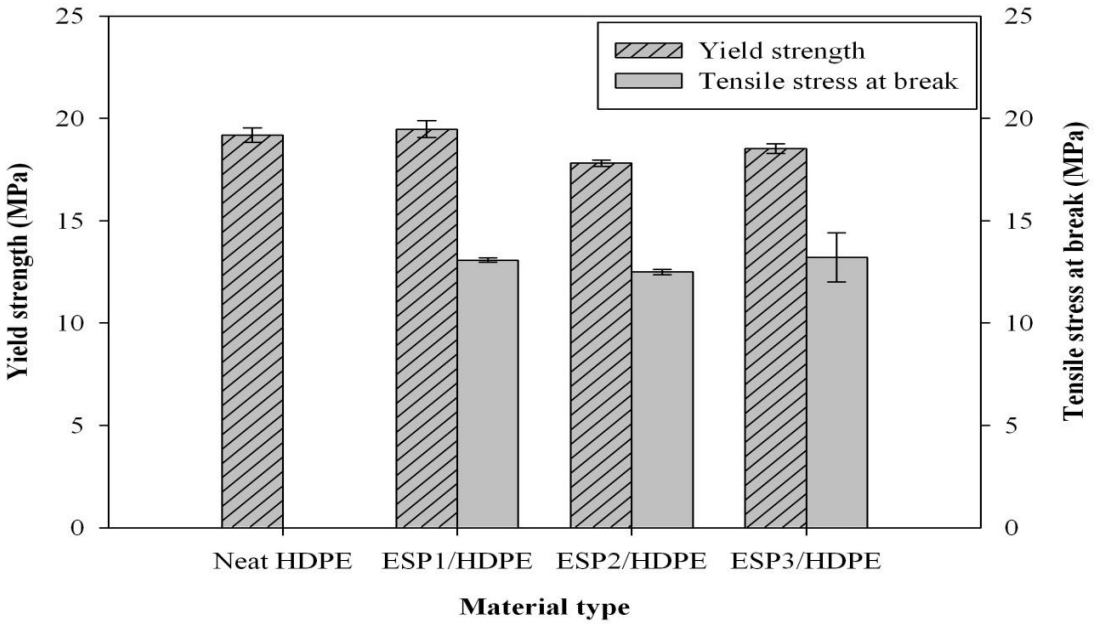

Figure 4.13 Plots of yield strength and tensile stress at break of neat HDPE and HDPE composite prepared with ESP1, ESP2 and ESP3 at 20 wt.%.

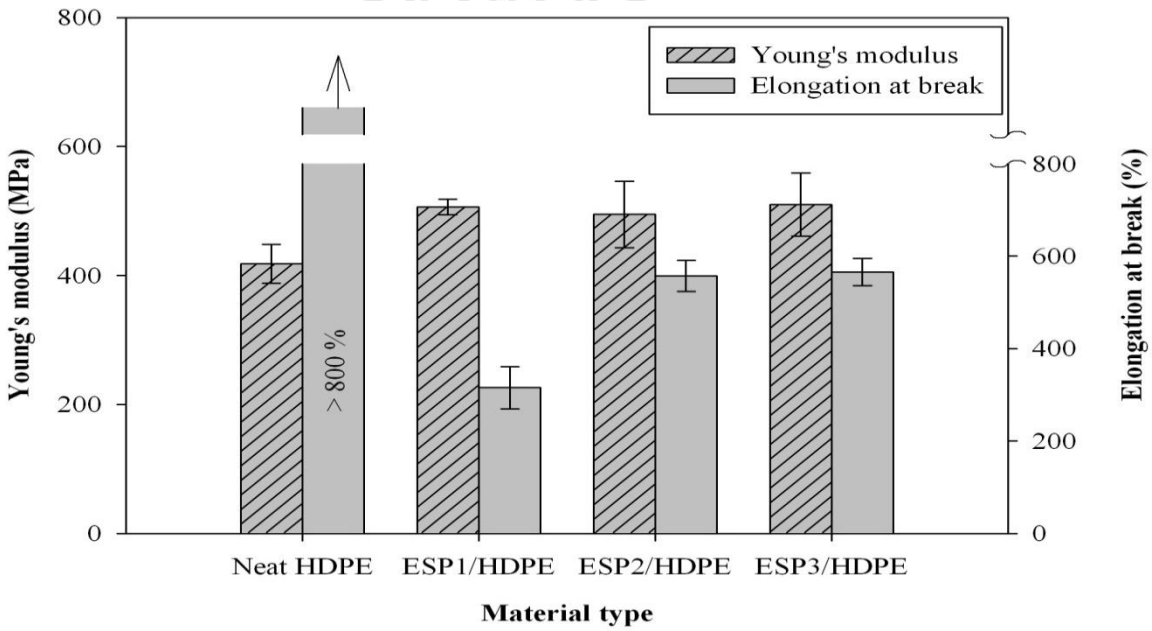

Figure 4.14 Plots of Young's modulus and elongation at break of neat HDPE and HDPE composite prepared with ESP1, ESP2 and ESP3 at 20 wt.%.

Flexural modulus and flexural strength of neat HDPE and HDPE composite filled with ESP1, ESP2 and ESP3 are shown in Figure 4.15. Incorporation of ESP1, ESP2 and ESP3 slightly improved flexural modulus of HDPE. This was due to the addition of hard particle of ESP. Flexural strength of neat HDPE did not much different from ESP/HDPE composites. In addition, flexural strength of HDPE composite was slightly decreased when ESP2 was added. However, HDPE composites prepared with three different particle sizes of ESP had no significant differences in flexural modulus and flexural strength of HDPE composites.

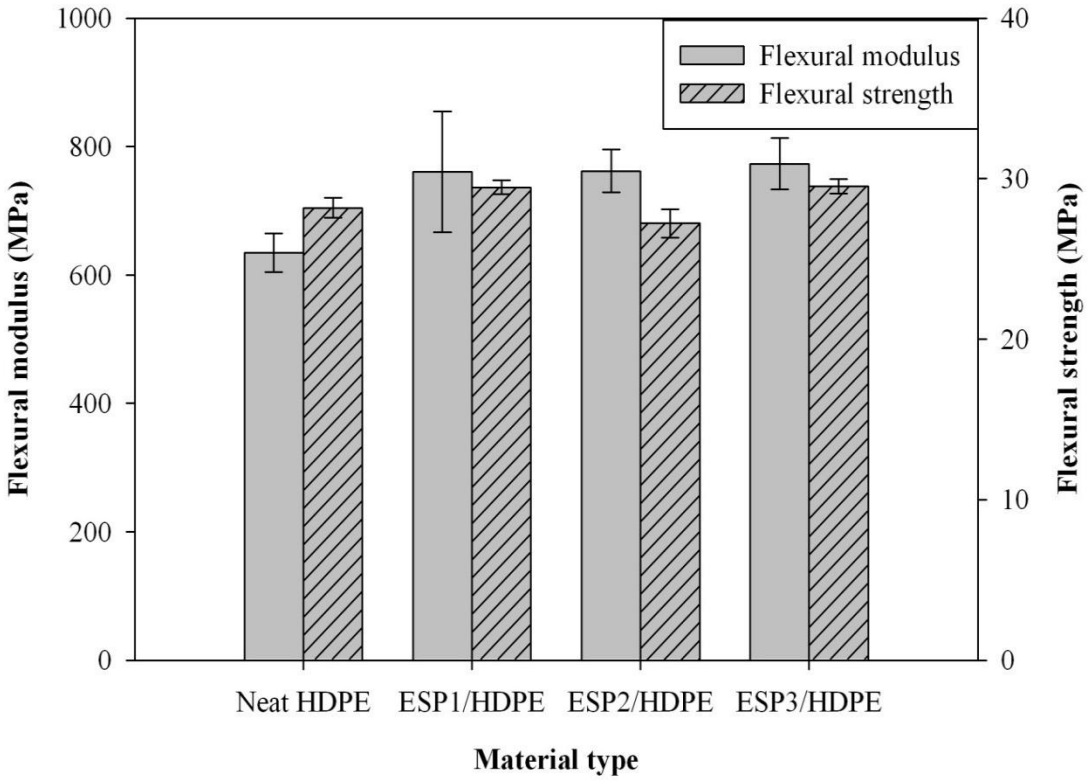

Figure 4.15 Plots of flexural modulus and flexural strength of neat HDPE and HDPE composite prepared with ESP1, ESP2 and ESP3 at 20 wt.%.

Impact strength of neat HDPE and HDPE composites filled with ESP1, ESP2 and ESP3 is presented in Figure 4.16. Neat HDPE did not rupture within an instrumentation limit. However, under impact loading, the HDPE composite with smaller eggshell particle size had higher impact strength than the composites with larger eggshell particle size. This was because the voids size from the HDPE composite prepared with smaller particle of ESP3 were lower extended than that of the composite prepared with larger particle of ESP2 and ESP1. These voids acted as stress concentrator which made the composite prepared with ESP3 fractured at higher stress (Zuiderduin, Westzaan, Huetink and Gaymans, 2003).

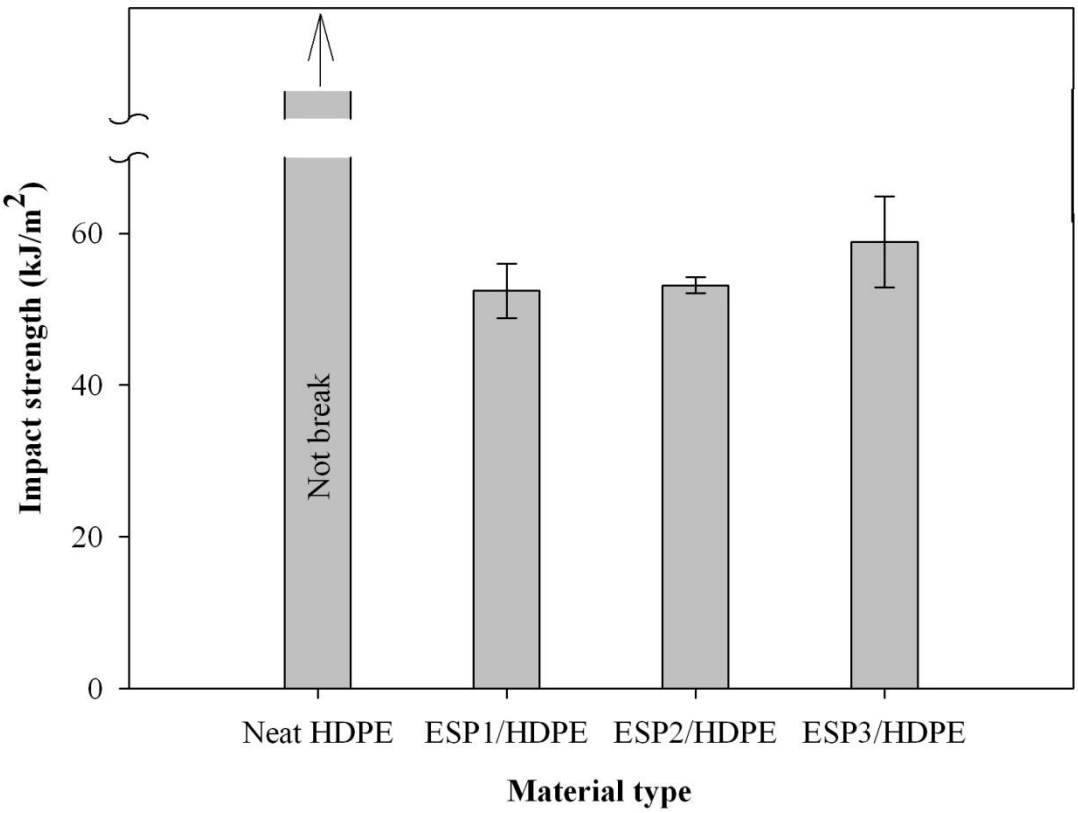

Figure 4.16 Plot of impact strength of neat HDPE and HDPE composite prepared with ESP1, ESP2 and ESP3 at 20 wt.%.

Table 4.8 Young's modulus, elongation at break, yield strength, tensile stress at break, flexural modulus, flexural strength, flexural strength and impact strength of neat HDPE and 20 wt.% ESP/HDPE composites prepared with ESP1, ESP2 and ESP3 at 20 wt.%.

HDPE composite	Young's modulus (MPa)	Elongation at break (%)	Yield strength (MPa)	Tensile stress at break at break (MPa)	Flexural modulus (MPa)	Flexural strength (MPa)	Impact strength (kJ/m^2)
Neat HDPE	418.1±31.0	Not break	19.1±0.3	Not break	634.5±30.0	28.1±0.6	Not break
ESP1/HDPE	506.0±12.0	315.3±46.0	19.4±0.4	13.2±1.2	760.9±24.0	29.4±0.4	52.4±3.5
ESP2/HDPE	494.6±51.2	557.2±33.4	17.8±0.1	12.4±0.1	762.1±33.6	27.2±0.8	53.1±1.0
ESP3/HDPE	510.0±49.0	565.7±29.0	18.5±0.2	13.0±0.1	773.3±40.0	29.5±0.4	58.8±6.0

4.2.2.4 Fracture surface morphology

Fracture surface morphology of neat HDPE and 20 wt.% ESP/HDPE composites with ESP particle sizes of 35.30 µm (ESP 1), 20.35 µm (ESP2) and 13.96 µm (ESP3) are shown in Figure 4.17. It was observed that interfacial adhesion between ESP1, ESP2 and ESP3 surface and HDPE matrix was not good. This indicated that eggshell particle sizes did not affect interfacial adhesion between ESP and HDPE. Moreover, the particles distribution in HDPE matrix of ESP1, ESP2 and ESP3 were the same. In addition, several holes were observed on the fracture surface. These holes were caused from detaching of ESP particle from HDPE matrix. The surface topology of HDPE filled with ESP1, ESP2 and ESP 3 indicated that the filled HDPE still ruptured in a ductile manner similar to that of neat HDPE.

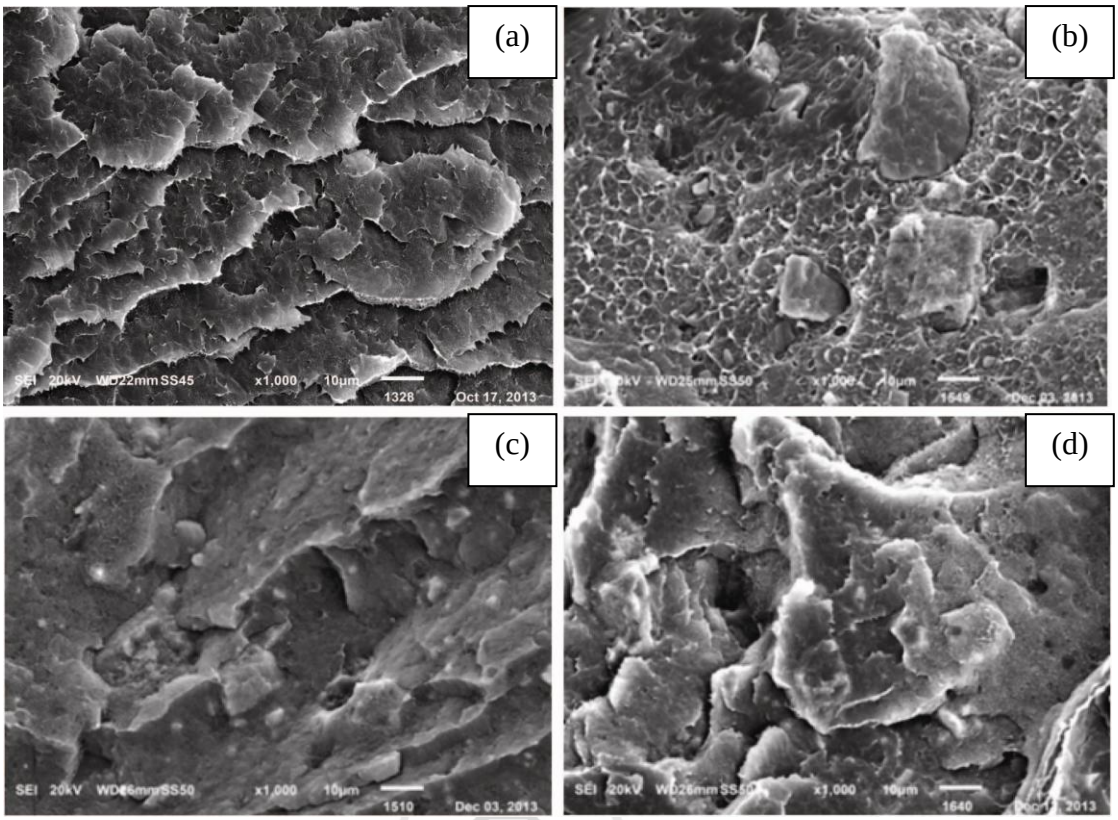

Figure 4.17 SEM micrographs (x1000) of neat HDPE (a) and HDPE composites filled with ESP1 (b), ESP2 (c) and ESP3 (d) at 20 wt.%.

4.2.2.5 Decomposition temperature

TGA and DTGA curves of neat HDPE and HDPE composites filled with ESP1, ESP2 and ESP3 are shown in Figure 4.18. Neat HDPE thermally decomposed as a single transition at 483^{o}C whereas HDPE composites thermally decomposed into two transition steps. The first transition due to decomposition of HDPE matrix was at 485^{o}C, 490^{o}C and 492^{o}C for HDPE filled with ESP1, ESP2, and ESP3, respectively. The second transition derived from decomposition of eggshell calcium carbonate was around 747^{o}C, 750^{o}C and 754^{o}C for HDPE filled with ESP1, ESP2, and ESP3, respectively. The ESP particle size did influence thermal decompsition of HDPE matrix. The decomposition temperature of HDPE matrix incresaed with decreasing ESP particle size. Moreover, the decomposition temperature of ESP filled in HDPE matrix slightly increased with decreasing eggshell particle size.

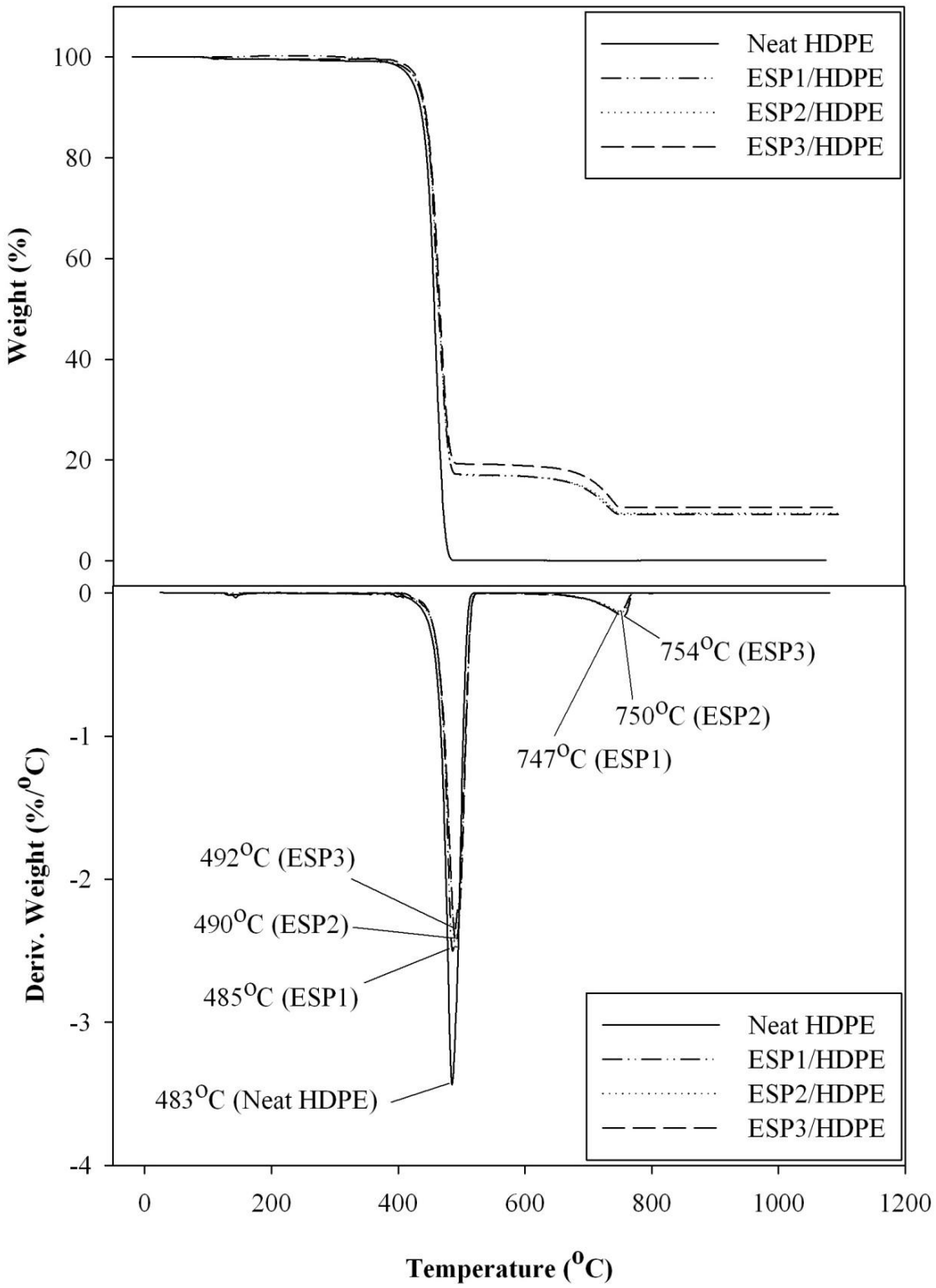

Figure 4.18 TGA and DTGA curves of neat HDPE and HDPE composite filled with ESP1, ESP2 and ESP3 at 20 wt.%.

4.2.2.6 Melting and crystallization temperature

DSC curves of neat HDPE and HDPE composites prepared with ESP1, ESP2 and ESP3 are shown in Figure 4.19. In the first heating curve, neat HDPE and HDPE filled with ESP1, ESP2 and ESP3, showed a single melting behavior during heating process, as observed in Figure 4.19 (a). With different eggshell particle size, it presented that melting temperature of HDPE slightly changed. This indicated that eggshell particle size did not significantly affect melting of HDPE matrix. Similarly, the second heating scan, eggshell particle size did not also influence melting temperature of HDPE matrix, as shown in Figure 4.19 (b).

Figure 4.20 shows DSC curves obtained from the first cooling of neat HDPE and HDPE filled with ESP1, ESP2 and ESP3. It was found that the crystallization temperature of neat HDPE and HDPE filled with ESP1, ESP2 and ESP3 was not significantly different. In addition, degree of crystallinity of HDPE composite obtained from the first heating scan did not change with adding ESP1, ESP2 and ESP3, indicating ESP particle size had no effect on crystallization of HDPE matrix. However, at slow rate of the second heating scan, crystallinity degree of HDPE slightly decreased with decreasing ESP particle size. This might be due to the removal of thermal history by the second heating. Additionally, melting temperature, crystallization temperature and degree of crystallinity of HDPE composite prepared with ESP1, ESP2 and ESP3 are shown in Table 4.9.

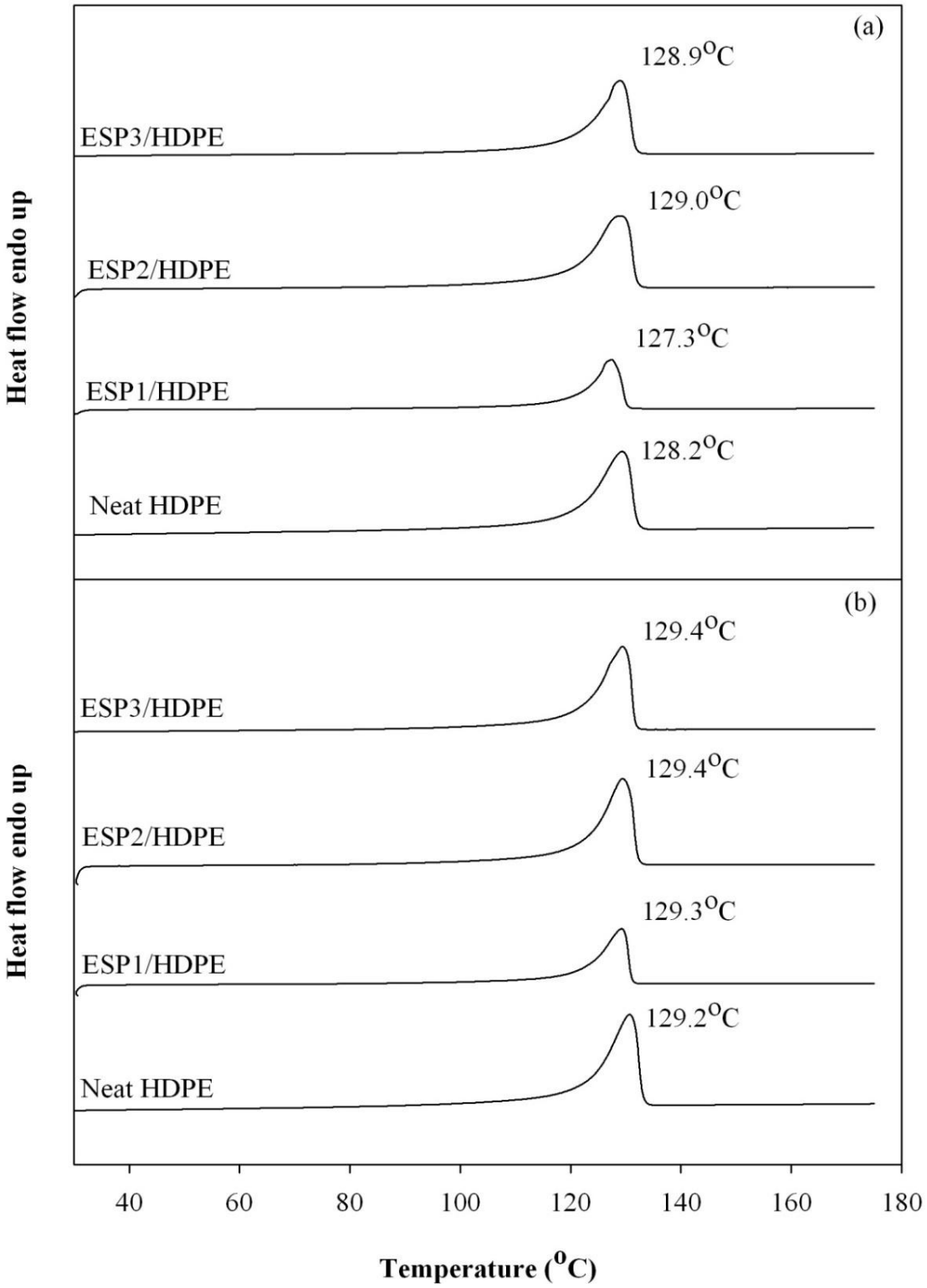

Figure 4.19 DSC curves of 1st heating (a) and 2nd heating (b) scan of neat HDPE and 20 wt.% ESP/HDPE composites prepared with ESP1, ESP2 and ESP3.

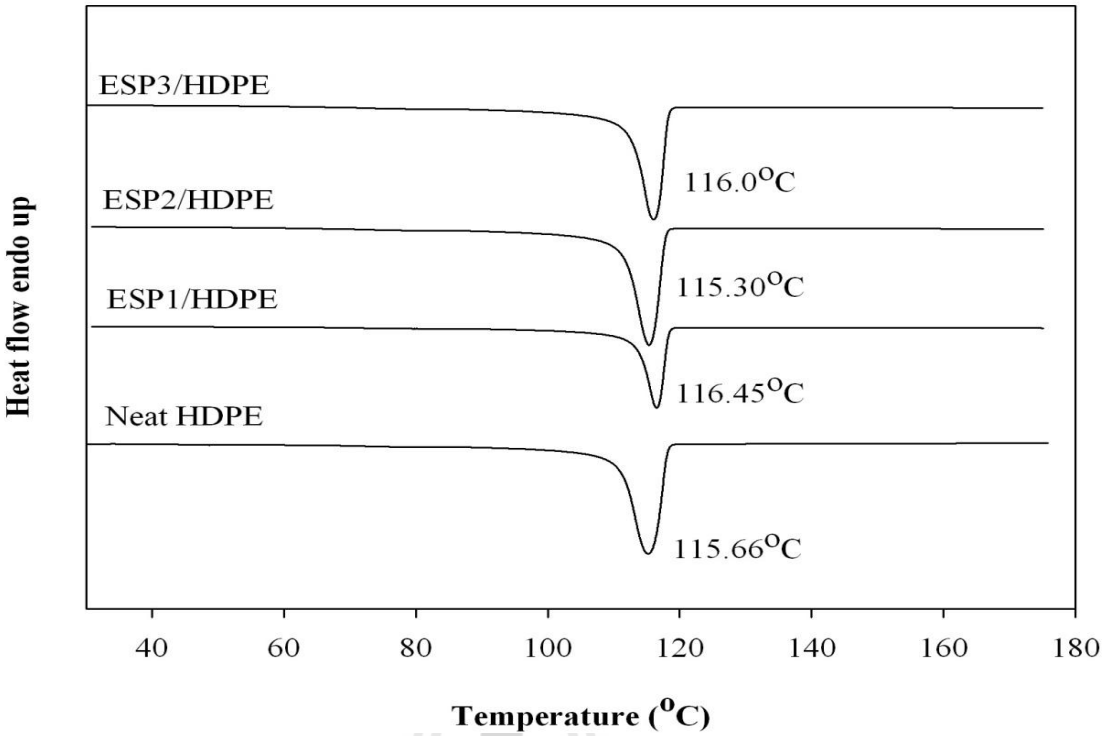

Figure 4.20 DSC curves obtained from the 1st cooling scan of neat HDPE and 20 wt.% ESP/HDPE prepared with ESP1, ESP2 and ESP3.

Table 4.9 Melting temperature (T_m), crystallization temperature (T_c) and degree of crystallinity of neat HDPE and HDPE composite filled with ESP1, ESP2 and ESP3 at 20 wt.%.

HDPE composites	T_d (°C)		T_m (°C)		T_c (°C)	Delta H (J/g)		X_c (%)	
	HDPE	ESP	1st scan	2nd scan		1st scan	2nd scan	1st scan	2nd scan
Neat HDPE	483	-	128.3	129.3	115.7	206.3	227.9	70.5	77.9
ESP1	485	747	127.3	129.3	116.5	255.5	279.1	69.9	76.3
ESP2	490	750	129.1	129.4	115.3	254.5	275.7	69.6	75.4
ESP3	492	754	129.0	129.4	116.0	252.6	272.2	69.1	74.4

4.2.3 Effect of compatibilization on physical properties of ESP2/HDPE composites

4.2.3.1 Flow property

MFI of the uncompatibilized and compatibilized of 20 wt.% ESP2/HDPE composite at various compositions of HDPE-g-MAH and EPR-g-MAH is listed in Table 4.10. It was revealed that MFI of compatibilized HDPE composite slightly decreased with increasing HDPE-g-MAH content. Comparatively, with increasing EPR-g-MAH content, MFI of compatibilized HDPE composite insignificantly changed from uncompatibilized HDPE composite. However, at high content of the compatibilizer, the HDPE composite modified with EPR-g-MAH had higher MFI than the HDPE composite modified with HDPE-g-MAH.

Table 4.10 MFI of 20 wt.% ESP2/HDPE composite at various HDPE-g-MAH, and EPR-g-MAH contents.

Compatibilizer content (wt.%)	**MFI (g/10min)**	
	HDPE-g-MAH[a]	**EPR-g-MAH[b]**
0	7.10	
2	7.01	7.03
5	6.14	7.01
8	5.03	6.82
10	4.40	6.82

a = MFI of HDPE-g-MAH compatibilized HDPE composite

b = MFI of EPR-g-MAH compatibilized HDPE composite

4.2.3.2 Stress-strain behavior

Figure 4.21 shows tensile stress-strain curves of compatibilized 20 wt.% ESP2/HDPE composites at various compositions of HDPE-g-MAH and EPR-g-MAH. The uncompatibilized and compatibilized HDPE composites showed cold drawing region before the test specimen was fractured. Moreover, it was seen that increasing HDPE-g-MAH content significantly improved the ductility of ESP2/HDPE composite. On the other hand, the ductility of compatibilized ESP2/HDPE composites significantly decreased with increasing EPR-g-MAH content. This might be due to the fact that HDPE-g-MAH contained ethylene of 99 wt.% whereas EPR-g-MAH contained 43 wt.% ethylene and 53 wt.% propylene. This implied that the HDPE-g-MAH backbone was more compatible to HDPE matrix than EPR-g-MAH backbone. With increasing HDPE-g-MAH content, the compatibility of the composite was increased leading to the reduction of a gap between ESP and HDPE, resulting in an increasing of ductility.

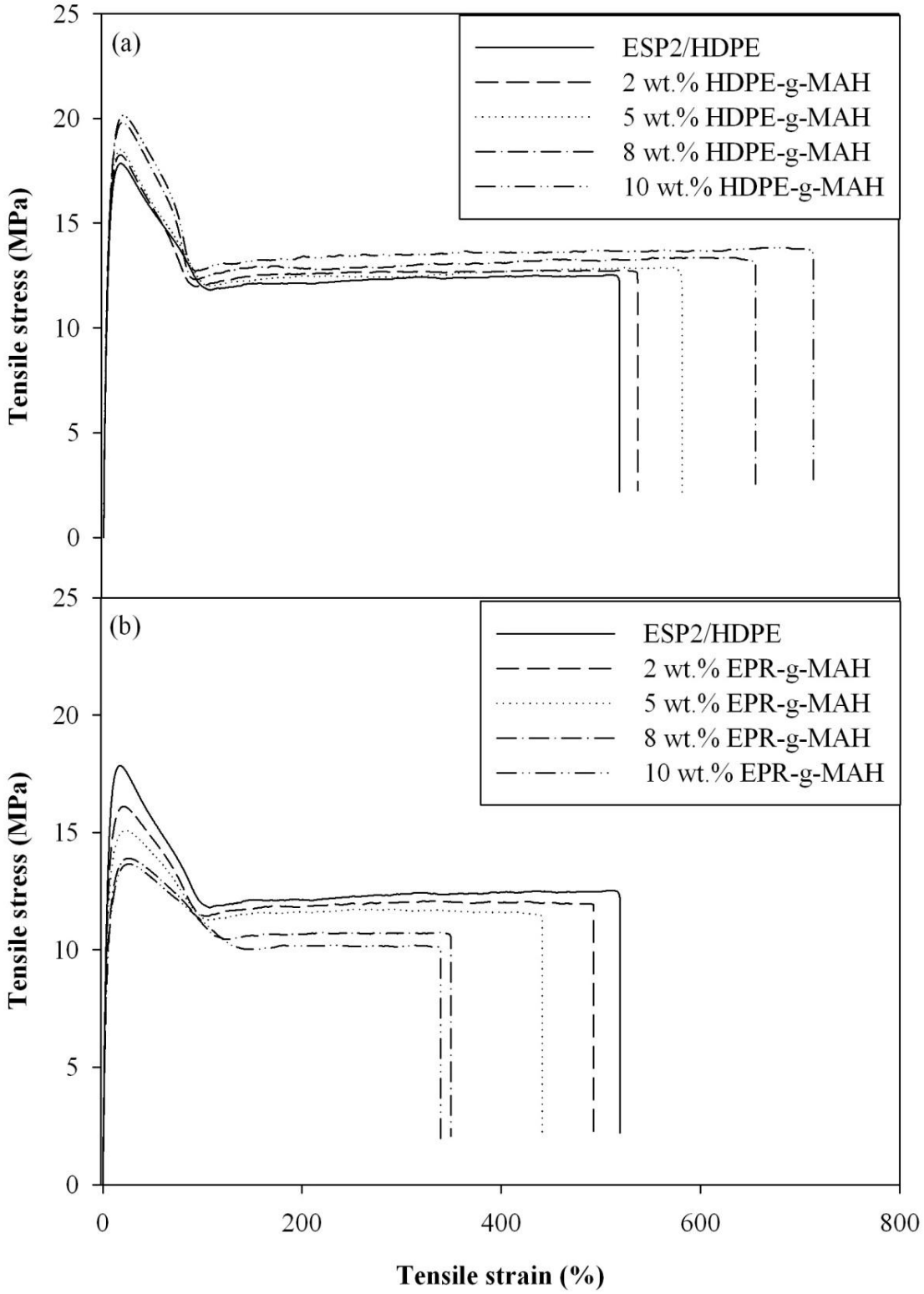

Figure 4.21 Tensile stress-strain curves of 20 wt.% ESP2/HDPE composites at various HDPE-g-MA (a) and EPR-g-MA (b) contents.

4.2.3.3 Mechanical properties

Figure 4.22 shows plots of tensile stress at break of 20 wt.% ESP2/HDPE composite at various compositions of HDPE-g-MAH and EPR-g-MAH. It presented that HDPE-g-MAH enhanced tensile stress at break of the composite. With increasing HDPE-g-MAH content, tensile stress at break of compatibilized HDPE composites gradually improved. On the other hand, addition of EPR-g-MAH led to the negative effect on tensile stress at break of the composite. This was because HDPE matrix more disliked EPR-g-MAH than HDPE-g-MAH as mentioned in 4.2.3.2.

Plots of Young's modulus and elongation at break of 20 wt.% ESP2/HDPE composite at various compositions of HDPE-g-MAH and EPR-g-MAH are shown in Figure 4.23. It was found that Young's modulus of HDPE composite was not significantly influenced by addition of HDPE-g-MAH. With increasing HDPE-g-MAH content, Young's modulus of compatibilized HDPE composite was not much different. Comparatively, Young's modulus of the composite slightly decreased when EPR-g-MAH was added. Additionally, the HDPE-g-MAH compatibilized HDPE composite had higher elongation at break than the uncompatibilized HDPE composite but EPR-g-MAH compatibilized HDPE composite had lower elongation at break. Moreover, elongation at break of compatibilized HDPE composite was improved with increasing HDPE-g-MAH content. However, elongation at break of the composite decreased with increasing EPR-g-MAH content.

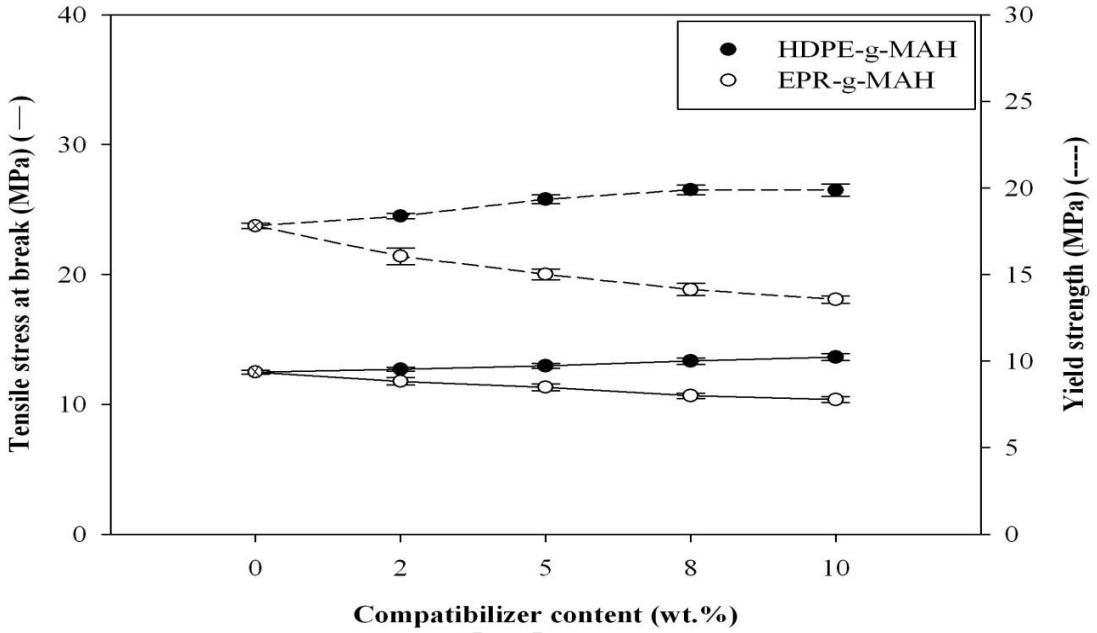

Figure 4.22 Plots of tensile stress at break (—) and yield strength (---) of 20 wt.% ESP2/HDPE composite vs compatibilizer content.

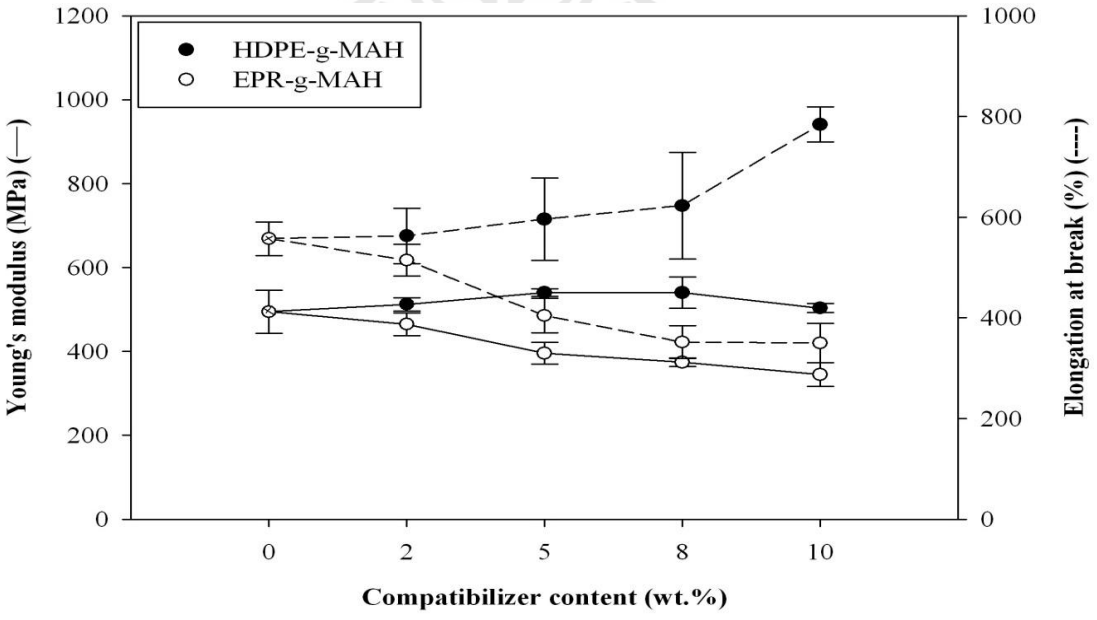

Figure 4.23 Plots of Young's modulus (—) and elongation at break (---) of 20 wt.% ESP2/HDPE composite vs compatibilizer content.

Figure 4.24 shows flexural modulus of 20 wt.% ESP/HDPE composite at various compositions of HDPE-g-MAH and EPR-g-MAH. Flexural modulus of HDPE composite was improved with increasing HDPE-g-MAH content. On the other hand, flexural modulus of the composite was increased at 2 wt.% EPR-g-MAH. At 5-10 wt.% EPR-g-MAH, flexural modulus of the compatibilized HDPE compiosites decreased with increasing EPR-g-MAH content.

Flexural strength of 20 wt.% ESP/HDPE composite at various compositions of HDPE-g-MAH and EPR-g-MAH are shown in Figure 4.24. It was found that HDPE-g-MAH slightly increased flexural strength of the composite. With increasing HDPE-g-MAH content, flexural strength of the compatibilized HDPE composite was slightly increased. On the other hand, as increasing EPR-g-MAH content, flexural strength of the composite was significantly decreased. In addition, tensile properties of 20 wt.% ESP/HDPE composite at various compositions of HDPE-g-MAH and EPR-g-MAH are summarized in Table 4.11. Moreover, flexural modulus and flexural strength of 20 wt.% ESP/HDPE composite at various compositions of HDPE-g-MAH and EPR-g-MAH are listed in Table 4.12.

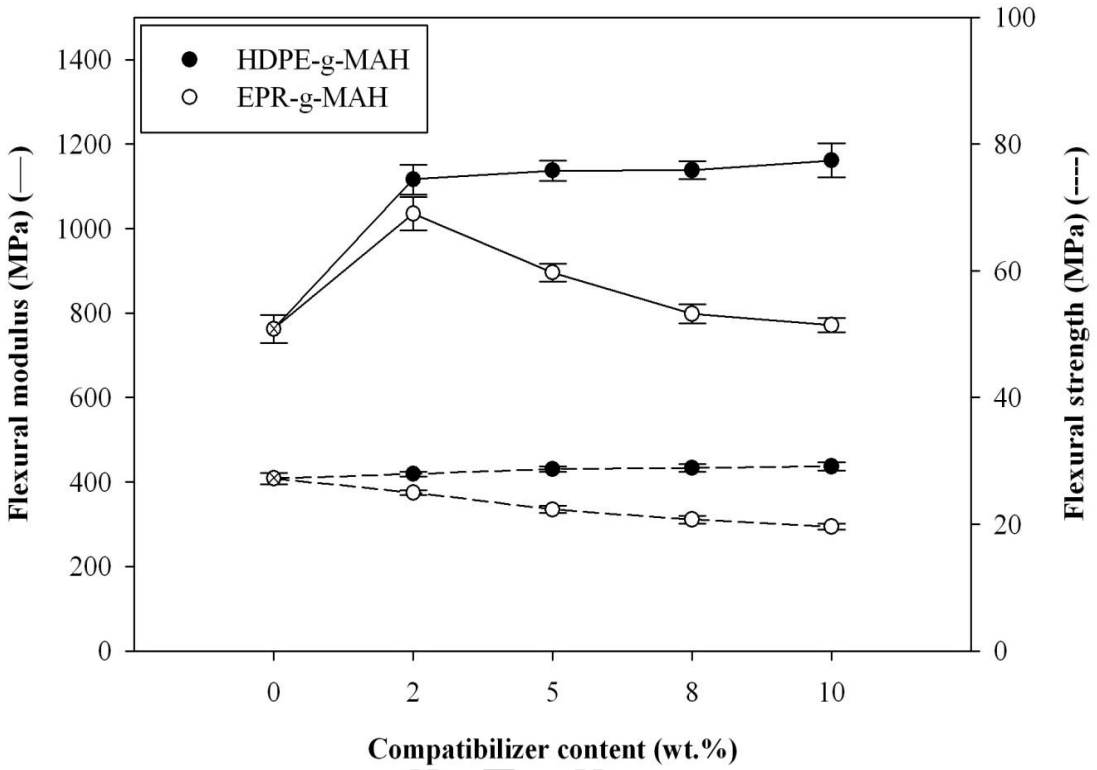

Figure 4.24 Plots of flexural modulus (—) and flexural strength (---) of 20 wt.% ESP2/HDPE composite vs compatibilizer content.

Table 4.11 Yield strength, tensile stress at break, Young's modulus, and elongation at break of the uncompatibilized and compatibilized ESP2/HDPE composite at various HDPE-g-MAH and EPR-g-MAH content.

Compatibilizer (wt%)	Yield strength (MPa)		Tensile stress at break (MPa)		Young's modulus (MPa)		Elongation at Break (%)	
	HDPE-g-MAH	EPR-g-MAH	HDPE-g-MAH	EPR-g-MAH	HDPE-g-MAH	EPR-g-MAH	HDPE-g-MAH	EPR-g-MAH
0	17.8±0.1		12.4±0.1		494.6±51.2		557.2±33.4	
2	18.3±0.1	16.0±0.4	12.7±0.1	11.7±0.2	512.1±15.3	465.2±27.0	562.9±55.4	514.7±31.2
5	19.3±0.2	15.0±0.3	12.9±0.2	11.3±0.2	540.1±8.8	395.8±25.7	596.2±82.3	404.4±34.3
8	19.8±0.2	14.1±0.3	13.3±0.2	10.6±0.2	540.3±36.8	374.5±10.4	623.0±106.0	351.8±32.5
10	19.8±0.3	13.5±0.2	13.6±0.2	10.3±0.2	503.4±10.5	344.7±28.0	784.2±34.8	350.0±38.7

Table 4.12 Flexural modulus and flexural strength of the uncompatibilized and compatibilized ESP2/HDPE composite at various HDPE-g-MAH and EPR-g-MAH content.

Compatibilizer content (wt.%)	Flexural modulus (MPa)		Flexural strength (MPa)	
	HDPE-g-MAH	EPR-g-MAH	HDPE-g-MAH	EPR-g-MAH
0	762.1±33.6		27.2±0.8	
2	1116.4±35.2	1035.0±39.5	27.9±0.3	24.9±0.4
5	1137.3±24.2	895.9±21.4	28.7±0.4	22.3±0.5
8	1138.1±21.7	797.9±22.2	28.8±0.6	20.7±0.6
10	1161.7±41.0	771.1±16.6	29.1±0.6	19.6±0.4

Impact strength of 20 wt.% ESP/HDPE composite at various compositions of HDPE-g-MAH and EPR-g-MAH are shown in Table 4.13. It was found that impact strength of the composites significantly increased when HDPE-g-MAH was added. In addition, the compatibilized HDPE composites at 5, 8, 10 wt.% HDPE-g-MAH did not rupture within instrumentation limit. Comparatively, as increasing EPR-g-MAH content, impact strength of the composite significantly decreased.

From the mechanical properties, it was revealed that HDPE-g-MAH improved tensile stress at break, yield strength, Young's modulus, elongation at break, flexural modulus and flexural strength. These results could be attributed by chemical bonding and ion-dipole interaction between the C=O group of the maleic anhydride and Ca^{2+} ion of eggshell calcium carbonate (Li, Mai, Feng and Haung, 2006). On the other hand, HDPE composites modified with EPR-g-MAH had lower mechanical properties than the HDPE composites modified with HDPE-g-MAH. This might be because the HDPE-g-MAH backbone was more compatible to HDPE matrix than EPR-g-MAH backbone as mentioned in 4.2.3.2.

Table 4.13 Impact strength of the uncompatibilized and compatibilized ESP2/HDPE composite at various HDPE-g-MAH and EPR-g-MAH content.

Compatibilizer content (wt.%)	**Impact strength (kJ/m^2)**	
	HDPE-g-MAH	**EPR-g-MAH**
0	53.1±1.0	
2	57.4±0.4	51.2±3.0
5	>130	50.7±0.9
8	>130	48.7±1.9
10	>130	45.6±1.7

4.2.3.4 Fracture surface morphology

Fracture surface morphology of 20 wt.% ESP2/HDPE composites at various compositions of HDPE-g-MAH and EPR-g-MAH are shown in Figure 4.25. The better interfacial adhesion between ESP2 surface and HDPE phase was observed for the composite compatibilized with HDPE-g-MAH. This was indicated by more HDPE matrix adhering on ESP2 surface as observed from Figure 4.43 (a1) – (a4). This result well corresponded with and improvement of yield and impact strength, mentioned previously. Comparatively, the poor interfacial adhesion between ESP2 surface and HDPE phase was observed for the composite compatibilized with EPR-g-MAH as shown in Figure 4.25 (b1)-(b4). The addition of HDPE-g-MAH and EPR-g-MAH, the particle distribution in ESP2/HDPE was the same. However, the surface topology of the ESP2/HDPE composite compatibilized with HDPE-g-MAH and EPR-g-MAH indicated that the compatibilized HDPE composites still ruptured in a ductile manner.

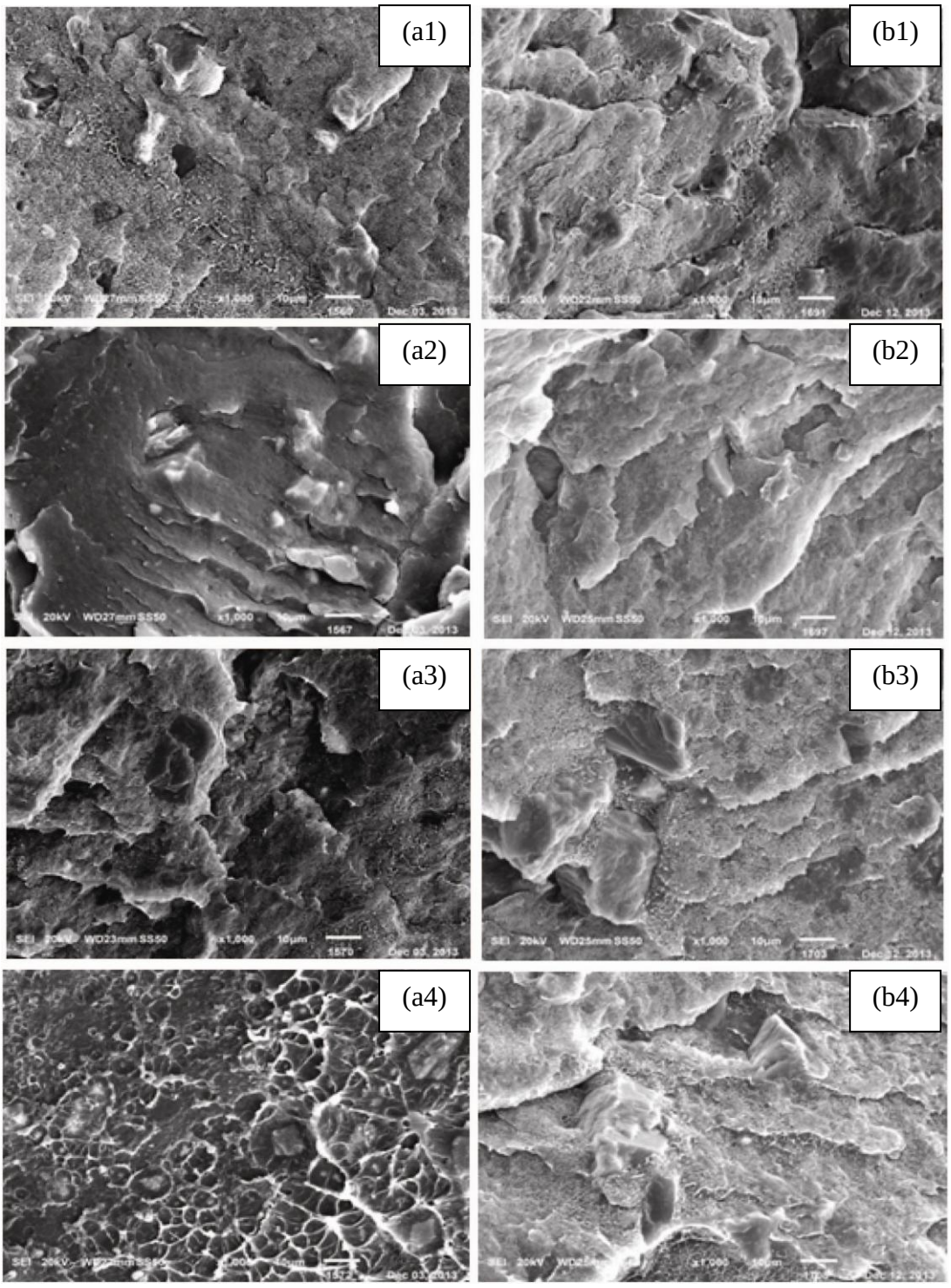

Figure 4.25 SEM micrographs (x1000) of the compatibilized 20 wt.% ESP2/HDPE composite at 2 wt.% (1), 5 wt.% (2), 8 wt.% (3) and 10 wt.% (4) of HDPE-g-MAH (a), and EPR-g-MAH (b).

4.2.3.5 Decomposition temperature

TGA and DTGA curves of compatibilized 20 wt.% ESP2/HDPE composite at various composition of HDPE-g-MAH and EPR-g-MAH are shown in Figure 4.26 and 4.27, respectively. The uncompatibilized and compatibilized HDPE composite at various compositions of HDPE-g-MAH and EPR-g-MAH showed two thermal transitions. The first transition, from 488^{o}C to 490^{o}C was due to the decomposition of HDPE matrix. The second transition from 754^{o}C to 758^{o}C was derived from the decomposition of ESP2. The decomposition temperature of ESP2 insignificantly increased with increasing HDPE-g-MAH and EPR-g-MAH content. However, the decomposition temperature of HDPE matrix was not influenced by addition of HDPE-g-MAH and EPR-g-MAH. In addition, thermal decomposition of 20 wt.% ESP2/HDPE composite at various content of HDPE-g-MAH and EPR-g-MAH are listed in Table 4.14.

Table 4.14 Thermal decomposition of 20 wt.% ESP2/HDPE composite at various contents of HDPE-g-MAH and EPR-g-MAH.

Compatibilizer content (wt.%)	**Composite decomposition temperature (^{o}C)**			
	with HDPE-g-MAH		**with EPR-g-MAH**	
	HDPE	**ESP**	**HDPE**	**ESP**
0	490	754	490	754
2	490	754	489	755
5	490	757	489	757
8	490	757	488	758
10	489	758	488	757

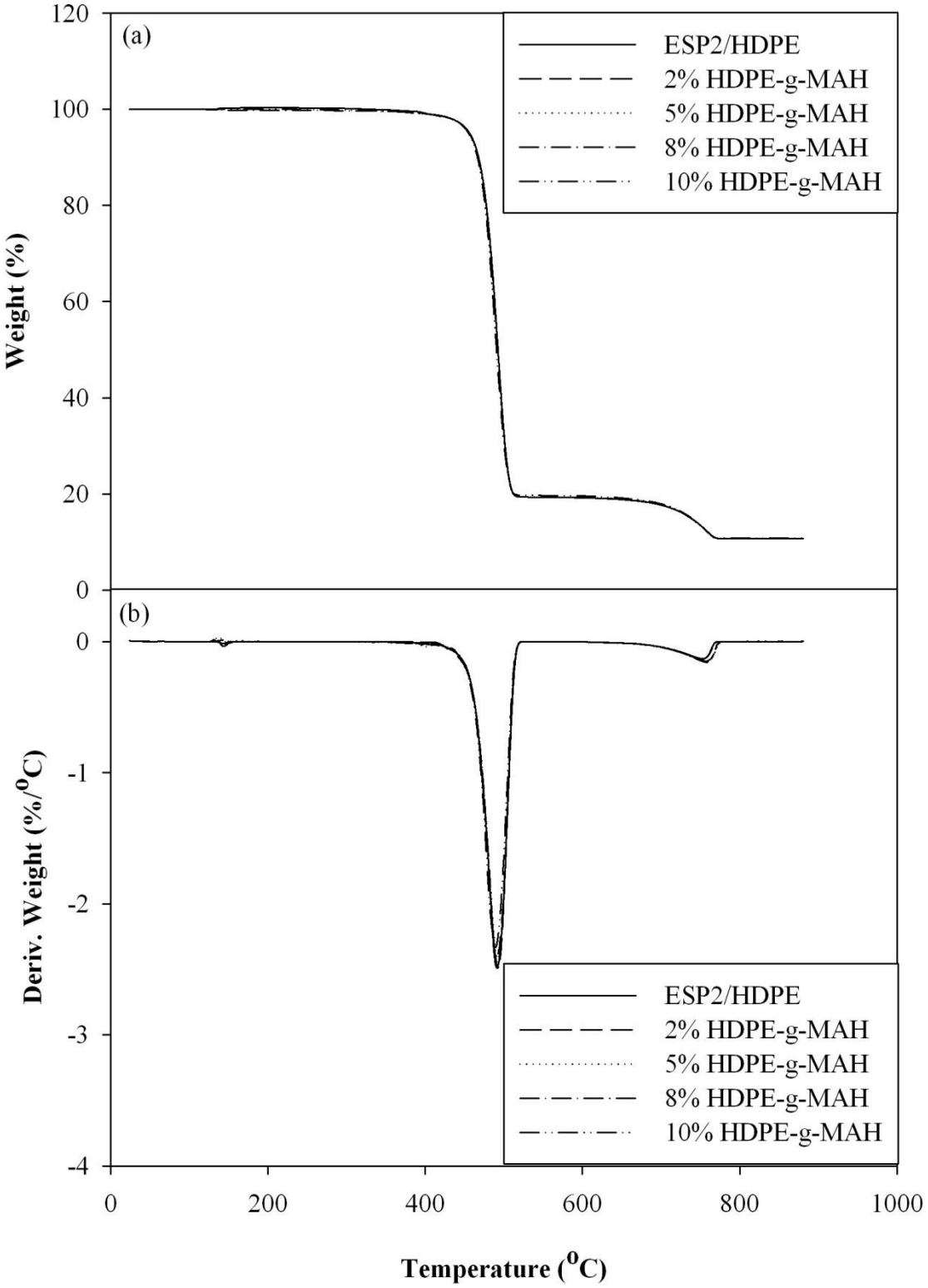

Figure 4.26 TGA (a) and DTGA (b) curves of 20 wt.% ESP2/HDPE composite at various HDPE-g-MAH contents.

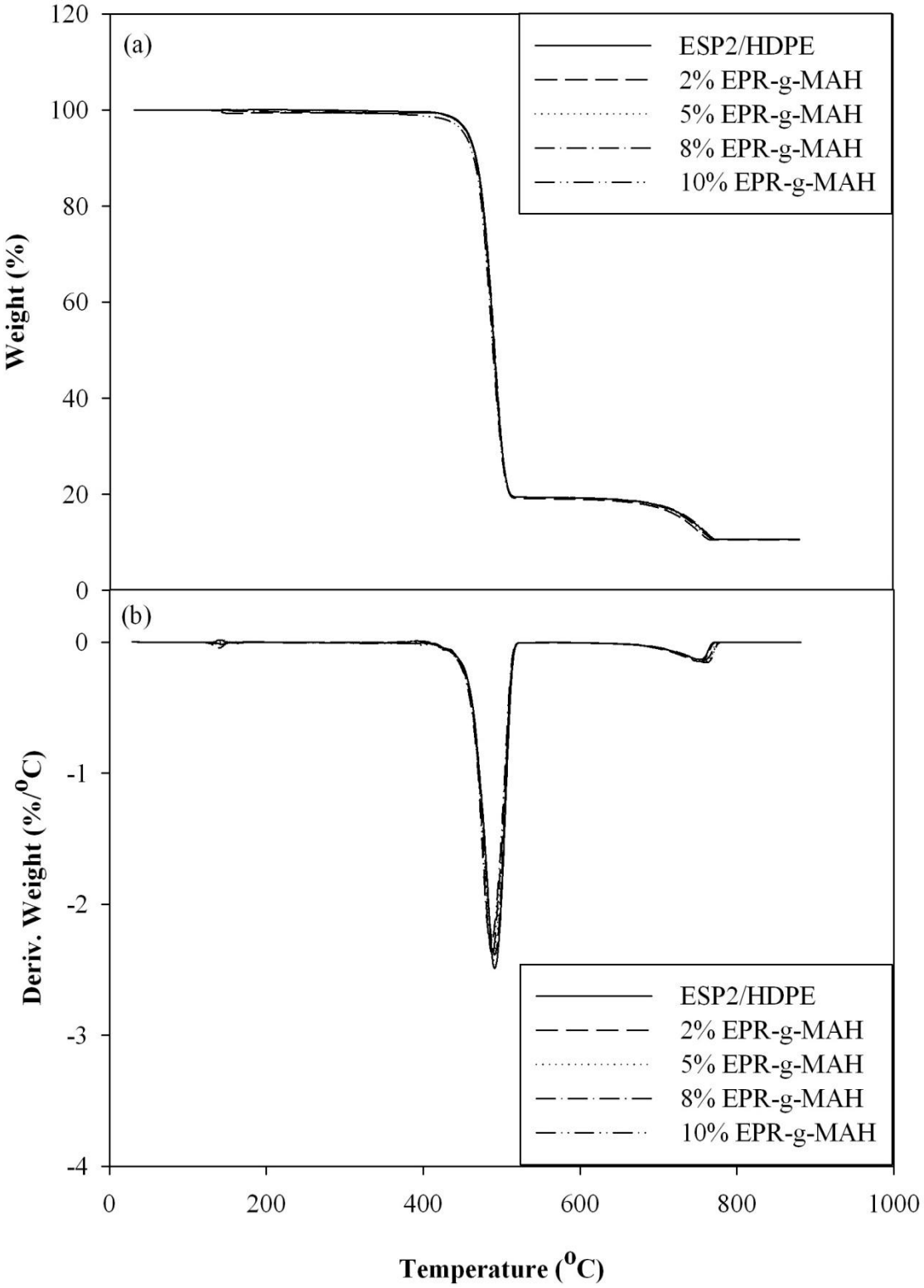

Figure 4.27 TGA (a) and DTGA (b) curves of 20 wt.% ESP2/HDPE composite at various EPR-g-MAH contents.

4.2.3.6 Melting and crystallization temperature

DSC curves of the ESP2/HDPE composite compatibilized with HDPE-g-MAH and EPR-g-MAH are shown in Figure 4.28 and 4.29, respectively. In the first heating curve, the uncompatibilized and compatibilized HDPE with HDPE-g-MAH, shows a single melting behavior, as observed in Figure 4.28 (a). It was found that adding HDPE-g-MAH did not influence melting temperature of HDPE matrix. With increasing HDPE-g-MAH content, melting temperature of HDPE did not change. Similarly, from the second heating scan, HDPE-g-MAH did not affect melting temperature of HDPE matrix, as shown in Figure 4.28 (b).

Melting tempertures of compatibilized ESP2/HDPE composite at 2, 5, 8 and 10 wt.% EPR-g-MAH are presented in Figure 4.29. It was revealed from the first heating scan that addition of EPR-g-MAH did not affect melting temperature of HDPE matrix. With increasing EPR-g-MAH, melting temperature was not much different. Moreover, the second heating scan, EPR-g-MAH content did not affect melting temperature of HDPE matrix as well.

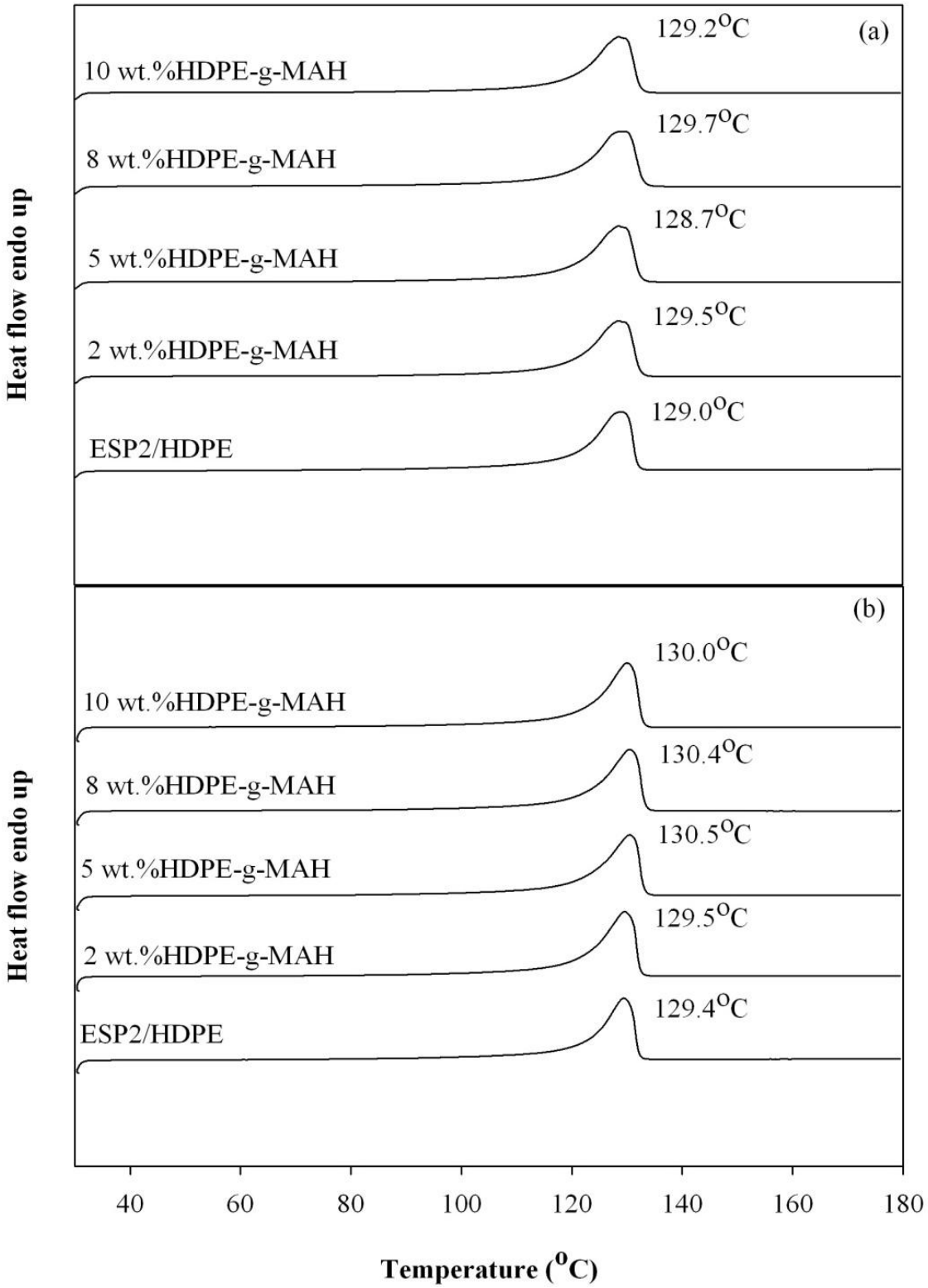

Figure 4.28 DSC curves of 1st heating (a) and 2nd heating (b) scan of 20 wt.% ESP2/HDPE composites at various HDPE-g-MAH contents.

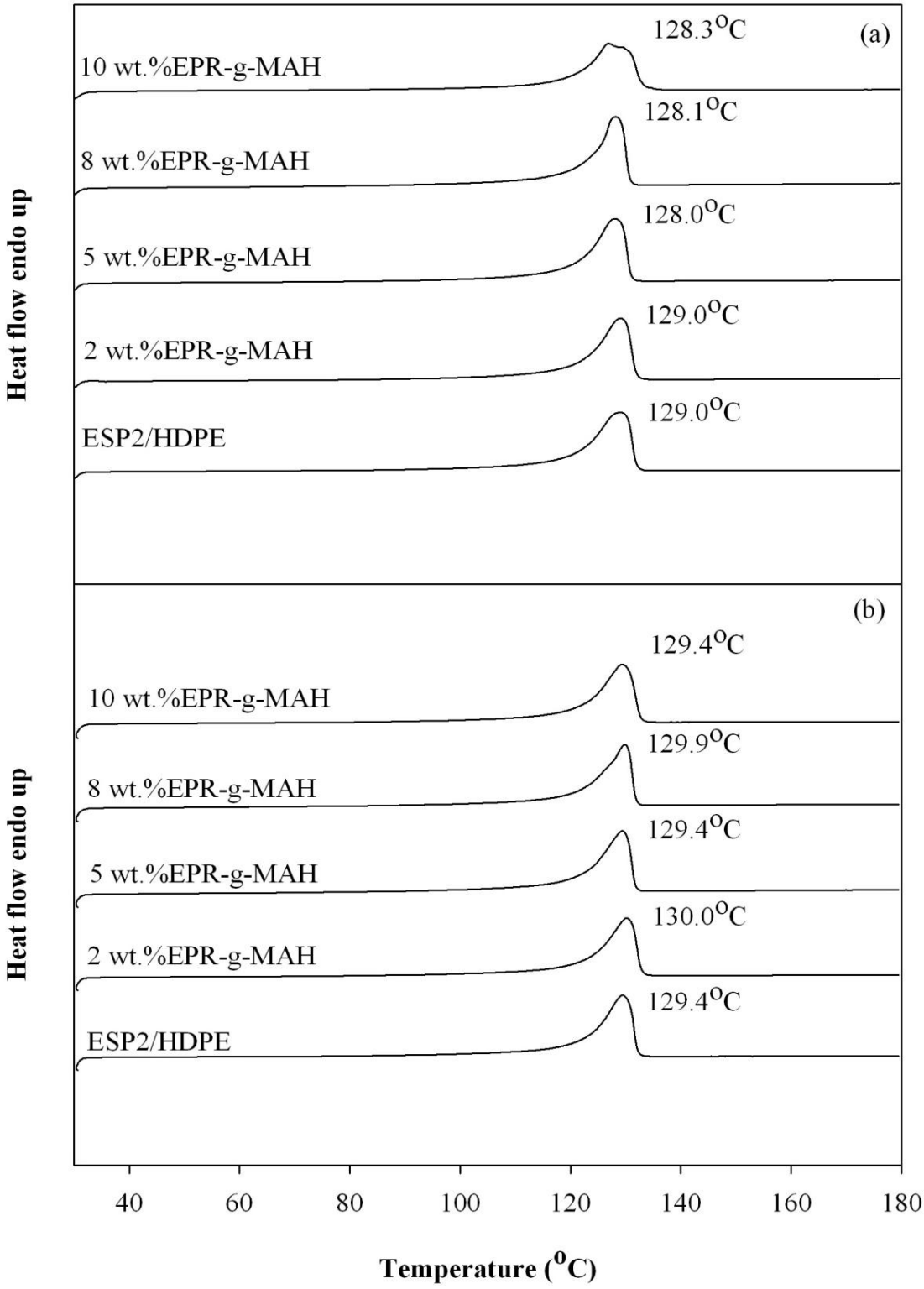

Figure 4.29 DSC curves of 1st heating (a) and 2nd heating (b) scan of 20 wt.% ESP2/HDPE composites at various EPR-g-MAH contents.

Figure 4.30 (a) shows DSC curves obtained from the first cooling of uncompatibilized and compatibilized 20 wt.% ESP2/HDPE composite at 2, 5, 8 and 10 wt.% HDPE-g-MAH. It presented that crystallization temperature of HDPE matrix did not change with the addition of HDPE-g-MAH. With increasing HDPE-g-MAH content, the melting temperature of HDPE matrix did not change, as well. Similarly, the incorporation of EPR-g-MAH in ESP2/HDPE composite insignificantly affect crystallization temperature of HDPE matrix, as observed from Figure 4.30 (b).

Nevertheless, degree of crystallinity of HDPE composites compatibilized with EPR-g-MAH was higher than that of HDPE composites compatibilized with HDPE-g-MAH. As mentioned previously, HDPE matrix more disliked EPR-g-MAH than HDPE-g-MAH, as observed from SEM micrograph in Figure 4.25, therefore during HDPE matrix was crystallization, as foreigners, elastomeric backbone of EPR-g-MAH less disturbed the crystallization process than polyethylene backbone of HDPE-g-MAH did. Adding EPR-g-MAH into ESP2/HDPE composite insignificant affected HDPE's crystallinity. On the other hand, adding 2 wt.% HDPE-g-MAH resulted in significant decrease of crystallinity of HDPE matrix comparing to that of uncompatibilized ESP2/HDPE composite. Nevertheless, the crystallinity increased when adding 5-10 wt.% HDPE-g-MAH.

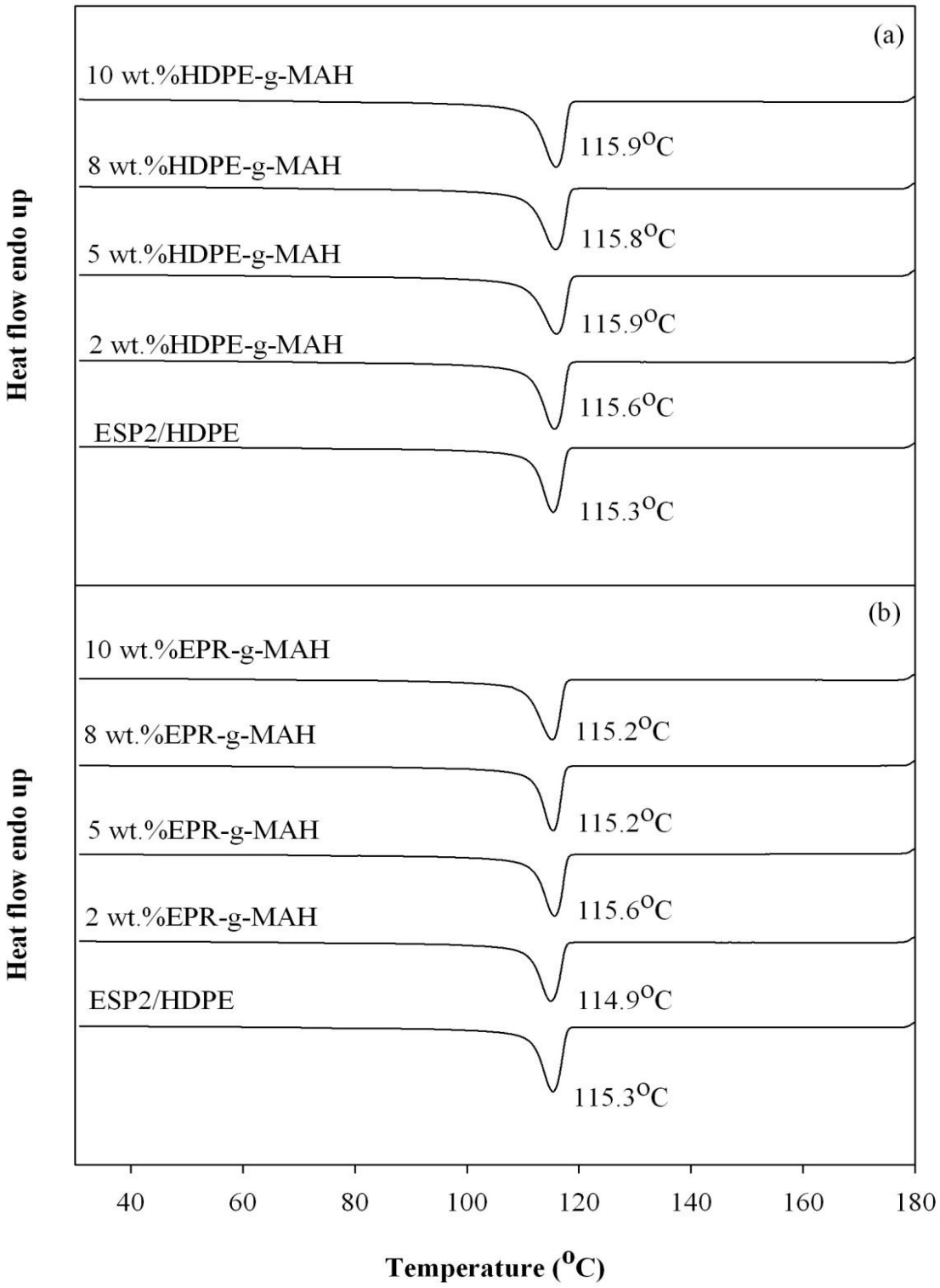

Figure 4.30 DSC curves obtained from the 1st cooling scan of 20 wt.% ESP2/HDPE composite at various HDPE-g-MAH (a) and EPR-g-MAH (b) contents.

Table 4.15 Melting temperature (T_m) and crystallization temperature (T_c) of 20 wt.% ESP/HDPE composite at various HDPE-g-MAH and EPR-g-MAH contents.

Compatibilizer content (wt.%)	T_m, 1st scan (^oC)		T_m, 2nd scan (^oC)		T_c (^oC)	
	HDPE-g-MAH	EPR-g-MAH	HDPE-g-MAH	EPR-g-MAH	HDPE-g-MAH	EPR-g-MAH
0	129.0		129.4		115.3	
2	129.5	129.0	129.5	130.0	115.6	114.9
5	128.7	128.0	130.5	129.4	115.9	115.6
8	129.7	128.1	130.4	129.9	115.8	115.2
10	129.2	128.3	130.0	129.4	115.9	115.2

Table 4.16 Degree of crystallinity (X_c) of 20 wt.% ESP/HDPE composite at various HDPE-g-MAH and EPR-g-MAH contents.

Compatibilizer content (wt.%)	Delta H (J/g), 1st scan		Delta H (J/g), 2nd scan		X_c, 1st scan (%)		X_c, 2nd scan (%)	
	HDPE-g-MAH	EPR-g-MAH	HDPE-g-MAH	EPR-g-MAH	HDPE-g-MAH	EPR-g-MAH	HDPE-g-MAH	EPR-g-MAH
0	213.5		221.6		58.3		60.5	
2	191.3	222.3	219.5	230.8	51.2	59.5	58.8	61.8
5	203.3	225.9	220.6	238.2	52.8	58.6	57.3	61.8
8	226.7	233.2	255.0	242.0	57.0	58.6	64.1	60.8
10	227.9	235.4	261.7	235.4	56.0	57.9	64.4	57.9

4.3 Characterization of PESP/HDPE composites

4.3.1 Effect of PESP content on physical properties of PESP/HDPE composites

4.3.1.1 Flow property

MFI of neat HDPE and PESP/HDPE composite at various PESP content is listed in Table 4.17. It was revealed that MFI of neat HDPE was higher than that of PESP/HDPE composites. Furthermore, MFI of PESP/HDPE composite was slightly decreased with increasing PESP content.

Table 4.17 MFI of neat HDPE, and PESP/HDPE composite at various PESP contents.

PESP content (wt.%)	MFI (g/10 min)
0	11.47
5	10.80
10	10.25
20	7.61

4.3.1.2 Stress-strain behavior

For tensile properties, the tensile stress-strain curves of neat HDPE and PESP/HDPE composite are shown in Figure 4.31. At tension rate of 10 mm/sec within instrumentation limit. The specimens of neat HDPE and PESP/HDPE composite at 5 and 10 wt.% PESP did not break. At 20 wt.% PESP content, the tensile stress-strain curve of HDPE composite showed cold drawing region before the specimen fractured. It might be because the hard and rigid particles of PESP restricted

the mobility and deformation of the polymer matrix as increasing PESP content (Yun Fu, Qiao Feng, Lauke and Wing Mai, 2008).

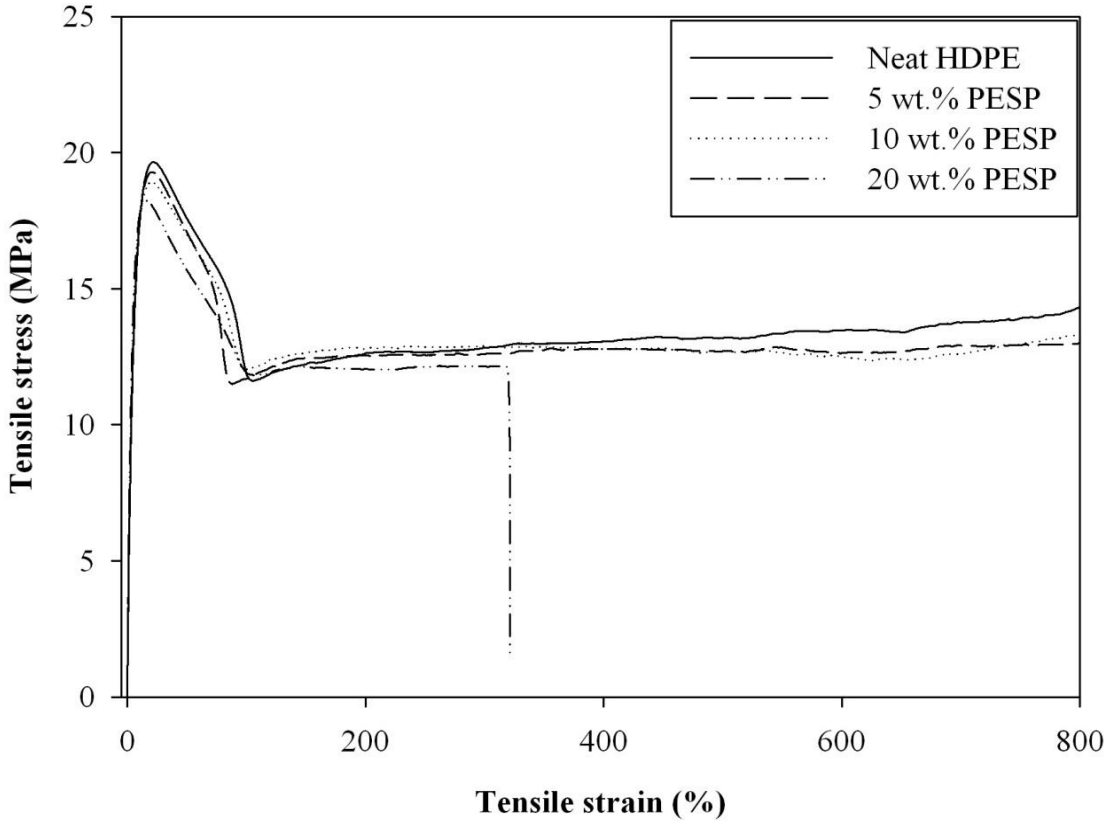

Figure 4.31 Tensile stress-strain curve of neat HDPE, and PESP/HDPE composite at various PESP contents.

4.3.1.3 Mechanical properties

From Figure 4.32, yield strength of neat HDPE and HDPE composite significantly decreased with increasing PESP content. In addition, tensile stress at break of PESP/HDPE composite is shown in Figure 4.32 as well. The specimens of neat HDPE and PESP/HDPE composite at 5 and 10 wt.% PESP did not break. However, at 20 wt.% PESP, HDPE composite showed tensile stress at break.

This might be because of formation of PESP particle aggregation. This aggregation led to a decrease of tensile stress at break and yield strength.

Young's modulus and elongation at break of neat HDPE and PESP/HDPE composite are shown in Figure 4.33. It was found that Young's modulus of the composite slightly increased with increasing PESP content. This was due to the incorporation of rigid particle of PESP. From elongation at break, the specimens of neat HDPE, and PESP/HDPE composite at 5 and 10 wt.% PESP did not break within an instrumentation limit. However, elongation at break of PESP/HDPE composite decreased with the addition of 20 wt.% PESP.

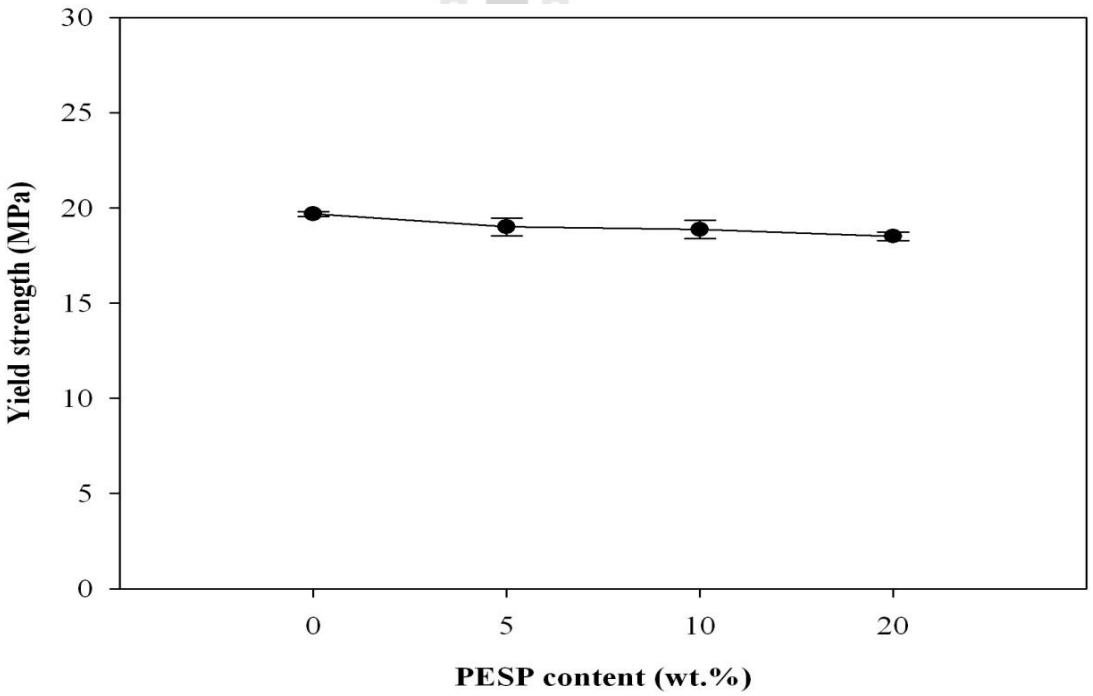

Figure 4.32 Plots of yield strength vs PESP content of PESP/HDPE composite.

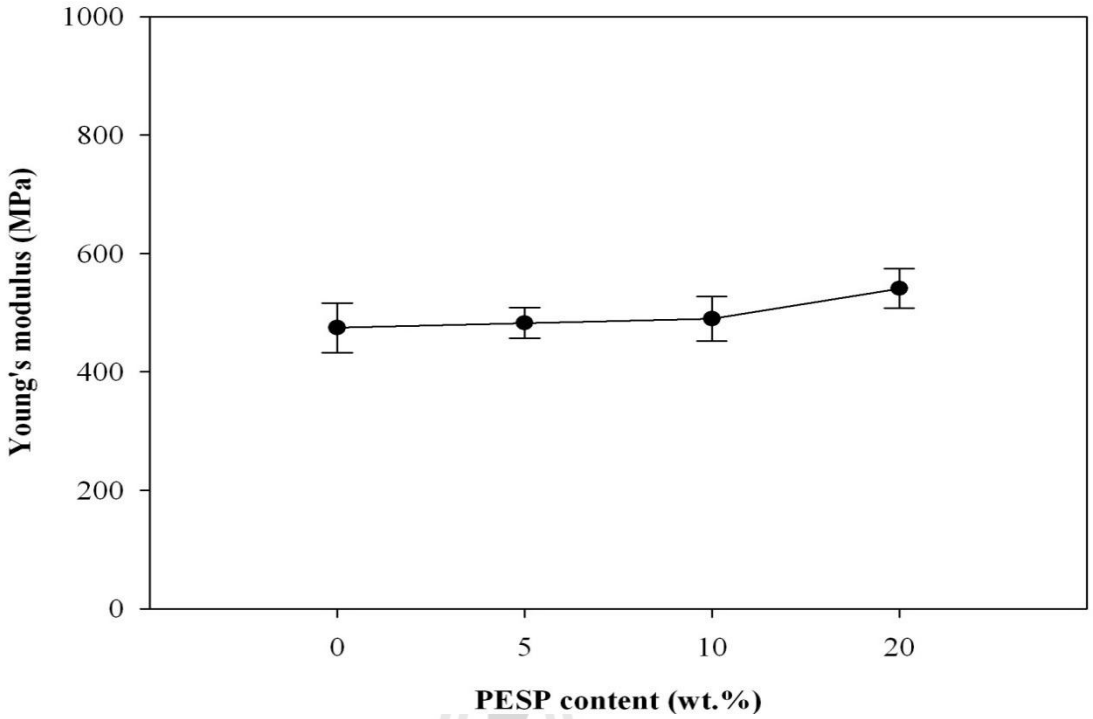

Figure 4.33 Plots of Young's modulus vs PESP content of PESP/HDPE composite.

Figure 4.34 shows flexural modulus and flexural strength of neat HDPE and PESP/HDPE composite with various PESP contents. It was observed that flexural modulus improved via the addition of PESP and their modulus was slightly increased with increasing PESP content. However, flexural strength of neat HDPE and HDPE composite at various PESP contents was insignificantly different. In addition, mechanical properties of HDPE composite prepared with PESP are summarized in Table 4.19.

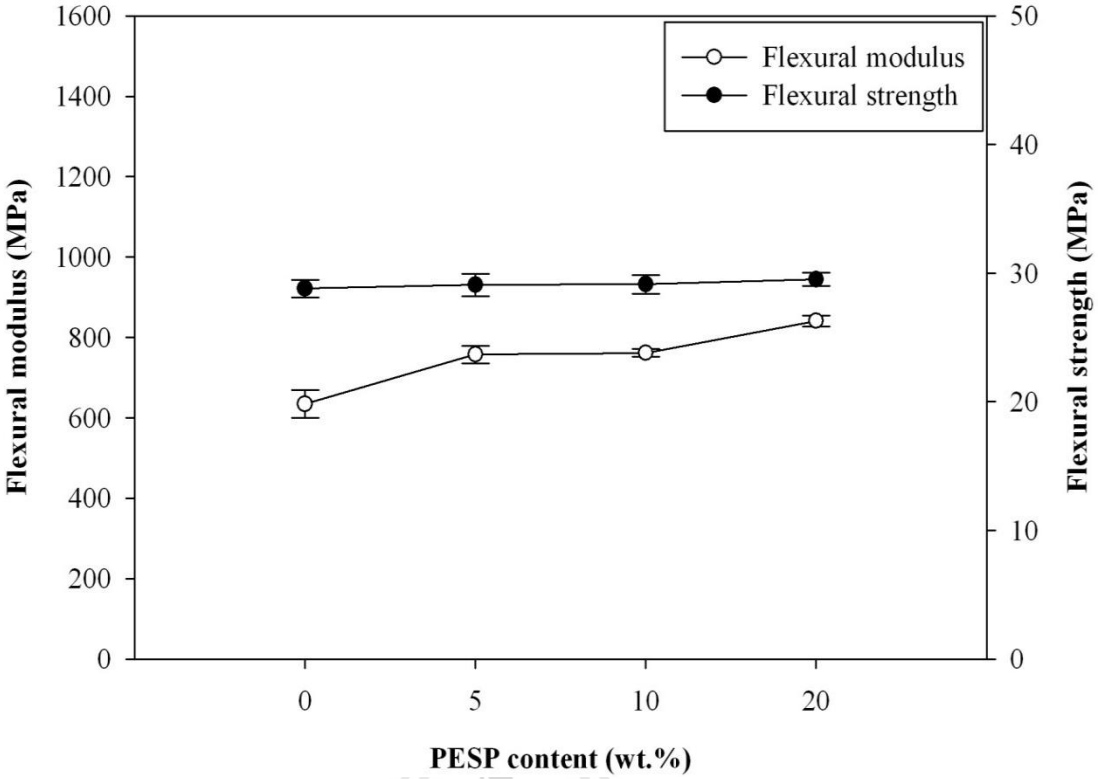

Figure 4.34 Plots of flexural modulus and flexural strength vs PESP content of PESP/HDPE composite.

Impact strength of neat HDPE and PESP/HDPE composite at various PESP content is presented in Table 4.18. The result showed that the incorporation of PESP filler at 20 wt.% decreased impact strength of the filled HDPE. Nevertheless, the impact strength of neat HDPE and PESP/HDPE composite at 5 and 10 wt.% PESP was not obtained because they did not break within an instrumentation limit. In addition, impact strength of HDPE composite prepared with 5 and 10 wt.% PESP was still higher than 130 kJ/m^2.

Table 4.18 Impact strength of neat HDPE, and PESP/HDPE composite at various PESP contents.

PESP content (wt.%)	Impact strength (kJ/m^2)
0	>130
5	>130
10	>130
20	46.0±5.8

Table 4.19 Young's modulus, elongation at break, yield strength, tensile stress at break, flexural modulus and flexural strength of PESP/HDPE composite at various PESP contents.

PESP content (wt.%)	Young's modulus (MPa)	Elongation at break (%)	Yield strength (MPa)	Tensile stress at break (MPa)	Flexural modulus (MPa)	Flexural strength (MPa)
0	474.4±42.0	>800	19.6±0.1	Not obtained	634.5±31	28.8±0.6
5	482.6±26.0	>800	19.0±0.4	Not obtained	757.7±22.1	29.0±0.8
10	489.6±37.9	>800	18.8±0.4	Not obtained	761.7±9.3	29.1±0.7
20	540.8±33.6	353.3±87.4	18.5±0.2	10.1±1.9	841.5±13.3	29.5±0.5

4.3.1.4 Fracture surface morphology

Fracture surface morphologies of PESP/HDPE composite at various PESP contents are shown in Figure 4.35. It is seen that PESP/HDPE composites had a rough surface with PESP aggregate which was in sphere, cubic and irregular shape. When PESP content increased to 20 wt.%, PESP aggregate was obviously observed: this led to poor mechanical properties of PESP/HDPE composite. Distribution of PESP particles in HDPE matrix was hardly observed from fracture surface of HDPE with 5 wt.% PESP. Nevertheless, the HDPE filled with PESP still ruptured in a ductile manner.

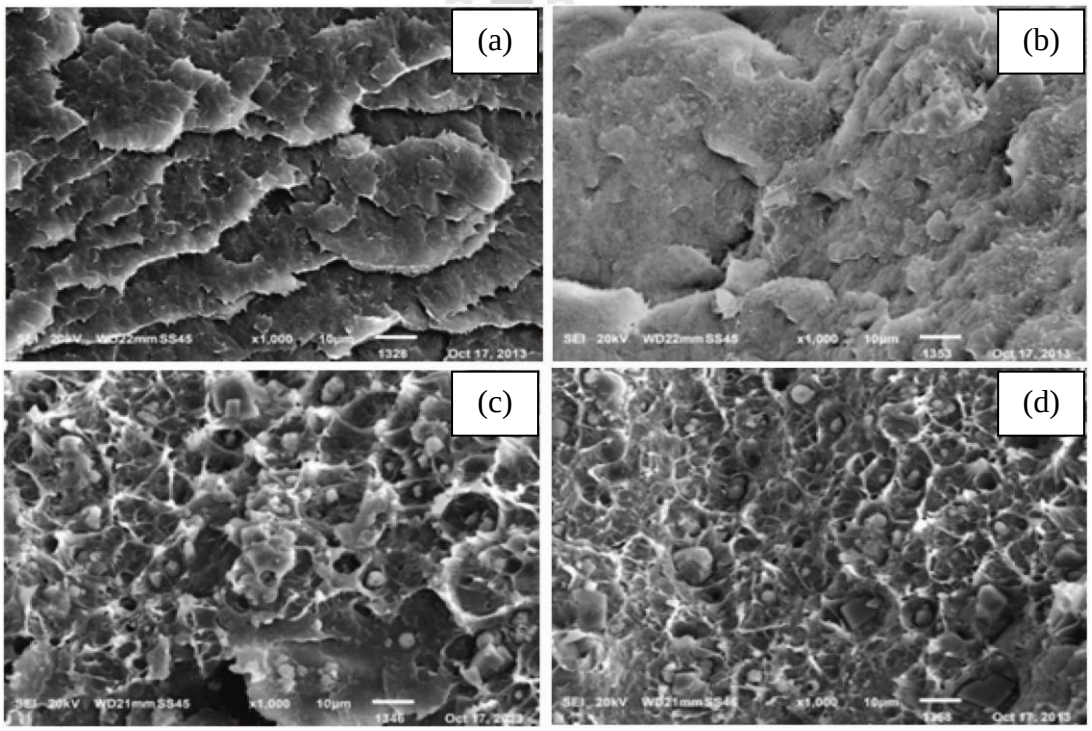

Figure 4.35 SEM micrographs (x1000) of neat HDPE (a), and PESP/HDPE composite at 5 wt.% PESP (a), 10 wt.% PESP (b) and 20 wt.% PESP (c).

4.3.1.5 Decomposition temperature

TGA and DTGA curves of neat HDPE and PESP/HDPE composite at various PESP contents are shown in Figure 4.36. Neat HDPE thermally decomposed as a single transition at 481^{o}C whereas PESP/HDPE composites decomposed with two thermal transitions. The first transitions due to decomposition of HDPE matrix were 484, 486 and 489^{o}C for HDPE filled with 5, 10 and 20 wt.% PESP, respectively. The second transition derived from decomposition of precipitated eggshell calcium carbonate was around 733, 754, 764 and 777^{o}C for HDPE filled PESP with 5, 10 and 20 wt.%, respectively. The addition of PESP into HDPE significantly increased thermal decomposition temperature of HDPE matrix. In addition, the decomposition temperature of PESP in the composite increased with increasing PESP content.

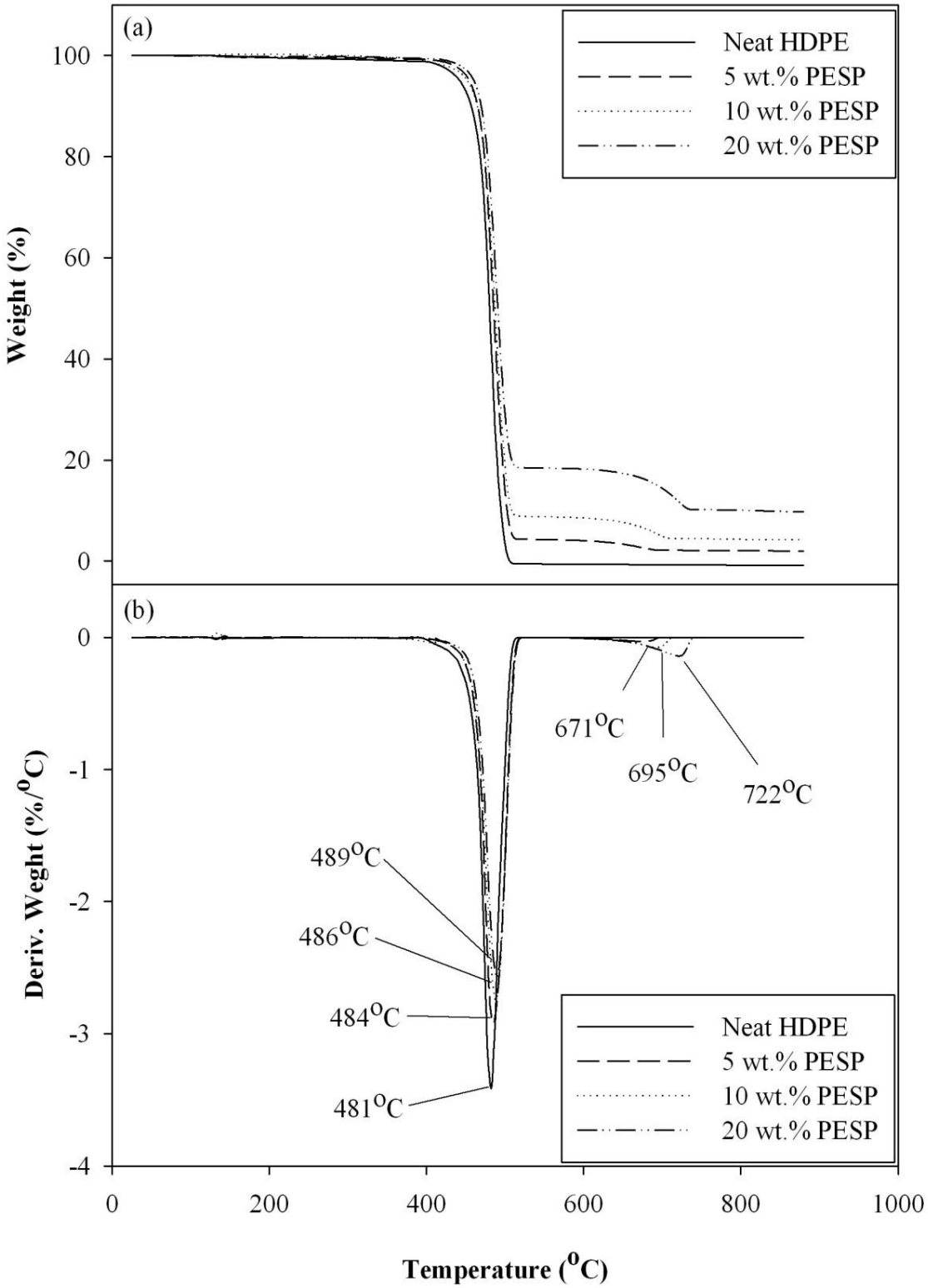

Figure 4.36 TGA (a) and DTGA (b) curves of neat HDPE, and PESP/HDPE composite at various PESP contents.

4.3.1.6 Melting and crystallization temperature

DSC curves of neat HDPE and PESP/HDPE composites at vartous PESP contents are shown in Figure 4.37. In the first heating scan, neat HDPE and ESP3/HDPE composites, showed a single melting behavior during heating process. It was found that incorporation of PESP into HDPE decreased melting temperature of HDPE matrix. With increasing PESP content, the melting temperature slightly decreased. However, for the 2^{nd} heating scan, PESP content did not significantly affect melting temperature of HDPE matrix.

From Figure 4.38, PESP content slightly affect crystallization temperature of HDPE matrix. Incorporation of PESP resulted in higher crystallization temperature of HDPE matrix. This was because PESP acted as a nucleating agent for HDPE crystallinity. However, PESP content did not resulting in any change of HDPE crystallization temperature. On the other hand, degree of crystallinity of PESP/HDPE composites slightly decreased with increasing PESP content. Melting temperature, crystallization temperature and crystallinity's degree of neat HDPE and PESP/HDPE composite at various PESP contents are listed in Table 4.20.

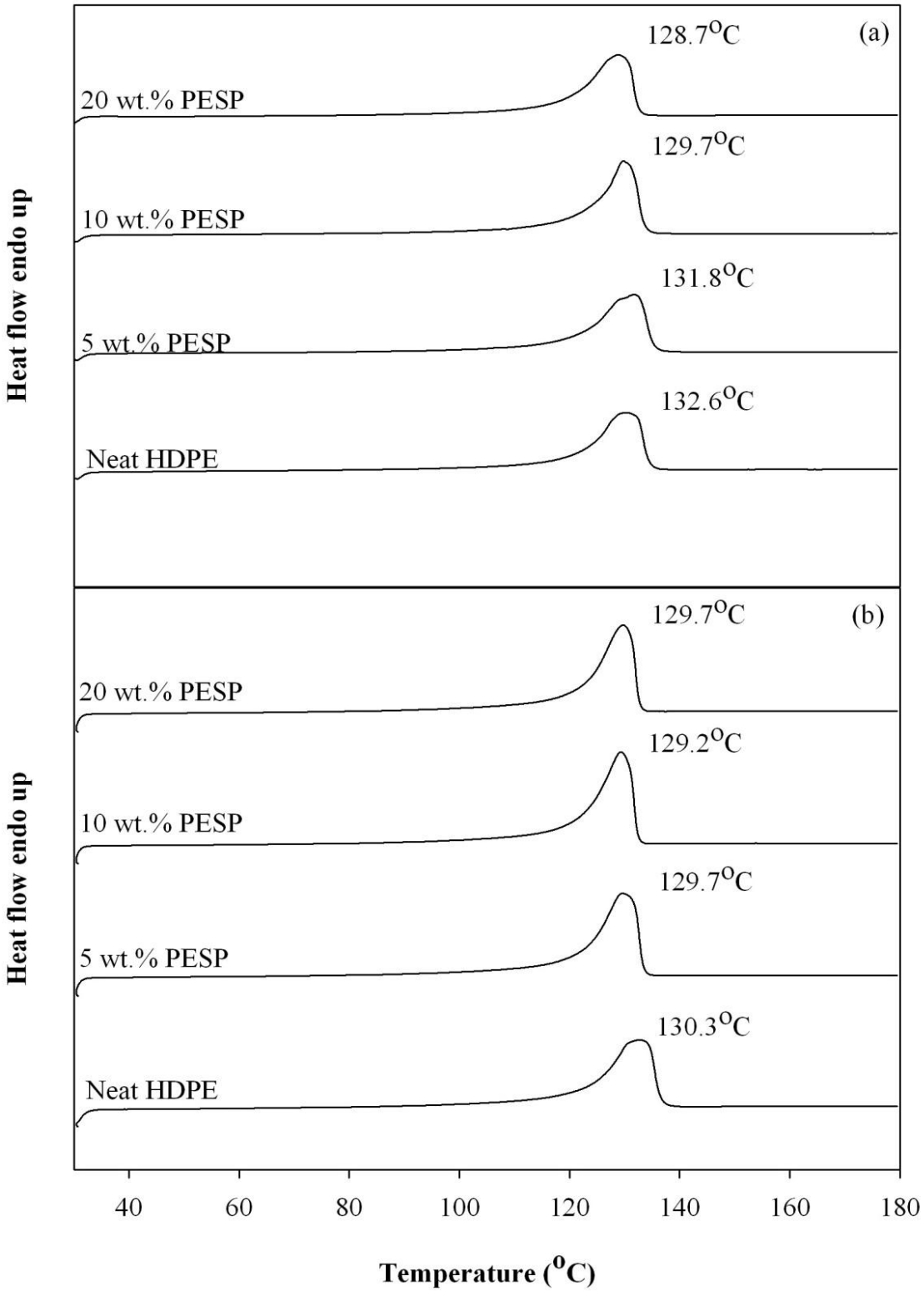

Figure 4.37 DSC curves of 1st heating (a) and 2nd heating (b) scan of PESP/HDPE composites.

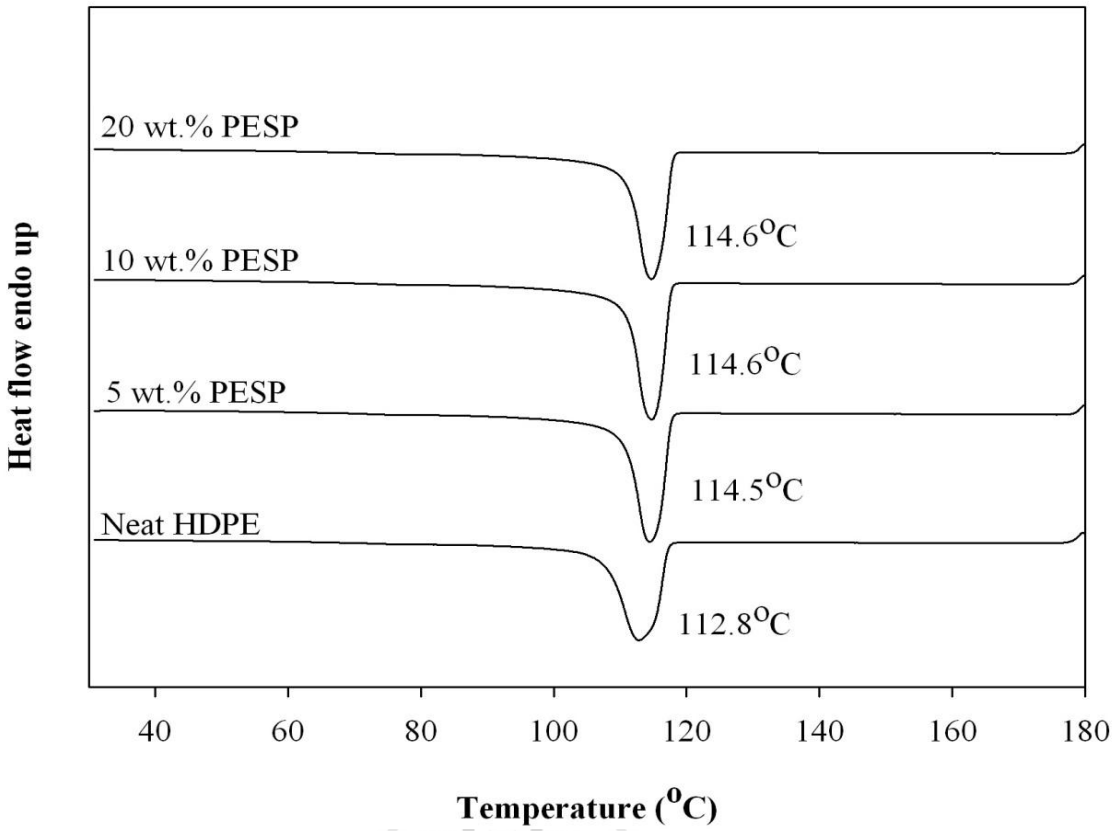

Figure 4.38 DSC curves obtained from the 1st cooling scan of PESP/HDPE at various PESP contents.

Table 4.20 Melting temperature (T_m), crystallization temperature (T_c) and degree of crystallinity (X_c) of neat HDPE and HDPE composite at various PESP contents.

PESP content (wt.%)	T_d (^oC)		T_m (^oC)		T_c (^oC)	Delta H (J/g)		X_c (%)	
	HDPE	PESP	1st scan	2nd scan		1st scan	2nd scan	1st scan	2nd scan
Neat HDPE	481	-	130.3	132.6	112.8	206.3	227.9	70.5	77.9
5	484	671	131.8	129.7	114.5	205.1	226.6	66.6	73.6
10	486	695	129.7	129.2	114.6	210.8	224.7	64.8	69.1
20	489	722	128.7	129.7	114.6	220.7	223.5	60.4	61.1

4.3.2 Comparative physical properties of ESP3/HDPE and PESP/HDPE composites

4.3.2.1 Flow property

MFI of HDPE filled with 20 wt.% of ESP3 and PESP are shown in Table 4.21. The PESP/HDPE composite was slightly higher than the ESP3/HDPE composite. This was because PESP had two type of crystal form; vaterite and calcite. The hardness of vaterite crystal had lower than that of calcite crystal form. Thus, PESP might lower restrict the mobility and flow of polymer chain than the ESP3.

Table 4.21 MFI of HDPE composite filled with ESP3 and PESP.

Material	MFI (g/10 min)
ESP3/HDPE	6.08
PESP/HDPE	7.61

4.3.2.2 Stress-strain behavior

The tensile stress-strain curves of ESP3/HDPE and PESP/HDPE composite are shown in Figure 4.39. At 20 wt.% filler content, the tensile stress-strain curve of ESP3/HDPE and PESP/HDPE composites showed cold drawing region before fracture at a tension rate of 10 mm/sec. However, ESP3/HDPE composite had higher extension region than the PESP/HDPE composite before the test specimen was fractured. This is an indication that, under tensile deformation, the HDPE composite with ESP3 particle in calcite form was able to absorb more applied energy prior to the composite rupture than the composite with PESP. This was

corresponded with the PESP particles had higher dispersion than the ESP3 particle in HDPE matrix as observed from SEM micrograph in Figure 4.41.

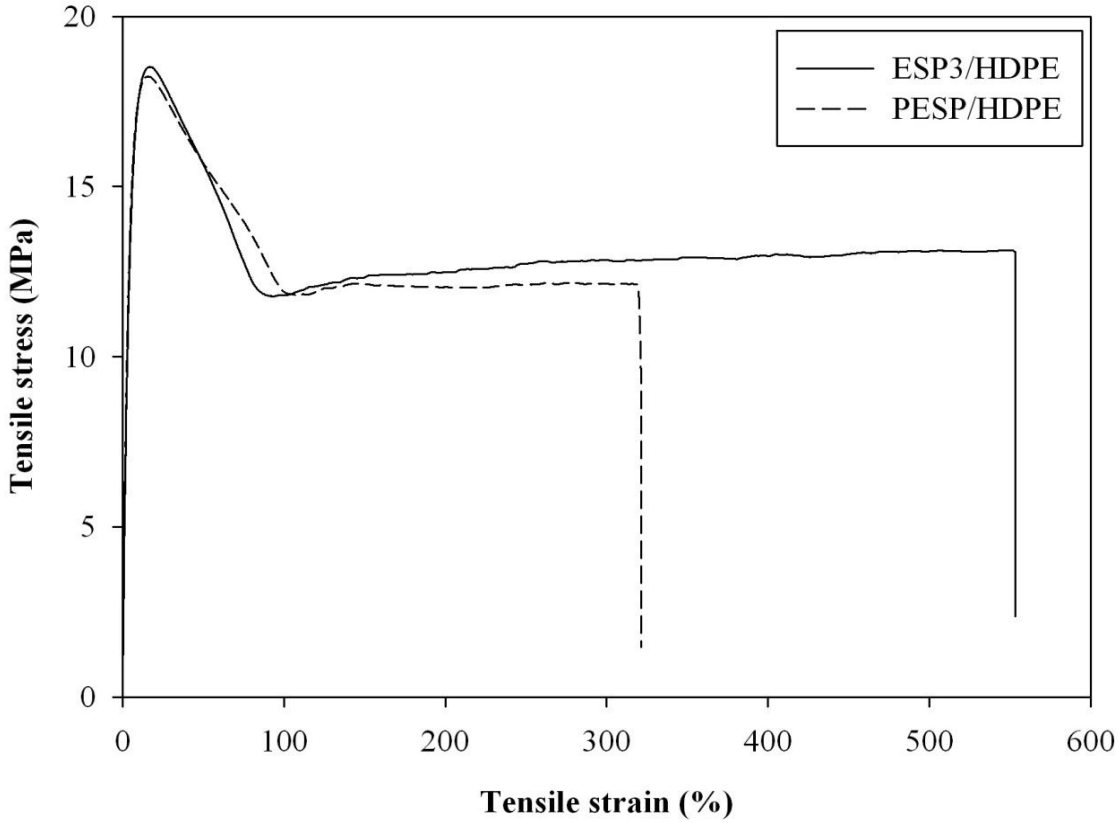

Figure 4.39 Tensile stress-strain curves of 20 wt.% ESP3/HDPE and PESP/HDPE composites.

4.3.2.3 Mechanical properties

Figure 4.40 shows Young's modulus, elongation at break, yield strength, tensile stress at break, flexural modulus, flexural strength and impact strength of ESP3/HDPE and PESP/HDPE composites. Actually, yield strength and tensile stress at break of ESP3/HDPE and PESP/HDPE composite were not different.

Comparatively, Young's modulus of PESP/HDPE composite was slightly higher than that of the ESP3/HDPE composite. In addition, elongation at break of the composite with ESP3 was higher than that of the composite with PESP. This might be due to the different in shape and polymorph between ESP3 and PESP. ESP3 contained purely calcite polymorph. PESP contained not only calcite but also vaterite form. The calcite form was higher hardness than the vaterite form (Xu et al., 2011). Therefore, the incorporation of ESP3 into HDPE resulted in improved the toughness properties of the composite. However, the particle size of ESP3 and PESP was not much different.

Flexural modulus of PESP/HDPE composite was slightly higher than that of ESP3/HDPE composite. However, there was no significant difference in flexural strength of ESP3/HDPE and PESP/HDPE composite. Under impact loading, it was found that the ability to absorb impact energy of HDPE composite prepared with ESP3 was higher than that of the composite prepared with PESP. This result well corresponded with area under stress-strain curve from tensile test of the ESP3/HDPE and PESP/HDPE composite. It indicated that the different particle characteristics of ESP3 and PESP did affect mechanical properties of the filled HDPE, except slight different in toughness and impact strength.

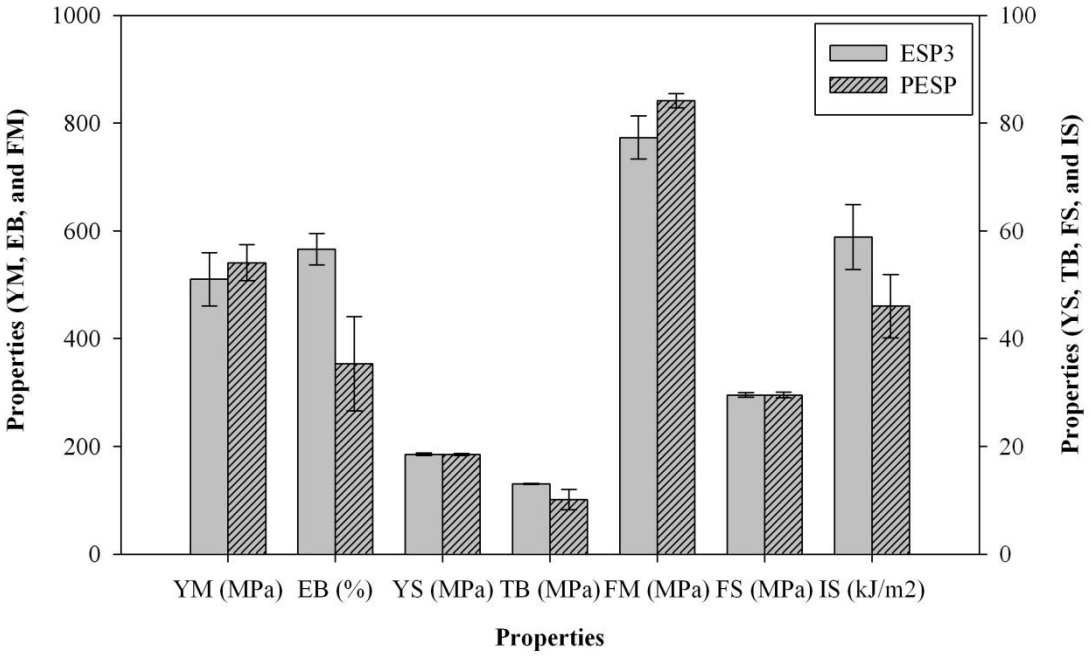

Figure 4.40 Plots of Young's modulus (YM), elongation at break (EB), yield strength (YS), tensile stress at break (TB), flexural modulus (FM), flexural strength (FS) and impact strength (IS) of 20 wt.% ESP3/HDPE and 20 wt.% PESP/HDPE composites.

Table 4.22 Young's modulus, elongation at break, yield strength, tensile stress at break, flexural modulus, flexural strength and impact strength of HDPE composite filled with 20 wt.% ESP3 and 20 wt.% PESP.

HDPE composite	Young's modulus (MPa)	Elongation at break (%)	Yield strength (MPa)	Tensile stress at break (MPa)	Flexural modulus (MPa)	Flexural strength (MPa)	Impact strength (kJ/m^2)
ESP3/HDPE	510.0±49.0	565.7±29.0	18.5±0.2	13.0±0.1	773.3±40.0	29.5±0.4	58.8±6.0
PESP/HDPE	540.8±33.6	353.3±87.4	18.5±0.2	10.1±1.9	841.5±13.3	29.5±0.5	46.0±5.8

4.3.2.4 Fracture surface morphology

Fracture surface morphology of ESP3/HDPE and PESP/HDPE composites is shown in Figure 4.41. Several holes were observed on the fracture surface of ESP3/HDPE and PESP/HDPE composite. These holes were caused from detaching of ESP3 and PESP particle from HDPE matrix. This was because the interfacial adhesion between fillers surface and HDPE matrix was not good. However, the composite with PESP in Figure 4.41 (b) exhibited better distribution of PESP particle in HDPE matrix than the composite with ESP3 in Figure 4.41 (a). However, the surface topology of HDPE filled with ESP3 and PESP indicated that the filled HDPE still ruptured in a ductile manner.

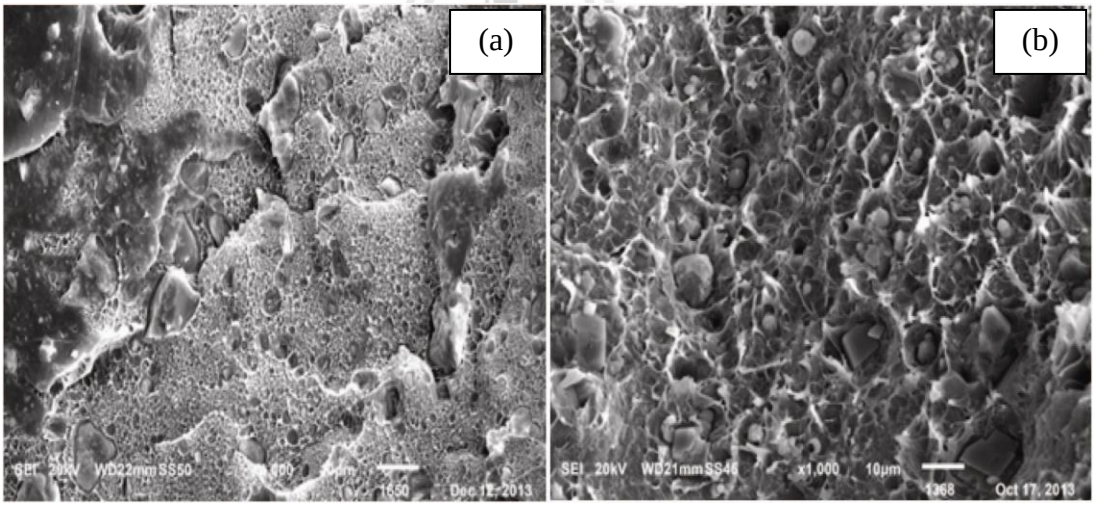

Figure 4.41 SEM micrographs (x1000) of 20 wt.% ESP3/HDPE composite (a) and 20 wt.% PESP/HDPE composite (b).

4.3.2.5 Decomposition temperature

Figure 4.42 shows TGA and DTGA curves of ESP3/HDPE and PESP/HDPE composites. The ESP3/HDPE and PESP/HDPE composites displayed the decomposition process in two stages. The first transition was at the temperature about 487^{o}C due to the thermal decomposition of the HDPE matrix. The second transition occurred in the temperature at 753 and 723^{o}C for HDPE filled with ESP3 and PESP respectively. The ESP3 and PESP did not affect decomposition temperature of HDPE matrix. Nevertheless, the decomposition temperature of PESP in the composite was lower than that of the ESP3 in the composite. This was probably because the vaterite form in PESP was an unstable phase (Xu et al., 2011). Moreover, the particle size range of PESP was quite homogenous and narrow than that of ESP3 leading to good in heat transfer, resulting in decomposition at lower temperature.

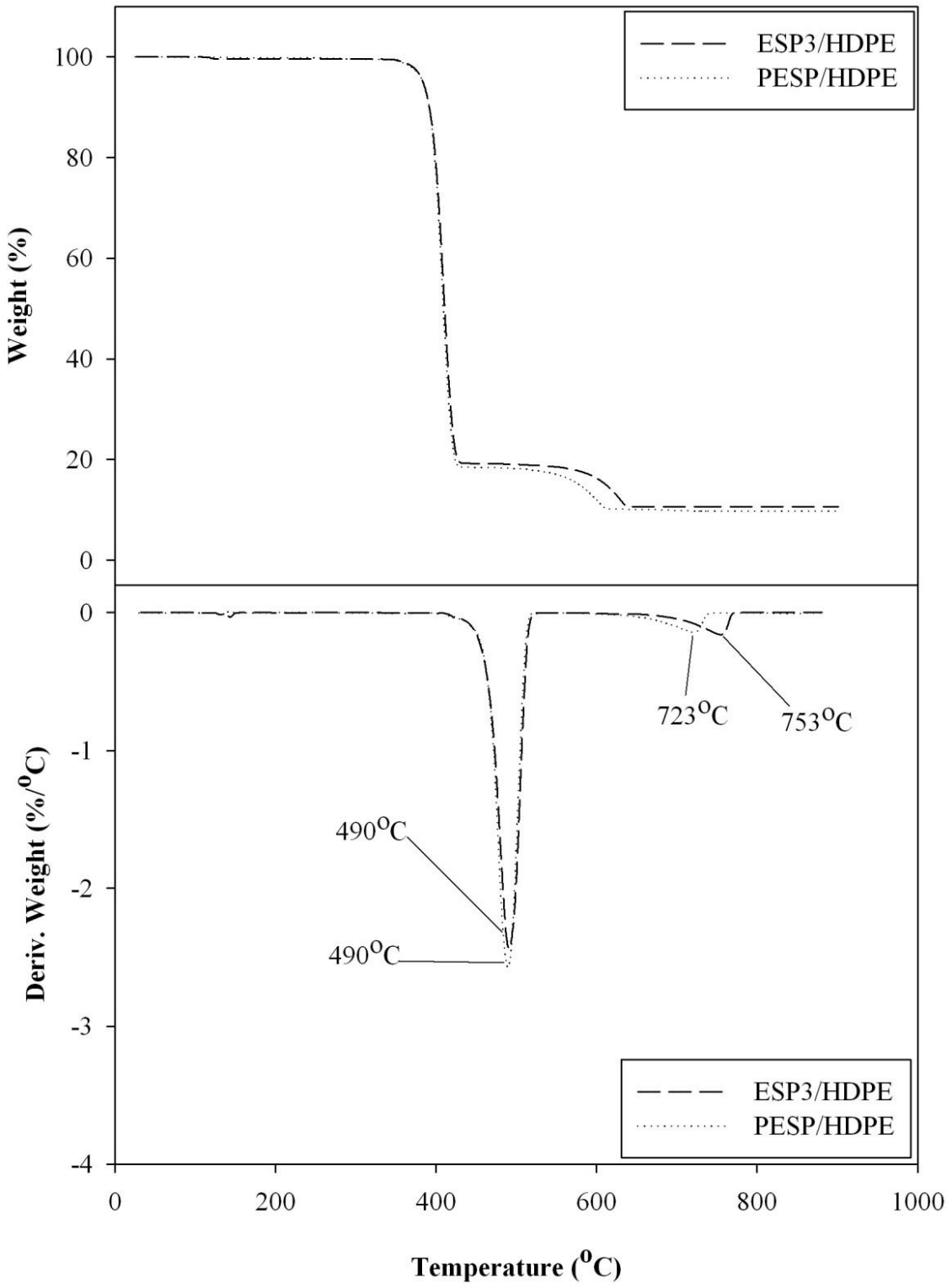

Figure 4.42 TGA and DTGA curves of neat HDPE, 20 wt.% ESP/HDPE and 20 wt.% PESP/HDPE composites.

4.3.2.6 Melting and crystallization temperature

DSC curves of 20 wt.% ESP3/HDPE and 20 wt.% PESP/HDPE composites are shown in Figure 4.43. It was found from the first heating scan that the ESP3 and PESP particles did not affect melting temperature of HDPE matrix. Furthermore, the second heating scan showed a single melting behavior during heating process. It was found that incorporation of ESP3 and PESP did not influence melting temperature of HDPE matrix as well.

From Figure 4.44, HDPE filled with ESP3 had slightly higher crystallization temperature than the HDPE filled with PESP. In addition, HDPE filled with ESP3 had higher crystallinity degree than the HDPE filled with PESP. Melting temperature, crystallization temperature and crystallinity degree of HDPE composite prepared with ESP3 and PESP are shown in Table 4.23.

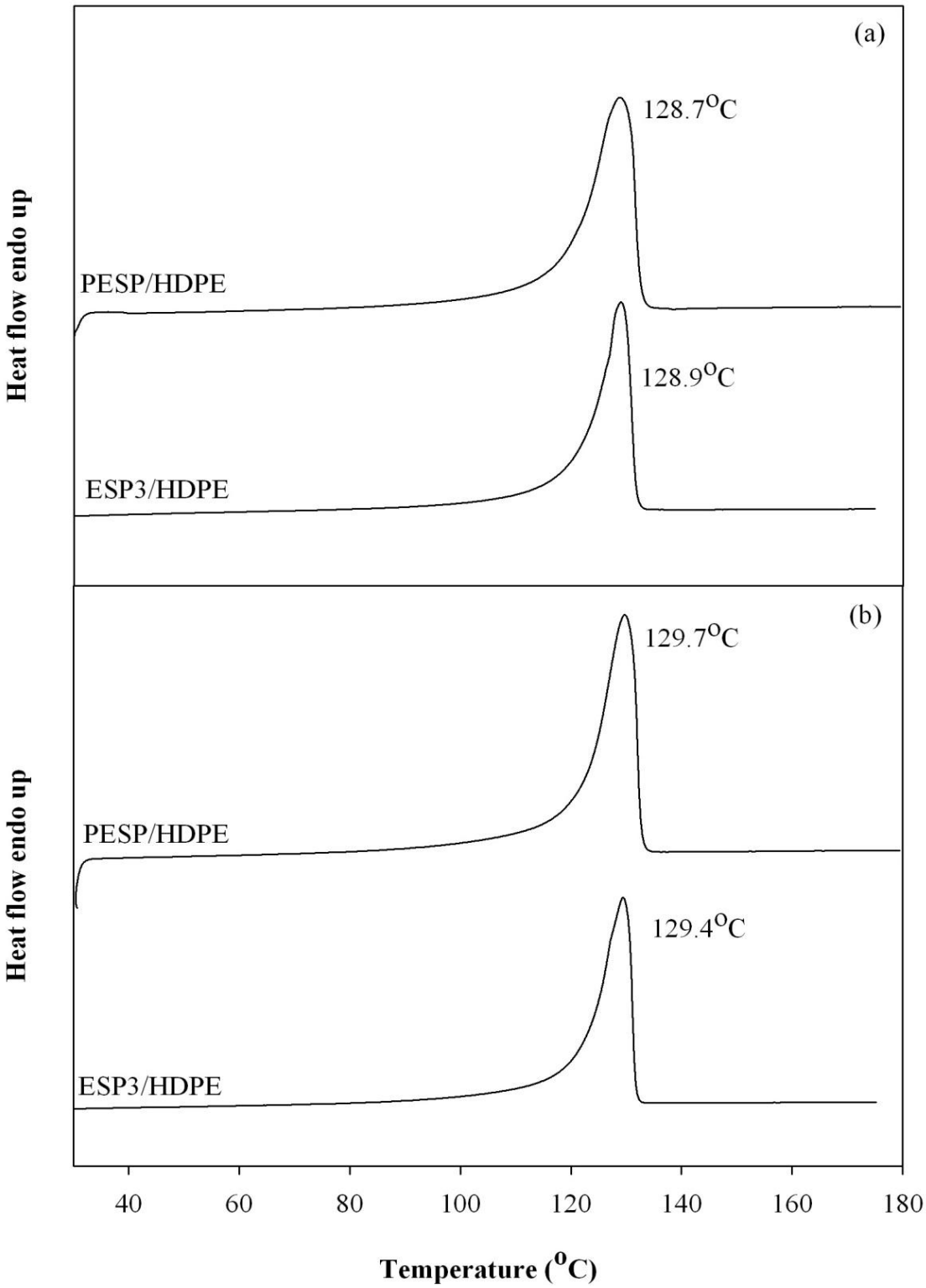

Figure 4.43 DSC curves of 1st heating (a) and 2nd heating (b) scan of HDPE composite prepared with ESP3 and PESP.

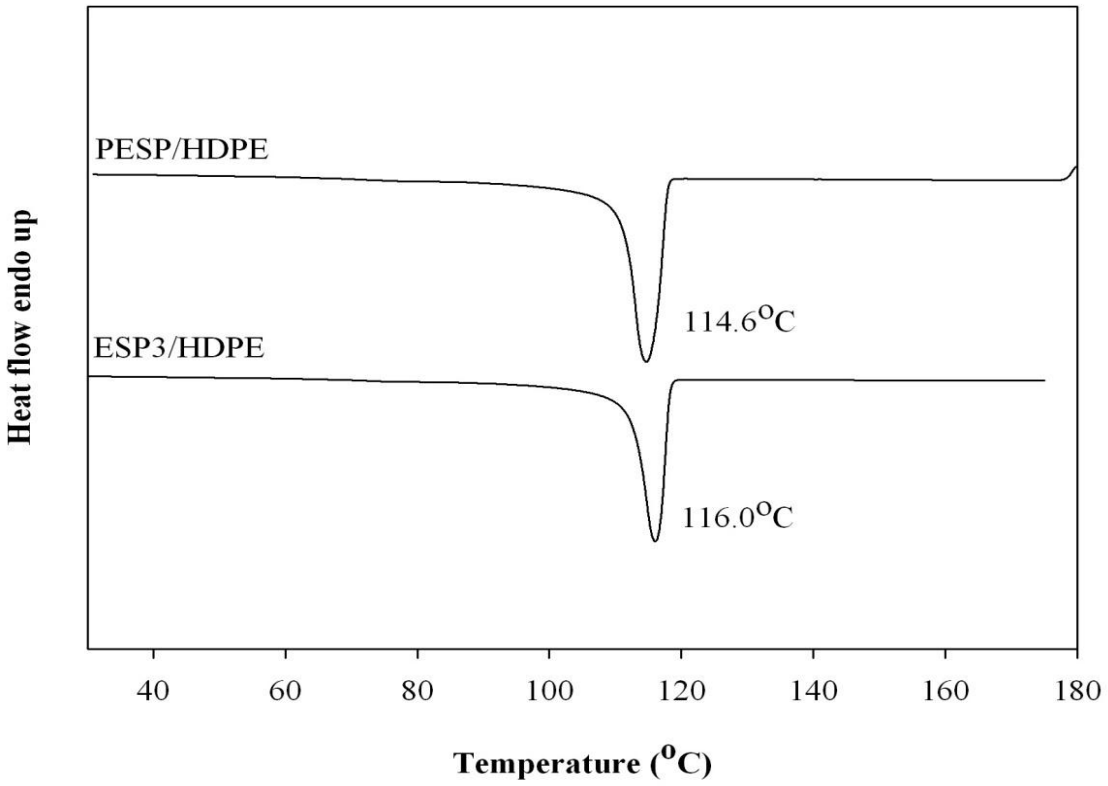

Figure 4.44 DSC curves obtained from the 1st cooling scan of HDPE composite prepared with ESP3 and PESP.

Table 4.23 Melting temperature (T_m), crystallization temperature (T_c), and degree of crystallinity (X_c) of HDPE composite filled with ESP3 and PESP.

Material	T_d (^oC)		T_m (^oC)		T_c (^oC)	Delta H (J/g)		X_c (%)	
	HDPE	ES	1st scan	2nd scan		1st scan	2nd scan	1st scan	2nd scan
ESP3/HDPE	490	753	128.9	129.4	116.0	252.6	272.2	69.1	74.4
PESP/HDPE	490	723	128.7	129.7	114.6	220.7	223.5	60.4	61.1

4.4 Characterization of ESP3/PBS composites

4.4.1 Effect of ESP content on physical properties of ESP3/PBS composites

4.4.1.1 Flow property

The melt flow index (MFI) of neat PBS and ESP3/PBS composite at various ESP3 content is summarized in Table 4.24. MFI of neat PBS was higher than that of the PBS composites. MFI of PBS composites decreased with increasing ESP3 content. The decrement of MFI of PBS composite as increasing ESP3 content resulted from the ESP3 particle disturbed the flow of polymer and hindered the mobility of chain segments in melt flow (Yun Fu, Qiao Feng, Lauke and Wing Mai, 2008).

Table 4.24 MFI of neat PBS and ESP3/PBS composite at various ESP3 contents.

ESP3 content (wt.%)	MFI (g/10 min)
0	35.48
10	28.46
20	25.57
30	22.46
40	20.51

4.4.1.2 Stress-strain behavior

Tensile stress-strain curves of neat PBS, and ESP3/PBS composite at various ESP3 contents are shown in Figure 4.45. At a tension rate of 10 mm/min, the tensile stress-strain curve of neat PBS shows yield point, cold drawing region and strain hardening region before specimen rupture. In addition, the ductile-brittle transition of the PBS composite occurred at 10 wt.% ESP3. At 20 wt.% ESP3, PBS composite fractured in a brittle manner. However, tensile stress-strain curves of the composite at 10-20 wt.% ESP3 exhibited yield point without cold drawing region before fracture. With increasing ESP3 content to 30-40 wt.%, the PBS composites fractured prior to yielding. This was probably because the ESP3 particle restricted the mobility of polymer chains as increasing ESP3 content (Yun et al., 2008). PBS filled with 10-40 wt.% ESP3 broke in a brittle manner.

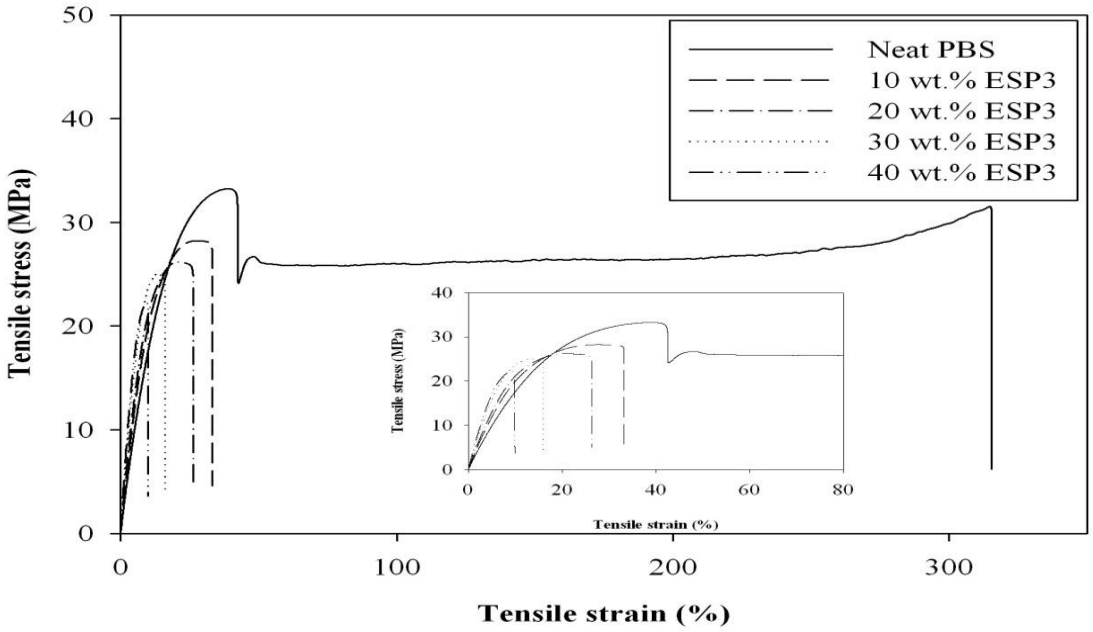

Figure 4.45 Tensile stress-strain curves of neat PBS and ESP3/PBS composite at various ESP3 contents.

4.4.1.3 Mechanical properties

From a plot of tensile strength vs ESP content of ESP3/PBS composite shown in Figure 4.46, it was revealed that tensile strength of the PBS composites gradually decreased with increasing ESP3 content. This indicated that the content of ESP3 had effect on tensile strength of the filled PBS. It was previously reported that tensile strength of silica powder/PBS composite decreased with increasing silica powder content as well (Bian et al., 2010). Additionally, the PBS composite fractured prior to yielding when ESP3 was added at 30-40 wt.%.

Figure 4.47 shows Young's modulus of neat PBS and ESP3/PBS composite at various ESP3 contents. Young's modulus of PBS composite improved by addition of ESP3. In addition, Young's modulus of PBS composite increased with increasing ESP3 content. This was caused by the incorporation of rigid particle of ESP3 which is stiffer than PBS.

With increasing ESP content, elongation at break of ESP3 filled PBS decreased and, was much lower than that of the unfilled PBS as presented in Figure 4.47. This is an indication that with higher content in ESP3, the PBS composite lossed ability to plastically flow prior to composite fracture.

The PBS composite with higher content in ESP3 had lower impact strength than that of the composite with lower ESP3 content and lower than that of unfilled PBS as shown in Table 4.25. However, the PBS composite at 10 wt.% ESP3 and neat PBS did not rupture within an instrumentation limit of 130 kJ/m^2. This result well corresponded with the area under stress-strain curves shown in Figure 4.45, that toughness of the PBS composites decreased with increasing ESP3 content.

Figure 4.48 shows the plots of flexural modulus and flexural strength of ESP3/PBS composite at various ESP3 contents. It presents that the flexural modulus of the PBS composite increased with increasing ESP3 content. The flexural strength of neat PBS and ESP3/PBS composites had not much difference in flexural modulus. Tensile strength, Young's modulus, elongation at break, flexural modulus and flexural strength of ESP3/PBS composites are summarized in Table 4.26.

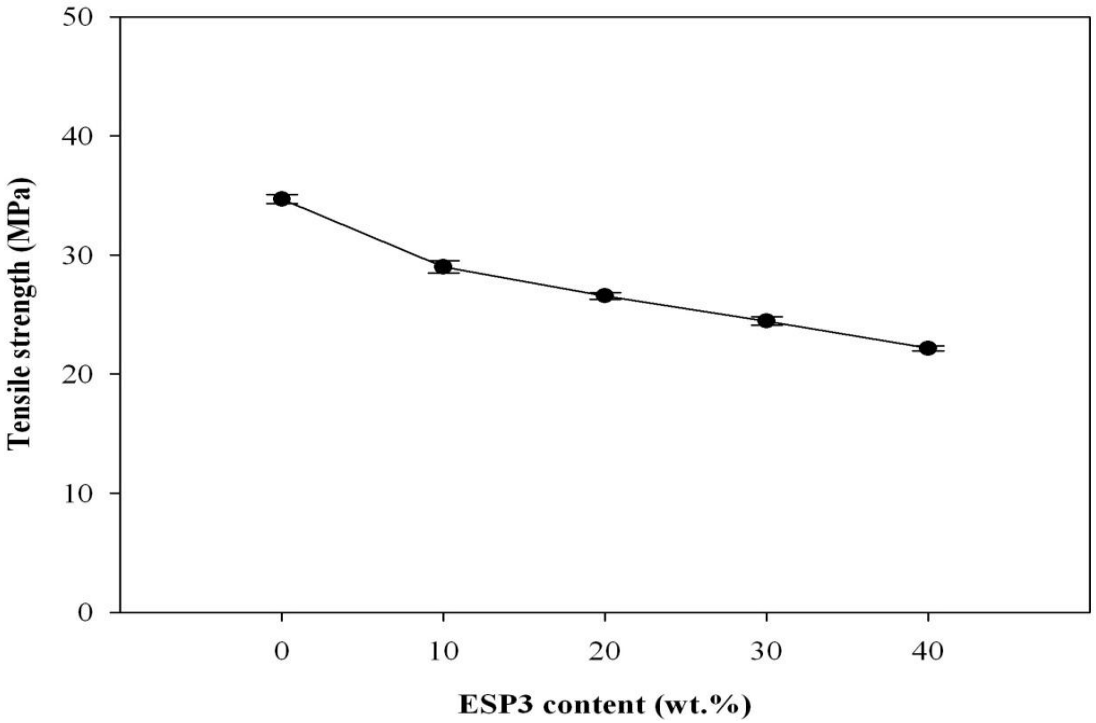

Figure 4.46 Plots of tensile strength vs ESP3 content of ESP3/PBS composite.

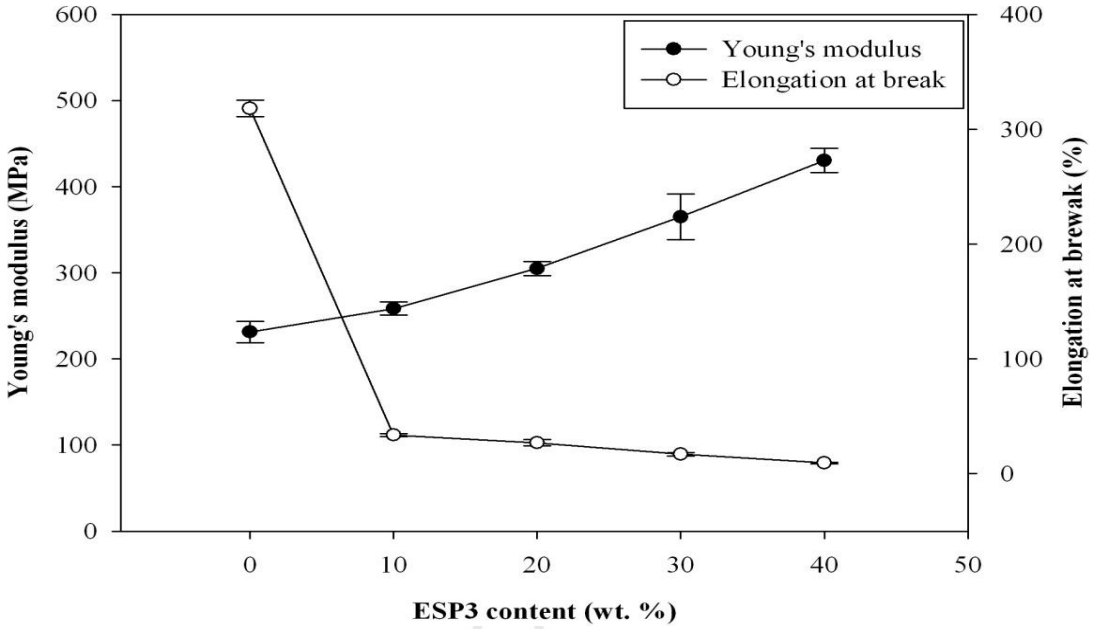

Figure 4.47 Plots of Young's modulus and elongation at break vs ESP3 content of ESP3/PBS composite.

Table 4.25 Impact strength of neat PBS and ESP3/PBS composite at various ESP3 contents.

ESP3 content (wt.%)	Impact strength (kJ/m^2)
0	>130
10	>130
20	60.4±9.6
30	39.1±7.0
40	26.5±6.7

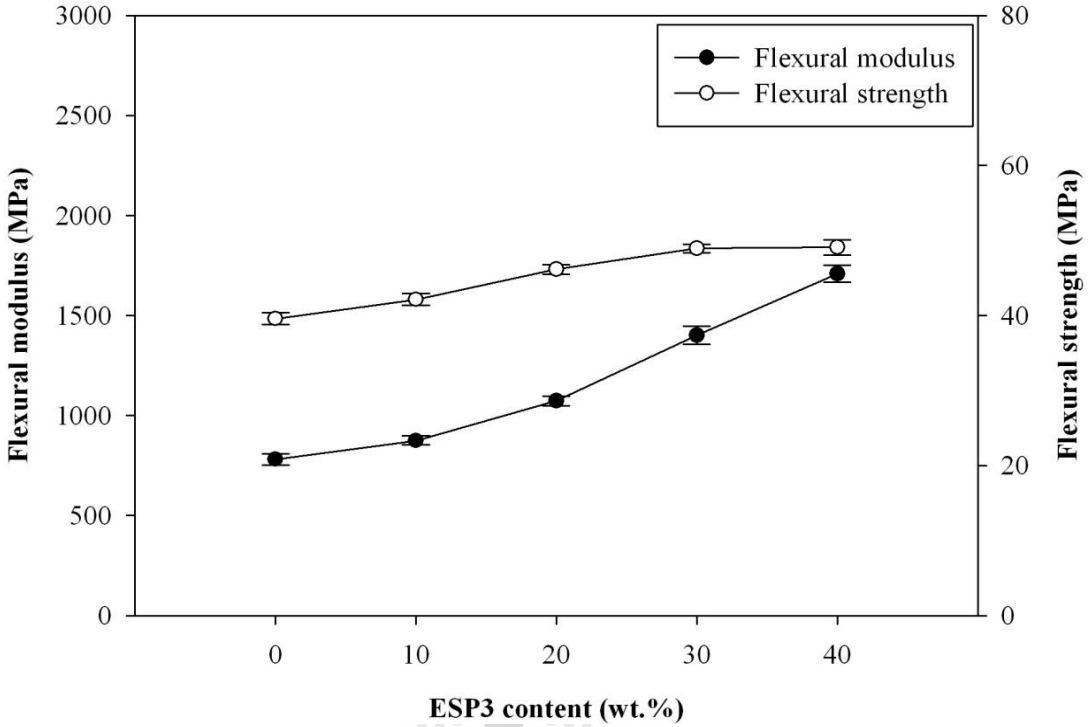

Figure 4.48 Plots of flexural modulus and flexural strength vs ESP3 content of ESP3/PBS composite.

Table 4.26 Tensile strength, Young's modulus, elongation at break, flexural modulus and flexural strength of neat PBS and ESP3/PBS composite at various ESP3 content.

ESP3 content (wt.%)	Tensile strength (MPa)	Young's modulus (MPa)	Elongation at Break (%)	Flexural modulus (MPa)	Flexural strength (MPa)
0	34.7±0.3	231.3±12.3	318.1±7.0	781.4±28.6	39.5±0.7
10	29.0±0.5	258.4±7.6	33.7±1.2	875.4±22.4	42.1±0.7
20	26.5±0.2	304.8±8.2	27.0±2.5	1073.0±24.1	46.1±0.6
30	25.2±0.2	364.9±26.5	17.0±1.4	1400.6±45.8	48.9±0.5
40	22.4±0.3	430.5±14.2	9.4±0.6	1709.1±42.5	49.0±1.0

4.4.1.4 Fracture surface morphology

SEM micrographs of neat PBS and ESP3/PBS composites illustrate that neat PBS and PBS composite had a rough fracture surface with poor distribution of eggshell particles as observed in Figure 4.49 (a2) - (a5). The higher the ESP content, the poorer the ESP3 dispersed within PBS matrix. The poor distribution of the filler particle was responsible for the decrease of tensile stress at break and impact strength. With a larger magnification of SEM micrographs in Figure 4.49 (b2)-(b5), the detachment of PBS matrix from ESP3 surface with partial PBS left on the surface was observed. This indicated that the interfacial adhesion between PBS matrix and ESP3 particle was probably formed (Wang, Lu and Wang, 1997; Li, Mai, Feng and Huang, 2006; Intharapat, Kongnoo and Kateungngan, 2013). The mechanism of the interaction between eggshell calcium carbonate and PBS are shown in Figure 4.50. In addition, the surface topology of neat PBS indicated that it ruptured in a ductile manner. For addition more of ESP3, brittle fracture of the composites was indicated by the smooth surface of PBS matrix with increasing ESP3 content.

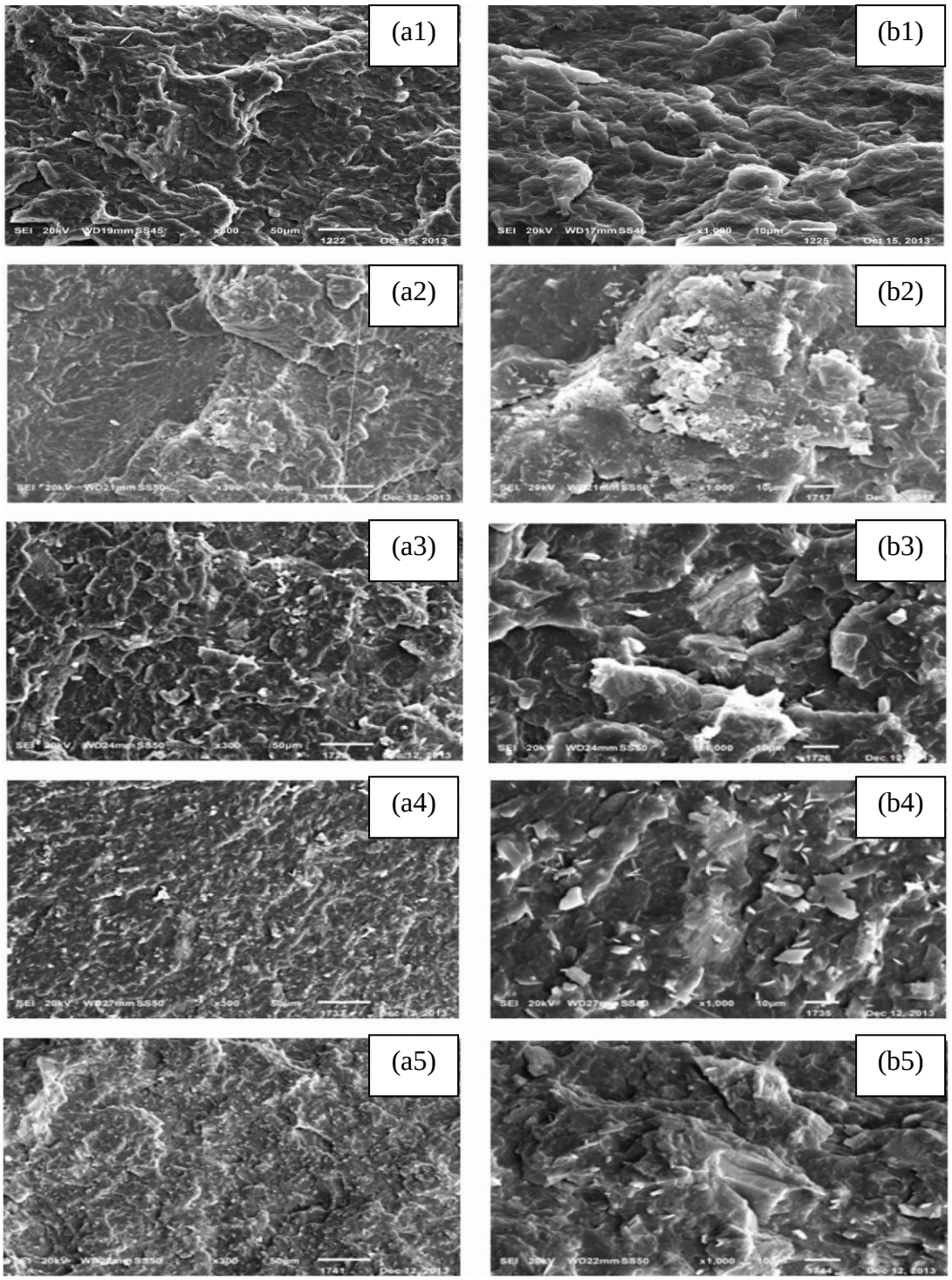

Figure 4.49 SEM micrographs (x300 (a) and x1000 (b)) of neat PBS (1), ESP3/PBS composite at 10 wt.% ESP3 (2), 20 wt.% ESP3 (3), 30 wt. % ESP3 (4) and 40 wt.% ESP3 (5).

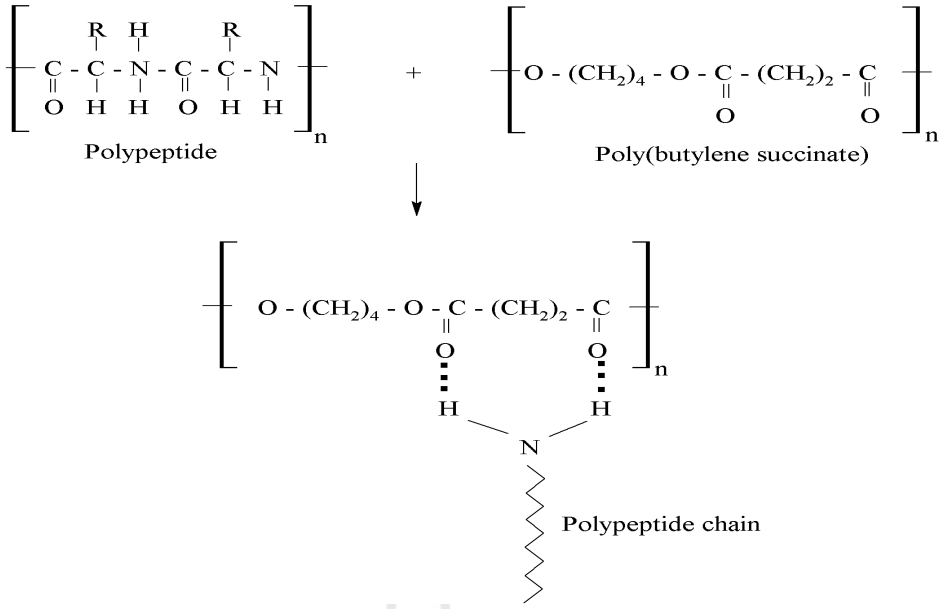

(a) The interaction between matrix protein exist at surface of ESP and PBS

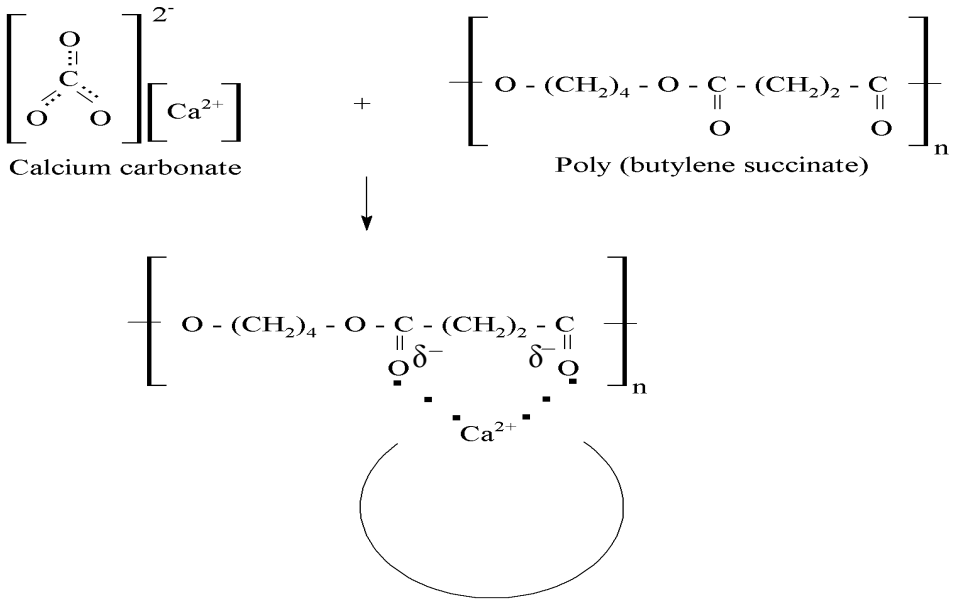

(b) The interaction between eggshell calcium carbonate and PBS

Figure 4.50 Schematic represent the mechanism of the interaction between matrix protein and PBS (a), and the interaction between eggshell calcium carbonate and PBS (b) (Ji, Zhu, Qi and Zeng, 2009; Intharapat, Kongnoo and Kateungngan, 2013).

4.4.1.5 Decomposition temperature

Figure 4.51 shows TGA and DTGA curves of ESP3/PBS composites. Neat PBS thermally decomposed as a single transition at 414^{o}C. In addition, ESP3/PBS composites had three thermal transitions. The first transition at 413^{o}C was due to the decomposition of unbound PBS matrix. The second transition occurred at 486, 483, 485 and 481^{o}C due to the decomposition of the bound PBS of 10, 20, 30 and 40 wt.% ESP3/PBS composites, respectively. It was expected that the possible formation of ion-dipole interaction between the C=O groups in PBS and Ca^{2+} ion of ESP3 and/or the formation of hydrogen bonding of the C=O groups in PBS with the small amount of polar amine (-NH_2) groups in protein (i.e., polypeptide) that existed on the filler surfaces (Wang, Lu and Wang, 1997; Ji, Zhu, Qi and Zeng, 2009; Intharapat, Kongnoo and Kateungngan, 2013).

In similarity, Li, Mai, Feng and Huang (2006) reported that the DTGA peak of nano $CaCO_3$ encapsulated by poly (styrene-co-maleic anhydride) exhibited an additional peak at 485^{o}C. This result suggested that the interfacial interaction between Ca^{2+} ion at surface of nano $CaCO_3$ particles and C=O groups of MAH in poly (styrene-co-maleic anhydride) took place. The third transition at 743^{o}C, 758^{o}C and 775^{o}C was derived from the decomposition of 10, 20, and 30-40 wt.% ESP3 deposited in the composite, respectively. With increasing ESP3 content, ESP3 thermally decomposed at higher temperature. However, the decomposition temperature of unbound PBS matrix was not influenced by an existence of ESP3. Decomposition temperatures (T_d) of neat PBS and ESP3/PBS composite are summarized in Table 4.27.

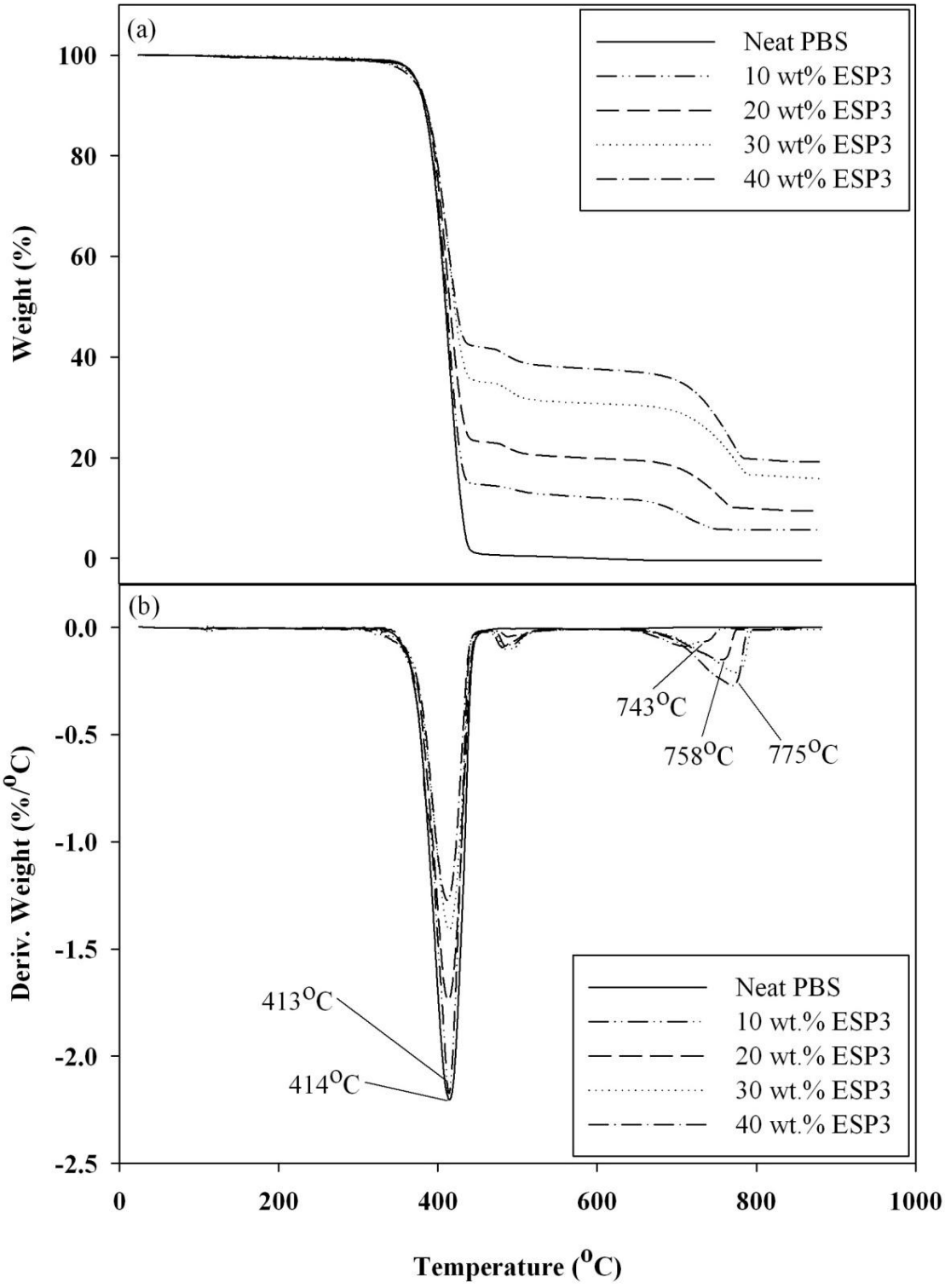

Figure 4.51 TGA (a) and DTGA (b) curves of neat PBS and PBS composites at 10, 20, 30 and 40 wt.% ESP3.

4.4.1.6 Melting and crystallization temperature

Figure 4.52 shows DSC curves of neat PBS and ESP3/PBS composite obtained from the first heating and second heating scan. In the first heating curve, neat PBS and ESP3/PBS composites, show a single melting behavior during heating process. It revealed that melting temperature of PBS did not change when adding ESP3. With increasing ESP3 content, their melting temperatures did not change as observed in Figure 4.52 (a). This indicated that ESP3 did not significantly affect melting temperature of PBS matrix. Moreover, from the first heating, the cold crystallization temperature of PBS appeared at 99^{o}C. The addition of ESP3, the cold crystallization peak of the composite slightly decreased with increasing ESP3 content.

In addition, the second heating curves of neat PBS and ESP3/HDPE composites are presented in Figure 4.52 (b). The second heating curves of neat PBS shows double melting peaks. The melting peaks at higher temperature belonged to the more perfect crystalline structure than that at lower temperature. The less perfect crystals have enough time to melt and reorganize into crystals with higher structure perfection and remelt at higher temperature (Qiu, Komura, Ikehara and Nishi, 2003). In corporation of ESP3 at 10 wt.%, PBS matrix still showed double melting peaks. However, at 20-40 wt.% ESP3, PBS matrix showed only single melting peak of high endotherm at 110^{o}C close to that of the 10 wt.% ESP3/PBS composite. Cold crystallization was also observed at ESP3 content of 10, 20, 30, and 40 wt.%. This indicated that ESP3 did not significantly affect melting process of PBS matrix. As observed from Table 4.27, the melting temperature of neat PBS obtained from the first heating was not significantly different from those obtaining from the high melting endotherm of ESP3/PBS composites from the second heating scan.

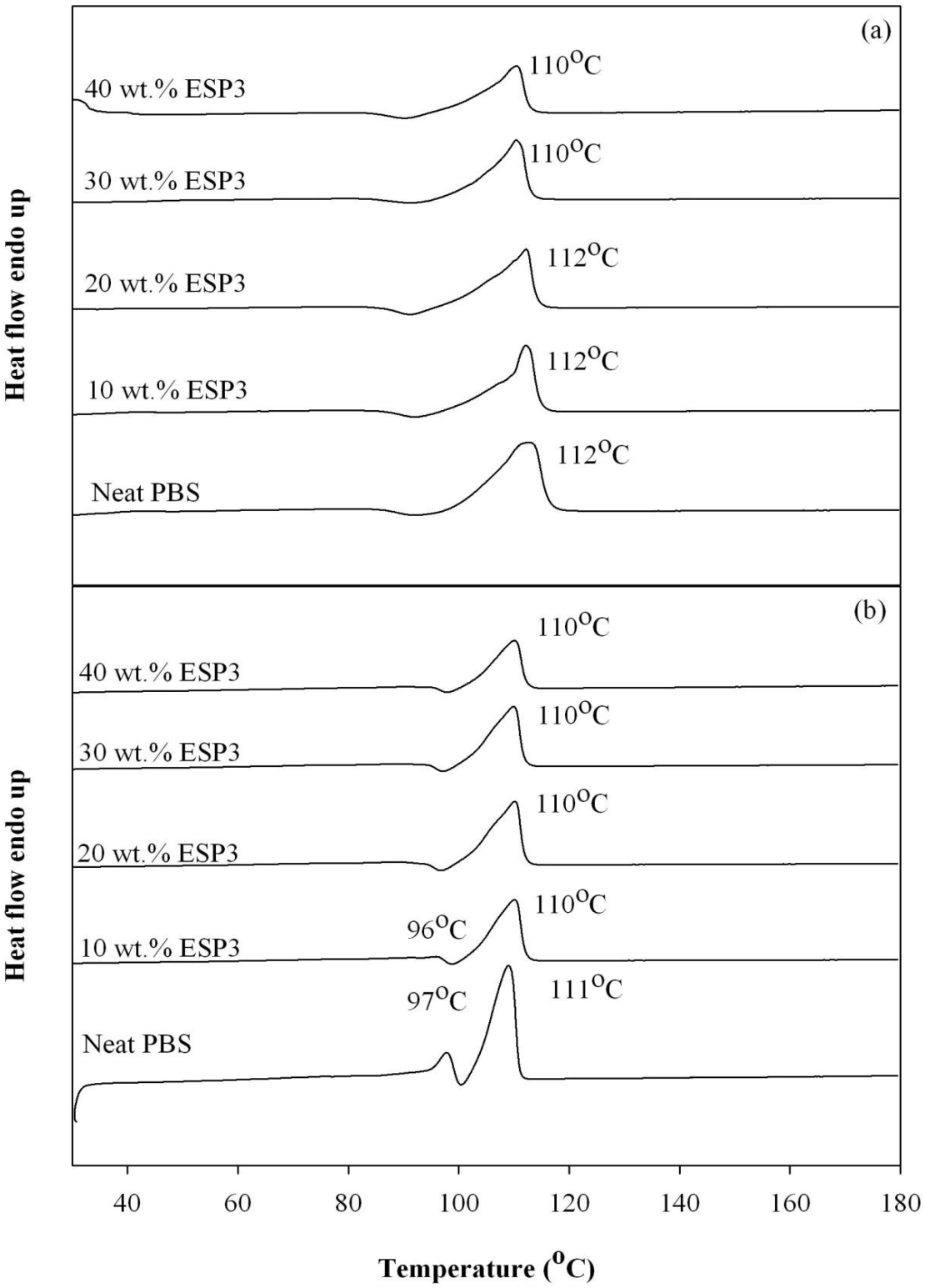

Figure 4.52 DSC curves of 1st heating (a) and 2nd heating (b) scan of neat PBS and PBS composites at 10, 20, 30 and 40 wt.% ESP3.

It was found that the adding ESP3 into PBS resulted in decreased crystallization temperature of PBS matrix as shown in Figure 4.53. Guo, Zhang, and Zang (2013) reported that the T_c of HA/PBS composites decreased with increasing content of HA due to the decrease of molecular weight of PBS during processing. In addition, crystallization temperature of PBS composites did not change when ESP3 was added at 20-40 wt.%. It clearly indicated that ESP3 did not act as a nucleating agent for PBS matrix. Accordingly, degree of crystallinity of PBS composite decreased with increasing ESP content. This was due to ESP3 particles obstructed the PBS chain mobility during reentry into specific lamellar.

In addition, degree of crystallinity of neat PBS and PBS composites obtained from the second heating scan was not much different from that of the first heating scan. Melting temperature, crystallization temperature and degree of crystallinity of neat PBS and PBS composite at 10, 20, 30 and 40 wt.% ESP3 are listed in Table 4.27.

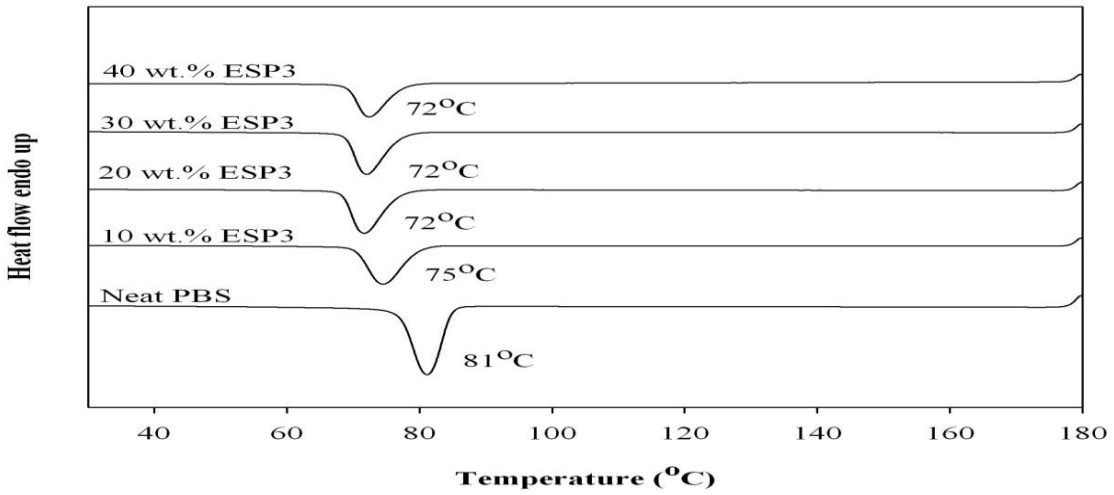

Figure 4.53 DSC curves obtained from the 1st cooling scan of neat PBS and PBS composites at 10, 20, 30 and 40 wt.% ESP3.

Table 4.27 Decomposition temperature (T_d), melting temperature (T_m), crystallization temperature (T_c) and degree of crystallinity (X_c) of neat PBS and ESP3/PBS composite at various ESP3 content.

ESP3 content (wt.%)	T_d (^oC)			T_m (^oC)			T_c (^oC)	Delta H (J/g)		X_c (%)	
	PBS	Bound PBS	ESP3	1st scan	2nd scan			1st scan	2nd scan	1st scan	2nd scan
					low	high					
0	414	-	-	112	97	111	81	58.6	48.8	53.1	44.2
10	413	486	743	112	96	110	75	51.4	51.6	42.0	42.1
20	413	483	758	112	-	110	72	48.6	56.0	35.2	40.6
30	413	485	775	110	-	110	72	42.3	46.9	26.9	29.8
40	413	481	775	110	-	110	72	37.0	39.8	20.1	21.6

4.5 Characterization of PESP/PBS composite

4.5.1 Effect of PESP content on physical properties of PESP/PBS composites

4.5.1.1 Flow property

The melt flow index (MFI) of neat PBS and PESP/PBS composite at various PESP contents is listed in Table 4.28. The addition of PESP into PBS increased MFI of the PBS composites. In addition, MFI of PBS composite increased with increasing PESP content. This was probably because PESP had two type of crystal form; vaterite and calcite. The hardness of vaterite crystal had lower than that of calcite crystal form. When increasing PESP content, vaterite crystal was increased, resulting in reduction of restriction the mobility and flow of polymer chain.

Table 4.28 MFI of neat PBS, and PESP/PBS composite at various PESP contents.

PESP content (wt.%)	MFI (g/10 min)
0	35.48
5	36.35
10	42.39
20	45.26

4.5.1.2 Stress-strain behavior

Figure 4.54 shows tensile stress-strain curves of neat PBS and PESP/PBS composite at various PESP contents. Tensile stress-strain curve of neat PBS shows yield point, cold drawing region with strain hardening region before the

test specimen ruptured. In addition, the 5 wt.% PESP/PBS composites fractured in the ductile-brittle transition. The tensile stress-strain curve of PESP filled with 5-10 wt.% PESP exhibited yield point without cold drawing region and strain hardening region before the specimen fractured. With increasing PESP content as 20 wt.%, the PBS composite fractured prior to yielding. This was probably because the PESP particle restricted the mobility of polymer chains as increasing PESP content (Yun et al., 2008).

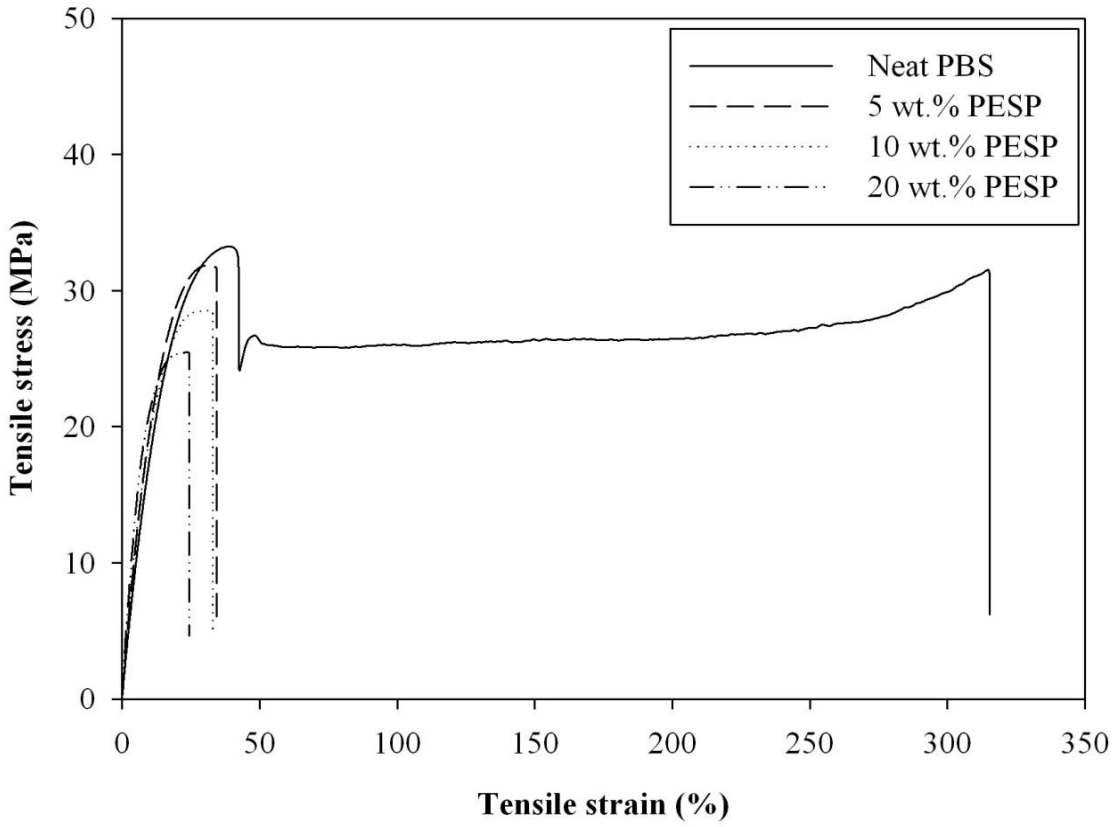

Figure 4.54 Tensile stress-strain curves of PESP/PBS composite at various PESP contents.

4.5.1.3 Mechanical properties

Figure 4.55 shows tensile strength of neat PBS and PESP/PBS composite at various PESP contents. Incorporation of PESP, tensile strength of the composites was lower than that of neat PBS. With increasing PESP content, tensile strength of the PBS composite was slightly decreased. In addition, at 20 wt.% PESP, the PBS composite fractured before yielding.

Figure 4.56 shows Young's modulus and elongation at break of PESP/PBS composite at various PESP contents. Young's modulus of the composite gradually increased with increasing PESP content. The increase of Young's modulus was caused by the incorporation of rigid particles of PESP. However, elongation at break of the composite decreased with increasing PESP contents, and much lower than that of neat PBS.

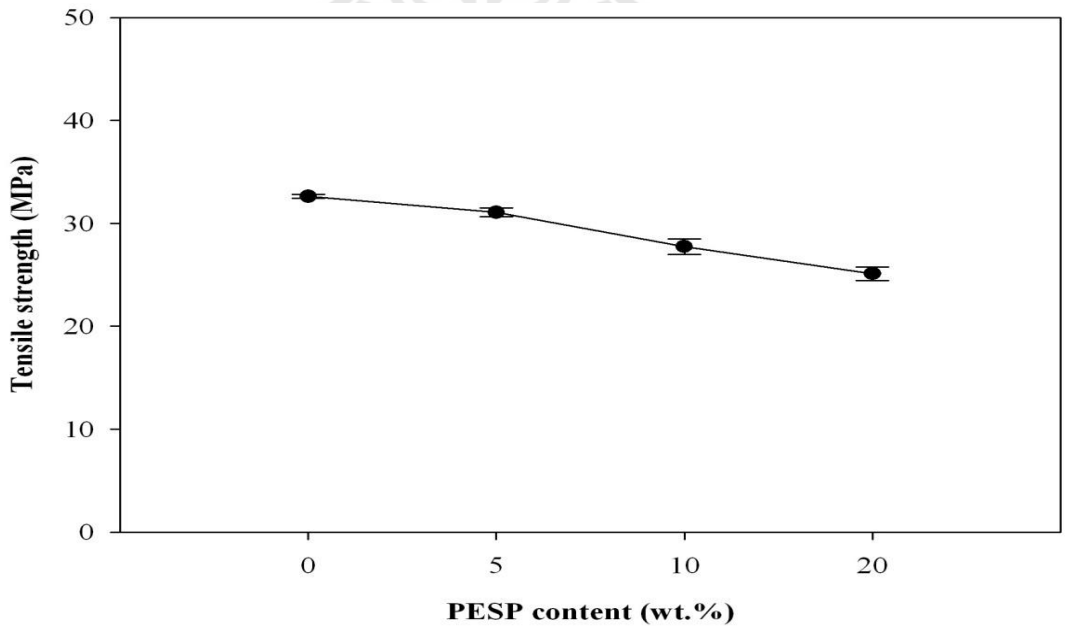

Figure 4.55 Plots of tensile strength of PESP/PBS composite at various PESP contents.

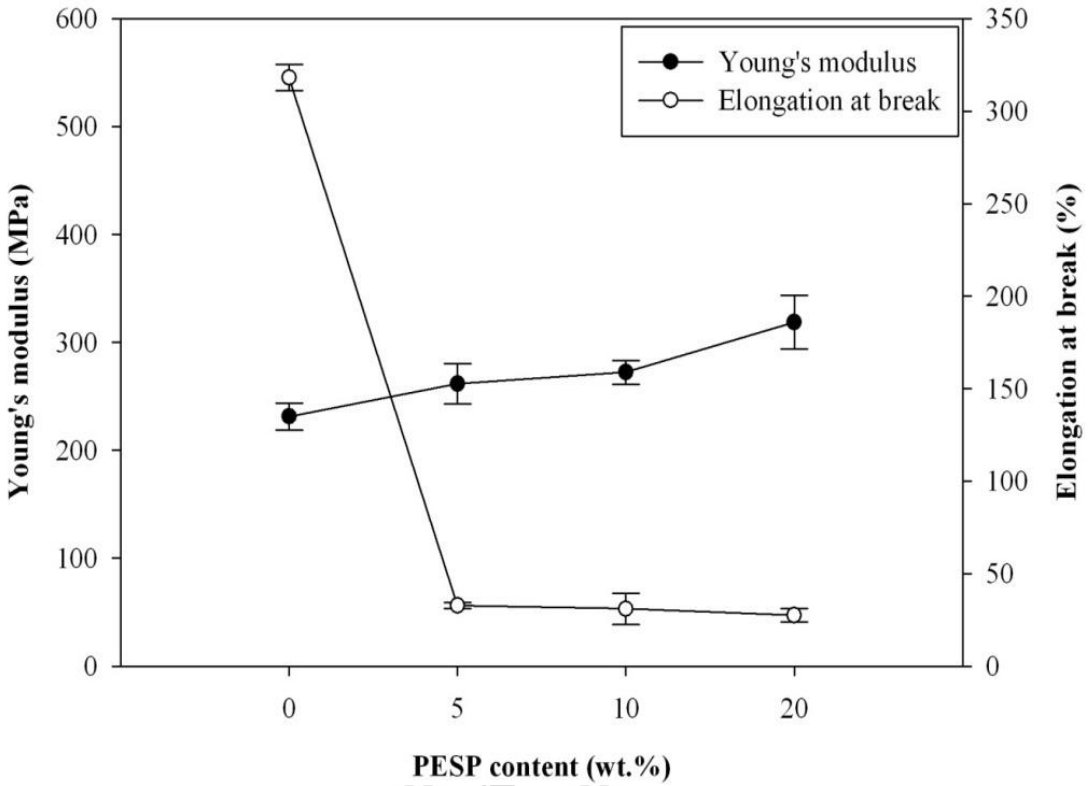

Figure 4.56 Plots of Young's modulus and elongation at break of PESP/PBS composite at various PESP contents.

Figure 4.57 shows flexural modulus and flexural strength of PESP/PBS composite at various PESP contents. The flexural modulus of PBS containing 0-20 wt.% PESP significantly increased. This indicated that the incorporation of PESP into PBS caused improvement bending resistance of the composites. Moreover, the flexural strength of the composite slightly increased with increasing PESP contents.

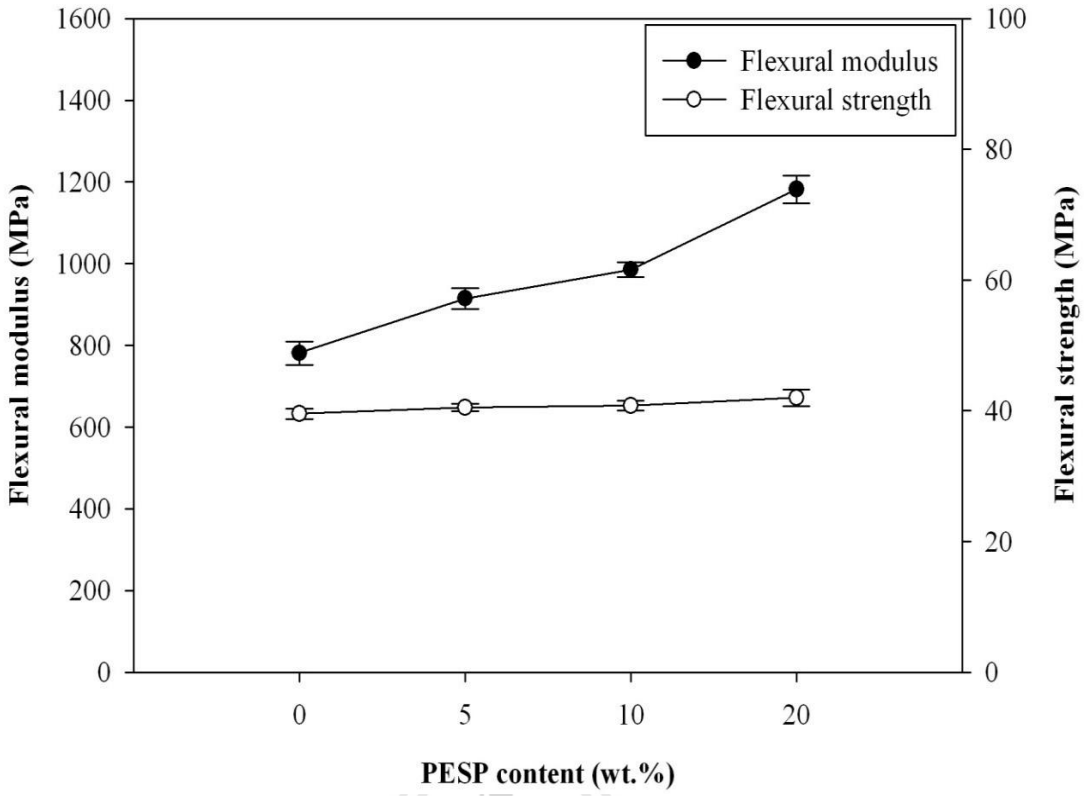

Figure 4.57 Plots of flexural modulus and flexural strength of PESP/PBS composite at various PESP contents.

Impact strength of PESP/PBS composites is listed in Table 4.29. With increasing PESP content, the test specimens of 0, 5 and 10 wt.% PESP/PBS composites did not break within instrumentation limit of more than 130 kJ/m^2. However, at 20 wt.% PESP, impact strength of the composite was 31.74 kJ/m^2. This is an indication that with higher content of PESP, the PBS composite lossed ability to absorb impact energy prior to composite fracture. Tensile strength, Young's modulus, elongation at break, flexural modulus and flexural strength are summarized in Table 4.30.

Table 4.29 Impact strength of neat PBS and PESP/PBS composite at various PBSP contents.

PESP content (wt.%)	Impact strength (kJ/m^2)
0	>130
5	>130
10	>130
20	31.7±1.0

Table 4.30 Tensile strength, Young's modulus, elongation at break, flexural modulus and flexural strength of PESP/PBS composites at various PESP contents.

PESP content (wt.%)	Tensile strength (MPa)	Young's modulus (MPa)	Elongation at Break (%)	Flexural modulus (MPa)	Flexural strength (MPa)
0	34.7±0.3	231.3±12.3	318.1±7.0	781.4±28.6	39.5±0.7
5	31.6±0.4	261.7±18.5	32.6±1.7	915.1±25.5	40.5±0.5
10	28.2±0.7	272.2±10.8	30.9±8.2	985.9±17.7	40.7±0.7
20	25.5±0.5	318.6±24.8	27.4±3.5	1182.6±33.8	41.9±1.2

4.5.1.4 Fracture surface morphology

SEM micrographs of PESP/PBS composites at various PESP contents are shown in Figure 4.58. The PBS composites showed a coarse fracture surface morphology with aggregated PESP particles. The higher the PESP content, the poorer the PESP dispersed within PBS matrix. The aggregation and poor distribution of the PESP particles led to poor mechanical properties such as tensile stress at break and impact strength. In addition, the surface topology of PBS matrix indicated that it ruptured in a brittle manner.

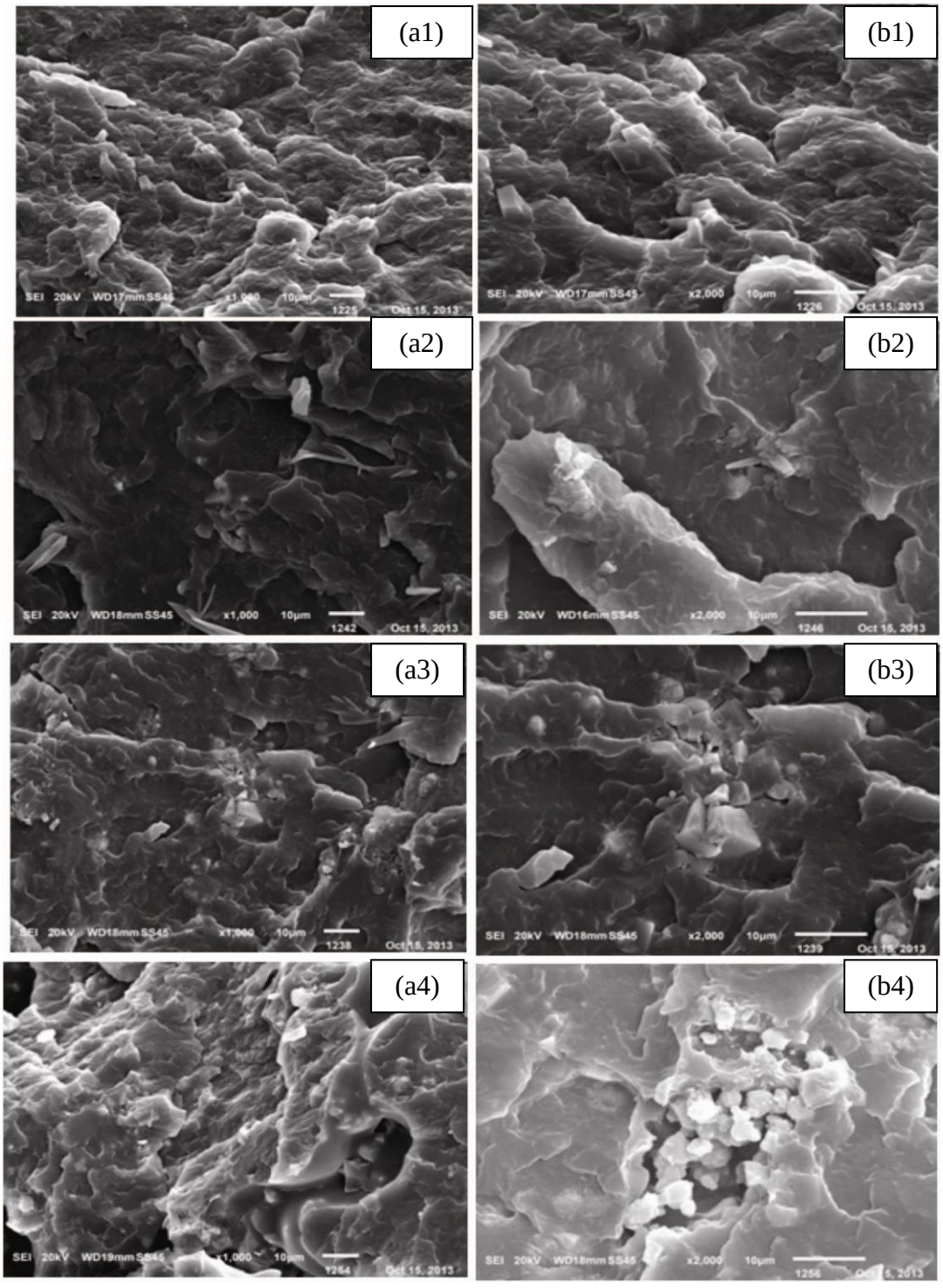

Figure 4.58 SEM micrographs (x1000 (a) and x2000 (b)) of neat PBS (1), PESP/PBS composite at 5 wt.% PESP (2), 10 wt.% PESP (3) and 20 wt. % PESP (4).

4.5.1.5 Decomposition temperature

TGA and DTGA curves of neat PBS and ESP3/PBS composites are shown in Figure 4.59. Neat PBS thermally decomposed as a single transition at 409^{o}C. The PESP/PBS composites had three thermal transitions. The first transition at 406^{o}C was due to the decomposition of unbound PBS matrix. The second transition occurred at 495, 485 and 477^{o}C due to the decomposition of the bound PBS of 5, 10 and 20 wt.% PESP/PBS composites, respectively. It was expected that the interaction between the PBS matrix and PESP particle was occurred, as mentioned in 4.4.1.5. The third transition at 710, 727 and 732^{o}C was derived from the decomposition of PESP deposited in the composite at 5, 10, and 20 wt.%, respectively. With increasing PESP content, PESP thermally decomposed at higher temperature. However, the decomposition temperature of PBS matrix was not influenced by an existence of PESP.

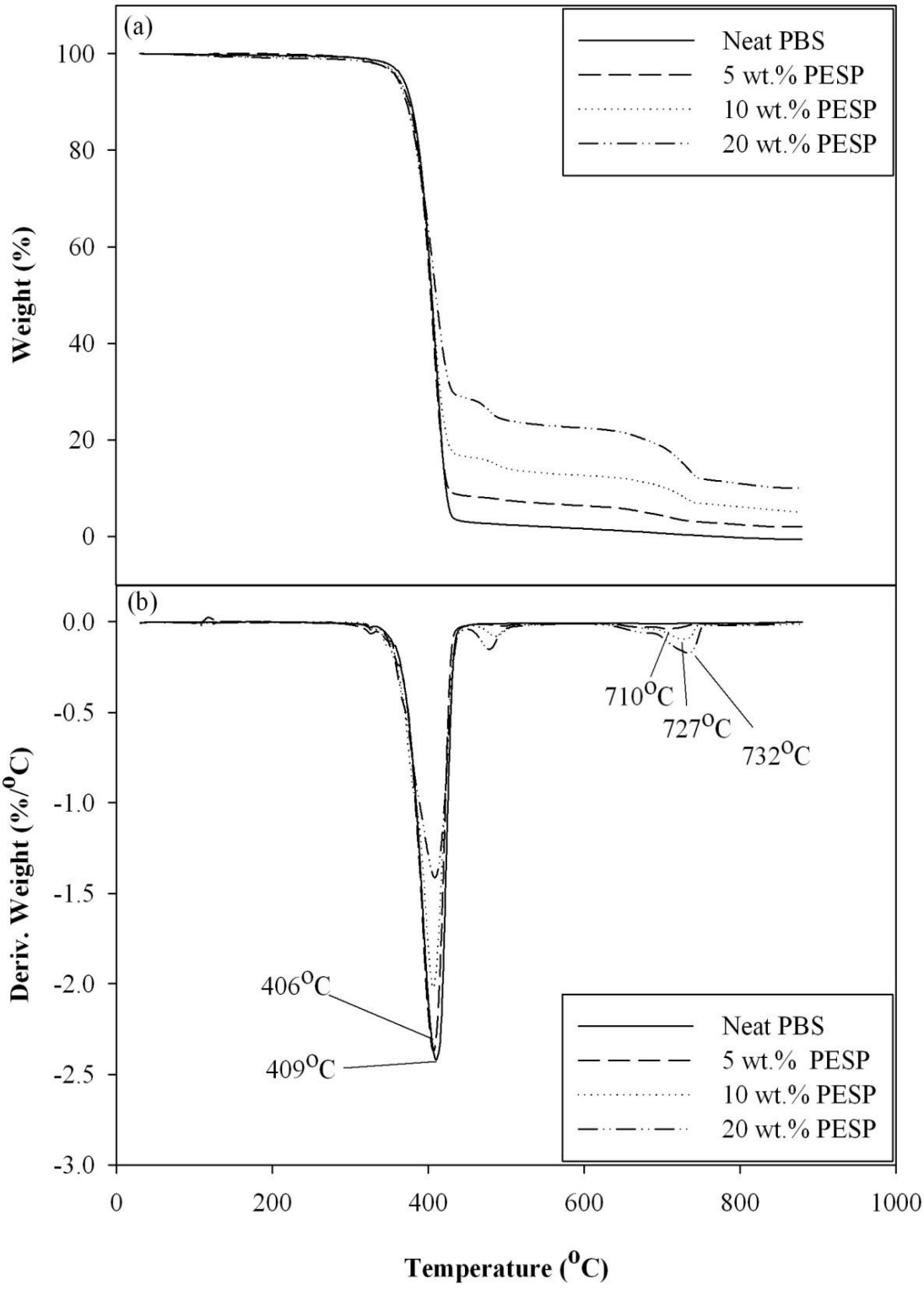

Figure 4.59 TGA (a) and DTGA (b) curves of neat PBS and PESP/PBS composite at various PESP contents.

4.5.1.6 Melting and crystallization temperature

Figure 4.60 shows DSC curves obtained from the first heating and second heating scan of neat PBS and PESP/PBS composites at various PESP contents. In the first heating curve, neat PBS showed a single melting behavior during heating process and cold crystallization about 99^{o}C. With addition of PESP, it was found that the PESP content did not significantly affect melting temperatures and cold crystallization of the PBS matrix as presented in Figure 4.60 (a). In addition, the second heating curves of neat PBS shows double melting peaks. It was mentioned in 4.4.1.6. However, adding PESP, the melting peak of PBS matrix shows single melting peak at 110^{o}C, indicating that PESP did not significantly affect melting temperature of PBS matrix. Cold crystallization was also observed of PESP content of 5, 10, and 20 wt.%. In addition, the small shoulder peak at 107^{o}C from the 2nd heating scan of the PESP/PBS composite was observed. Phua, Chow and Ishak (2011) studied the thermal behavior of PBS and OMMT/PBS composites. They explained that the small shoulder peak of PBS during heating scan was due to the occurrence of a different crystal lamella thickness. Therefore, the occurrence of the shoulder peak at 107^{o}C of PESP/PBS composite was an indication that PBS crystallized into several lamella thickness with the inclusion of PESP as well.

From Figure 4.61, PESP content slightly effect crystallization temperature of PBS matrix. Incorporation of PESP resulted in lowering of crystallization temperature of PBS matrix. PESP might strongly affect crystallization at high temperature. Furthermore, PESP content did not affected crystallization temperature of PBS. Accordindly, degree of crystallinity of PESP/PBS composites was slightly decreased with increasing PESP content. Melting temperature,

crystallization temperature and degree of crystallinity of neat PBS and PESP/PBS composite at various PESP contents are summarized in Table 4.31.

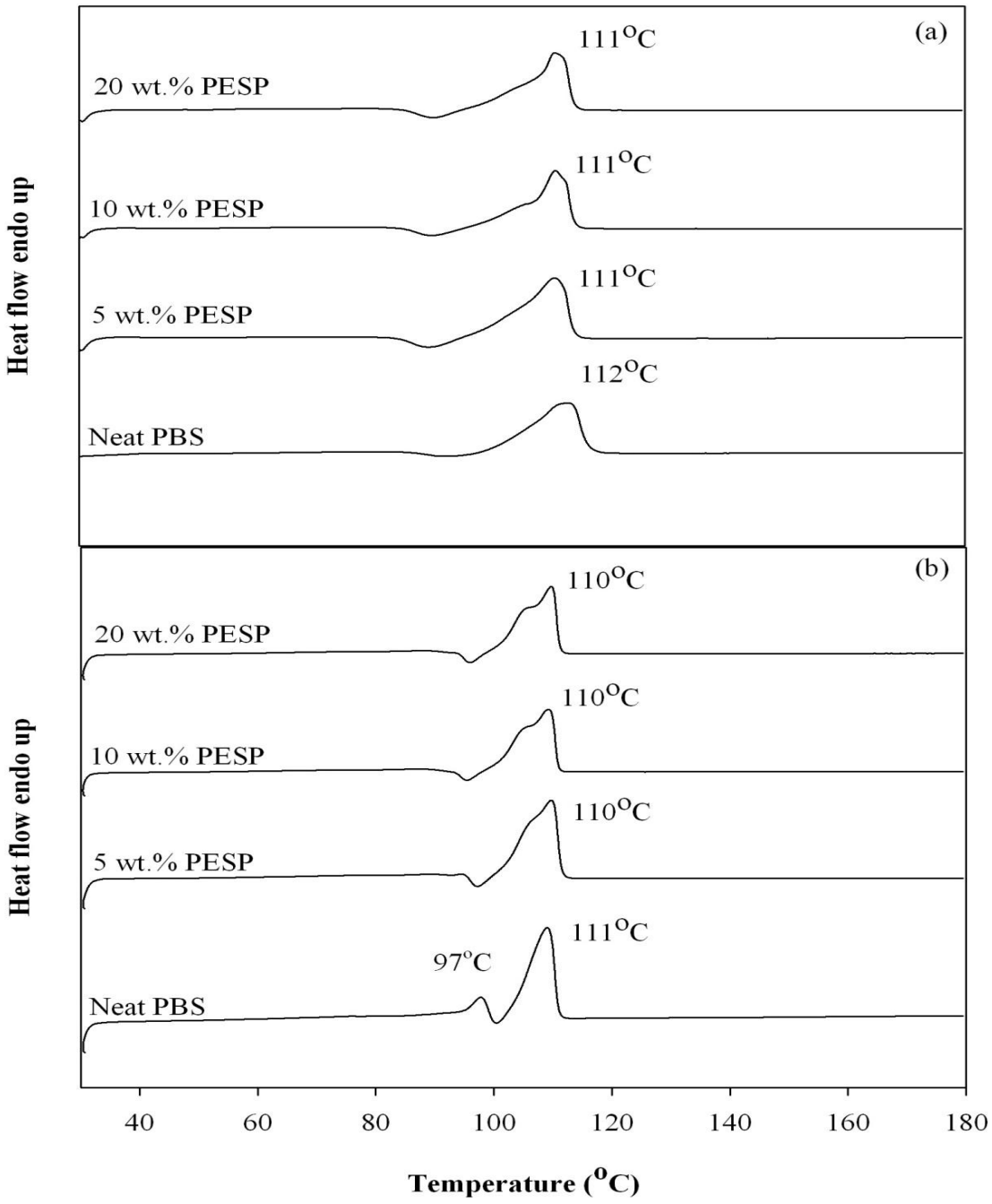

Figure 4.60 DSC curves of the 1st heating (a) and the 2nd heating (b) scan of neat PBS and PESP/PBS composite at various PESP contents.

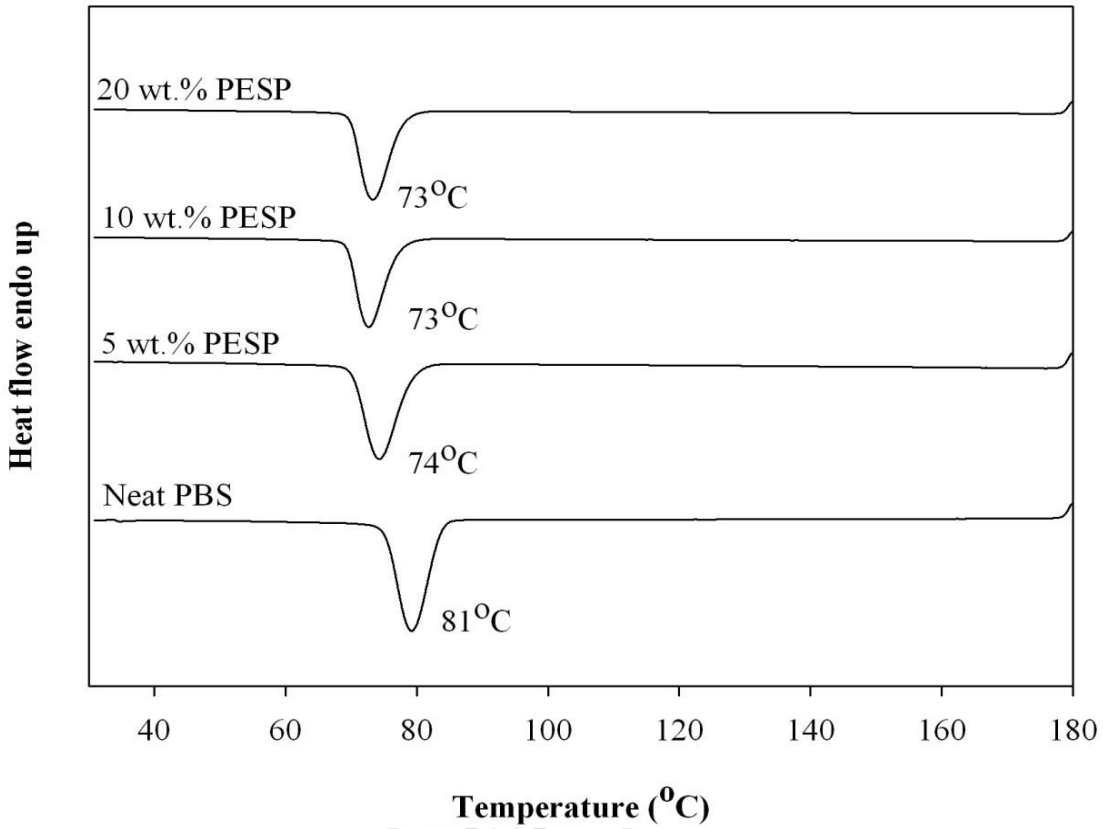

Figure 4.61 DSC curves obtained from the 1st cooling scan of neat PBS and PESP/PBS composite at various PESP contents.

Table 4.31 Decomposition temperature (T_d), melting temperature (T_m), crystallization temperature (T_c) and degree of crystallinity (X_c) of neat PBS and PESP/PBS composite at various PESP contents.

PESP content (wt.%)	T_d (^oC)			T_m (^oC)			T_c (^oC)	Delta H (J/g)		X_c (%)	
	PBS	Bound PBS	PESP	1st scan	2nd scan			1st scan	2nd scan	1st scan	2nd scan
					low	high					
0	409	-	-	112	97	111	79	58.6	48.7	53.1	44.2
5	406	495	710	111	-	110	74	61.2	61.0	52.7	52.5
10	406	485	727	111	-	110	73	61.9	61.5	50.5	50.2
20	406	477	732	111	-	110	73	60.5	61.0	43.9	44.2

4.5.2 Comparative physical properties of ESP3/PBS and PESP/PBS composites

4.5.2.1 Flow property

MFI of PBS filled with ESP3 and PESP at 20 wt.% filler content are shown in Table 4.32. MFI of the PESP/HDPE composite was higher than that of the ESP3/PBS composite. This was probably due to calcite is more stable than others polymorphs at ambient temperature and atmospheric pressure whereas vaterite is mostly unstable (Piskin and Ozdemir, 2012). Therefore, the stable calcite could be more restricted the mobility of polymer matrix than the unstable vaterite.

Table 4.32 MFI of neat PBS, 20 wt.% ESP3/PBS and 20 wt.% PESP/PBS composites.

PBS composites	MFI (g/10 min)
ESP3/PBS	25.57
PESP/PBS	45.26

4.5.2.2 Stress-strain behavior

The tensile stress-strain curves of ESP3/PBS and PESP/PBS composites are shown in Figure 4.62. At 20 wt.% filler content, the tensile stress-strain curve of ESP3/PBS composites exhibited yield point without cold drawing region and strain hardening region before the specimen fractured whereas the PESP/PBS composite was fractured prior to yielding at a tension rate of 10 mm/sec. In addition, the ESP3/PBS composite had higher toughness, determined from an area under tensile stress-strain curve, than the PESP/PBS composite. This indicated that

the aggregation of PESP did affect flow behavior of PBS composite. Their aggregated PESP was obviously formed leading to poor toughness properties in PESP/PBS composite as observed from SEM micrograph in Figure 4.64 (b) (Zuiderduin, Westzaan, Huetink and Gaymans, 2003).

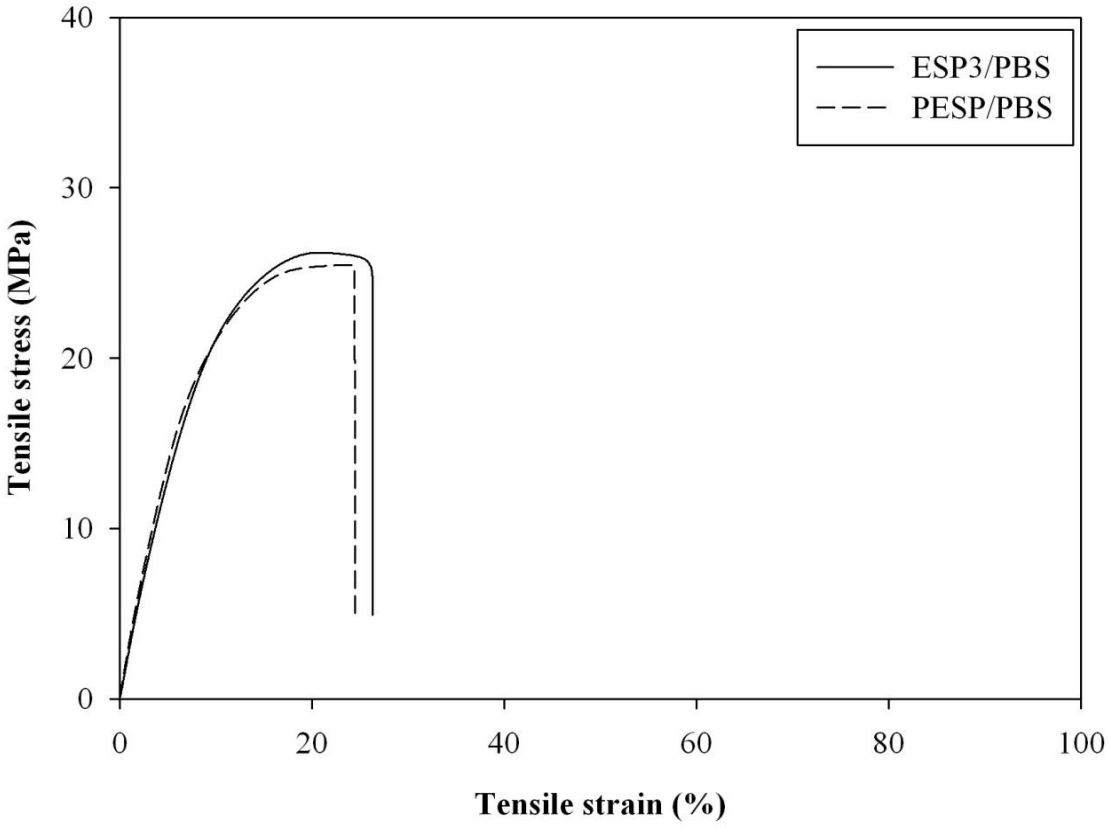

Figure 4.62 Tensile stress-strain curves of ESP3/PBS and PESP/PBS composite.

4.5.2.3 Mechanical properties

Plots of Young's modulus, elongation at break, tensile strength, flexural modulus, flexural strength and impact strength of ESP3/PBS and PESP/PBS composites at 20 wt.% filler content are shown in Figure 4.63. Adding ESP3 and PESP into PBS, Young's modulus of the PESP/PBS composite was slightly

higher than that of the ESP3/PBS composite. In addition, elongation at break and tensile strength of ESP3/PBS and PESP/PBS composite were insignificantly different.

In addition, it was found that PESP was more effective than ESP3 for improving flexural modulus of the composite. On the other hand, flexural strength of the PESP/PBS composite was slightly lower than that of the ESP3/PBS composite. Impact strength of ESP3/PBS and PESP/PBS composites are presented in Figure 4.63, as well. The ESP3/PBS composite had higher impact strength than the PESP/PBS composite. It could be implied that the addition of ESP3 into PBS can improve the toughness of the composite more than the addition of PESP into PBS, determined from area under tensile stress-strain curve. In addition, the aggregated PESP in PBS matrix led to lower in toughness of the composite as well. Young's modulus, elongation at break, tensile strength, flexural modulus, flexural strength and impact strength of ESP3/PBS and PESP/PBS composites at 20 wt.% filler content are summarized in Table 4.33.

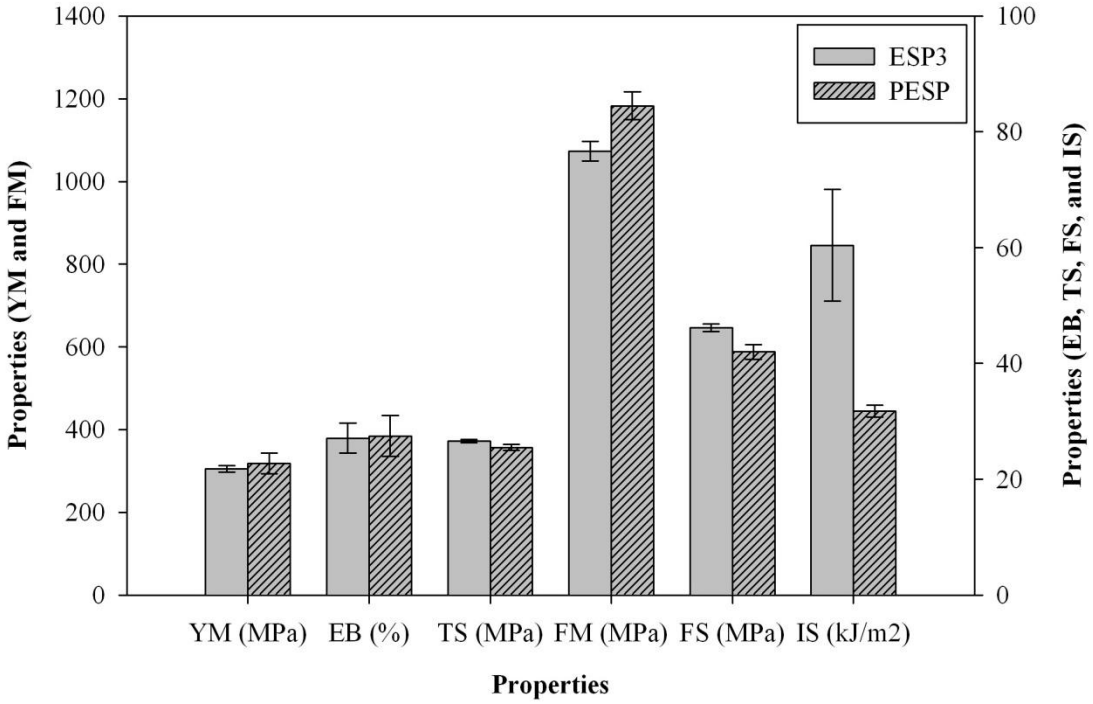

Figure 4.63 Plots of Young's modulus (YM), elongation at break (EB), tensile strength (TS), flexural modulus (FM), flexural strength (FS) and impact strength (IS) of ESP3/PBS and PESP/PBS composites at 20 wt.% filler content.

Table 4.33 Tensile strength, Young's modulus, elongation at break, flexural modulus, flexural strength and impact strength of ESP3/PBS and PESP/PBS composites at 20 wt.% filler content.

PBS composites	Tensile strength (MPa)	Young's modulus (MPa)	Elongation at Break (%)	Flexural modulus (MPa)	Flexural strength (MPa)	Impact strength (kJ/m^2)
ESP3/PBS	26.5±0.2	304.8±8.2	27.0±2.5	1073.0±24.1	46.1±0.6	60.4±9.6
PESP/PBS	25.5±0.5	318.6±24.8	27.4±3.5	1182.6±33.8	41.9±1.2	31.7±1.0

4.5.2.4 Fracture surface morphology

Figure 4.64 shows SEM micrographs of the fracture surface of the ESP3/PBS and PESP/PBS composites. It was found that the ESP3/PBS and PESP/PBS composites showed rough fracture surface as shown in Figure 4.64 (a) and (b) respectively. When compared with ESP3, the particle distribution of PESP within the PBS matrix was not uniform. Moreover, Figure 4.64 (b) shows aggregated PESP particle from the fracture surface. In addition, the interfacial adhesion between PBS matrix and filler particle of ESP3/PBS composite was obviously higher than that of the PESP/PBS composite. The result corresponded to the lower impact strength of the PESP/PBS composite. However, the detachment of PBS matrix from ESP3 and PESP surface with partial PBS left on the surface was observed. Furthermore, the surface topology of PBS filled with ESP3 and PESP still ruptured in a brittle manner.

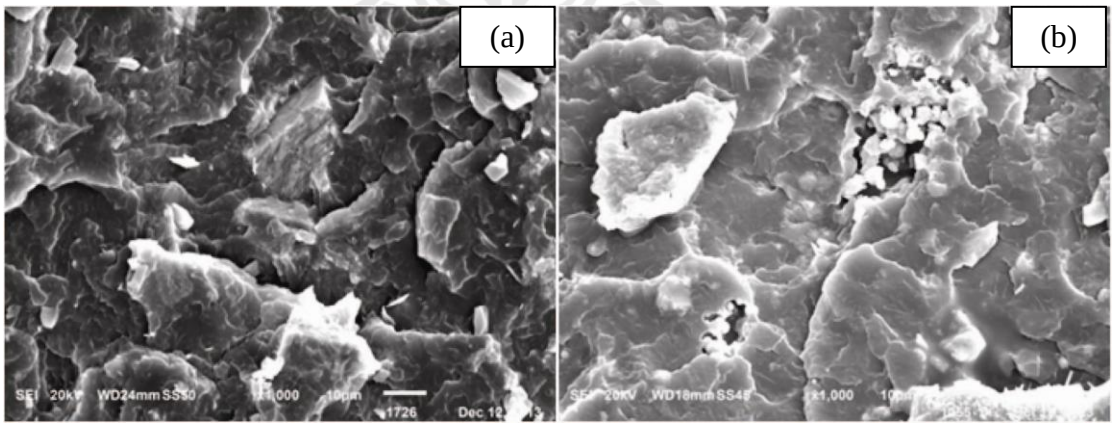

Figure 4.64 SEM micrograph (x1000) of 20 wt.% ESP3/PBS (a) and 20 wt.% PESP/PBS (b) composites.

4.5.2.5 Decomposition temperature

TGA and DTGA curves of neat PBS and PBS composites are shown in Figure 4.65 (a) and (b) respectively. The first transition around 413 and 406^{o}C corresponded to the thermal decomposition of PBS matrix within the ESP3/PBS and PESP/PBS composites, respectively. The second transition at 483 and 477^{o}C was caused by the thermal decomposition of bound PBS in the ESP3/PBS and PESP/PBS composites, respectively, as mentioned in 4.3.1.3. The third transition at 758 and 732^{o}C was the thermal decomposition of ESP3 and PESP within the composites respectively. Comparatively, the decomposition temperature of the PBS matrix in the PESP/PBS composite was lower than that of the ESP3/PBS composite. This illustrated that the incorporation of PESP did affect thermal stability of PBS matrix. Moreover, the bound PBS and PESP had lower decomposition temperature than the bound PBS and ESP3 as well. This might be because the vaterite form of PESP was unstable at ambient temperature resulting in decomposed at low temperature (Piskin and Ozdemir, 2012). Decomposition temperature of ESP3/PBS and PESP/PBS composites at 20 wt.% filler content are listed in Table 4.34.

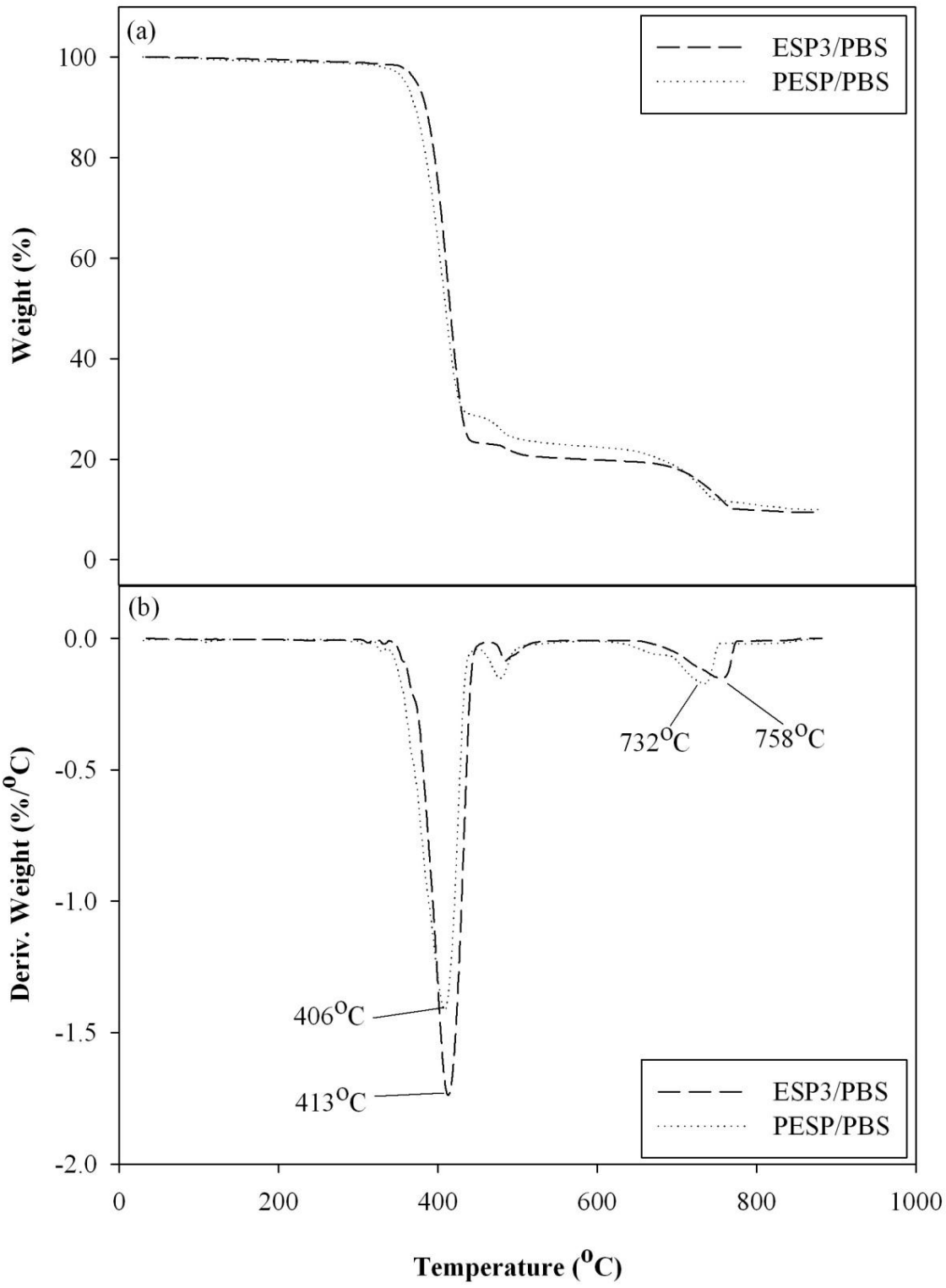

Figure 4.65 TGA (a) and DTGA (b) curves of ESP3/PBS and PESP/PBS composite at 20 wt.% filler content.

4.5.2.6 Melting and crystallization temperature

DSC curves obtained from the first heating and second heating scan of ESP3/PBS and PESP/PBS composites at 20 wt.% filler content are displayed in Figure 4.66. It was found from the first heating scan that the ESP3 and PESP particles did not differently affect melting temperature and cold crystallization temperature of PBS matrix. From the second heating scan, it was revealed that incorporation of ESP3 and PESP did not influence the high melting temperature and cold crystallization temperature of PBS matrix as well. However, the low melting temperature was cleanly observed for PBS filled PESP.

Figure 4.67 shows DSC curves obtained from the first cooling scan of ESP3/PBS and PESP/PBS composites at 20 wt.% filler content. It was found that PBS filled with PESP had higher crystallization temperature than the PBS filled with ESP3. Nevertheless, the degree of crystallinity obtained from the second heating of PBS filled with ESP3 and PESP was so close. Accordingly, PBS filled with PESP had higher crystallinity degree than the PBS filled with ESP3. Melting temperature, crystallization temperature and crystallinity degree of PBS composite prepared with ESP3 and PESP are shown in Table 4.34.

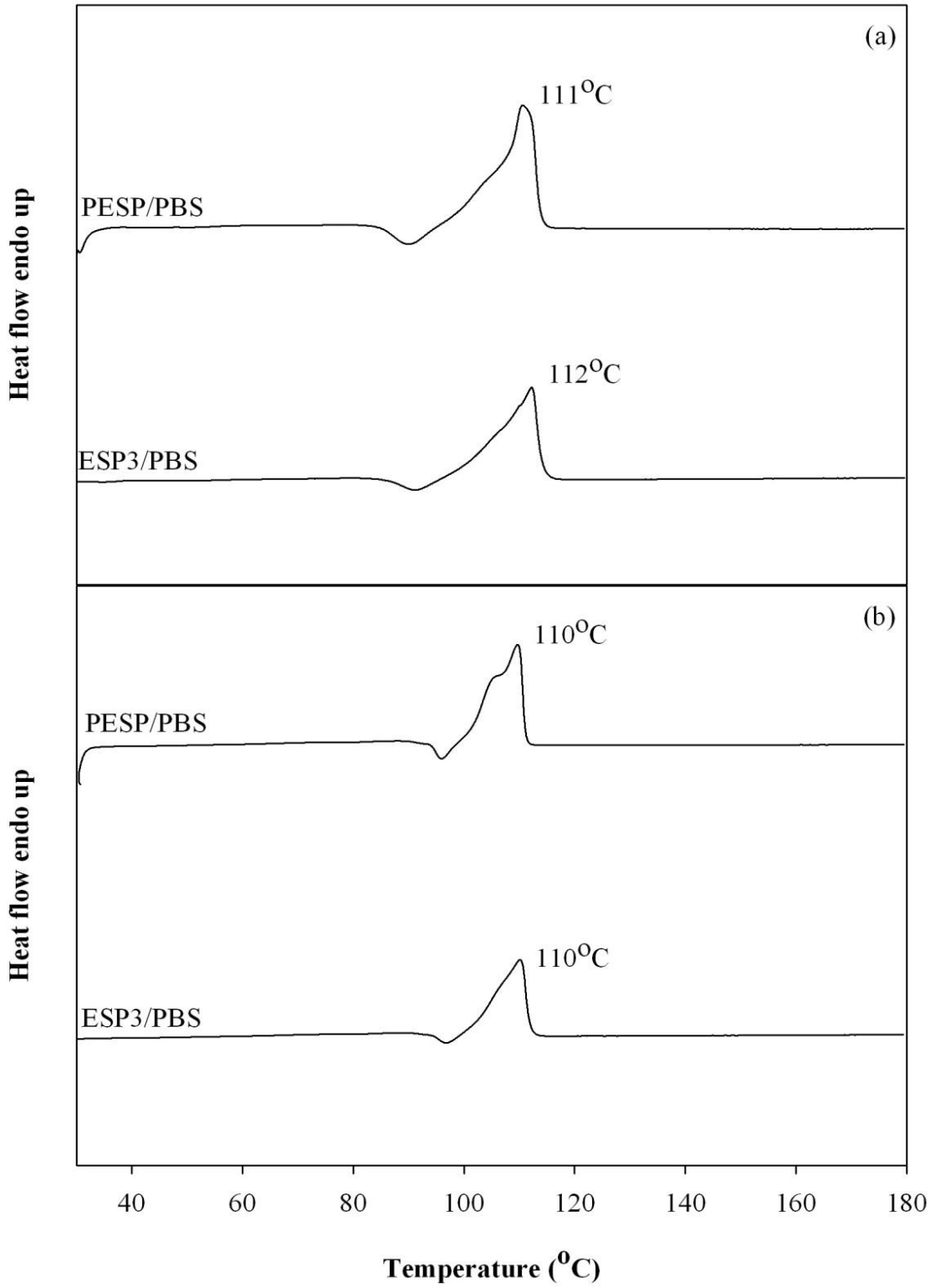

Figure 4.66 DSC curves obtained from the 1st heating (a) and the 2nd heating (b) scan of ESP3/PBS and PESP/PBS composites at 20 wt.% filler content.

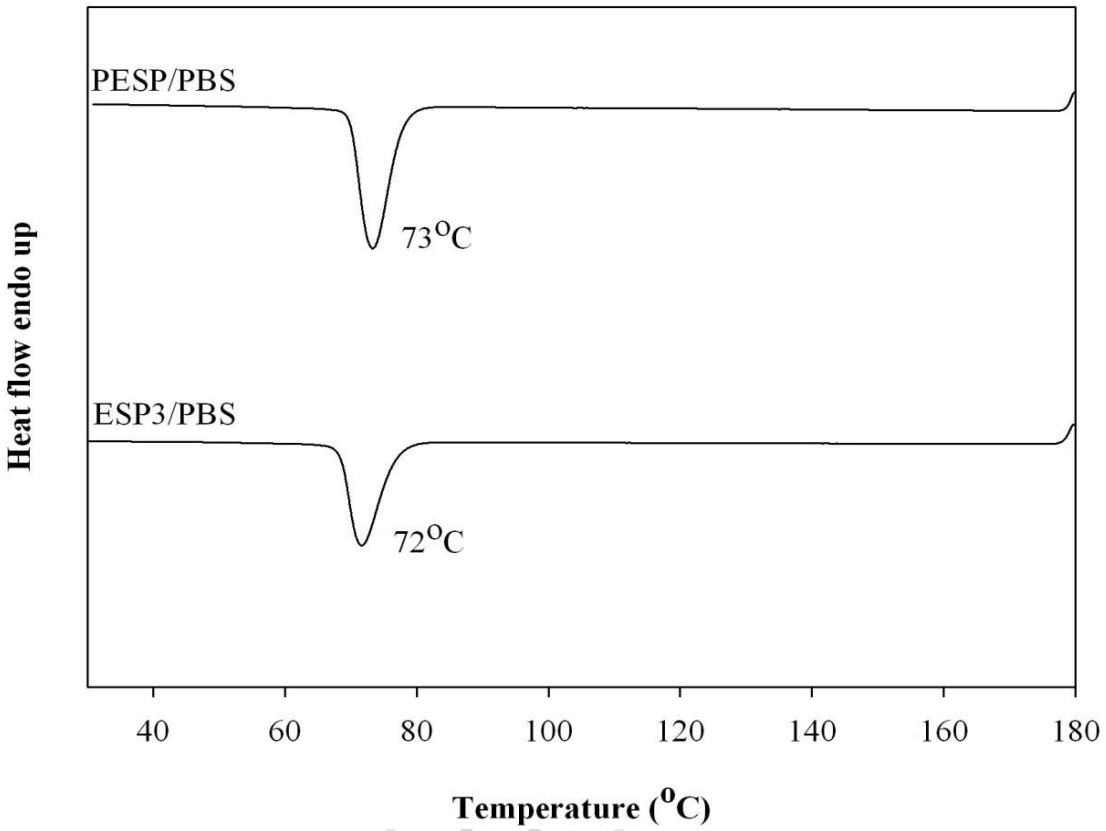

Figure 4.67 DSC curves obtained from the 1st cooling scan of ESP3/PBS and PESP/PBS composites at 20 wt.% filler content.

Table 4.34 Decomposition temperature (T_d), melting temperature (T_m), crystallization temperature (T_c) and degree of crystallinity (X_c) of ESP3/PBS and PESP/PBS composites at 20 wt.% filler content.

PBS composites	T_d (^oC)				T_m (^oC)		T_c (^oC)	Delta H (J/g)		X_c (%)	
	PBS	Bound PBS	ESP3	PESP	1st scan	2nd scan		1st scan	2nd scan	1st scan	2nd scan
ESP3/PBS	413	483	758	-	112	110	72	48.5	56.0	35.2	40.6
PESP/PBS	406	477	-	732	111	110	73	60.5	61.0	43.9	44.2

CHAPTER V

CONCLUSIONS

In this study, chicken eggshell was used in forms of eggshell powder (ESP) and precipitated eggshell powder (PESP) for high density polyethylene (HDPE) composite and poly (butylene succinate) (PBS) composite. The eggshell powder contained calcium carbonate ($CaCO_3$) about 94 wt.% in calcite polymorph. The precipitated eggshell powder (PESP) comprised $CaCO_3$ as main component in calcite and vaterite polymorph. In addition, some organic compounds of eggshell matrix were removed by ESP precipitation.

For ESP/HDPE composite, the ESP with average particle size of 13.96 μm was used for preparing the composite. MFI of the composite decreased with increasing ESP content. Ductile to brittle transition of the composite occurred at 30 wt.% ESP. Yield strength, tensile stress at break and impact strength of the composite decreased. However, Young's modulus and flexural modulus significantly increased and flexural strength of the composites slightly increased with increasing ESP content. The addition of ESP at various contents did not influence decomposition, melting and crystallization temperature of HDPE matrix. However, degree of crystallinity of HDPE composite decreased with increasing ESP content.

For studying effect of ESP particle size, it was found that the smaller particle size of 13.96 μm of ESP improved elongation at break and impact strength of 20 wt.% ESP/HDPE composite. However, MFI, yield strength, tensile stress at break, Young’s

modulus, flexural strength and flexural modulus of the filled HDPE did not depend on ESP particle size. On the other hand, the ESP particle size did influence thermal decomposition of HDPE matrix. The decomposition temperature of HDPE matrix increased with decreasing ESP particle size. Melting temperature, crystallization temperature, and degree of crystallinity of the HDPE composite were not influenced by ESP particle size.

For compatibilized ESP/HDPE composite, the 20 wt.% ESP with average particle size of 20.35 μm was used for preparing the uncompatibilized and compatibilized HDPE composites. MFI slightly decreased, yield strength, flexural properties gradually increased and impact strength significantly improved with increasing HDPE-g-MAH content. With increasing HDPE-g-MAH content, Young's modulus of HDPE composites compatibilized with various HDPE-g-MAH composition was not much different. HDPE-g-MAH helped reduce brittleness of 20 wt.% ESP/HDPE composite whereas EPR-g-MAH had negative effect on tensile properties, flexural properties and impact strength of the compatibilized HDPE composites. However, with increasing EPR-g-MAH content, MFI of compatibilized HDPE composite insignificantly change compare to that of uncompatibilized HDPE composite. Decomposition, melting, and crystallization temperatures insignificantly influenced by addition of HDPE-g-MA and EPR-g-MAH. Adding EPR-g-MAH into HDPE composite insignificant affected HDPE's crystallinity. On the other hand, adding 2 wt.% HDPE-g-MAH resulted in significant decrease of crystallinity of HDPE matrix compared to that of uncompatibilized HDPE composite. Nevertheless, the crystallinity increased when adding 5-10 wt.% HDPE-g-MAH.

For PESP/HDPE composite, ductile to brittle transition occurred at PESP content of 20 wt.%. MFI, yield strength, tensile stress at break, elongation at break and impact strength of HDPE composite slightly decreased with increasing PESP content. However, Young's modulus, flexural modulus of the composite slightly increased with increasing PESP content. Nevertheless, flexural strength of HDPE composites at various PESP contents was insignificantly different. The addition of PESP into HDPE significantly increased degradation temperature of HDPE matrix. PESP content did not significantly affect melting and crystallization temperature of HDPE matrix. Degree of crystallinity of HDPE composites slightly decreased with increasing PESP content.

In comparison of physical properties between ESP/HDPE and PESP/HDPE composites, MFI, Young's modulus and flexural modulus of the PESP/HDPE composite were slightly higher than ESP/HDPE composite. Yield strength, tensile stress at break and flexural strength of ESP/HDPE and PESP/HDPE composite were not different. Impact strength of ESP/HDPE composite was higher than that of PESP/HDPE composite. The ESP and PESP did not affect decomposition and melting temperature of HDPE matrix. HDPE filled with ESP had higher crystallization temperature and cyrstallinity than HDPE filled with PESP.

For ESP/PBS composite, prepared with ESP having average particle size of 13.96 μm, MFI, tensile strength, elongation at break and impact strength of PBS composites decreased with increasing ESP content. However, the ESP/PBS composites ruptured before yielding under the tensile force. Young's modulus, flexural modulus and flexural strength of PBS composite increased with increasing ESP content. ESP did not affect decomposition and melting temperature of PBS

matrix. Adding ESP into PBS resulted in decreased crystallization temperature of PBS matrix. Degree of crystallinity of the composite decreased with increasing ESP content.

For PESP/PBS composite, MFI, flexural modulus and flexural strength of PBS composites increased with increasing PESP content. Tensile strength, elongation at break and impact strength of PBS composites decreased with increasing PESP content. However, the PESP/PBS composite ruptured before yielding under the tensile test. PESP did not affect decomposition and melting temperature of PBS matrix. Adding PESP into PBS resulted in slightly decreased crystallization temperature of PBS matrix. Degree of crystallinity of the composite decreased with increasing PESP content.

For comparison of physical properties between ESP/PBS and PESP/PBS composites at 20 wt.% ES filler, MFI, flexural modulus of the PESP/HDPE composite were higher than those of ESP/HDPE composite. Elongation at break and tensile strength of ESP/PBS and PESP/PBS composite were insignificantly different. Flexural strength of the PESP/PBS composite was slightly lower than that of the ESP/PBS composite. The ESP/PBS composite had higher impact strength than the PESP/PBS composite. Furthermore, the ESP/PBS and PESP/PBS composites did not yield at 20 wt.% filler content. ESP and PESP particles did not affect melting temperature of PBS matrix. Moreover, PBS filled with PESP had slightly higher decomposition and crystallization temperature than the PBS filled with ESP. However, PBS filled with PESP had higher degree of crystallinity than the PBS filled with ESP.

REFERENCES

Atikler, U., Basalp, D. and Tihminlioğlu, F. (2006). Mechanical and morphological properties of recycled high-density polyethylene, filled with calcium carbonate and fly ash. **J. Appl. Polym. Sci.** 102: 4460–4467.

Bartczak, Z., Argon, A. S., Cohen, R. E. and Weinberg, M. (1999). Toughness mechanism in semi-crystalline polymer blends: II. High-density polyethylene toughened with calcium carbonate filler particles. **Polymer**. 40: 2347-2365.

Benham, E. and McDaniel, M. (2003). Ethylene polymers, HDPE. **Enc. Polym. Sci. Tech.** 2: 382-412.

Bian, J., Wang, X., Wen, X., Han, C., Wang, S., and Dong, L. (2010). Nonisothermal crystallization behavior and mechanical properties of poly (butylene succinate)/silica nanocomposites. **J. Appl. Polym. Sci**. 116: 902–912.

Chojnacka, K. (2005). Biosorption of Cr (III) ions by eggshells. **J. Haz. Mater.** 121: 167–173.

Chrissafis, K., Paraskevopoulos, K. M., Tsiaoussis, I. and Bikiaris, D. (2009). Comparative study of the effect of different nanoparticles on the mechanical properties, permeability, and thermal degradation mechanism of HDPE. **J. Appl. Polym. Sci.** 114: 1606–1618.

Cordeiro, C. M. and Hincke, M. T. (2011). Recent patents on eggshell: shell and membrane applications. **Recent patents on food nutrition agriculture**. 3: 1-8.

Cusack, M., Fraser, A. C. and Stachel, T. (2003). Magnesium and phosphorus distribution in the avian eggshell. **Comp. Bioch. Phys. Part B: Biochemistry and Molecular Biology.** 134: 63-69.

Dangtungee, R. and Shawaphun, S. (2008). Mechanical properties of polypropylene filled with egg shell. **J. KMUTNB.** 18: 9-15.

Dasgupta, P., Singh, A., Adak, S. and Purohit, K. M. (2004). Synthesis and characterization of hydroxyapatite produced from eggshell. **International Symposium of Research Students on Mater. Sci. Eng.** (pp. 1-6). Chennai, India

Dauphin, Y., Cuif, J. P., Salomé, M., Susini, J. and Williams, C. (2006). Microstructure and chemical composition of giant avian eggshells. **Analyt. Bioa. Chem.** 386: 1761-1771.

Dennis, J. E., Xiao, S. Q., Agarwal, M., Fink, D. J., Heuer, A. H. and Caplan, A. I. (1996). Microstructure of matrix and mineral components of eggshells from White Leghorn chickens (Gallus gallus). **J. Morph.** 228: 287-306.

Dobiášová, L., Kužel, R., Šichová, H. and Kopeček, J. (2009). The egg-shell microstructure studied by powder diffraction. online positing. http://www.xray.cz/epdic/abstracts/293.htm.

Elleithy, R. H., Ali, I., Ali, M. A. and Al-Zahrani, S. M. (2010). High density polyethylene/micro calcium carbonate composites: A study of the morphological, thermal, and viscoelastic properties. **J. Appl. Polym. Sci.** 117: 2413–2421.

Egg Basics for the Consumer. Online posting. http://foodsafety.suencs.com/060909-egg-basics-for-the-consumer.

Freire, M. N. and Holanda, J. N. F. (2006). Characterization of avian eggshell waste aiming its use in a ceramic wall tile paste. **Cerâmica**. 52: 240-244.

Funabashi, M., Flores, E., Kunioka, M. (2010). Biomass carbon ratio of polymer composites measured by accelerator mass spectrometry. **J Polym Environ**. 18: 85–93.

Gautron, J. and Nys, Y. (2007). Eggshell matrix proteins. In R. Huopalahti, R. López-Fandiño, M. Anton, & R. Schade (eds.) **Bioactive Egg Compounds** (pp. 103-108). Berlin Heidelberg: Springer.

Ghani, S. A. and Young, H. C. (2010). Conductive polymer based on polyaniline-eggshell powder (PANI-ESP) composites. **J. Phys. Sci.** 21: 81-97.

Gil, K. B. and Mok, L. S. (2007). Removal of heavy metals using waste eggshell. **J. Env. Sci.** 19: 1436–1441.

Glatz, P., Miao, Z. and Rodda, B. (2011). Handling and treatment of poultry hatchery waste: a review. **Sustainability**. 3: 216-237.

Gongruttananun, N. (2011). Influence of red light on reproductive performance, eggshell ultrastructure, and eye morphology in Thai-native hens. **Poult Sci.** 90: 2855-2863.

Goran, G. V., Crivneanu, V., Tudoreanu, L. and Udrea, D. (2010). Dynamics of some mineral elements in hen eggs. **Bulletin UASVM, Veterinary Medicine**. 67: 88-94.

Gungor, A. (2007). Mechanical properties of iron powder filled high density polyethylene composites. **Materials and Design**. 28: 1027-1030.

Guo, W., Zhang, W. (2013). Mechanical properties and crystallization behavior of hydroxyapatite/poly (butylene succinate) composites. **J Biomed Mater Res Part A.** 191: 2500–2506.

Hassan, S. B., and Patrick, S. N. (2012). Development of polyester/eggshell particulate composites. **Trib Ind.** 34: 217-225.

Hincke, M. T., Chien, Y.-C., Gerstenfeld, L. C. and McKee, M. D. (2008). Colloidal-gold immunocytochemical localization of osteopontin in avian eggshell gland and eggshell. **J Histochem Cytochem.** 56: 467–476.

Hincke, M. T., Gautron, J., Panheleux, M., Garcia-Ruiz, J., McKee, M. D. and Nys, Y. (2000). Identification and localization of lysozyme as a component of eggshell membranes and eggshell matrix. **Matrix Biology.** 19: 443-453.

Hoidy, W., Al-Mulla, E. and Al-Janabi, K. (2010). Mechanical and thermal properties of PLLA/PCL modified clay nanocomposites. **J. Polym. Env.** 18: 608-616.

Hunton, P. (2005). Research on eggshell structure and quality: An historical overview. **Brazil. J. Poul. Sci.** 7: 67-71.

Intharapat, P., Kongnoo, A., and Kateungngan, K. (2013). The potential of chicken eggshell waste as a bio-filler filled epoxidized natural rubber (ENR) composite and its properties. **J Polym Environ.** 21: 245–258.

Jai, P. H., Jeong, S. W., Yang, J. K., Kim, B. G. and Lee, S. M. (2007). Removal of heavy metals using waste eggshell. **J. Env. Sci.** 19: 1436-1441.

Ji, G., Hongqi, Z., Chenze, Q. and Minfeng, Z. (2009). Mechanism of interactions of eggshell microparticles with epoxy resins. **Polym. Eng. Sci.** 49: 1383-1388.

Kim, H., Biswas, J. and Choe, S. (2006). Effects of stearic acid coating on zeolite in LDPE, LLDPE, and HDPE composites. **Polymer.** 47: 3981-3992.

Kim, H. S., Kim, H. J., Lee, J. W. and Choi, I. G. (2006). Biodegradability of bio-flour filled biodegradable poly(butylene succinate) bio-composites in natural and compost soil. **Polym. Degrad. Stab.** 91: 1117-1127.

King'ori, A. M. (2011). A review of the uses of poultry eggshells and shell membranes. **Inter. J. Poul. Sci.** 10: 908-912.

Kobeleva, A. R. and Poilov, V. Z. (2007). Technology for production of calcium carbonate with prescribed properties. **Russ. J. Appl. Chem.** 80: 1447-1452.

Krishna, D. S. R., Siddharthan, A., Seshadri, S. K. and Kumar, T. S. S. (2007). A novel route for synthesis of nanocrystalline hydroxyapatite from eggshell waste. **J. Mater. Sci. Mater. Med.** 18: 1735–1743.

Krishna, D. S. R., Siddharthan, A., Seshadri, S. K. and Kumar, T. S. S. (2007). A novel route for synthesis of nanocrystalline hydroxyapatite from eggshell waste. **J. Mater. Sci. Mater. Med.** 18: 1735-1743.

Kwon, S., Kim, K. J., Kim, H., Kundu, P. P., Kim, T. J., Lee, Y. K., Choe, S. (2002). Tensile property and interfacial dewetting in the calcite filled HDPE, LDPE, and LLDPE composites. **Polymer.** 43: 6901-6909.

Lee, M. W., Han, S. O. and Seo, Y. B. (2008). Red algae fibre/poly(butylene succinate) biocomposites: The effect of fibre content on their mechanical and thermal properties. **Comp. Sci. Tech.** 68: 1266-1272.

Lee, S. J. and Oh, S. H. (2003). Fabrication of calcium phosphate bioceramics by using eggshell and phosphoric acid. **Mater. Lett.** 57: 4570-4574.

Li, G., Mai, K. C., Feng, K. C., and Huang, Y. P. (2006). Preparation and characterization of nano-$CaCO_3$ encapsulated by copolymerization of styrene and maleic anhydride. **Polym Int.** 55: 891–897.

Li, H., Zheng, M. and Xu, X. (2001). A study on HDPE/sulfonated EPDM-treated $CaCO_3$ blends. **J. Appl. Polym. Sci.** 80: 2140–2144.

Liu, Z. H., Kwok, K. W., Li, R. K. Y. and Choy, C. L. (2002). Effects of coupling agent and morphology on the impact strength of high density polyethylene/$CaCO_3$ composites. **Polymer.** 43: 2501-2506.

Liu, Z. H., Zhu, X. G., Li, Q., Qi, Z. N. and Wang, F. S. (1998). Effect of morphology on the brittle ductile transition of polymer blends: 5. The role of $CaCO_3$ particle size distribution in high density polyethylene/$CaCO_3$ composites. **Polymer.** 39: 1863-1868.

Mine, Y. (2008). **Egg bioscience and biotechnology** (pp. 1-168): Hoboken, N.J.

Mnifa, N., Massardiera, V., Kallel, T. and Elleuch, B. (2010). New (PP/EPR)/nano-$CaCO_3$ based formulations in the perspective of polymer recycling. Effect of nanoparticles properties and compatibilizers. **Polym. Adv. Technol.** 21: 896–903.

Murakami, F. S., RodriguesI, P. O., Campos, C. M. T. and Silva, M. A. S. (2007). Physicochemical study of $CaCO_3$ from egg shells. **Ciência e Tecnologia de Alimentos.** 27: 658-662.

Osman, M. A., Atallah, A. and Schweizer, T., and Ottinger, H. C. (2004). Particle-particle and particle-matrix interactions in calcite filled high-density polyethylene steady shear. **J. Rheol.** 48: 1167-1184.

Osman, M. A. and Atallah, A. (2005). Interparticle and particle–matrix interactions in polyethylene reinforcement and viscoelasticity. **Polymer.** 46: 9476-9488.

Osman, M. A. and Atallah, A. (2006). Effect of the particle size on the viscoelastic properties of filled polyethylene. **Polymer.** 47: 2357-2368.

Pakdeechote, P. (2010). Preparation of chicken eggshell for high density polyethylene composites. Master of Engineering, Thailand, Nakhon Ratchasima.

Pakdeechote, P., Suppakarn, N., Ruksakulpiwat, Y. and Sutapun, W. (2010) August 26-27. Rheological, mechanical and morphological properties of eggshell powder (esp.) filled high density polyethylene (HDPE). Paper presented at **The The Sixth Thailand Materials Science And Technology Conference** (MSAT-6), Bangkok.

Park, H. J., Jeong, S. W., Yang, J. K., Kim, B. G. and Lee, S. M. (2007). Removal of heavy metals using waste eggshell. **J. Env. Sci.** 19: 1436-1441.

Phua, Y. J., Chow, W. S. and Mohd Ishak, Z. A. (2011). The hydrolytic effect of moisture and hygrothermal aging on poly(butylene succinate)/organo-montmorillonite nanocomposites. **Polym. Degrad. Stab.** 96: 1194-1203.

Phua, Y. J., Chow, W. S. and Mohd Ishak, Z. A. (2011). Mechanical properties and structure development in poly (butylene succinate)/organo-montmorillonite nanocomposites under uniaxial cold rolling. **EXPRESS Polym. Lett.** 5: 93-103.

Phueakbuakhao, N., Ouajai, W. and Kreua-Ongarjnukool, N. (2008). Effect of coupling agents on mechanical properties and morphology of $CaCO_3$-filled recycled high density polyethylene. **J Miner Met Mater Soc.** 18: 131-135.

Pines, M., Knopov, V. and Bar, A. (1996). Involvement of osteopontin in egg shell formation in the laying chicken. **Matrix Biology.** 14: 765-771.

Popescu, M. A., Matei, C., Fagarasan, G., and Plesu, V. (2013). Thermal decomposition of calcium carbonate polymorphs precipitated in the presence of ammonia and alkylamines. **Adv Pow Tech.** 1: 1-8.

Qiu, Z., Komura, M., Ikehara, T., and Nishi, T. (2003). DSC and TMDSC study of melting behaviour of poly (butylene succinate) and poly (ethylene succinate). **Polym.** 44: 7781–7785.

Renaudin, G., Bertrand, A., Dubois, M., Gomes, S., Chevalier, P. and Labrosse, A. (2008). A study of water releases in ground (GCC) and precipitated (PCC) calcium carbonates. **J. Phys. Chem. Sol.** 69: 1603-1614.

Reza, S. M., Ramezani, D. H. and Akbar, G. (2008). Mechanical properties and vulcanization characteristics of styrene-butadiene rubber (SBR) based compounds filled with eggshell powder as a bio-filler. **AIP Conference Proceedings.** 1042: 312-314.

Rose, M. and Hincke, M. (2009). Protein constituents of the eggshell: eggshell-specific matrix proteins. **Cell. Mol. Life. Sci.** 66: 2707-2719.

Sabriye, Pişkin, Ö. D. Ö. (2012). Effect of process conditions on crystal structure of precipitated calcium carbonate ($CaCO_3$) from fly ash: Na_2CO_3 preparation. **IJBEES.** 1: 2277-4394.

Saeb, N. R., Khonakdar, H. A., Heinrich, G., and Wagenknecht, U. (2012). A comparative study on curing characteristics and thermomechanical properties of elastomeric nanocomposites: the effects of eggshell and calcium carbonate nanofillers. **J. Appl. Polym. Sci.** 127: 4241-4250.

Sahebian, S., Zebarjad, S. M., Khaki, J. V. and Sajjadi, S. A. (2009). The effect of nano-sized calcium carbonate on thermodynamic parameters of HDPE. **J. Mater. Process. Tech.** 209: 1310-1317.

Sahebian, S., Zebarjad, S. M., Sajjadi, S. A., Sherafat, Z. and Lazzeri, A. (2007). Effect of both uncoated and coated calcium carbonate on fracture toughness of HDPE/$CaCO_3$ nanocomposites. **J. Appl. Polym. Sci.** 104: 3688-3694.

Sahnoune, F., Cuesta, J. M., and Crespy, A. (1999). Effect of elastomer interfacial agents on tensile and impact properties of $CaCO_3$ filled HDPE. **J. Mater. Sci.** 34: 535-544.

Salam, Z. A. A., Abdou, A. M. and Harith, M. A. (2006). Elemental and utrastructure analysis of the eggshell: Ca, Mg and Na distribution during embryonic development via LIBS and SEM techniques. **Inter. J. Poul. Sci.** 5: 35-42.

Scala, J. N. L., Boleli, I., Ribeiro, L., Freitas, D. and Macari, M. (2000). Pore size distribution in chicken eggs as determined by mercury porosimetry. **Rev. Bras. Cienc. Avíc.** 2: 1-10.

Shih, Y. F., Chen, L. S. and Jeng, R. J. (2008). Preparation and properties of biodegradable PBS/multi-walled carbon nanotube nanocomposites. **Polymer.** 49: 4602-4611.

Shuhadah, S. and Supri, A. G. (2009). LDPE-Isophthalic acid-modified egg shell powder composites (LDPE/ESPI). **J. Phys. Sci.** 20: 87–98.

Stadelman, W. J. and Cotterill, O. J. (1995). Quality identification of eggshell (4th ed.). **Egg science and technology** (pp. 39-151). The Haworth press, Inc.

Suwanprateeb, J. (2000). Calcium carbonate filled polyethylene: correlation of hardness and yield stress. **Compos. Part A- Appl S.** 31: 353-359.

Suzuki, F. K., Wang, P. Y., Weatherspoon, J. B. and Mead, L. C. (2012). Method of producing eggshell powder. Online posting. http://www.google.com/patents/US20060062857.

Tanniru, M. and Misra, R. D. K. (2005). On enhanced impact strength of calcium carbonate-reinforced high-density polyethylene composites. **Mater. Sci. Eng.** 405: 178–193.

Tanniru, M., Misra, R. D. K., Berbrand, K. and Murphy, D. (2005). The determining role of calcium carbonate on surface deformation during scratching of calcium carbonate-reinforced polyethylene composites. **Mater. Sci. Eng: A.** 404: 208-220.

Teir, S., Eloneva, S. and Zevenhoven, R. (2005). Production of precipitated calcium carbonate from calcium silicates and carbon dioxide. **Energ. Conv. and Managem.** 46: 2954-2979.

Teixeira, S. C. S., Moreira, M. M., Lima, A. P., Santos, L. S., Rocha, B. M. d., Lima, E. S. d., Coutinho3, F. M. B. (2006). Composites of high density polyethylene and different grades of calcium carbonate: Mechanical, rheological, thermal, and morphological properties. **J. Appl. Polym. Sci.** 101: 2559–2564.

Toro, P., Quijada, R., Yazdani-Pedram, M. and Arias, J. L. (2007). Eggshell, a new bio-filler for polypropylene composites. **Mater. Lett.** 61: 4347-4350.

Tsai, W. T., Yang, J. M., Lai, C. W., Cheng, Y. H., Lin, C. C. and Yeh, C. W. (2006). Characterization and adsorption properties of eggshells and eggshell membrane. **Biores. Tech.** 97: 488-493.

Tsai, W.-T., Yang, J.-M., Hsu, H.-C., Lin, C.-M., Lin, K.-Y. and Chiu, C.-H. (2008). Development and characterization of mesoporosity in eggshell ground by planetary ball milling. **Micropor. Mesopor. Mater.** 111: 379-386.

Vassiliou, A. A., Mabrouk, K. E., and Kontopoulou, M. (2011). Effect of evolved interactions in poly (butylene succinate)/fumed silica biodegradable in situ prepared nanocomposites on molecular weight, material properties, and biodegradability. **J. App. Polym. Sci.** 119: 2010–2024.

Virta, R. L. (2002). Clay and shaleu.s. **Geological Survey Minerals Yearbook** (pp. 18.11-18.27).

Wang, W. Y., Zeng, X. F., Wang, G. Q. and Chen, J. F. (2007). Preparation and characterization of calcium carbonate/low-density-polyethylene nanocomposites. **J. Appl. Polym. Sci.** 106: 1932–1938.

Wei, H., Shen, Q., Zhao, Y., Zhou, Y., Wang, D. and Xu, D. (2005). On the crystallization of calcium carbonate modulated by anionic surfactants. **J. Crys. Growth.** 279: 439-446.

Witoon, T. (2011). Characterization of calcium oxide derived from waste eggshell and its application as CO2 sorbent. **Ceram. Inter.** 37: 3291-3298.

Wypych, G. (2000). Calcium carbonate (2nd ed.). Handbook of fillers (pp. 48-58).

Xanthos, M. (2010). Calcium carbonate (2nd ed.). **Functional fillers for plastics** (pp. 291-305): Wiley-VCH.

Xie, T., Liu, H., Ou, Y. and Yang, G. (2005). Property transitions in high-density polyethylene/maleated poly(ethylene–octene)/calcium carbonate ternary composites. **J. Appl. Polym. Sci.** 101: 3361–3366.

Xu, N., Zou, J., Shi, W., Feng, J. and Gong, M. (2005). Unsaturated hyperbranched polyester as a surface modifier of $CaCO_3$ and enhanced effect on mechanical properties of HDPE/$CaCO_3$ composites. **Polym. Adv. Tech.** 16: 378–386.

Xu, X., Zhao, Y., Lai, Q. and Hao, Y. (2011). Effect of polyethylene glycol on phase and morphology of calcium carbonate. **J. Appl. Polym. Sci.** 119: 319-324.

Dauphin, J. C., M Salomé, J Susini , CT Williams. (2006). Microstructure and chemical composition of giant avian eggshells. **Anal. Bioanal. Chem**. 386: 1761-1771.

Yang, Y.-L., G'Sell, C., Hiver, J. M. and Bai, S.-L. (2007). Dynamic mechanical properties and morphology of high-density polyethylene/$CaCO_3$ blends with and without an impact modifier. **J. Appl. Polym. Sci.** 103: 3907–3914.

Yoo, S., Hsieh, J. S., Zou, P. and Kokoszka, J. (2009). Utilization of calcium carbonate particles from eggshell waste as coating pigments for ink-jet printing paper. **Biores. Tech.** 100: 6416-6421.

Yun, F., Qiao, F., Lauke, and Wing, M. (2008). Effects of particle size, particle/matrix interface adhesion and particle loading on mechanical properties of particulate–polymer composites. **Compos Part B**. 39: 933-961.

Zweifel, H. (2008). Calcium carbonate Plastics (5th ed.). **Additives Handbook** (pp. 932-934).

APPENDIX A

DEFINITION OF SYMBOL FOR PARTICLE SIZE AND SIZE DISTRIBUTION

Definition of symbol for particle size and size distribution

D [4, 3] = Mean diameter value by volume

D [0, 1] = 10 volume percent less than or equal to a given diameter

D [0, 5] = 50 volume percent less than or equal to a given diameter

D [0, 9] = 90 volume percent less than or equal to a given diameter

APPENDIX B

LIST OF PUBLICATIONS

List of Publications

Buakaew, W., Ruksakulpiwat, Y., Suppakarn, N., and Sutapun, W. (2013). Effect of compatibilizers on mechanical and thermal properties of high density polyethylene filled with bio-filler from eggshell. **Adv. Mater. Res.** 699: 57-62.

Buakaew, W., Ruksakulpiwat, Y., Suppakarn, N., and Sutapun, W. (2013). Effect of filler particle size on mechanical and thermal properties of high density polyethylene filled with bio-filler from eggshell waste. In **Proceeding of the Pure and Applied Chemistry International Conference 2013** (pp 607-610). Chon Buri, Thailand.

Buakaew, W., Ruksakulpiwat, Y., Suppakarn, N., and Sutapun, W. (2013). Mechanical, thermal and morphological properties of poly (butylene succinate) filled with bio-functional filler from eggshell waste. **Adv. Mater. Res.** 747: 72-75.

Advanced Materials Research Vol. 699 (2013) pp 57-62
Online available since 2013/May/27 at www.scientific.net

doi:10.4028/www.scientific.net/AMR.699.57

Effect of Compatibilizers on Mechanical and Thermal Properties of High Density Polyethylene Filled with Bio-Filler from Eggshell

Wanikorn Buakaew[1, 2, a], Yupaporn Ruksakulpiwat[1, b], Nitinat Suppakarn[1, c], and Wimonlak Sutapun[1, d]

[1]School of Polymer Engineering, Institute of Engineering, Suranaree University of Technology, NakhonRatchasima, 30000 Thailand

[2]Center of Excellence on Petrochemical, and Materials Technology, Chulalongkorn University, Bangkok, 10330 Thailand

[a]wanikorn102@gmail.com, [b]yupa@sut.ac.th, [c]nitinat@sut.ac.th, [d]wimonlak@sut.ac.th

Keywords: Eggshell, Calcium Carbonate, ESP/HDPE composite, compatibilizer.

Abstract. In this research work, the effect of compatibilizers on mechanical and thermal properties of ESP/HDPE composites was investigated. High density polyethylene grafted with maleic anhydride (HDPE-g-MA) and ethylene propylene rubber grafted with maleic anhydride (EPR-g-MA) were used to compatibilize the ESP/HDPE composites. The ESP/HDPE composite with and without the compatibilizes was prepared at 20 wt.% ESP. The volume average particle size of ESP was 20.35 µm. The compatibilized HDPE composites were prepared at 2, 5, 8 and 10 wt.% of HDPE-g-MA and at 2, 5, 8 and 10 wt.% of EPR-g-MA, as well. It was found that ultimate stress, yield strength, and elongation at break of the ESP/HDPE composites prepared with HDPE-g-MA increased with increasing HDPE-g-MA content. In addition, Young's modulus was maximum at 8 wt.% HDPE-g-MA. The composites filled with HDPE-g-MA had improved impact strength with increasing HDPE-g-MA content. On the other hand, the composites with EPR-g-MA showed a decrease in tensile properties and impact strength when increasing EPR-g-MA content. The impact strength of the HDPE composites compatibilized with EPR-g-MA decreased with increasing EPR-g-MA content. In addition, degree of crystallinity of the composites with EPR-g-MA was higher than that of the composite with HDPE-g-MA. Furthermore, compatibilizing ESP/HDPE composites with either HDPE-g-MA or EPR-g-MA did not influence HDPE and ESP decomposition temperatures, HDPE melting temperature and HDPE crystallization temperature.

Introduction

Avian eggshell contains approximately 94 wt.% calcium carbonate, 1 wt.% magnesium carbonate, 1 wt.% calcium phosphate and 4 wt.% organic matters [1]. Chicken eggshell from hatchery industry, food industry and household is commonly disposed to landfill by which enormous amount of the eggshell waste, about 250,000 tons per annum, was left in environment [2]. Actually, the waste comprised valuable $CaCO_3$ of 94 wt.%; this content is close to purity of ground calcium carbonate (GCC) filler, 80 wt.%, used in plastic industry [3]. High density polyethylene (HDPE), a semicrystalline polymer, is one of the most consumed thermoplastics and the demand market of HDPE is annually increasing. Its vast application includes automotive, industrial, and household applications. However, its application has been limited, according to its mechanical properties are not high enough for some sectors of industrial application such as pipe and containers [4]. HDPE has therefore been compounded with some reinforcing mineral fillers. More than 60% of the reinforcing fillers used in HDPE are calcium carbonate as GCC and PCC (precipitated calcium carbonate) [5]. By the way, raw material as sedimentary rock for calcium carbonate production takes so long time for accumulating in nature. Therefore, eggshell is one of good GCC filler replacement due to its availability and high content in calcium carbonate. Most importantly, it is regenerated from bio-source. It has been reported that ground eggshell was used as a filler for non polar polymers such as HDPE [6], LDPE [7] and PP [8] in which eggshell calcium carbonate helped improve Young's modulus of the filled polymers. However, their tensile and impact strength were significantly

deteriorated since interfacial adhesion between non polar polymers and eggshell calcium carbonate was not well enough [9]. It was also reported that at eggshell calcium carbonate content of not more than 20 wt.%, the filled polymers were still ruptured in a ductile manner [10]. Several research works have been reported that the interaction between surface of $CaCO_3$ particles and HDPE matrix was able to enhance via compatiblization [11, 12]. The objective of this study was to investigate the effect of compatibilizer content on the mechanical and thermal properties of ESP filled HDPE composites. In addition, the filled HDPE was compatibilized by either high density polyethylene grafted with maleic anhydride (HDPE-g-MA) or ethylene propylene rubber grafted with maleic anhydride (EPR-g-MA).

Experimental

Materials. Chicken eggshell waste of Bolvans Goldlind and ISA Brown (hybrid) breeds was obtained from SUT farm, Suranaree University of Technology. High density polyethylene (EL-Lene™ H5814J) was purchased from SCG Chemicals Co., Ltd. High density polyethylene grafted with maleic anhydride, HDPE-g-MA, (Fusabond® MB100D, DuPont™) was kindly supplied by ChemicalInnovation Co., Ltd. Ethylene propylene rubber grafted with maleic anhydride, EPR-g-MA, (Exxerlor™ VA1803) was purchased from Global Connections Co., Ltd. The content of maleic anhydride of HDPE-g-MA and EPR-g-MA were 0.9 and 1.14 wt.%, respectively.

Eggshell Powder Preparation. First of all, chicken eggshell waste was thoroughly cleaned with tap water to remove residual of chicken dung, albumen (egg white) and yolk from the eggshell. After that, the cleaned eggshell was dried in an open air for 24 h. The eggshell from this step was referred as a raw eggshell. Eggshell powder (ESP) was prepared by grinding the raw eggshell via ball milling for 24 h. Subsequently, the ground eggshell was sieved using sieves of 325 and 450 mesh number.

HDPE Composites Preparation. To prepare ESP/HDPE composite, 80 wt.% HDPE and 20 wt.% ESP were mixed in an internal mixer (Hakke Rheomix 3000p). For HDPE-g-MA and EPR-g-MA compatibilized ESP/HDPE composite, the composite was prepared at the compatibilzer content of 2, 5, 8, and 10 wt.% based on HDPE. ESP was dried in an oven overnight at 70°C before mixixed. To prepare compatibilized ESP/HDPE composites, a mixture of HDPE and a compatibilizer was first melted for 5 min in an internal mixer (Hakke Rheomix 3000p) and ESP was then added into the mixing chamber. The mixing process was operated at 190°C under a rotor speed of 70 rpm and mixing time of 15 min. Subsequently, ESP/HDPE composite and compatibilized HDPE composites were pelletized before further molded into test specimens by an injection machine (Chuan Lih Fa, CLF 80T). The injection process was carried out with a melting temperature of 200°C, a screw speed of 208 rpm, an injection speed of 19.5 mm/sec, a holding pressure of 840 kg/cm^2 and a mold temperature of 30°C.

ESP Characterizations. Particle size and size distribution of ESP were determined via a particle size analyzer (Malvern Instruments, Mastersizer 2000) equipped with a He-Ne laser source of 633 nm at a beam length of 2.35 mm. Thermal decomposition temperature of ESP was monitored by a thermogravimetric analyzer (TA Instrument, SDT2960) with a heating rate of 20°C/min under a nitrogen atmosphere. The particle morphology of ESP was investigated by a scanning electron microscope (JSM 5800LV) with an accelerating voltage of 14 kV.

ESP/HDPE Composite Characterizations. Tensile properties of HDPE composites were determined in uniaxial tension using a universal testing machine (Instron model 5565) at a crosshead speed of 10 mm/min. The tensile test was conducted in accordance with ASTM D638. Unnotched Izod impact strength of the HDPE composites was evaluated under impact tester (Atlas, BPI) with 5.4 J hammer following ASTM D256. Thermal decomposition temperatures of HDPE and HDPE composites was monitored by a thermogravimetric analyzer (TA Instrument, SDT2960) with a heating rate of 20°C/min under a nitrogen atmosphere. Melting temperature (T_m), crystallization temperature (T_c) and crystallinity degree (X_c) of HDPE composites was determined using a differential scanning calorimetry, DSC, (Perkin Elmer Instruments Model UNIX DSC-7). For DSC analysis, a sample was heated to 180°C and cooled to 25°C under nitrogen atmosphere. The heating and cooling rate was 10°C/min. Melting and crystallization temperature were obtained according to ASTM D3417. Degree of HDPE composites' crystallinity was calculated using Eq. 1 as shown below.

$$X_c = [(\Delta H_f)/(\Delta H_{f^*})(W_f)] \times 100 \quad (1)$$

Where, H_f is the enthalpy of fusion of the sample, H_{f^*} is the enthalpy of fusion of a 100% crystalline HDPE as 292.60 J/g [5] and W_f is the weight fraction of HDPE matrix.

Freeze fracture surface morphology of those ESP/HDPE composites was investigated by a scanning electron microscope (JSM 5800LV) operated at acclerating voltage of 14 kV. The composites were fractured under liquid nitrogen and coated with gold for 10 min.

Results and Discussion

The ESP had a volume average diameter of 20.35 μm, was D_{10} of 3.46 μm, D_{50} of 18.47 μm, D_{90} of 39.60 μm with the particle range of 0.34-63.43 μm. The size distribution curve of ESP is shown in Fig. 1 (a) before the investigation SEM micrographs of ESP, in Fig. 1 (b), show that ESP was in cubic and irregular shape. Actually, particle shape of ground calcium carbonate was cubic in shape [13].

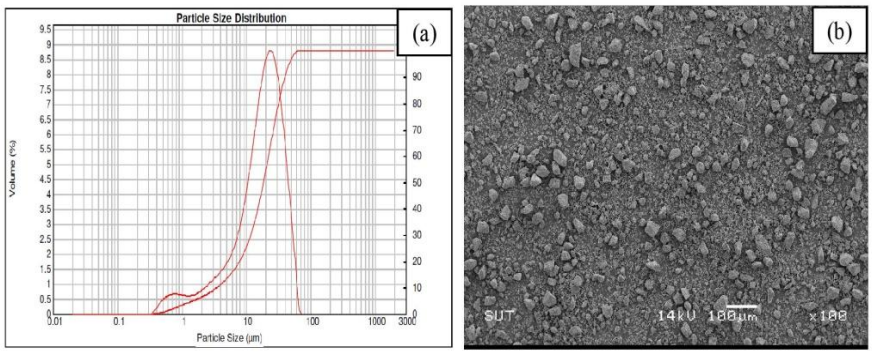

Figure 1. Particle size distribution curve (a), and SEM micrograph (x100) of ESP (b).

From Fig. 2, plots of mechanical properties vs compatibilizer content of ESP/HDPE composites, it was revealed that HDPE-g-MA enhanced ultimate stress, yield strength, and elongation at break of the composites. With increasing HDPE-g-MA, those mechanical properties gradually improved. Unnotched impact strength of the composites significantly increased and the compatibilized HDPE composites at 5, 8, 10 wt.% HDPE-g-MA did not rupture within instrumentation limit. These results could be attributed by chemical bonding and ion-dipole interaction between the C=O group of the maleic anhydride and Ca^{2+} ion of eggshell calcium carbonate [14]. However, Young's modulus of HDPE composite was not significantly influenced by addition of HDPE-g-MA. On the other hand, ultimate stress, yield strength, elongation at break and unnotched impact strength were decreased with increasing EPR-g-MA content. In addition, Young's modulus of compatibilized HDPE composite gradually decreased with increasing EPR-g-MA content. Furthermore, HDPE composites modified with EPR-g-MA had ultimate stress, yield strength and impact strength lower than those of HDPE composites modified with HDPE-g-MA. This might be due to the fact that HDPE-g-MA contained ethylene of 99 wt.% whereas EPR-g-MA contained 43 wt.% ethylene and 53 wt.% propylene. This implied that the HDPE-g-MA backbone was more compatible to HDPE matrix than EPR-g-MA backbone.

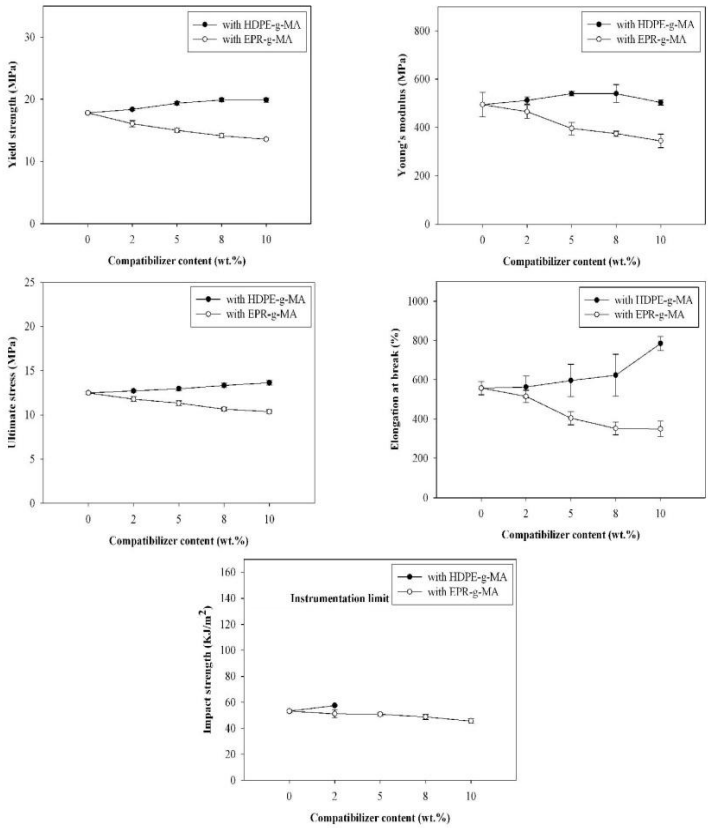

Figure 2. Plots of yield strength, ultimate stress, Young's modulus, elongation at break, and impact strength of 20 wt.% ESP/HDPE composites vs compatibilizer content.

From TGA and DTGA curves shown in Table 1, ESP/HDPE composites, uncompatibilized and compatibilized with HDPE-g-MA and EPR-g-MA, had two thermal transitions. The first transition from 488°C to 490°C was due to the decomposition of HDPE matrix. The second transition from 754°C to 758°C was derived from the decomposition of ESP. The decomposition of ESP slightly increased with increasing HDPE-g-MA and EPR-g-MA content. However, the decomposition temperature of HDPE matrix was not influenced by addition of HDPE-g-MA and EPR-g-MA.

Table 1. Decomposition temperatures of 20 wt.% ESP/HDPE composites at various HDPE-g-MA and EPR-g-MA contents.

Compatibilizer content (wt.%)	Decomposition temperature (°C)			
	with HDPE-g-MA		with EPR-g-MA	
	HDPE	ESP	HDPE	ESP
0	490	754	490	754
2	490	754	489	755
5	490	757	489	757
8	490	757	488	758
10	489	758	488	757

As shown in Table 2, HDPE-g-MA and EPR-g-MA did not significantly affect melting temperature and crystallization temperature of HDPE matrix of the composites. Degree of crystallinity of HDPE composites compatibilized with EPR-g-MA was higher than that of HDPE composites compatibilized with HDPE-g-MA. As mentioned before, HDPE matrix more disliked EPR-g-MA than HDPE-g-MA therefore during HDPE matrix was crystallizing, as foreigners, elastomeric backbone of EPR-g-MAH disturbed the crystallization process less than polyethylene backbone of HDPE-g-MA did. Adding EPR-g-MA into ESP/HDPE composite insignificant in affected HDPE's crystallinity. On the other hand, adding 2 wt% HDPE-g-MA resulted in significant decrease of crystallinity of HDPE matrix comparing to that of uncompatibilized ESP/HDPE composite. Nevertheless, the crystallinity became increasing when adding 5-10 wt.% HDPE-g-MA.

Fracture surface morphology of 20 wt.% ESP/HDPE composites at 0 wt.% and 5 wt.% HDPE-g-MA and EPR-g-MA are shown in Fig. 3. The better interfacial adhesion between ESP surface and HDPE phase was observed for the composite compatibilized with HDPE-g-MA indicated by more HDPE matrix adhering on ESP surface as observed from Fig. 3(b). This result well corresponded with and improvement of yield and impact strength as previously mentioned.

Table 2. Melting temperature (T_m), crystallization temperature (T_c), and degree of crystallinity (X_c) of 20 wt.% ESP/HDPE composites at various compatibilizer contents.

Compatibilizer content (wt.%)	T_m (°C)		T_c (°C)		X_c (%)	
	HDPE-g-MA	**EPR-g-MA**	**HDPE-g-MA**	**EPR-g-MA**	**HDPE-g-MA**	**EPR-g-MA**
0	129.06		115.30		58.37	
2	129.59	129.06	115.64	114.95	51.25	59.56
5	128.71	128.05	115.96	115.62	52.81	58.67
8	129.70	128.17	115.80	115.29	57.02	58.66
10	129.24	128.36	115.97	115.29	56.08	57.93

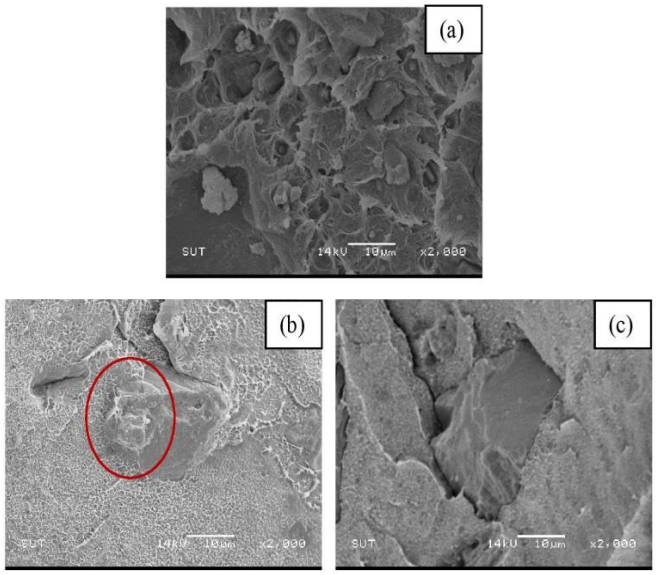

Figure 3. SEM micrographs of 20 wt.% ESP/HDPE composites: uncompatibilized (a) and compatibilized with 5 wt.% HDPE-g-MA (b) and 5 wt.% EPR-g-MA (c).

Summary

In this study, it was found that HDPE-g-MA helped reduce brittleness of 20 wt.% ESP/HDPE composite whereas EPR-g-MA had negative effect on tensile properties and impact strength of the HDPE composite. For ESP/HDPE composite with HDPE-g-MA, yield strength gradually increased and impact strength significantly improved with increasing HDPE-g-MA content. Decomposition, melting, and crystallization temperatures insignificantly influenced by addition of HDPE-g-MA. The optimum content of HDPE-g-MA for compatibilizing the ESP/HDPE composite was around 8-10 wt.%. At this content range, degree of crystallinity of the composite did not much differ from that of ESP/HDPE composite without HDPE-g-MA. On the other hand, EPR-g-MA negatively affected both tensile properties and impact strength and did not influence decomposition, melting, and crystallization temperatures of ESP/HDPE composite, as well. However, the degree of crystallinity of the composites filled with EPR-g-MA was comparable to that of the composite without EPR-g-MA.

Acknowledgement

The authors sincerely thank Suranaree University of Technology and Center of Excellence on Petrochemical, and Materials Technology, Chulalongkorn University for financial support and SUT farm for supplying chicken eggshell. The special thank is also attributed to Chemical Innovation Co., Ltd. for supplying the HDPE-g-MA compatibilizer.

References

[1] M.T. Hincke, U, J. Gautron, M. Panheleux, J. G. Ruiz, M. D. McKee, Y. Nys: Matrix Biol.Vol. 19 (2000), p. 443-453.
[2] N. Verma, V. Kumar, M. C. Bansal: Pol J Environ Stud. Vol. 21 (2012), p. 491-497.
[3] R. N. Rothon: *Mineral Fillers in Thermoplastics: Filler Manufacture and Characterisation* (United Kingdom, 1998).
[4] M. Saeedi, S. J. Sharahi, in: Proceedings of International Conference on Nanotechnology and Biosensors (2011), p. 34-38.
[5] S. Sahebian, S. M. Zebarjad, J. V. S. A. Sajjadi: J. Mat. Process. Tech. Vol. 209 (2009), p. 1310-1317.
[6] P. Pakdeechote, Y. Ruksakulpiwat, N. Suppakarn, W. Sutapun, in: Proceedings of the Sixth Thailand Materials Science and Technology Conference (2010), p. 168-170.
[7] S. Shuhadahand, A.G. Supri: J Phys. Sci. Vol. 20. (2009), p. 87–98.
[8] R. Dangtungee, S. Shawaphun: J KMUTNB. Vol. 18 (2008), p. 9-15.
[9] P. Pakdeechote, Y. Ruksakulpiwat, N. Suppakarn, W. Sutapun, in: Proceedings of the 11th Pacific Polymer Conference (2009), p. 154.
[10] P. Pakdeechote. in: *Preparation of chicken eggshell for high density polyethylene composites*, School of Polymer Engineering, Suraree University of Technology, Thailand (2010).
[11] N. Phueakbuakhao, W. P. Ouajai, N. K. Ongarjnukool: J. Met. Mater. Min. Vol 18 (2008), p. 131-135.
[12] Z. H. Liu, K. W. Kwok, R. K. Y. Li, C. L. Choy: Polym. Vol. 43 (2002), p. 2501-2506.
[13] M. N Freire, J. N. F. Holanda: Cerâmica. Vol. 52 (2006), p. 240-244.
[14] G. Li, K. C. Mai, K. C. Feng, Y. P. Huang: Polym Int. Vol. 55 (2006), p. 891–897.

EFFECT OF FILLER PARTICLE SIZE ON MECHANICAL AND THERMAL PROPERTIES OF HIGH DENSITY POLYETHYLENE FILLED WITH BIO-FILLER FROM EGGSHELL WASTE

Wanikorn Buakaew[1,2], Yupaporn Ruksakulpiwat[1], Nitinat Suppakarn[1], Wimonlak Sutapun[1*]

[1]School of Polymer Engineering, Institute of Engineering, Suranaree University of Technology, Nakhon Ratchasima, 30000 Thailand
[2]Center of Excellence on Petrochemical, and Materials Technology, Chulalongkorn University, Bangkok, 10330 Thailand

[*]Author for correspondence; E-mail: wimonlak@sut.ac.th, Tel. +66 44 224435, Fax. +66 44 224605

Abstract: In this work, eggshell calcium carbonate in a form of powder was used as bio-filler for HDPE. Three different average sizes of eggshell powder (ESP), 35.30, 20.35 and 13.96 µm were used. The effect of eggshell particle size on mechanical and thermal properties of 20 wt.% ESP/HDPE composites was investigated. It was found that HDPE composites prepared with three different particle sizes of ESP had no significant differences in Young's modulus, yield strength and ultimate stress. HDPE filled with smaller particle size of ESP had higher elongation at break and impact strength than the one with larger particle size. In addition, the HDPE composite with smaller particle size of ESP had higher decomposition temperature of HDPE matrix and ESP filler. On the other hand, melting temperature crystallizing temperature and degree of crystallinity of HDPE composite were not influenced by ESP particle size.

1. Introduction

High density polyethylene (HDPE), a semi-crystalline polymer, is widely used as a commodity polymer with high-tonnage production due to its distinctive mechanical and physical properties. Several particulate mineral fillers as calcium carbonate, clay, talc, silica, mica and wollastonite etc., have been incorporated into HDPE [1]. The main function of the fillers is to improve certain properties such as mechanical properties weathering resistance and environmental stress cracking resistance, as well as to reduce material cost. Calcium carbonate as ground calcium carbonate (GCC) and precipitated calcium carbonate (PCC) are the most consumed reinforcing filler for HDPE, more than 60% of total filler usage [2]. By the way, raw material as sedimentary rock for calcium carbonate production takes so long time for accumulating in nature. In order to prolong this natural resource, other source for calcium carbonate should have been looking for. Eggshell calcium carbonate is one of good replacements for calcium carbonate filler due to its renewability, availability and high content in calcium carbonate (94 wt.%). Most importantly, it is regenerated from avian such as hen, duck and bird. It was reported that eggshell calcium carbonate was successfully applied as reinforcing filler for LDPE [3], PP [4] and epoxy [5]. The mechanical and flow properties of those polymers filled with eggshell powder were comparable to those properties of the polymers filled with GCC [6]. In addition, ESP content of less than 20-30 wt.% would not significantly affect deformation and failure behavior of the filled polymers under tensile loading. Apart from filler content, filler particle size is one of important material parameters affecting physical properties of particulate filled polymers [7].

The objective of this study was to investigate the effect of ESP particle size (35.30, 20.35 and 13.96 µm) on mechanical and thermal properties of HDPE filled with ESP.

2. Materials and Methods

2.1 Materials

High density polyethylene, HDPE, (EL-Lene™ H5814J) with a melt flow index of 14 g/10 min and a density of 0.958 g/cm^3 was purchased from SCG Chemicals Co., Ltd. Three different sizes of eggshell powder were used, ESP 1, ESP 2 and ESP 3. They were prepared from Chicken eggshell waste of Bolvans Goldlind and ISA Brown (hybrid) breeds, supplied by SUT farm, Suranaree University of Technology. Their average particle size (D [4,3]), size distribution, and BET surface area are shown in Table 1.

Table 1: Volume average particle size, size distribution and BET surface area of ESP fillers.

Eggshell Powder	Particle size distribution (µm)				BET surface area (m^2/g)
	D [4,3]	D [0,1]	D [0,5]	D [0,9]	
ESP 1	35.30	2.33	33.69	74.41	3.71
ESP 2	20.35	3.46	18.47	39.60	3.90
ESP 3	13.96	2.64	12.37	27.56	4.23

2.2 HDPE composite preparation

HDPE composites were prepared with ESP 1, ESP 2 and ESP 3 at 20 wt.% eggshell powder in an internal mixer (Hakke, Rheomix 3000p). Eggshell powder was dried in an oven overnight at 70°C before mixed with

HDPE. HDPE was first melted for 5 min in the mixer and eggshell powder was then added. The mixing process was operated at 190°C under a rotor speed of 70 rpm and mixing time of 15 min. Subsequently, the HDPE composites were pelletized by a grinding machine before further molded into test specimens using an injection machine (Chuan Lih Fa, CLF 80T). The injection process was carried out at a melting temperature of 200°C, a screw speed of 208 rpm, an injection speed of 19.5 mm/sec, a holding pressure of 840 kg/cm^2 and a mold temperature of 30°C.

2.3 ESP characterization

The X-ray diffractometer (Bruker, D5005) was used to determine crystal polymorph of calcium carbonate eggshell and ground $CaCO_3$. The measurement was carried out using CuK_α radiation (λ = 0.15406 nm) with an accelerating voltage of 40 kV and a current of 40 mA, 2θ between 5 and 70°C, a scan step of 0.02°, and a scan speed of 0.5 s/step.

Thermal decomposition temperature of eggshell powder was monitored by a thermogravimetric analyzer, TGA (Mettler Toledo, TGA/DSC1) with a heating rate of 20°C/min under a nitrogen atmosphere.

Particle morphology of eggshell powder was investigated by a scanning electron microscope (JEOL, JSM 5800LV) with an accelerating voltage of 14 kV.

2.4 ESP/HDPE composite characterization

Tensile properties of neat HDPE and ESP/HDPE composites were determined in uniaxial tension using a universal testing machine equipped with of 5 kN load cell, (Instron, Series 5565). The tensile test was conducted in accordance with ASTM D638 at a crosshead speed of 10 mm/min.

Unnotched Izod impact strength of neat HDPE and ESP/HDPE composites was evaluated on an impact tester (Atlas, BPI) equipped with a pendulum hammer of 5.4 J, following ASTM D256.

Thermal decomposition temperature of neat HDPE and ESP/HDPE composites was monitored by a thermogravimetric analyzer, TGA (Mettler Toledo, TGA/DSC1) with a heating rate of 20°C/min under a nitrogen atmosphere.

Melting temperature crystallizing temperature and degree of crystallinity of neat HDPE and ESP/HDPE composites were determined using a differential scanning calorimetry, DSC (Perkin Elmer, UNIX DSC-7). For DSC analysis, a sample was heated to 180°C and subsequently cooled to 25°C under a nitrogen atmosphere with a heating and cooling rate of 10°C/min. Melting and crystallizing temperatures were obtained according to ASTM D3417. Degree of crystallinity was calculated using the equation shown below.

$$X_c\,(\%) = [(\Delta H_f)/(\Delta H_{f^*})(W_f)]\times 100 \qquad (1)$$

Where, H_f is the enthalpy of fusion of the sample, H_{f^*} is the enthalpy of fusion of a 100% crystalline HDPE as 292.60 J/g [2] and W_f is the weight fraction of HDPE matrix.

Freeze fractured surface morphology of neat HDPE and ESP/HDPE composites was investigated by a scanning electron microscope (JEOL, JSM 5800LV) operated at an accelerating voltage of 14 kV. The HDPE and composites were fractured under liquid nitrogen and coated with gold for 10 min.

3. Results and Discussion

X-ray diffraction (XRD) patterns of ESP 1, ESP 2 and ESP 3, and ground $CaCO_3$ were comparatively illustrated in Figure 1. The pattern of ESP and ground $CaCO_3$ was well matched. The strongest peak of the calcium carbonate eggshell occurred at 2θ of 29.5°. The XRD patterns of eggshell powder are the pattern of calcite polymorph with a crystal system of rhombohedral hexagonal structure (a= 4.98900, b=4.98900, c=17.06200, α=90°, β=90°, γ=120°)

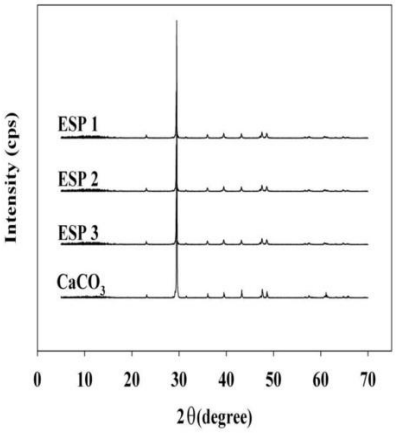

Figure 1. XRD patterns of ground $CaCO_3$, ESP 1, ESP 2, and ESP 3.

TGA and DTGA curves as well as SEM micrographs of ESP 1, ESP 2 and ESP 3 were shown in Figure 2 (a) and 2 (b), respectively. From TGA and DTGA curves, eggshell powder shows two major thermal transitions. The first transition occurred at 230-330°C, was derived from the decomposition of organic matter of eggshell matrix and membrane. The second transition at 814°C, 809°C and 777°C were derived from thermal decomposition of eggshell $CaCO_3$ of ESP 1, ESP 2 and ESP 3, respectively [8]. The results showed that thermal stability of eggshell $CaCO_3$ decreased with smaller particle of the eggshell. The smaller particle size had larger surface area that contributes to high efficiency of heat transfer [9]. Therefore, with larger surface, ESP decomposed at lower temperature. SEM micrographs of ESP, in Figure 2 (b), show that ESP particle was in cubic and irregular shape.

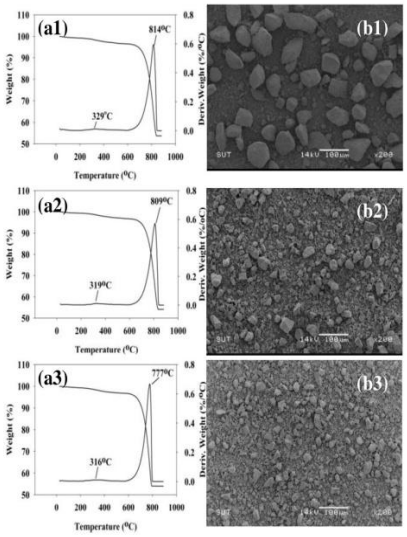

Figure 2. TGA and DTGA curves (a) and SEM micrographs (x200) (b), of ESP 1 (1), ESP 2 (2), and ESP 3 (3).

For tensile properties, ESP particle size did not affect Young's modulus, ultimate stress, and yield strength, of filled HDPE composites, as observed from Figure 3 (a) and 3 (b). However, elongation at break of ESP/HDPE composite depended on particle size of ESP. Elongation at break of the composite with smaller ESP particle size (ESP 2 and ESP 3) was higher than that of the composite with the larger size of ESP 1. This is an indication that, under tensile deformation, the HDPE composite with ESP particle size smaller than 35.30 µm was able to absorb more applied energy prior to the composite rupture. However, under impact loading, the ability to absorb impact energy of those composites prepared with ESP 1, ESP 2, and ESP 3 was insignificantly different.

From TGA and DTGA curves shown in Figure 4, neat HDPE thermally decomposed as a single transition at 483°C whereas ESP/HDPE composites decomposed with two thermal transitions. The first transition due to decomposition of HDPE matrix was at 485°C, 490°C and 492°C for HDPE filled with ESP1, ESP2, and ESP3, respectively. The second transition derived from decomposition of eggshell calcium carbonate was around 750°C [10]. The ESP particle size did influence thermal decompsition of HDPE matrix. The decomposition temperature of HDPE matrix and ESP filler were increased with decreasing ESP particle size. This was possibly due to the increased efficiency of heat transfer of smaller particle of ESP [9].

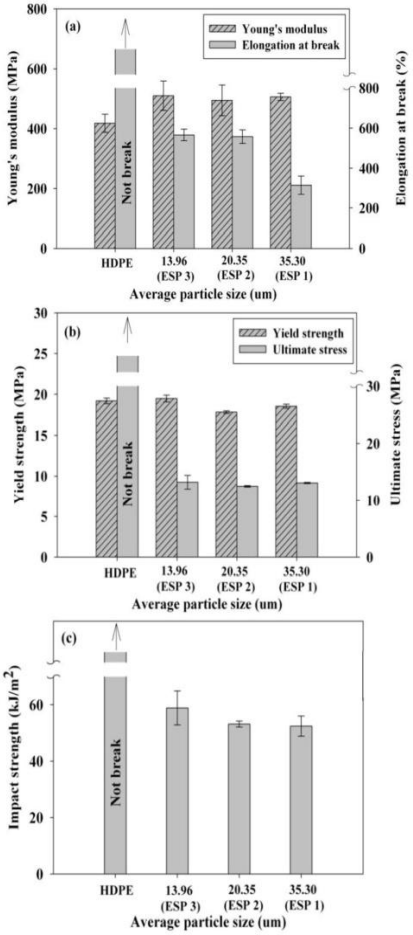

Figure 3. Plots of Young's modulus and elongation at break (a), yield strength and ultimate stress (b), and impact strength (c) of ESP/HDPE composite vs ESP particle size.

As shown in Table 3, ESP particle size did not significantly affect melting temperature, crystallizing temperature and degree of crystallinity of HDPE matrix of HDPE filled with ESP.

Fracture surface morphology of 20 wt.% ESP/HDPE composites with ESP particle sizes of 35.30 (ESP 1) and 13.96 (ESP 3) µm are shown in Figure 5 (a) and 5 (b). It was observed that interfacial adhesion between ESP surface and HDPE matrix was not good. Several holes were observed on the fracture surface. These holes were caused from detaching of ESP particle from HDPE matrix. The surface topology of HDPE filled with ESP 1 and ESP 3 indicated that the filled HDPE still ruptured in a ductile manner.

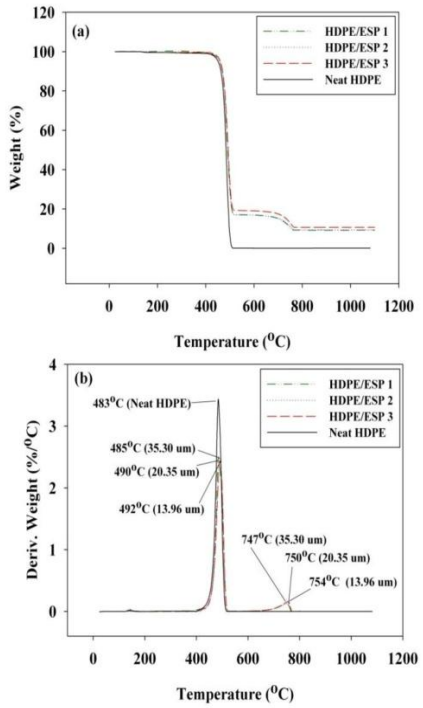

Figure 4. TGA (a) and DTGA (b) curves of neat HDPE and HDPE composites filled with ESP 1, ESP 2, and ESP 3.

Table 3: Melting temperature (T_m), crystallizing temperature (T_c), and degree of crystallinity (X_c) of neat HDPE and HDPE composites filled with ESP 1, ESP 2, and ESP 3.

HDPE Composites	T_m (°C)	T_c (°C)	X_c (%)
HDPE	128.29	115.66	70.51
ESP 1/HDPE	127.30	116.45	69.87
ESP 2/HDPE	129.06	115.30	69.58
ESP 3/HDPE	128.97	116.00	69.06

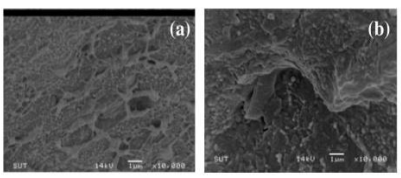

Figure 5. SEM micrographs (x10000) of freeze fractured surface of 20 wt.% ESP/HDPE composites prepared with ESP 1 (a) and ESP 3 (b).

4. Conclusions

In this study, it was found that under tensile deformation, HDPE composite prepared with 20 wt.% absorbed more applied energy prior to composite rupture when particle size of ESP was less than 35.30 µm. However, ESP particle size did not much affect impact strength of the HDPE composite. Yield strength, ultimate stress and Young's modulus of the filled HDPE did not depend on ESP particle size. On the other hand, decomposition temperatures of ESP/HDPE composite were significantly influenced by ESP particle size. The decomposition temperatures of HDPE matrix and ESP filler was higher with smaller size of ESP. Melting and crystallizing temperature, and degree of crystallinity of the HDPE composite did not much differ from that of neat HDPE.

Acknowledgements

The authors sincerely thank Suranaree University of Technology and Center of Excellence on Petrochemical, and Materials Technology, Chulalongkorn University for financial support and SUT farm for supplying chicken eggshell. The special thank is also attributed to Scientific Promotion Co., Ltd. for kindly supplying air jet sieving machine (Retsch, AS 200 jet).

References

[1] R.H. Elleithy, L. Ali, M. A. Ali and S. M. Al-Zahrani,J. Appl. Polym. Sci.117 (2010) 2413–2421.
[2] S. Sahebian, S. M. Zebarjad, K. J. Vahdati and S. A. Sajjadi, J. Mater. Process. Tech. 209(2009) 1310-1317.
[3] S. Shuhadah and A. G. Supri, J. Phys. Sci. 20 (2009) 87–98.
[4] R. Dangtungee and S. Shawaphun, J. KMUTNB. 18 (2008) 9-15.
[5] G. Ji, Z. Hongqi, Q. Chenze and Z. Minfeng, Polym. Eng. Sci.49 (2009) 1383-1388.
[6] S. Fu, X. Feng, B. Lauke and Y. Mai, Compos. B. 39 (2008) 933-961.
[7] M. Hancock, P. Tremayne and J. D. Rosevear, J. Polym. Sci. 18 (1980) 3211.
[8] M. N. Freire and J. N. F. Holanda, Cerâm. 52 (2006) 240-244.
[9] M. Mohamed, S. Yusupand and S. Maitra, J. Eng. Sci. Tech. 7 (2012) 1 - 10.
[10] F.S. Murakami, P. O. Rodringuesl, C. M. T. Campos and M. A. S. Silval, Ciênc. Tecnol. Aliment. Campinas. 27 (2006) 658-662.

Advanced Materials Research Vol. 747 (2013) pp 72-75
Online available since 2013/Aug/30 at www.scientific.net

doi:10.4028/www.scientific.net/AMR.747.72

Mechanical, Thermal and Morphological Properties of Poly(butylene succinate) Filled with Bio-Functional Filler from Eggshell Waste

Wanikorn Buakaew[1, 2, a], Yupaporn Ruksakulpiwat[1, b], Nitinat Suppakarn[1, c], and Wimonlak Sutapun[1, d]

[1]School of Polymer Engineering, Institute of Engineering, Suranaree University of Technology, Nakhon Ratchasima, 30000 Thailand

[2]Center of Excellence on Petrochemical, and Materials Technology, Chulalongkorn University, Bangkok, 10330 Thailand

[a]wanikorn102@gmail.com, [b]yupa@sut.ac.th, [c]nitinat@sut.ac.th, [d]wimonlak@sut.ac.th

Keywords: eggshell, calcium carbonate, PBS/ESP composite

Abstract. In this work, calcium carbonate derived from eggshell, in a form of eggshell powder (ESP) with an average particle size of 13.96 μm, was used as bio-reinforcing filler for poly (butylene succinate), (PBS). The effect of ESP content on mechanical, thermal, and morphological properties of ESP filled PBS was investigated. The ESP/PBS composites were prepared at various ESP contents of 10, 20, 30 and 40 wt.%. It was found that incorporation of ESP into PBS matrix resulted in an improvement of Young's modulus but it resulted in a decrease of tensile stress at break, yield strength and impact strength of the composite. In addition, increasing ESP content did not significantly influence decomposition temperature and melting temperature of PBS matrix. On the other hand, with increasing ESP content, crystallization temperature of the composite decreased but degree of crystallinity increased. Fracture surface morphology of the PBS composites obtained from scanning electron microscope indicated agglomeration and poor distribution of ESP within the composite matrix. Partial adhesion between ESP surface and PBS matrix was observed as well.

Introduction

In recent years, eco-friendly biodegradable polymers have gained increasing attention because of growing worldwide recognition of the need to reduce global environmental pollution. These polymers are completely degraded in natural ecosystems such as natural soil, lake and marine [1]. Nowadays, biodegradable polymers such as poly(lactic acid) (PLA), poly(butylenes succinate) (PBS) and poly(butylene adipate-co-terephthalate) (PBAT) are used to replace non-degradable polymer [2]. Among these biodegradable polymers, Poly(butylene succinate) (PBS), one of biodegradable polyester, is becoming the biodegradable material of choice for replacing traditional polyethylene (PE) and polypropylene (PP) in the near future due to their biodegradability and availability, and also comparable physical properties to those commodity thermoplastics. PBS is produced by the condensation reaction of the glycols 1,4-butanediol and aliphatic dicarboxylic acid, which is succinic acid [3]. Presently, PBS is not yet widely used as consumer product because it is too expensive, 10 $/kg (source: Fresh Bag Co., Ltd). However, it has been predicted that within the nearest 5 years, the consumer product from PBS will be spreadly commercialized. Nevertheless, PBS is able to compounded with several reinforcing fillers for reduction of material cost and/or enhancement of stiffness. There are many studies concerning the use of mineral filler, from bio sources, as reinforcment in bio-composites system such as shellfish shell [4], oyster and mussel shell [5]. The chicken eggshell is a waste from hatchery and food industry. Mostly, eggshell is commonly disposed without any utilization even though it comprised valuable CaCO3 upto 94 wt.%, close to purity of ground calcium carbonate (GCC) used as a plastic filler [6]. Thus, eggshell is interesting, apart from high in CaCO3 content, because it is derived from renewable bio-source and abundant. Presently, there are studies about incoperating GCC into some biodegradable polymers such as PLA [7] and PBAT [8]. The results showed improvement of Young's modulus of those composites with increasing GCC content.

Therefore, the aim of this study was to employ eggshell powder (ESP), prepared from eggshell waste, as biofiller for PBS. The effect of ESP content on the mechanical, thermal and morphological properties of PBS filled with ESP was then investigated.

Experimental

Materials. Chicken eggshell waste of Bovans Goldline and ISA Brown (hybrid) breeds was obtained from SUT farm, Suranaree University of Technology. The eggshell powder (ESP) was prepared from the eggshell waste. The procedure for ESP preparation was mentioned elsewhere [9]. The average particle size, size distribution and BET surface area of ESP are shown in Table 1. Poly (butylene succinate), (GS Pla AZ91TN), with a melt flow index of 4 g/10 min and a density of 1.26 g/cm^3 was supplied by Mitsubishi Chemical Performance Polymer, Inc.

Table 1. Average particle size, size distribution and BET surface area of ESP

Material	Particle size distribution (μm)					BET surface area (m^2/g)
	D[0,1]	D[0,5]	D[0,9]	D[4,3]	Range	
ESP	2.64	12.37	27.56	13.96	0.34-40.02	4.2308

ESP/PBS Composite Preparation. Poly (butylene succinate), PBS, filled with 10, 20, 30 and 40 wt% ESP was prepared in an internal mixer (Hakke, Rheomix 3000p). The ESP was dried in an oven overnight at 70°C before mixed with PBS. To prepare ESP filled PBS, PBS was first melted for 2 min in an internal mixer and ESP was then added into the mixing chamber. The mixing process was operated at 120°C under a rotor speed of 60 rpm and a mixing time of 3 min. Subsequently, ESP/PBS composites were ground and further molded into test specimens by an injection machine (Chuan Lih Fa, CLF 80T). The injection molding was carried out with a melting temperature of 190°C, a screw speed of 130 rpm, an injection speed of 47 mm/sec, a holding pressure of 617 kg/cm^2 and a mold temperature of 30°C.

ESP/PBS Composite Characterizations. Tensile properties of PBS and PBS composites were determined in uniaxial tension using a universal testing machine (Instron, Series 5565). The tensile test was conducted in accordance with ASTM D638 at a crosshead speed of 10 mm/min. Unnotched Izod impact strength of PBS and PBS composites was evaluated under an impact tester (Atlas, BPI) equipped with 5.4 J hammer, following ASTM D256. Thermal decomposition temperature of PBS and PBS composites was monitored by a thermogravimetric analyzer (Mettler Toledo, TGA/DSC1) with a heating rate of 20°C/min under a nitrogen atmosphere. Melting temperature (Tm), crystallizing temperature (T_c) and crystallinity degree (X_c) of PBS and PBS composites were determined using a differential scanning calorimetry, DSC, (Perkin Elmer, UNIX DSC-7). For DSC analysis, a sample was heated to 180°C and cooled to 25°C under nitrogen atmosphere. The heating and cooling rate was 10°C/min. Melting and crystallizing temperature were obtained according to ASTM D3417. Crystallinity degree (Xc) of PBS composites was calculated using Eq. 1, as shown below.

$$X_c\,(\%) = [(\Delta H_f)/(\Delta H_{f^*})(W_f)]\times 100 \qquad (1)$$

Where, H_f is the enthalpy of fusion of the sample, H_{f^*} is the enthalpy of fusion of a 100% crystalline PBS as 110.3 J/g [10] and W_f is the weight fraction of PBS matrix.

Freeze fracture surface morphology of those ESP/PBS composites was investigated by a scanning electron microscope (JOLE, JSM 5800LV) operated at acclerating voltage of 14 kV. The composites were fractured under liquid nitrogen and coated with gold for 10 min.

Results and Discussion

From plots of tensile properties vs ESP content of ESP/PBS composite, it was revealed that tensile stress at break and yield strength of the composites gradually decreased with increasing ESP content, as observed from Fig. 1 (a). In addition, Young's modulus of the composites was improved by addition of ESP. This was caused by the incorporation of rigid particle of ESP which is stiffer than PBS. With increasing ESP content, elongation at break of ESP filled PBS decreased and was much lower than that of unfilled PBS. This is an indication that with higher content of ESP, the PBS composite lossed ability to absorb applied energy prior to composite fracture. This result well corresponded with the result obtained from an impact test of the PBS composite. The PBS composite with higher content in ESP had lower impact strength than that of the composite with lower ESP content and lower than that of unfilled PBS. However, the PBS composite at 10 wt.% ESP and neat PBS did not rupture within an instrumentation limit.

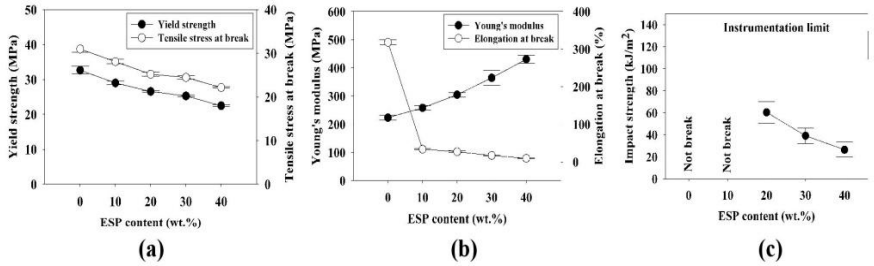

Figure 1. Plots of yield strength & tensile stress at break (a), Young's modulus & elongation at break (b) and impact strength (c) vs ESP content of ESP/PBS composite.

Decomposition temperatures of ESP/PBS composites are shown in Table 2. ESP/PBS composites had two thermal transitions. The first transition at 413°C and 414°C was due to the decomposition of PBS matrix. The second transition at 743°C, 758°C and 775°C was derived from the decomposition of 10, 20, and 30-40 wt.% ESP within the composite, respectively. With increasing ESP content, ESP thermally decomposed at higher temperature. However, the decomposition temperature of PBS matrix was not influenced by an existence of ESP.

In addition, ESP content did not significantly affect melting temperature of PBS, composite matrix. Crystallizing temperature of the composite decreased with increasing ESP content. This indicated that ESP did not act as a nucleating agent for PBS. On the other hand, degree of crystallinity of PBS composite was increased with increasing ESP content.

Table 2. Decomposition temperature (T_d), melting temperature (T_m), crystallizing temperature (T_c) and degree of crystallinity (X_c) of ESP/PBS composite at various ESP contents.

ESP content (wt.%)	T_d (°C)		T_m (°C)	T_c (°C)	X_c (%)
	PBS	ESP			
0	414	-	112	81	51
10	413	743	112	74	56
20	413	758	110	72	58
30	413	775	110	72	62
40	413	775	110	72	65

SEM micrographs of ESP/PBS composites shown in Fig. 2 illustrate that PBS composite has a rough fracture surface with agglomerated eggshell particles. The higher the ESP content, the poorer the ESP dispersed within PBS matrix. The agglomeration and poor distribution of the filler particle

was responsible for the decrease of yield strength, tensile stress at break and impact strength. The detachment of PBS matrix from ESP surface with partial PBS left on the surface was observed. In addition, the surface topology of PBS matrix indicated that it still ruptured in a ductile manner as same as neat PBS.

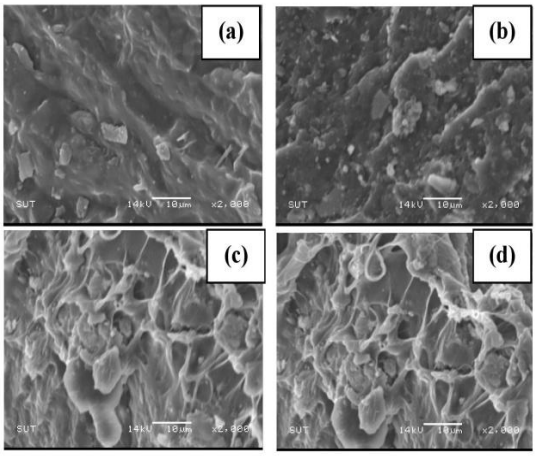

Figure 2. SEM micrographs of freeze fracture surface of ESP/PBS composites prepared with 10 wt.% (a), 20 wt.% (b), 30 wt.% (c) and 40 wt.% (d) ESP.

Summary

In this study, it was found that increasing content of ESP had negative effect on yield strength, tensile stress at break and impact strength of ESP/PBS composite. However, addition of ESP resulted in an increase of Young's modulus of the composite. For thermal properties, decomposition temperature of PBS matrix was not influenced by an inclusion of ESP. However, decomposition temperature of ESP filler was higher when it was added more into the PBS matrix. Melting temperature of the PBS matrix did not much differ from that of neat PBS. On the other hand, crystallizing temperature of the composite matrix decreased, however, degree of crystallinity of the PBS composite increased with increasing ESP content.

Acknowledgements

The authors sincerely thank Suranaree University of Technology for financial support and SUT farm for supplying chicken eggshell. The special thank is also attributed to Scientific Promotion Co., Ltd. for kindly supplying air jet sieving machine (Retsch, AS 200 jet).

References

[1] Y. F. Shih and Y. C. Chieh: Macromol. Theory Simul. Vol. 16 (2007), p. 101-110.
[2] W. Hoidy, E. A. Mulla, K. A. Janabi: J. Polym. Environ. Vol. 18 (2010), p. 608-616.
[3] Y. F. Shih, L. S. Chen, R. J. Jeng: J. Polym. Vol. 49 (2008), p. 4602-4611.
[4] H. S. Kim, H. J. Kim, J. W. Lee, I. G. Choi: Polym. Degrad. Stabil. Vol. 91 (2006), p. 1117-1127.
[5] M. W. Lee, S. O. Han, Y. B. Seo: Compos. Sci. Technol. Vol. 68 (2008), p. 1266-1272.
[6] M. Cusack, A. C. Fraser, T. Stachel: Comp. Biochem. Phys. B. Vol. 134 (2003), p. 63-69.
[7] H. S. Kim: J. Appl. Polym. Sci. Vol. 109 (2008), p. 3087–3092.
[8] Z. Shi, J. Dong, and W. Ma: Adv. Mat. Res. Vol. 602 – 604 (2013), p. 768-771.
[9] R. Dangtungee and S. Shawaphun: J. KMUTNB. Vol. 18 (2008), p. 9-15.
[10] Y. J. Phua, W. S. Chow, and Z. A. M. Ishak: Express. Polym. Lett. Vol. 5 (2011), p. 93-103.

BIOGRAPHY

Mr. Wanikorn Buakaew was born on February 20, 1987 in Lampang province, Thailand. He has earned his Bachelor's Degree in Materials Science (Rubber Industry) from Maejo University (MJU), Chiang Mai, in 2009. After that, he continued his Master's Degree in Polymer Engineering at School of Polymer Engineering, Institute of Engineering, Suranaree University of Technology. During his master degree's study, he presented one oral presentation entitle: **"Effect of compatibilizers on mechanical and thermal properties of high density polyethylene filled with bio-filler from eggshell"** at the 2013 International Conference on Materials Science and Chemical Engineering (MSCE 2013) in Singapore. Moreover, he presented three poster presentations entitle: **"Effect of filler particle size on mechanical and thermal properties of high density polyethylene filled with bio-filler from eggshell waste"** at the Pure and Applied Chemistry International Conference 2013 (PACCON 2013) in Chon Buri, Thailand, **"Effect of a compatibilizer on mechanical, thermal and morphological properties of high density polyethylene filled with bio-filler from eggshell waste"** at the 4th Research Symposium on Petrochemical and Materials Technology and the 19th PPC Symposium on Petroleum, Petrochemicals, and Polymers (PETROMAT and PPC SYM 2013) in Bangkok, Thailand, and finally **"Mechanical, thermal and morphological properties of poly (butylene succinate) filled with bio-functional filler from eggshell waste"** in the 4th International Conference on Multi-Functional Materials and Structures in Bangkok, Thailand.